DEVELOPMENT OF AN ULTRAVIOLET-PROTECTIVE GLASS FIBRE REINFORCED EPOXY COMPOSITE

TSZ-TING WONG

Ph.D
The Hong Kong Polytechnic University
2017

The Hong Kong Polytechnic University

Department of Mechanical Engineering

Development of an Ultraviolet-protective Glass Fibre Reinforced Epoxy Composite

Tsz-ting Wong

A thesis submitted in partial fulfilment of the

requirements for the degree of Doctor of Philosophy

September 2016

Certificate of Originality

I hereby declare that this thesis is my own work and that, to the best of my knowledge and belief, it reproduces no material previously published or written, nor material that has been accepted for the award of any other degree or diploma, except where due acknowledgement has been made in the text.

__________________________________ *(Signature)*

Isabel Tsz-ting Wong *(Name of Student)*

Dedication

To my supervisor, husband, family, fellows and friends.

I dedicate my research works in sincere gratitude for their love and support.

Abstract

With the increasing utilization of fibre reinforced polymer-based composites (FRPs) in aircraft, civil construction and automobile engineering industries, long-term durability is critical to FRPs. In another word, it is essential to maintain the structural strength of FRPs under various environmental effects (such as UVR, temperature and moisture) with the change of time. FRPs are inevitably in contact with UVR from sunlight during service. Nowadays, at least 50% fuselage materials of commercial aircraft A350 and B787 are implemented with FRPs. The roofs and facades on buildings and deck panels on bridges made by FRPs are found everywhere.

Ultraviolet radiation (UVR), an inherent stimulus to human body and polymer-based materials, poses negative effects to the health of exposed organisms and strength of exposed materials. To protect polymer-based materials from UVR degradation, inorganic zinc oxide (ZnO) particle is proposed to alleviate the chemical UVR absorption of polymers and simultaneously enhance the physical UVR absorption. ZnO is able to physically absorb UVR and gives full UVR spectrum absorption. Besides, it is relatively inexpensive and easy for processing. Moreover, nanoparticle dissolution out of polymers could happen when contacting with UVR and ionic solutions. Hollow glass fibre (HGF) is introduced to protect the nanoparticles from dissolution and simultaneously reinforce the polymer surface from wearing problem as hollow glass fibre generally has high wearability. As a result, ZnO/HGF is engineered to be the top lamina of glass fibre reinforced epoxy composite for the protection purpose.

100nm ZnO particle is found in present research performing with optimized results in UVR absorption with good particle dispersion in epoxy, unsaturated polyester, epoxy-based and styrene-based shape memory polymers (EP- and S-SMPs). 4 wt.% 100nm ZnO particle mixed with epoxy is filled into HGF by using vacuum infiltration technique and exhibits uniform particle dispersion and good rheology properties. 4 wt.% 100nm ZnO/HGF lamina achieves high UVR absorption among the tested samples including epoxy, 2 wt.% and 7 wt.% 100nm ZnO/HGF laminas. Particle agglomeration occurs when the particle content is increased to 7 wt.% which its lamina results in having the lowest UVR absorption. 4 wt.% 100nm ZnO also exhibits good particle dispersion, UVR absorption and therefore is able to maintain the surface hardness and shape memory effects in EP- and S-SMPs after UVA exposure.

The surface morphology and tensile properties of glass fibre unsaturated polyester composite with 6 wt.% 100nm ZnO implemented in the first three layers of glass fabric underwent accelerated continuous and cyclic UVA exposure are compared. Their surface morphology has no significant difference but their tensile properties are found otherwise. The rate of change of the Young's modulus of the composite underwent continuous UVA exposure is 2 times higher than that with cyclic UVA exposure. Similar result is found in the tensile strength which is 1.16 times higher. Mechanical properties should be the determinant for the degradation rate of composites and estimation on their service life.

Theoretical model is developed for the parameter optimization in designing the configuration of ZnO/HGF lamina based on stress transfer ability. Together with the results obtained from experimental analysis, 4 wt.% 100nm ZnO/HGF lamina with longer length of HGF has good stress transfer ability, load carrying capability, particle dispersion and UVR resistibility.

Up to the moment in present research, it has been revealed that there are plenty of potential in the investigation of the UVR degradation and resistance in polymer-based composites. More details will be addressed in the last chapter of this thesis, Chapter Nine Concluding Remarks and Suggestions for Future Development.

Publications Arising from the Project

International Journals

Based on my research outcomes, my published articles have attracted over 21 citations to date.

1. Kin-tak Lau, **Tsz-ting Wong**, Jinsong Leng and David Hui. Property enhancement of polymer-based composites at cryogenic environment by using tailored carbon nanotubes. Composites Part B: Engineering. 2013;54:41-43.

2. **Tsz-ting Wong**, Kin-tak Lau, Wai-yin Tam, Jinsong Leng and Julie A. Etches. UV resistibility of a nano-ZnO/glass fibre reinforced epoxy composite. Materials and Design. 2014;56:254-257.

3. **Tsz-ting Wong**, Wai-yin Tam, Julie A. Etches, Wen-xin Wang, Jinsong Leng and Kin-tak Lau. Feasibility of using ZnO/epoxy filled hollowed glass fibres (HGFs) for UV resistant polymer composites. Materials Letters. 2014;128:220-223.

4. **Tsz-ting Wong**, Kin-tak Lau, Wai-yin Tam, Jinsong Leng, Wenxin Wang, Wenbing Li and Hongqiu Wei. Degradation of nano-ZnO particles filled styrene-based and epoxy-based SMPs under UVA exposure. Composite Structures. 2015;132:1056-1064.

5. **Tsz-ting Wong**, Kin-tak Lau, Wai-yin Tam, Julie A Etches, Jang-kyo Kim and Ying Wu. Effects of silane surfactant on nano-ZnO and rheology properties of nano-ZnO/epoxy on the UV absorbability of nano-ZnO/epoxy/micron-HGF epoxy composite. Composite Part B: Engineering. 2016;90:378-385.

Conference Proceedings

1. **Tsz-ting Wong**, Kin-tak Lau, Wai-yin Tam and Julie A. Etches. A nano-ZnO filled hollow glass fibre reinforced epoxy composite with UV resistibility. 3rd International Conference on Nanomechanics and Nanocomposites (ICNN3). Hong Kong. 22-25 May 2014.

2. **Tsz-ting Wong**, Kin-tak Lau, Wai-yin Tam and Julie A. Etches. Hollow glass fibre reinforced epoxy composite filled with nano-ZnO possesses UV absorbability. 1st International Conference on Computational and Experimental Methods for Composite Materials and Structures (ICCEMCMS). Harbin. 10-12 September 2014.

3. **Tsz-ting Wong**, Kin-tak Lau, Wai-yin Tam, Jinsong Leng, Jang-kyo Kim, Julie A. Etches and Ying Wu. Prevention of UVR degradation on polymer-based composites by nano-ZnO & HGFs. 20th International Conference on Composite Materials (ICCM20). Copenhagen. 19-24 July 2015.

4. **Tsz-ting Wong**, Kin-tak Lau and Julie A Etches. Ultraviolet radiation on polymer-based composites. 17th European Conference on Composites Materials (ECCM17). Munich. 26-30 June 2016.

5. **Tsz-ting Wong**, Kin-tak Lau and Julie A Etches. The degradation and resistance of glass fibre polymer composites against ultraviolet radiation energy by using ZnO nanoparticles. 24th International Conference on Composites/Nano Engineering (ICCE24). Hainan Island. 17-23 July 2016.

Honours

1. Conference Committee Member of International Technical Program Committees, 2016 International Conference on Advanced Materials Research and Manufacturing Technologies (AMRMT 2016), 18-20 August 2016, Singapore.

2. Reviewer of International Journals:
   Composites Part B: Engineering; and
   International Journal of Advanced Materials and Production (IJAMP).

3. Invited Talks in Different Universities:
   University of Cambridge, Department of Materials Science and Metallurgy, United Kingdom, 7 April 2015;
   University of Bristol, Department of Aerospace Engineering, United Kingdom, 27 July 2015;
   Royal Melbourne Institute of Technology University, School of Engineering, Australia, 25 February 2016;
   University of New South Wales, School of Civil and Environmental Engineering, Australia, 29 February 2016; and
   The Hong Kong Polytechnic University, Research Institute for Sustainable Urban Development, Hong Kong, 22 March 2016.
   Georgia Institute of Technology, School of Aerospace Engineering, United States, 3 May 2016.

Acknowledgement

I would like to express my sincere gratitude to my PhD chief supervisor, Professor Alan Kin-tak Lau, for every support and opportunity he has given throughout the whole period of my study. It is also important for me to deeply thank my husband, Thomas Lau, my co-supervisor, Dr. Wai-yin Tam, family and friends. Without their support, I would never have arrived at this stage of my life.

Special thank you would like to be made for every person who have given me the opportunities and who have collaborated with me in this research, Professor Michael Wisnom, Professor David Hui, Professor Jinsong Leng, Professor Jang-kyo Kim, Dr. Julie A. Etches, Ying Wu, Wenbing Li and Hongqiu Wei. I am grateful for the comments on my PhD research from two external examiners, Professor Ayman S. Mosallam and Dr. Alexander Djordjevich, of which their comments are very useful for my future development. I also wish to thank you departmental staff for their supports.

Last but not least, thank you Professor San-qiang Shi to be my supervisor during the period of May 2016 to August 2016 after Professor Alan Kin-tak Lau has been relocated to Australia. And thank you for the support from the Hong Kong Polytechnic University Grant.

Table of Contents

Chapter One

Chapter Two

Chapter Three

Chapter Four

Chapter Five

Chapter Six

Chapter Seven

Chapter Eight

Chapter Nine

List of Figures

List of Tables

List of Abbreviations

Technical Terms

2D	2-dimentional
3D	3-dimentional
$–CH_3$	methyl group (Me)
$–CH=CH_2$	Vinyl function group
–OH	Hydroxyl group
–OCH	Hydroxyl group
$–NH_2$	Amino group (amine)
AFM	Atomic-force microscopy
APEI	Poly(amide-ester-imide)
APTES	γ-aminopropyltriethoxysilane (KH550)
ASTM	International Standards Organization
CFRP	Carbon fibre reinforced polymer-based composite
CoF	Coefficient of friction
CO	Carbon monoxide
CO_2	Carbon dioxide
CTE	Coefficient of thermal expansion
DMA	Dynamic mechanical analysis
DSC	Differential scanning calorimetry
EP	Epoxy
EP-SMP	Epoxy-based shape memory polymer
EDX	Energy-dispersive X-ray spectroscopy
EDS	Energy-dispersive X-ray spectroscopy
EIS	Electrochemical impedance spectroscopy
FBG	Fibre-optic Bragg gating

FRP	Fibre reinforced polymer-based composite
FTIR	Fourier transform infrared spectroscopy
GF	Glass fibre
GFRP	Glass fibre reinforced polymer-based composite
GLARE	Glass fibre/aluminum laminate
GPTMS	γ-glycidoxypropyltrimethoxysilane (KH560)
H	Hydrogen
H_2O	Water
HALS	Hindered amine light stabilizer
HB	Brinell hardness
HGF	Hollow glass fibre
HK	Knoop hardness
HV	Vickers hardness
ISO	International Organization for Standardization
LDPE	Low density polyethylene
LOI	Limiting oxygen index
MEKP	Methyl ethyl ketone peroxide
Mo	Metal oxide
MPS	γ-methacryloxypropyltrimethoxysilane (KH570)
O_2	Oxygen
O_2^-	Superoxide radical
O_3	Ozone
ODSs	Ozone-depleting substances
OH^-	Hydroxyl radical
OM	Optical microscope
PAI	Poly(amide-imide)
PBIA	Poly(benzimidazole-amide)
PEA	Poly(ester-amide)
PMMA	Poly(methyl methacrylate)

PS	Polystyrene
PU	Polyurethane
PUA	Polyurethane Acrylate
QUV	Accelerated weathering tester
R	Functional groups in polymer chain
ROM	Rule of mixtures
RT	Room temperature
S	Styrene
SEM	Scanning electron microscope
Si	Silane
SME	Shape memory effect
SMP	Shape memory polymer
S-SMP	Styrene-based shape memory polymer
ToF-SIMS	Time of flight-secondary ion mass spectrometry
UIT	Ultraviolet imaging telescope
UP	Unsaturated polyester
UVA	Ultraviolet A (315nm-400nm)
UVB	Ultraviolet B (280nm-315nm)
UVC	Ultraviolet C (100nm-280nm)
UVR	Ultraviolet radiation
UVPS	UV photoelectron spectroscopy
VTES	Vinyltriethoxysilane (KH151)
WARP & WEFT	Fibre woven bi-direction
XμCT	X-ray micro computed tomography
XLPE	Silane cross-linked polyethylene
XPS	X-ray photoelectron spectroscopy
XRD	X-ray powder diffraction
Zn	Zinc
ZnO	Zinc oxide

Equation Parameters

Abs	Absorption of UVR
$\%T$	Percentage of transmission
λ	Wavelength
I	Intensity
h	Hole in band gap of metal oxide
e^-	Electron in band gap of metal oxide
ρ	Density
μ	Poisson's ratio
n	Refractive index
θ	Degree of angle
d	Distance
x	Magnification
λ	Thermal conductivity
T_g	Glass transition temperature
T_m	Melting temperature
T_d	Decomposition temperature
R	Universal gas constant
ΔS	Entropy of activation
ΔH	Enthalpy of activation
k_B	Boltzmann constant
E_a	Activation energy
A	Pre-exponential factor
R^2	Coefficient of determination
R_r	Shape recovery ratio
T_r	Recovery reaction time
T_f	Full recovery time
F	Force
A	Area

E	Modulus of elasticity
σ	Stress
ε	Strain
G	Fracture toughness
τ	Shear stress
γ	Shear deformation
μ	Coefficient of friction
r_b	Radius of epoxy base
$r_{A_{bf}}$	Radius of adhesive layer, A_{bf}
r_f	Radius of HGF
$r_{A_{fc}}$	Radius of adhesive layer, A_{fc}
r_c	Radius of [ZnO/epoxy] core
L_f	Length of HGF
b	Epoxy base
A_{bf}	Adhesive layer between epoxy base and HGF
f	HGF
A_{fc}	Adhesive layer between HGF and [ZnO/epoxy] core
c	[ZnO/epoxy] core
E_b	Young's modulus of epoxy base
E_f	Young's modulus of HGF
E_c	Young's modulus of [ZnO/epoxy] core
G_A	Shear modulus of adhesive layers, A_{bf} and A_{fc}
N_b	Tensile force applied on epoxy base
$N_{A_{bf}}$	Tensile force applied on adhesive layer, A_{bf}
N_f	Tensile force applied on HGF
$N_{A_{fc}}$	Tensile force applied on adhesive layer, A_{fc}
N_c	Tensile force applied on [ZnO/epoxy] core
$\tau_{A_{bf}f}(x, r_f)$	Shear stress applied on adhesive layer, A_{bf}

$\tau_{A_{fc}C}(x,r_c)$	Shear stress applied on adhesive layer, A_{fc}
U_b	Axial displacement of epoxy base
U_f	Axial displacement of HGF
U_c	Axial displacement of [ZnO/epoxy] core
$\delta_{A_{bf}}$	Relative displacement of adhesive layer, A_{bf}
$\delta_{A_{fc}}$	Relative displacement of adhesive layer, A_{fc}
π	pi (3.14159)
x-axis	Horizontal axis
r-axis	Radial axis
y-axis	Vertical axis

Units

%	Percentage (Ratio)
wt.%	Weight percentage (Ratio)
eV	Electronvolt (Band gap energy)
mW/cm^2	Milliwatt per square centimetre (UVR intensity)
mW/(cm^2•nm)	Milliwatt per square centimetre per nanometer (Irradiance)
W/(m^2•nm)	Watt per square metre per nanometer (Irradiance)
s	Second (Time)
min	Minute (Time)
hour	Hour (Time)
km	Kilometre (Length)
m	metre (Length)
cm	Centimetre (Length)
mm	Millimetre (Length)
µm	Micrometre (Length)
nm	Nanometre (Length)
fm	Femtometre (Length)

m^2/g	Square metre per gram (Specific surface area)
t	Tonne (Weight)
g/cm^3	Gram per cubic centimetre (Density)
°	Degree (Angle)
℃	Celsius degree (Temperature)
K	Kelvin (Temperature)
K^{-1}	Per Kelvin (Coefficient of thermal expansion)
J/(mol·K)	Joule per mole per Kelvin (Heat capacity)
W/(m·K)	Watt per metre per Kelvin (Thermal conductivity)
cps	Counts per second (Intensity of XRD)
nm/min	Millimetre per minute (Rate)
s^{-1}	per second (Shear rate)
Hz	Hertz (Frequency)
Nm^{-2}	Newton per square metre (Young’s modulus/ Strength)
Pa	Pascal (Young’s modulus/ Strength)
gf	Gram force (Force)
N	Newton (Force)
mmHg	Millimetre of mercury (Pressure)
Pa·s	Pascal second (Viscosity)
mPa·s	Millipascal second (Viscosity)

Chapter One

Introduction

In recent years, industries are searching for alternative ways to lower the carbon emissions during manufacturing and burning fuels and looking for sustainable resources and materials for urban development to tackle the continuously growing global pollution problems. On the other hand, the alternative solutions are required to comply with the economic commitment which should be effective and possess potentials for investment.

In materials development, metallic materials are conventionally used for different engineering applications because of their good mechanical properties. However, the supply of unsustainable metallic materials is expected to fall behind the demand within the next 100 years according to the report pressing in 2012 from the University of Massachusetts Institute of Technology [Alonso el al., 2012]. As indicated, the inequality between supply and demand will cause a variety of global problems including price increases, humanitarian and environmental disregard. Jones [2013], was the Journalist for Nature and Yale Environmental 360, reported in 2013 that researchers are now working to find renewable alternatives to critical metals or better ways to recycle them. Polymeric materials are the other options besides metals. They are relatively abandon and cheaper in production which are generally synthesized from petroleum. In environmental concern, researchers have conducted investigations on producing polymers from sources which are more sustainable and environmental-friendly than petroleum [Meier et al., 2007; Meier et al., 2011].

One of the alternative is the fibre reinforced polymer-based composites (FRPs), such as glass or carbon fibres reinforced polymer-based composites (GFRPs or CFRPs), which their demand is dramatically increasing in recent years. They have been introduced and have potential developments in aircraft, civil constructions and automobile industries due to their advantages of light weigh which save the use of fuel and lower the carbon emission during operations, high design varieties for possessing extraordinary mechanical properties, non-corrosive property, relatively abandon and could be sustainable and environmental-friendly.

Improving the durability and lengthen the service life of materials are as well the promising solutions to save the environment as this leads to less production of waste. Polymer-based materials have their deficiency under various environmental conditions, such as ultraviolet radiation (UVR), moisture and temperature changes. Researchers have studied the degradation effects of a combined environmental conditions in polymer-based materials. This makes a difficulty in understanding the effects of single UVR in the materials. On the other hand, the harmfulness of UVR attacked human bodies keeps on going to be a global concern. Ozone depletion is discovered above the South Pole and the neighboring countries, such as Australia. This allows UVC, which is almost all absorbed by Ozone layer, to penetrate and reach onto the Earth surface, human bodies and construction materials. At the moment, there is still a limited research indicating about the amount of UVC intensity that reaches onto the Earth surface. Disregard UVC, UVA has the highest intensity and penetration power to human bodies. Existing commercial methods to prevent the integrity of polymer-based materials from UVR degradation are to use UVR protective coatings and embedded UVR resistant additives into polymer base. However, the surface of these two materials are easily suffered from wearing and dissolution problems under objects strikes and chemicals contact which eventually their function of UVR resistance are lost and the core materials are subjected to UVR exposure inevitably.

In present research, hollow glass fibre (HGF), as a recognized new functionally structural material with multifunctional properties by filling substances with unique characteristic, is introduced to be the host to protect zinc oxide (ZnO) from wearing and dissolution out of the polymers while ZnO nanoparticle possesses its intrinsic properties for physical UVR energy absorption in cost effective way. A topmost protective lamina of ZnO/HGFRPs is proposed to help alleviating the degradation effects in the core laminate of GFRP underneath.

1.1 Aim and Objectives

This research is to develop a new generation of glass fibre reinforced polymer-based composite (GFRP) protected by a layer of ZnO/HGF and investigate the material in terms of their UVR absorbability as well as their mechanical properties to alleviate the degradation effects in the core layers of GFRP. HGF and GFRP were chosen for the first attempt of this novel technology.

The objectives of this research are:

- To identify the specific type of nano-ZnO for physical UVR absorption
- To develop an UVR shielding nano-ZnO/HGF lamina on top of GFRP core and investigate the UVR shielding capability of the lamina
- To optimize the configuration of nano-ZnO/HGF lamina regarding its UVR absorbability and stress transfer ability by using experimental and theoretical analysis

1.2 Outline of Thesis

Literature Review

Chapter Two reviews and summarizes the literatures regarding the usage of FRPs, the change of environment, the nature and the harmfulness of UVR, different UVR degradation tests on polymer-based materials and existing UVR resistance solutions for polymer-based materials. This chapter provides an overall and basis scenario for the present research.

Background of the Present Research

Chapter Three states the background of present research including the problem statement, the materials for experiments and the methodology implemented for experimental and theoretical analyses.

UVR Degradation Mechanisms in Polymer-based Materials

Polyakov [1966] studied the effects of UVR towards the strength and failure of polymers under vacuum and air conditions. The study indicates the UVR degradation effects towards the mechanical properties of the polymer in vacuum condition of 10^{-6}mmHg (high vacuum) tend to cease after 80hours of exposure. In Betteridge et al. [1977] set up a thermal degradation exposure chamber and tested the change of chemical compositions of polymers by using UV-photoelectron spectroscopy. The study points out the necessity to acquire analyzing techniques for monitoring the degradation products in the polymer.

Started from 1980, whereas the applications of polymer-based materials were expanding, the number of research papers concerning about the UVR effects in the materials were increasing at the same time. The UVR degradation mechanisms of polymer-based materials are reported in ***Chapter Four***.

UVR Absorption Mechanisms in Zinc Oxide and Zinc Oxide–Polymers

In recent years, researchers have started to discuss the methods to protect polymer-based materials against UVR attacks. ZnO nanoparticles are being commonly used for UVR resistance purpose because of its intrinsic and prominent physical UVR absorbability. Findings on the UVR absorption mechanisms of a ZnO atom and itself embedded in polymers are presented in ***Chapter Five***.

UVR Degradation in Zinc Oxide/Polymer Composites

Chapter Six reveals the effects of UVR degradation in ZnO/polymer composites from experimental analyses. Artificial UVR exposure was chosen in the experiment to effectively obtain the testing results and compare the effects of artificial continuous and cyclic UVR exposure in the polymer-based materials. Furthermore, four kinds of polymer-based materials, GF/EP composite, GF/UP composite, EP-SMP and S-SMP, filled with ZnO nanoparticles underwent artificial continuous UVR exposure were studied on their UVR degradation.

UVR Resistance of Zinc Oxide/Polymer Composites

Chapter Seven discusses the UVR resistance of ZnO embedded in polymers and ZnO/polymer filled into HGF. The dispersion of ZnO nanoparticle in epoxy and the rheology properties of ZnO/epoxy resin regarding the UVR resistance and manufacturing of the composite were concerned and discussed. The negative effect of silane-doped on ZnO nanoparticle for the UVR resistance of the composite was revealed in this chapter.

Theoretical Analysis for Parameters Optimization

Theoretical analysis of ZnO/HGF lamina, a five-cylindrical system, is deliberated in ***Chapter Eight***. The developed mathematical model provides a theoretical principle to evaluate and optimize the design parameter of a system constructed in similar way based on its stress transfer ability. In addition, the model provides a theoretical concept for the configuration of the lamina regarding the content of ZnO in the core, the length and the thickness of HGF, the shear strength and the thickness of adhesive layers in relation to the mechanical and geometric properties of all elements in the system.

Concluding Remarks and Suggestions for Future Development

A summarized conclusion for the present research is made in ***Chapter Nine*** which is the last chapter of this thesis. The investigation documented in this thesis is not the completion for the research on UVR degradation and resistance in polymer-based composites. Future potential development of the research on this subject is also suggested in this chapter indicating there are plenty of room to be exploited for the integrity of polymer-based composites.

This research aims at providing a feasible and durable solution for the UVR protection of FRPs employed in aircraft and civil building exposing under UVR constantly during their service.

Chapter Two

Literature Review

Chapter Two reviews and summarizes the literatures regarding the usage of FRPs, the change of environment, the nature and the harmfulness of UVR, different UVR degradation tests on polymer-based materials and existing UVR resistance solutions for polymer-based materials. This chapter provides an overall and basis scenario for the present research.

2.1 Fibre Polymer-based Composites Utilized under UVR

According to Chawla [2012], Chung [2010], Kendall [2007], Stewart [2011] and Nicolais et al. [2011], in their books and articles, indicate that FRPs has already been started its utilization in aircraft, road and marine transportation, civil construction, automobile and medical industries. The applications in three technology-leading industries, aircraft, civil construction and automobile engineering, will be further discussed in the following sections, ***section 2.1.1***, ***section 2.1.2*** and ***section 2.1.3***.

2.1.1 Aircraft Industry

In 1980, British Aerospace disclosed the earlier principles of design for a CFRP aircraft wing [Taig, 1980]. It indicated there were four technical factors dominating the design: designer for built-in and accidentally induced stress, design for structural stability, design for service environment, humidity and elevate temperature exposure and design for variability of structural performance. The aim of this paper was to propose the use of FRPs for minimizing the mass within the limits of safety of an aircraft.

The development of Airbus's long-haul aircraft, A350 XWB shown in ***Figure 2.1***, entred commercial service in 2015 and Boeing's short-haul aircraft, B787 Streamliner shown in ***Figure 2.2***, entred commercial service in 2011 has demonstrated the usage of FRPs which their fuselage shells employ around 50% by weight of FRPs to replace the traditional use of comparatively heavyweight aluminum materials. FRPs are also found in external fan blades in GEnx turbofan engine shown in ***Figure 2.3*** used in B787.

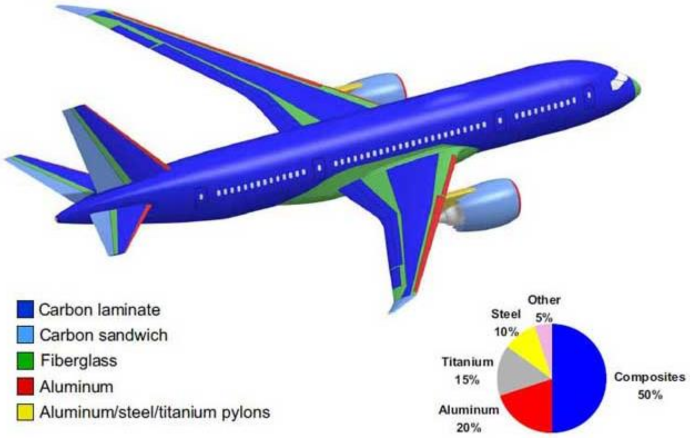

Figure 2.1 FRPs in Boeing B787 Streamliner [www.1001crash.com]

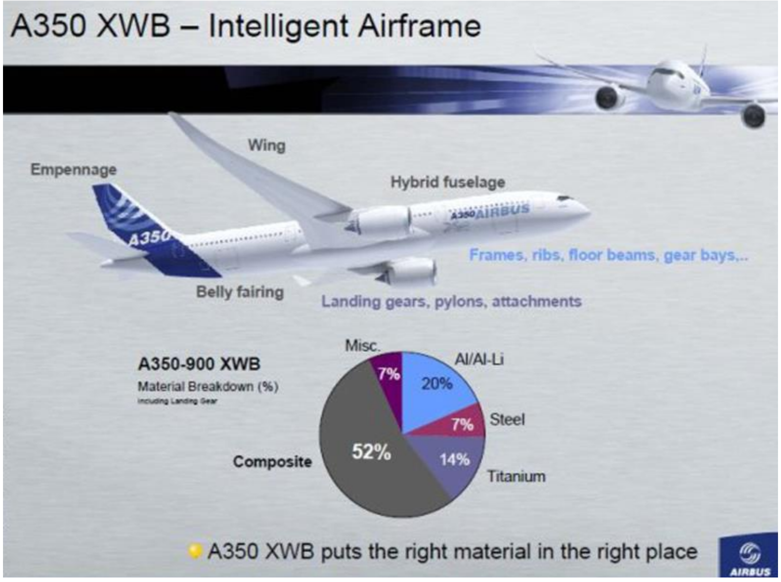

Figure 2.2 FRPs in Airbus A350 XWB [www.airbusgroup.com]

Figure 2.3 FRPs blades in GEnx engine [www.compositesworld.com]

FRP are being an alternative material for aircrafts is because they provide weight and fuel saving to lower emission of toxic substances. Scelsi et al. [2011] implemented a cradle-to-grave life cycle assessment (LCA) of structural materials, CFRP, GLARE (glass fibre/aluminum laminate used by Airbus A380) and aluminum alloy 2024 plates, to assess and compare the total emissions produced during manufacturing, use and disposal of aerospace materials and their selected components. It reported that for over 3600km, corresponding to approximately 5hours of air transport, an aircraft with a CFRP component for replacing a steel achieves the breakeven time in terms of overall environmental impacts, the emission of carcinogens and carbon dioxide, etc. Added that their high stiffness and strength properties allow the structural components to be pressurized under comparatively high stress level when aircrafts are flying at high altitude.

2.1.2 Civil Construction Industry

Civil engineering industry had started using FRPs first in small-scale components for building constructions [Kim et al., 2012; Mirmiran, 1996], such as protective jackets for pipes, deck panels on bridges and roof for shielding infrastructure. GFRP was used for the heli-deck of an offshore pipework platform in North Sea in the 1980s shown in ***Figure 2.4***; the first vehicle carrying with 9m long and 10 tonnes less weighed GFRP bridge deck located in Lancashire, England to span over a railway at Standen Hey Bridge was completed in 2008 shown in ***Figure 2.5***; the canopy at Dubai Airport utilized GFRPs in 1972 shown in ***Figure 2.6***; and also for the large-scale components with simple structures for building constructions, in 1974, Mondial House in London, England shown in ***Figure 2.7*** was built using GFRP for its façade which this was one of the most prestigious and ambitious building projects because of its size and complexity, where all the materials were constantly contacting external environmental impacts in their service period.

Figure 2.4 GFRP heli-deck of an offshore pipework platform in North Sea [Gibson, 2003]

Figure 2.5 GFRP bridge deck for Standen Hey Bridge in Lancashire, England [www.materialstoday.com]

Figure 2.6 GFRP roof for Dubai Airport in Dubai, United Arab Emirates [Shenoi et al., 2002]

Figure 2.7 GFRP cladding for Mondial House in London, England [Kendall, 2007]

In recent years, more complicated and dynamic shapes of structures shown in ***Figure 2.8*** [Kendall, 2007] have been built by using FRPs which the structures are unrealistic to be accomplished by using conventional concrete and steel materials to satisfy the building design. Holllaway [2010; 2013] published a review paper and written a book chapter discussing the present and future utilization of FRP composites in the civil engineering. The paper suggests the development of FRPs is growing from small scale application of retrofitting to structural scale of hybrid structural member combing with concrete and/or steel in new construction.

Figure 2.8 FRP architectural structures for Victoria House in London, England [Kendall, 2007]

2.1.3 Automotive Industry

Many renowned automobile companies have showed increased interest in utilizing FRPs as structural components in hybrid electric vehicles (HEVs), battery electric vehicles (BEVs), sports and private car for achieving the major goal to reduce the body weight in order to overcome the weight penalty from fuel and battery. 2013 McLaren MP4-12C supercar, a model from Mercedes-Benz, features a single-piece moulded FRP MonoCell tub shown in ***Figure 2.9*** and weighs less than 80kg. 2010 Audi A8, its spare wheel recess shown in ***Figure 2.10*** uses 60% FRP and contributes higher stiffness in chassis, 30% less in weight and 70% reduced in tooling investment [Stewart, 2011].

Figure 2.9 CFRP MonoCell tub from latest model of Mercedes-Benz [Stewart, 2011]

Figure 2.10 GFRP spare wheel recess of Audi [Stewart, 2011]

2.2 Nature of UVR

According to the report "Scientific Assessment of Ozone Depletion 2014" [WMO, 2014], it used the method of counting ozone-depleting substances (ODSs) to assess the ozone depletion and found that the trace gases that directly affect ozone and climate, such as HFCs, N_2O, CH_4, SF_6, NF_3 and SO_2F_2, were discovered to be variously increasing between tropospheric and stratospheric layers in few years before 2012. Ozone depletion and the subsequently varied UVR conditions outside and within ozone atmosphere will be discussed in detail in ***section 2.2.1***, ***section 2.2.2*** and ***section 2.2.3***.

2.2.1 UVR in Space

Atmosphere is divided into layers of troposphere, stratosphere, mesosphere, thermosphere and exosphere. Troposphere is about 20km high from the Earth surface while the layer of stratosphere is from 20-50km above the Earth surface. Sourced from NASA, approximate 90% of ozone is concentrated in stratosphere layer having 0.0003% of the total amount of gases in the stratosphere as shown in ***Figure 2.12***.

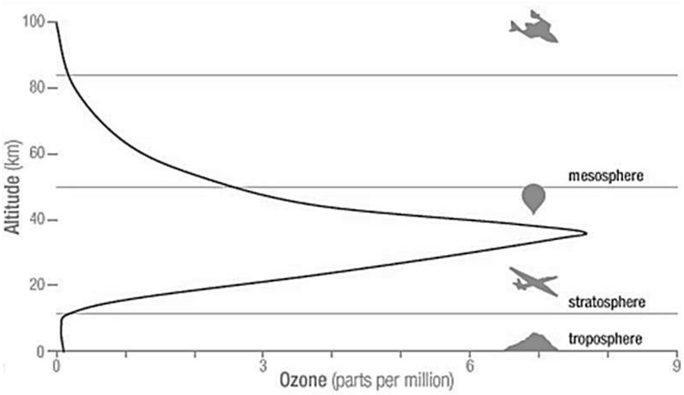

Figure 2.11 Change in ozone concentration with the change in altitude [Karentz, 2008]

Outside the ozone layer, in mesosphere or in the space, scientist used the data collected from satellites positioned outside the atmosphere and running around the Earth to detect UVR from the Sun and other astronomical objects. According to ***Figure 2.13*** taken by NASA's Ultraviolet Imaging Telescope (UIT) on the Astro-2 mission, it illustrated clouds of gas or particles containing newly formed stars are many times more massive than the Sun and glowing strongly in ultraviolet light [Karentz, 2008; US NASA, 2001].

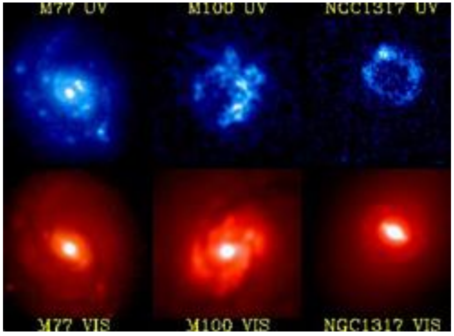

Figure 2.12 Three different galaxies taken in ultraviolet light (top) and visible light (bottom) [missionscience.nasa.gov]

UVR emission from the Sun is a kind of electromagnetic wave which is transmitted in waves or particles at different wavelengths and frequencies. UVR wave emits directly onto the half surface of the Earth and spiral its emission towards the side of the Earth facing away from the Sun due to the magnetic field around the Earth [US NASA, 2001].

UVR is a type of energy. Its energy is calculated in terms of radiation intensity or electromagnetic force. ***Figure 2.14*** sourced from NASA shows the amount of solar flux of UVR at the top of the atmosphere (outside ozone atmosphere) and on the Earth surface (within ozone atmosphere). It indicates space contains a considerable amount of UVA, UVB and also UVC at around 10^{-3}mW/(cm^2•nm) [US NASA, 2001].

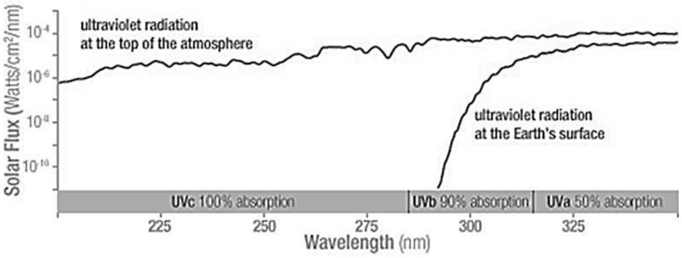

Figure 2.13 Absorption of UVR by ozone [Karentz, 2008]

2.2.2 Ozone Depletion

Ozone depletion is mainly caused by the increase of chemical gases. A hole is observed over Antarctica since the late 1970s, and spread widely to the neighbouring countries, such as Australia, New Zealand, Argentina and Chile. And it has been reported that Australia has the highest rate of skin cancer in the world [AIHW, 2014]. The ozone holes were found as largest as around 29.8 million square kilometres which is more than three and a half times the size of Australia. According to the adverse consequences, Montreal Protocol is an international agreement since 1987. Agreed countries are compiling the accordance stated in the agreement, in this way, some model simulations indicate that total column ozone outside of the tropics will recover to 1980s values by 2020 to 2050 and to 1960s values by 2025 to 2060 [WMO, 2014]. However, up to this moment, there are no any statistical data to reveal the intensity of UVC penetrated into the atmosphere and reach the Earth surface. And an increase in UVB is dramatically influencing the terrestrial biological and ecological system which is reflected in the increase in skin cancer rate in human body and the adverse time phase and biodiversity of living and agricultural species [AIHW, 2014; Caldwell et al., 1998; Diffey, 1991; Karentz, 2008; Paul et al., 2003; UNEP, 2010; US NASA, 2001].

2.2.3 UVR on the Earth

The primary natural source of UVR comes from the Sun and it is invisible to human eyes. Referring to ***Figure 2.11***, UVR has wavelength shorter than visible light (400-700nm) but longer than X-ray (<100nm) and it is subdivided into three groups adopted from WHO [2002] and UNEP [2010], UVA, UVB and UVC with different ranges of wavelength 315-400nm, 280-315nm and 100-280nm respectively, and different amount of energy reaching the Earth surface, 9.1105mW/cm^2 in average of UVA, 0.4795mW/cm^2 in average of UVB and 0mW/cm^2 in average of UVC respectively [Diffey, 2002]. Ozone layer is responsible for absorbing most part of UVB and all range of UVC. When ozone level decreases, higher level of UVB and UVC will be able to penetrate and reach the Earth surface.

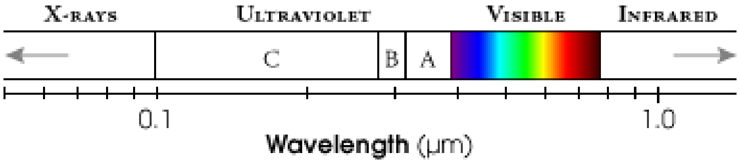

Figure 2.14 UVR region in electromagnetic spectrum [earthobservatory.nasa.gov]

Disregarding UVC, UVA has the longest wavelength, highest intensity and penetration power to human body. Referring to the data shown in ***Table 2.1***, it shows the comparison of typical properties of different UVR reaching the Earth surface.

Table 2.1 Typical properties of UVR reaching the Earth surface [Diffey, 2002; UNEP, 2010; WHO, 2002; www.skincancer.org]

	UVA	***UVB***	***UVC***
Wavelength	314-400nm	280-315nm	100-280nm
Radiation energy	Less energetic	Medium	Highest
Penetration on human's skin	Highest (to middle layer of skin)	Much lesser (to outer layer of skin)	Negligible
Level of intensity on the Earth surface	Highest	Medium	Almost none
Absorption by ozone	Almost none	Mostly absorbed	Practically all
Amount reaching the Earth surface	Approx. 95%	Approx. 5%	Negligible
Average amount of intensity reaching the Earth surface	9.1105 mW/cm^2	0.4795mW/cm^2	0mW/cm^2

2.3 Harmfulness of UVR

In average, UVR is alerted between 10am to 4pm for 6hours in every day [UNEP, 2010; WHO, 2002]. The intensity of UVR is various with weather, time of a day, geographical location and altitude from the Earth surface. Places, such as South Pole, Australia, New Zealand, Argentina and Chile, is suffered from higher intensity of UVA and UVB because of the ozone depletion. Countries, which are close to the equator, such as Pakistan, Philippines, are also affected by higher intensity of UVA and UVB because they locate at higher altitude from the Earth surface. It is the fact that every 1000m increases in altitude, 10-12% increases in UVR intensity [WHO, 2002]. Prolonged exposure to UVR is harmfulness to human body and polymer-based materials. The harmfulness of UVR is dependent on the susceptibility of the receiver and the amount of accumulative UVR energy. Their harmfulness will be disclosed in the following sections, ***section 2.3.1*** and ***section 2.3.2***.

2.3.1 Human Body

Comparing UVB, UVA has higher penetration power to the deeper layer of human skin as illustrated in ***Figure 2.15*** [Stiefel et al., 2015].

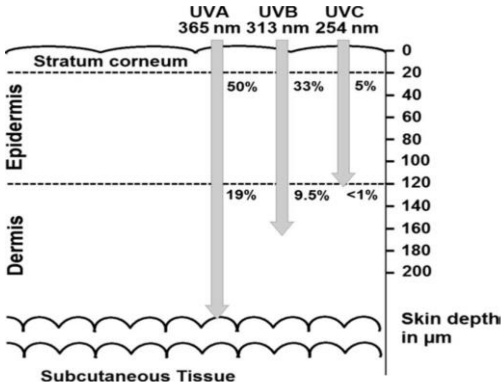

Figure 2.15 Schematic illustration of the penetration level of UVA, UVB and UVC in human skin [Stiefel et al., 2015]

The harmfulness of UVR in human body has been extensively studied from a few decades ago. The response of human skin and eye to UVR is classified in to acute effects and chronic effects. Experienced a short duration of excess UVR exposure can cause sunburn and tanning in skin shown in ***Figure 2.16*** and pain and snow blindness in eyes. Chronic effects are caused by experiencing a long duration of excess UVR exposure including two major health problems, skin cancer and cataracts shown in ***Figure 2.17*** [Diffey, 1991; Gallagher et al., 2006; Heiting, 2016; WHO, 2002]. UVR with high intensity is acutely induce a rapid response in human body for the damages.

Figure 2.16 Sunburn on human skin [bikinicladscientist.wordpress.com]

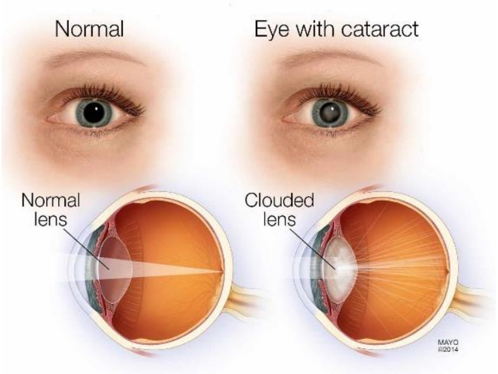

Figure 2.17 Cataracts in human eyes [healthlifemedia.com]

2.3.2 Polymer-based Materials

Most of the polymers, either synthetic polymer or natural polymeric wood, are susceptive to UVR. Thermoplastic and thermosetting plastic are the two divisions of synthetic polymer group. Thermosetting plastic is chosen for structural materials as it usually has promising mechanical properties than thermoplastic. Generally, with having enough amount of UVR energy, the bonds between atoms in polymer are ruptured, so the polymer is resulted in decolourization, loss of mechanical and thermal properties which limits the performance and service life of the material [Andrady et al., 1998; Kumar et al., 2009].

In a recent research [Awaja et al., 2011], FRPs underwent UVR exposure were tested the damaged integrity by using X-ray micro computed tomography (XμCT). The investigation was conducted on three types of composites, 3D-glass, E-glass and carbon fibres reinforced epoxy composites. The research indicated the damage in composite with 3D-glass was spherical voids formed in internal core, composite with E-glass showed different forms of damages, including microcracks, cracks and delamination, and the damage happened in both near surface and internal core of composite with carbon fibres.

In this sense, UVR effect in polymers is a crucial concern especially for materials used as structural components.

2.4 UVR Exposure Tests on Polymer-based Materials

The method of UVR exposure is a concern for testing the degradation on polymer-based materials. In the past research, some investigations were done by implementing natural UVR exposure test, however, this testing method takes a relatively long time for acquiring results. Therefore, there are many research choosing artificial UVR exposure test for experiments, and most of them utilized artificial continuous exposure test.

In this kind of environmental test, numerous factors, such as temperature, moisture, concentration of oxygen, affect experimental results. Meanwhile, a huge variety of polymer-based materials are specifically designed for different applications.

From the review of papers, it is not surprising to understand different results were obtained in the same samples underwent different UVR exposure methods. Exposure method for testing the degradation in polymer-based materials has to be unified and consolidated. In the following, testing equipment and standard will be reviewed in ***section 2.4.1*** and different testing methods will be introduced in ***section 2.4.2***, ***section 2.4.3*** and ***section 2.4.4***.

2.4.1 Natural UVR

The standard practice for natural UVR exposure testing of nonmetallic materials can be found in ASTM G7 launched in 2014. Five points of the significance of the test are

a. Exposures in several locations with different climates which represent a broad range of anticipated service conditions are recommended;
b. Several years of repeat exposures are needed to get an “average” test result for a given location;
c. Comparing results for materials exposure for short periods (less than one year) is not recommended unless materials are exposure at the same time in the same location;
d. Defining exposure periods in terms of total solar or solar-ultraviolet radiant energy can reduce variability in results from separate exposures;
e. Test specimens are placed on a single test panel or on test panels placed adjacent to each other during exposure to minimize the effect of temperature and wetness.

Kyrikou et al. [2011] conducted natural environmental (in soil including the exposure of UVR, temperature, moisture and other chemicals) exposure for examining the UVR effects in low density polyethylene (LDPE). In the same article, it mentions the artificial accelerated ageing test in the laboratory was also used for the examination which the test only considered the exposure of UVR and temperature and without considering the humidity. Added that the testing periods were held for approximately two consecutive months in 2005 and four consecutive months in 2006.

In accordance with the issues of the control difficulty in testing parameters and the lengthy testing period, artificial accelerated test is suggested.

2.4.2 Accelerated UVR

There are two kinds of UVR exposure equipment that are commonly being utilized for investigations, QUV chamber with UVR, temperature and moisture mode [Belec et al., 2015; Hulatt et al., 2002; Shanmugam et al., 2015; Yang et al., 2002; Yang et al., 2003] and accelerated degradation chamber with only UVR source [Awaja et al., 2009; Awaja et al., 2011]. UVR is mainly sourced from fluorescent or xenon lamp, other alternatives are mercury, quartz and tungsten lamp. The comparison on the feature of fluorescent and xenon arc lamp had been made by Diffey [2002] and fluorescent arc lamp is indicated as a solution to xenon having its problem of limited irradiation field.

Various systems for UVR exposure are available depending on the purpose of experiments. Testing method is also a concern for the experiments. Natural exposure discussed in ***section 2.4.1*** accelerated continuous discussed in ***section 2.4.3*** and accelerated cyclic discussed in ***section 2.4.4*** are the modes for UVR exposure being conducted to test the degradability of polymer-based materials. Regarding the testing method, a diversity of international ASTM standard practices was authorized as an accordance for UVR exposure test on nonmetallic materials (ASTM G7, ASTM G154 and ASTM G155), plastics (ASTM D4329, ASTM D2565 and ASTM D4459) and biodegradable plastics (ASTM D5275, ASTM D5208 and ASTM D5071). And there are no any specific testing methods in terms of UVR degradation standardized for particular fibre reinforced polymer-based composites.

It is worth noting that an international ASTM standard, ASTM G141, addresses the variability in various exposure testing of nonmetallic materials. Important notes for the variability in laboratory accelerated weathering tests are made on the repeatability and reproducibility. The specific factors that are responsible for the variability in the tests are light sources, irradiance and specimen temperatures, water contaminants, or impurities and poor spray quality and ambient temperature and humidity conditions. These factors have to be preciously controlled for conducting the experiments in order to give a reliable durability results.

2.4.2.1 Accelerated Continuous UVR

There are many research worked on a combined environmental effect of UVR, temperature, moisture and salt solutions to the polymer-based materials including UV resistant filled polymers [Chakrabarti et al., 2008; Shanmugam et al., 2015; Sil et al., 2010; Tcherbi-Narteh et al., 2013; Tcherbi-Narteh et al., 2014; Woo et al., 2007; Woo et al., 2008] and fibre polymer-based composites [Belec et al., 2015; Hulatt et al., 2002] by using the artificial accelerated continuous UVR exposure test. And there are also research limited to only focus on single UVR effects to UV resistant filled polymers [Kaczmarek et al., 2001; Liu et al., 2009; Selvi et al., 2014] and fibre polymer-based composites [Awaja et al., 2009; Awaja et al., 2011; Guillot et al., 2001; Lee et al., 1999].

Combining UVR with other environmental effects to study the impacts on polymer-based materials can not reflect the actual effect from single source of any of the factors. Although the combined environmental study may be associated with a particular end-use condition, effects from only source of UVR should be studied to equip a thorough understanding of the way it affects polymer-based materials.

Considering the research only focused on UVR effects to polymer-based materials by using artificial accelerated continuous accelerated UVR exposure test, there are no studies regarding the nanoparticle and glass fibre reinforced polymer-based composites. The damaging mechanism of UVR to nanoparticle and fibre reinforced polymer-based composites would be more complicated than that to UV resistant filled polymers or fibre polymer-based composite studied previously.

Comparing with artificial accelerated continuous UVR exposure test, artificial accelerated cyclic UVR exposure test has been rarely implemented.

2.4.2.2 Accelerated Cyclic UVR

A limited research are found in polymer-based materials of their UVR degradability by conducting artificial accelerated cyclic UVR exposure test. All of the research investigated a combined environmental effect of UVR, temperature, moisture and salt solutions based on particular international ASTM standard to polymer-based coating [Yang et al., 2002; Yang et al., 2003], UV resistant filled polymers [Gibson, 2003] and fibre polymer-based composites [Garcia-Espinel et al., 2015; Yan et al., 2015].

An investigation done by Agubra in nanoclay and E-glass fibre reinforced epoxy composite under a combined effect of UVR, moisture and rain is worth mentioning. Cyclic exposure was conducted according to a specific standard. Surface morphology, weight, flexural and dynamic mechanical properties were analyzed and reported in the paper [Agubra et al., 2014]. This research has made a model example to evaluate fibre nanocomposite under an environmental exposure.

There is still a lack of research on the effect from single source of UVR to the nanoparticle and fibre reinforced polymer-based composites.

2.5 UVR Degradation and Resistance Analysis on Polymer-based Materials

UVR degradation is a measurement of the change with time and it is a study of statistics. The degree and the rate of UVR degradation are two critical parameters for evaluating the degradability of materials. Different testing equipment were implemented for characterizing the UVR degradability of polymer-based composites which will be included in ***section 2.5.1***. There are few theoretical models analyzing the rate of degradation of polymer-based composites which will be listed in ***section 2.5.2***.

2.5.1 Experimental Analysis

A testing equipment of X-ray photoelectron spectroscopy (XPS) was utilized by Awaja et al. in 2010 [Awaja et al., 2010] and Nguyen et al. in 2011 [Nguyen et al., 2011] to observe the composition changes of the degraded topmost layer in 3D glass fibre and nanoparticle filled polymer composite respectively. The limitations of XPS are that in average less than 5nm depth from the top surface of materials can be analyzed and the sputtering technique for obtaining the depth distribution information of the material surface is limited for composite which contains different elements with a high deviation in reaction rate to ion milling. These affect the accuracy of the results obtained by using XPS to test the degradation properties of the surface of nanoparticle and/or fibre reinforced polymer-based composites.

Awaja et al. in 2009 and 2010 also implemented Time of Flight-Secondary Ion Mass Spectrometry (ToF-SIMS) [Awaja et al., 2009; Awaja et al., 2010] for characterizing the UVR degraded surface to obtain the information of its chemical compositions, imaging and depth profiling.

3D imaging for investigating the internal damages by UVR in polymer composites was demonstrated by Awaja et al. in 2011 [Awaja et al., 2011]. It was done by a testing equipment of X-ray Micro Computed Tomography (XμCT). Internal damages, such as micro cracks and delamination, were captured in different fibre composites underwent UVR exposure.

Yang et al. in 2003 and Lee et al. in 1999 correlated the change of electrical/ dieletric impedance and electrostatic properties of the UVR degraded polyurethane and glass fibre reinforced epoxy composite by using Electrochemical Impedance Spectroscopy (EIS) and Coronic Discharge Apparatus respectively [Lee et al., 1999; Yang et al., 2003].

UVR poses a potential in changing the colour of materials during degradation and the process is named as decolouration or decolourization. Total colour difference of materials were measured without and after UVR treatment using a spectrophotometer and it is the measurement of three factors including lightness and two chromaticity indices. The formula will be expressed in the next section [Cristea et al., 2010; Ghasemi-Kahrizsangi et al., 2015; Sun et al., 2012].

UV-vis Spectrophotometer is an instrument used for measuring the UVR transmission or absorption of a medium in solid or liquid form. It provides information of the degree of UVR transmittance or absorbance of materials against the wavelength of UVR. It is commonly used to compare the UVR resistibility of UVR resistant filled polymers to their primitive form [Jeeju et al., 2011; Kaczmarek et al., 2014; Kulyk et al., 2010; Li et al., 2001; Liu et al., 2009; Nouneh et al., 2011; Oral et al., 2004; Stevanovic et al., 2012; Tigges et al., 2010; Vidyasagar et al., 2011; Yang et al., 2004].

Other testing methods for characterizing UVR degradation of materials have

Fourier Transform Infrared Spectroscopy (FTIR), X-ray Powder Diffraction (XRD) and Energy-dispersive X-ray Spectroscopy (EDX) to state the radials formations and chemical changes in degraded materials; Atomic-force Microscopy (AFM) to test the roughness of degraded surface; film thickness gauge to measure the thickness of degraded surface; weight balance to count the weight loss explaining the number of voids happened in degraded materials; Scanning Electron Microscope (SEM) or Optical Microscope (OM) to observe the number of microcracks appeared in degraded materials and contact angle is measured to understand the energy of degraded surface.

In conjunction with the characterization, the degradability of materials were investigated by different mechanical property tests, such as micohardness and nanoindentation test for the degraded surface and tensile properties test, flexural properties test, fatigue test and Dynamic Mechanical Analysis (DMA) for the integral degraded materials.

2.5.2 Theoretical Analysis

There are few indicators and theoretical models developed for evaluating the degradability and resistibility of materials and they are listed as follows.

Equation 1 is the quantified measurement of the decolouration of materials in UVR degradation [Cristea et al., 2010; Ghasemi-Kahrizsangi et al., 2015; Sun et al., 2012]. Total colour difference, as mentioned in previous section, of materials is measured by a spectrophotometer and it measures three factors including lightness and two chromaticity indices. The formula is

$$\Delta \mathrm{E} = (\Delta L^{*2} + \Delta a^{*2} + \Delta b^{*2})^{1/2} \qquad (\textbf{\textit{Equation 1}})$$

where $\Delta \mathrm{E}$ represents the total colour difference; ΔL^* represents the changes of lightness; Δa^* and Δb^* represents the different between red-green and yellowblue colour coordinates respectively.

Equation 2 is the computation of carbonyl substance which is generated in the chemical UVR degradation of materials [Deka et al., 2012; Devi et al., 2013; Zhao et al., 2006]. Carbonyl index is developed as

$$\text{Carbonyl index} = {}^{I_C}/_{I_R}(100) \qquad \textbf{(Equation 2)}$$

where I_C is the intensity of the carbonyl absorption band (1700-1900cm^{-1}) and I_R is the intensity of the reference band (2900-2950cm^{-1}). The reference band is not affected by neither the irradiation of UVR nor the crystallinity of tested materials.

Equation 3 and ***Equation 4*** are the calculations of UVR transmission or absorption of materials filled with UVR absorbers to quantify the UVR resistance [Levchik et al., 2004; Sun et al., 2012]. From the ***Equation 4***, it is seen that the absorbance of a material is directly proportional to the material's thickness.

Beer-Lambert's Law:

$$\mathrm{A} = log_{10}(100/\%T) \qquad \textbf{(Equation 3)}$$

where A represents the absorption of UVR and $\%T$ represents the percentage of transmission

Beer's Law:

$$\mathrm{A} = \varepsilon b_{dry}c \qquad \textbf{(Equation 4)}$$

where ε represents the extinction coefficient that is the contact associated with the absorbent in mil^{-1}wt%$^{-1}$ unit, b_{dry} represents the thickness of dry film in mil unit and c represents the concentration of UVR absorbers in wt% unit.

Equation 5 is developed to calculate the photocatalysis of UVR absorber filled materials for chemical UVR resistance [Chakrabarti et al., 2008]. This measurement requires the implementation of Eosin Y as a sensitizing dye in the

UVR absorber filled polymer for understanding and developing the rate of degradation equation of the material.

$$\frac{-dW}{dt} = \frac{d[PVC^{\circ}]}{dt} = kW \qquad \textbf{(}\textbf{\textit{Equation 5}}\textbf{)}$$

where the lumped rate constant, $k = 2[\text{photocatalyst}]\left(\frac{I_f}{\rho l}\right)(k_1[EY] + k_2)$; W represents the mass of undegraded polymer; PVC° presents the degraded radicals of PVC attacked by active hydroxyl radicals; $[\text{photocatalyst}]$ presents the concentration of photocatalyst; I_f represents the intensity of UVR; ρ represents the density of polymer; l represents the thickness of polymer; $[EY]$ represents the concentration of sensitizing dye and k_1 and k_2 are defined from experiments.

2.6 UVR Resistance Solutions for Polymer-based Materials

The mechanisms for resisting UVR are by the method of scattering and absorption. Scattering is a physical reaction of the deviation of light radiation from a straight trajectory by one or more paths due to localized non-uniformities in the medium which the lights pass through and the reflected angles can be predicted by the law of reflection. UVR absorber absorbs the light radiation in two ways, chemical and physicals. In chemical reaction, it transfers the absorbed radiation energy into another form of substances called radicals which are usually reactive and harmful in nature to polymers. In physical reaction, it absorbs the radiation energy and dissipates the energy physically inside its atom. This reaction is usually done by semiconductors having inherent band gap inside its atom to possess intrinsic physical UVR absorbability.

UVR resistant substances are divided into two major groups, organic and inorganic. Organic UVR resistant usually takes up the UVR radiation energy and react the energy by chemical reaction while inorganic UVR resistant normally appears in the form of semiconductors. More information of organic and inorganic UVR additives for polymers will be introduced in ***section 2.5.1*** and ***section 2.5.2***. Further discussion on existing solutions for UVR protection in polymers will be made in ***section 2.5.3*** and ***section 2.5.4***.

2.6.1 Organic UVR Stabilizers

Organic stabilizers have been incorporated with polymers for reducing the rate of UVR degradation. However, there have been some disadvantages in mixing polymers with organic stabilizers [Chen et al., 2015; Jacobs et al., 2007; Selvi et al., 2014; Shanmugam et al., 2015; Stoecklein, 1999], such as hindered amine light stabilizers (HALS), hydroxyphenylbenzotriazole, oxalanilides and benzophenones, which they chemically disarrange the molecular structure of the original polymer system and accordingly alter the mechanical properties. Either mixed with or coated on polymers, organic UVR stabilizers entirely react with UVR through complex chains of chemical reaction. According to the research comparing the reaction with UVR of inorganic UVR additives and organic UVR stabilizers in sunscreen [Cockell et al., 1999; Kumar et al., 2009; Sambandan et al., 2011; Serpone et al., 2007; Stiefel et al., 2015], organic UVR stabilizers produce harmful radicals with irreversibly deteriorating themselves and their implemented medium. Organic UV absorber lacks of photostability which it becomes inactive to UVR absorption by a chain of reaction with UVR and even becomes photooxidizing agents [Serpone et al., 2007]. Furthermore, organic UVR stabilizers are usually composed of mixed inaccessible chemicals, in such a way their production are environmental unfriendly and ineffective.

2.6.2 Inorganic UVR Additives

A few metal oxides or semiconductors, for examples copper oxide (CuO) [Fleisch, 1982; Oral et al., 2004; Vidyasagar et al., 2011], zirconium dioxide (ZrO_2) [Rivera et al., 2007; Wan et al., 2014], aluminum oxide (Al_2O_3) [French et al., 1998; Xiao et al., 2015] and two commonly used zinc oxide (ZnO) [Cristea et al., 2010; Deka et al., 2012; Jeeju et al., 2011; Kulyk et al., 2010; Li et al., 2001; Li et al., 2006; Lowry et al., 2008; Sil et al., 2010; Tigges et al., 2010; Wang et al., 2013; Zhao et al., 2006; Zohdy et al., 2009] and titanium dioxide (TiO_2) [29,36,59,149,176], and also silver (Ag) nanoparticles [Kaczmarek et al., 2014; Nouneh et al., 2011; Stevanovic et al., 2012] have been demonstrated their UVR resistance properties in wood, synthetic polymers and fabrics.

CuO, ZrO_2, Al_2O_3 and Ag particles exhibit their intrinsic physical UVR absorbability. This property is achieved by the optical band gap located in their atomic structure and the dielectric ability on their surface. The degree of absorbability is dependent on the band gap energy of particle, the dielectric properties of particle and surrounding medium, the size and the shape of particle. The principle mechanism of UVR absorption of ZnO and TiO_2 particles are the same as CuO, ZrO_2, Al_2O_3 and Ag particles. ZnO and TiO_2 particles are more common for UVR resistance because they possess a wider UVR absorption spectrum and more detailed findings will be presented in the following section.

2.6.3 Comparison of Zinc Oxide with Titanium Dioxide

A comparison table is given in ***Table 2.2*** to clearly show the difference and similarity in the features of ZnO and TiO_2.

Table 2.2 Comparison of ZnO and TiO$_2$ [Dutta et al., 2009; El-Toni et al., 2010; Sambandan et al., 2011; Yang et al., 2004]

Features	***ZnO***	***TiO$_2$***
Wavelength	290 – 400nm	290 – 350nm
UVR protection	UVA1[*], UVA2[*] and UVB	UVA2[*] and UVB
Photocatalytic ability	A little lower	Higher
Band gap energy (temperature)	・ 3.436eV (-273°C) ・ 3.2eV (26°C)	・ 3.02eV (-273°C) in rutile ・ 3.2eV (-273°C) in anatase
Refractive index in visible light	1.9[#]	2.6[#]
Colour in visible light	・ Transparent (nano size) ・ White (RT[^]) to yellow (300°C)[&]	White or light coloured
Solubility	Hydrophilic	Hydrophilic
Antibacterial ability	Yes	Yes
Thermal conductivity	Relatively high	Lower
Heat capacity	43.1J/(mol·K)	50.0J/(mol·K) in rutile
Crystalline structure	・ Hexagonal wurtzite[%] ・ Cubic zinc-blende ・ Cubic sock-salt (NaCl type)	・ Rutile (tetragonal) ・ Anatase (tetragonal) ・ Brookite (orthorhombic)
Strengths	・ Completely photostable ・ Inexpensive ・ Chemically stable ・ Relatively abundant ・ Easy to incorporate into emulsions ・ Easy to prepare ・ Non-toxic ・ Stable to extremely high temperature (1800°C) ・ Anti-corrosion to humidity	・ Low cost ・ Chemically stable ・ Easy to incorporate into emulsions ・ Non-toxic
Limitations		・ Thermally unstable ・ Highly reactive to UVR[@]

[*] UVA1 (340 – 400nm) and UVA2 (315 – 340nm)

[#] Refractive index for water is 1.33

[^] RT represents room temperature

[&] Crystalline ZnO is thermochromic

[%] The most thermodynamically stable structure under ambient condition

[@] Photo excited to generate reactive oxygen species

ZnO is obviously an effective candidate in terms of the functions for UVR absorption, transparency and thermal stabilization. ZnO has an absorption spectrum for the whole range of UVR which TiO_2 does not have. Although TiO_2 has a higher reactivity to UVR than ZnO, it is not a good advantage for adopting it in polymers which this increase the rate of radical formation to further degrade the surrounding polymer. Because of the overwhelming advantages, ZnO is selected and incorporated into polymers for the present research. More information of ZnO will be revealed in the following sections.

2.6.4 Characteristics of Zinc Oxide Particle

The chemical structure of ZnO nanoparticles is shown in ***Figure 2.18***. ZnO particle embedded in polymers yields transparent when it is in nano size of which its diameter is smaller than 100nm. The physical UVR absorbability of ZnO particle is dependent on its band gap energy which is affected by its particle size. The relationship of ZnO particle size to its band gap energy shown in ***Figure 2.19*** has been studied by Dutta et al. [2009].

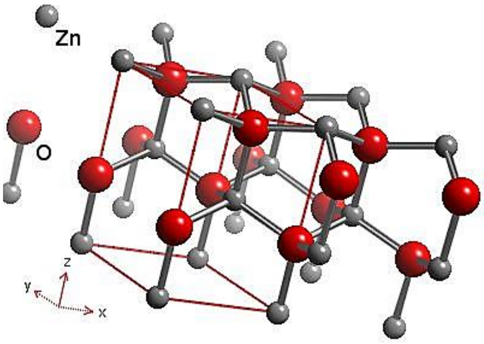

Figure 2.18 Chemical structure of ZnO nanoparticle [www.webelements.com]

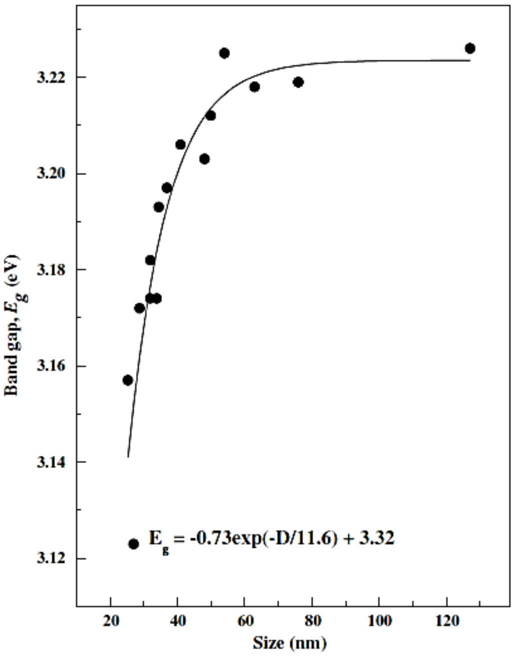

Figure 2.19 Band gap energy versus the size of milled ZnO particle [Dutta et al., 2009]

Larger diameter, in between 10nm and 200nm, of ZnO yields better UVR absorption at longer wavelength which is the UVA region [Dutta et al., 2009; Jeeju et al., 2011; Li et al., 2006]. Most research proved a low content of around 7 wt.% or below could be the optimum amount of ZnO particle to be implemented in polymers for good UVR absorption [Cristea et al., 2010; Lowry et al., 2008; Wang et al., 2013; Zhao et al., 2006].

2.6.5 Characteristics of Silane-Doped-Zinc Oxide Particle

Silane is one of the four major coupling agents for the modification of the surface of metal oxide nanoparticles [Mallakpour et al., 2015]. Numerous types of silane are commercially available in the market and have been incorporated onto ZnO nanoparticle surface for enhancing particles dispersion and their compatibility with polymer matrix. There are papers investigated the luminescence properties and UVR responses of silane-doped ZnO in the form of nanoparticle and filled in polymer resins. γ-aminopropyltriethoxysilane (APTES) [Abdolmaleki et al., 2012; Abdolmaleki et al., 2013; Costenaro et al., 2013; Grasset et al., 2003; Hang et al., 2015; Liu et al., 2012; Mallakpour et al., 2014; Mallakpour et al., 2015; Moghaddam et al., 2015; Ukaji et al., 2007], γ-glycidoxypropyltrimethoxysilane (GPTMS) [Huang et al., 2014; Zhang et al., 2015; Zhang et al., 2015] and γ-methacryloxypropyltrimethoxysilane (MPS) [Abdolmaleki et al., 2011; Bressy et al., 2012; Hsiang et al., 2010; Kim et al., 2012; Li et al., 2015; Mallakpour et al., 2012; Musat et al., 2014; Tang et al., 2007; Wang et al., 2010] are the three common types of silane coupling agent denoted by using their chemical code as KH550, KH560 and KH570. APTES (KH550) is frequently being used for ZnO nanoparticles with epoxy resin. Another silane coupling agent, Vinyltriethoxysilane (VTES) with chemical code of KH151 [Hu et al., 2009; Joshy et al., 2009; Kanimozhi et al., 2014; Ma et al., 2005], is usually being used for polyester resin which polystyrene is one of the compositions.

Table 2.3 compares the physical properties of APTES (KH550), GPTMS (KH560), MPS (KH570) and VTES (KH151).

Table 2.3 Physical properties of APTES (KH550), GPTMS (KH560), MPS (KH570) and VTES (KH151) [www.hengdachem.cn; www.sigmaaldrich.com]

	APTES (KH550)	***GPTMS (KH560)***	***MPS (KH570)***	***VTES (KH151)***
Classified group	Amino silane	Epoxy silane	Methacryloyl silane	Vinyl silane
Appearance	Colourless			
Viscosity	Low			
Density	0.947g/cm^3 at 20°C	1.055g/cm^3 at 20°C	1.055g/cm^3 at 20°C	0.9718g/cm^3 at 20°C
Molecular formula	$C_9H_{23}NO_3Si$	$C_9H_{20}O_5Si$	$C_{10}H_{20}O_5Si$	$C_8H_{18}O_3Si$

Molecular weight	221.37	236.34	248.35	190.31
Boiling point	217℃/760mmHg	290℃/760mmHg	255℃/760mmHg	123℃/760mmHg
Refractive index	1.420	1.4205	1.4205	1.3925
Flash point	96℃	110℃	108℃	22℃
Solubility	· Soluble in water (hydrolysis), aromatic or aliphatic hydrocarbons (alcohol) · Ketone, acetone and phenoxin are not recommended to be used as diluents	· Soluble in water (hydrolysis), aromatic or aliphatic solvents (alcohol, ether and ketone)	· Soluble in water (hydrolysis), aromatic or aliphatic solvents (alcohol, ether and ketone)	· Soluble in water (hydrolysis), aromatic or aliphatic hydrocarbons (alcohol, ether and ketone)

All of the silane coupling agents are colourless, have similar refractive index and low viscosity. KH151 silane has the lightest molecular weight followed by KH550, KH570 has the heaviest molecular weight. These four silane coupling agents have slightly difference in their applications. KH550, KH560 and KH570 are more feasible to be doped on the surface of ZnO particle. Among the three, KH550 has a widest application, KH560 works good with epoxy, polyester resin, etc., KH570 is used to improve water resistance and adhesion between radical cross-linked resin (e.g. unsaturated polyester resin) and inorganic substrate. KH151 is practical to be grafted in polymer to convert thermoplastic resin into thermosetting, to achieve better heat resistance, chemical resistance and mechanical strength than the original thermoplastic resin. It is used as a co-monomer for preparing moisture-curing silane cross-linked polymer (e.g. silane cross-linked polyethylene (XLPE), etc.) bridging with glass fibre and inorganic filler.

The chemical structures of APTES (KH550), GPTMS (KH560), MPS (KH570) and VTES (KH151) are shown in ***Figure 2.20, Figure 2.21, Figure 2.22 and Figure 2.23***. Their chemical formulae are $C_9H_{23}NO_3Si$, $C_9H_{20}O_5Si$, $C_{10}H_{20}O_5Si$ and $C_8H_{18}O_3Si$ respectively.

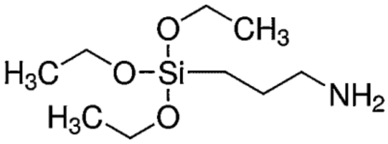

Figure 2.20 Chemical structure of APTES (KH550) [www.sigmaaldrich.com]

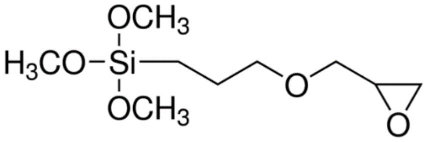

Figure 2.21 Chemical structure of GPTMS (KH560) [www.sigmaaldrich.com]

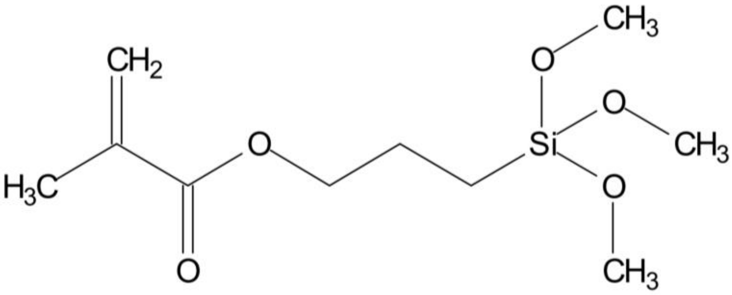

Figure 2.22 Chemical structure of MPS (KH570) [www.sigmaaldrich.com]

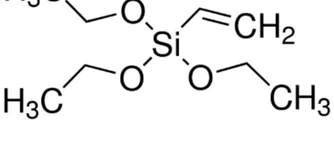

Figure 2.23 Chemical structure of VTES (KH151) [www.sigmaaldrich.com]

The chemical structure of KH550 silane-doped ZnO [Mallakpour et al., 2013], KH560 silane-doped ZnO [Li et al., 2015] and KH570 silane-doped ZnO [Musat et al., 2014] are shown in ***Figure 2.24, Figure 2.25 and Figure 2.26***. Functional groups (usually represents as R) in different silane react with polymer chains and inorganic ZnO particle with different strength depending on their attraction forces and the bridging length. $–NH_2$ is the amino group (amine) of KH550 silane, epoxy group (epoxide) in an equilateral triangle form appears on KH560 silane and $–CH_3$ is the methyl group (Me) of KH570 silane, these organic functional groups on silanes are responsible for reacting with polymers. On the other side, Si–OCH on silane and –OH on ZnO, hydroxyl groups, are attracted and bridged together to form the linkage of Si–O–ZnO. The chemical structure of KH151 silane-doped-fibre [Hu et al., 2009] is shown in ***Figure 2.27***. The vinyl functional group on silane represented as $–CH=CH_2$ provides a link for polymer chains and the other groups reciprocate with fibre.

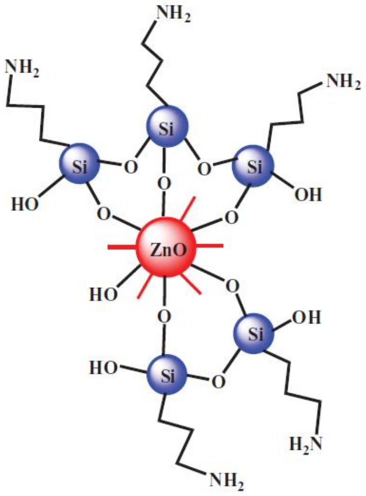

Figure 2.24 Chemical structure of KH550 silane-doped ZnO [Mallakpour et al., 2013]

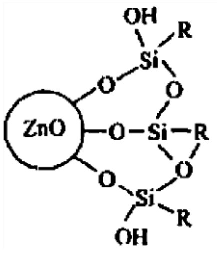

Figure 2.25 Chemical structure of KH560 silane-doped ZnO [Li et al., 2015]

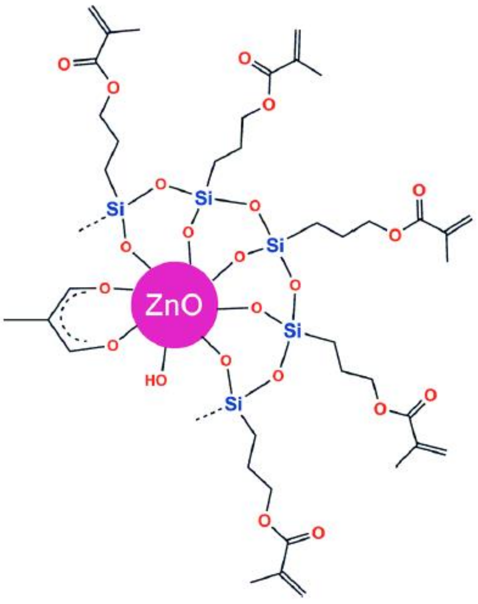

Figure 2.26 Chemical structure of KH570 silane-doped ZnO [Musat et al., 2014]

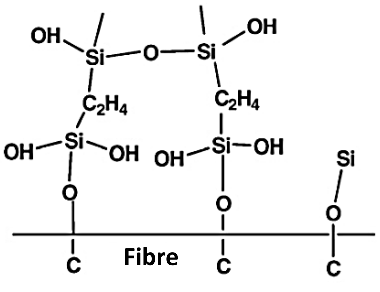

Figure 2.27 Chemical structure of KH151 silane-doped fibre [Hu et al., 2009]

Chapter Three

Background of the Present Research

Chapter Three states the background of present research including the problem statement, the materials for experiments and the methodology implemented for experimental and theoretical analyses.

3.1 Problem Statement

Base on the comprehensive literature review presented in previous chapter, UVR resistance in polymer-based composites is a crucial area in research for the health of materials during their service and the impact of materials to the environment. By introducing inorganic zinc oxide (ZnO) nanoparticles filled hollow glass fibre (HGF) to be the top protective lamina of fibre reinforced polymer composite (FRP), besides the full UVR spectrum and physical UVR absorbability of low-cost ZnO nanoparticles and therefore minimizing the UVR degradation effects in core composite in a cost effective way with a small amount of ZnO nanoparticle, at 7 wt.%, in polymer proven by other researchers to be sufficient for UVR absorption, the dissolution problem of nanoparticles under environmental erosion and the wearing problem of surface under mechanical strikes are also expected to be mitigated.

3.2 Materials for Experiment

In the development of top protective lamina of FRR to prevent the material from UVR degradation, two kinds of ZnO nanoparticle are introduced for the UVR absorption; HGF with micron diameter is used for the protection of ZnO nanoparticles and surface from dissolution and wearing out. Glass fibre reinforced polymer (GFRP) is suggested to the base material for comparison study. Three kinds of polymer resins, epoxy (EP), unsaturated polyester (UP) and shape memory polymer (SMP) are investigated with the implementation of ZnO nanoparticles and/or HGF. The following sections will introduce the kinds of composition being integrated in the novel material for investigating their UVR degradation and resistance in terms of their mechanical properties and UVR absorbabilities.

3.2.1 Zinc Oxide Nanoparticle

Two kinds of particles were implemented in tests. A comparison table is shown in ***Table 3.1***. Uncoated ZnO particle with 100nm diameter is denoted as 100nm ZnO throughout this entire thesis. Silane coupling agent-doped ZnO particle with 20nm diameter is represented as 20nm silane-doped ZnO. 1 wt.% silane coupling agent used is the common one, the γ-aminopropyltriethoxysilane (APTES), KH550. More information about the ZnO particle and silane coupling agent are discussed in ***section 2.6.5***.

Table 3.1 Properties of 100nm ZnO and 20nm silane-doped ZnO particles [adopted from manufacturers]

	Type 1	***Type 2***
Elements	ZnO	ZnO:KH550
Average particle size	100nm	20nm
Purity	99.9%	99:1%
Crystallinity	Single crystalline	Single crystalline
Type of manufacturing process	French	American
Surface treatment	No	Yes (KH550)
Colour	White	White
Shape	Nodular	Nodular
Specific surface area, m^2/g	9.0	20-60
Apparent (bulk) density, g/cm^3	0.560	0.532
pH	7.37	6.95
Compositions	· ZnO (99.9%)	· ZnO (99%)
	· CdO (0.005%)	· KH550* (1%)
	· PbO (0.001%)	· TiO_2 (0.051%)
	· H_2O Soluble Salts (0.02%)	· ZrO_2 (0.017%)
	· Fe_2O_3 (0.001%)	· Fe_2O_3 (0.008%)
	· Propionic acid (0.2% added)	· AgO_2 (0.027%)
Reactivity data	· React with Carbon Dioxide (CO_2) in air	
	· React with Carbon Monoxide (CO) or Hydrogen (H) to produce elemental Zinc (Zn)	
	· Sublime under normal pressure	
	· Do not occur polymerization	

Besides the difference in particle size (100nm and 20nm), the specific surface area ($9m^2/g$ and $20\text{-}60m^2/g$) and the surface property (undoped and KH550 doped) of two particles, their manufacturing process are different (French type and American type) which leads to a slightly variation of the physical composition of two particles. And the purity of 100nm ZnO (99.9%) is higher than 20nm silane-doped ZnO (99%). The similarity is that they both are single crystalline, in spherical shape, in white colour and having around 0.5 g/cm^3 of apparent density.

3.2.2 Hollow Glass Fibre

The HGF used in the tests were provided by the Faculty of Engineering, Bristol University. The glass type is an alkaline earth aluminosilicate glass for high temperature applications in electrical engineering and exhausted tube for halogen lamps for automotive, household and general lighting. ***Table 3.2*** shows the useful information of the HGF.

Table 3.2 Properties of HGF [adopted from Faculty of Engineering, Bristol University]

	Item	***Value***
Chemical composition	· SiO_2 · B_2O_3 · Al_2O_3 · BaO · CaO · MgO · Na_2O	60 wt.% 4.5 wt.% 14 wt.% 9 wt.% 10 wt.% 2.5 wt.% < 0.02 wt.%
Chemical resistance	· Hydrolytic resistance (ISO 719) · Acid resistance (DIN 12116) · Alkali resistance (ISO 695)	Class HGB 1 S3 A2
Physical data	Dimension	· 125µm (outer diameter) · 100µm (inner diameter) · 64% (hollowness K^2)*
	Coefficient of mean linear thermal expansion α (20°C) according to ISO 7991	$4.6 \times 10^{-6} K^{-1}$
	Transformation temperature T_g	720°C
	Density ρ at 25°C	$2.63 gcm^{-3}$
	Modulus of elasticity *E* (Young's modulus)	$81 \times 10^3 Nmm^{-2}$
	Poisson's ratio µ	0.24
	Thermal conductivity λ_w at 90°C	1.1W/(m·K)
	Refractive index n_d (λ=587.6nm)	1.538
	Coefficient of friction CoF	0.94 (for glass)

* hollowness $K^2=d^2/D^2$ (d and D represent the inner and outer diameter respectively)

It is worth noting that the dimension of HGF is one of the factors influencing the vacuum infiltrating process of ZnO/epoxy resin and the dispersion condition of ZnO particles in epoxy. The Young's modulus of the HGF is 81GPa (81 x 10^3Nmm^{-2}) which representing the strength it tolerates under fibre pull out action before delamination or failure happened.

3.2.3 Glass Fibre

Glass fibre used in the current investigation is the type of E-glass. It is a silica based with 50-60% SiO_2, inorganic and amorphous glass fibre. There are different woven patterns available in the market, plain woven is the common one which adaptable for various applications with its similar mechanical properties in plain transvers and longitudinal directions. The number of WARP and WEFT indicated in ***Figure 3.1*** are the determinants of the type of fibre. The one implemented in the present investigation is 431.8 per mm of WARP and 355.6 per mm of WEFT with thickness of 0.3mm and density of 175g/m^2.

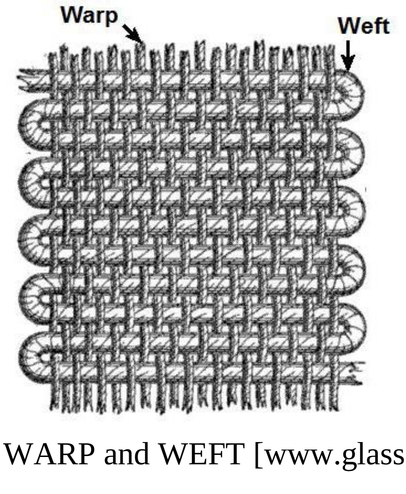

Figure 3.1 WARP and WEFT [www.glass-fiber.com]

It has advantages of good electrical insulation, good strength, reasonable Young's modulus and low density. Thus, it possesses good strength-to-weight ratio and moderate stiffness-to-weight ratio. The typical properties of E-glass fibre at room temperature are shown in ***Table 3.3***. It should be noted that glass fibres are susceptible to moisture and static fatigue as moisture decreases the strength of glass fibres and failure happens over a certain period of time under loads [Chawla, 2012].

Table 3.3 Typical properties of E-glass fibre [Chawla, 2012]

Tensile strength (GPa)	***Young's modulus (GPa)***	***Coefficient of thermal expansion*** $(10^{-6}\ K^{-1})$
1.5-2.5	70	4.7

3.2.4 Epoxy Resin

There are different types of commercial epoxy (EP) resin. The one utilized in present experiments are the most typical type, epoxy GY251 and hardener HY956. EP is a thermosetting plastic which contains an epoxide functional group, one oxygen and two carbon atoms, in its chemical structure illustrated in ***Figure 3.2*** [Strong, 2000].

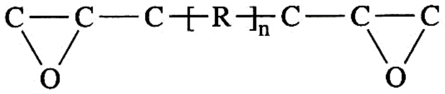

Figure 3.2 Schematic diagram of the repeating unit of epoxy [Strong, 2000]

EP is usually adopted for aerospace industry because of its good mechanical performance (high strength and toughness) together with the embedded fibre reinforcements. Besides, EP has advantages of higher chemical and fire resistance, higher strength, fairly impermeable to fluids (moisture) and relatively high dimension stability (low shrinkage) compared to unsaturated polyester (UP). EP is required to mix with hardener for curing process which the mixing ratio is according to the manufacturer’s recommendation, 5:1 of epoxy:hardener. ***Table 3.4*** shows the typical properties of EP [Chawla, 2012].

Table 3.4 Properties of EP [adopted from manufacturer]

Manufacturing properties of EP resin	
Mixing ratio	5:1 of GY251:HY956
Viscosity at 23°C	0.3-0.6Pa·s
Pot life	120mins at 23°C or 60mins 40°C
Gel time	60mins at 40°C or 15mins at 60°C
Minimum curing time	24hours at 23°C or 4hours at 23°C with 6hours 60°C
Properties of cured EP	
Density	1.1g/cm^3
Glass transition temperature	64°C
Thermal conductivity at 23°C	0.15W/(m.K)
Coefficient of thermal expansion	50-100 x 10^{-6}K^{-1}
Cure shrinkage	1-5%
Use temperature	150°C
Shore D hardness at 23°C	80
Poisson’s ratio	0.2 – 0.33
Modulus of elasticity at 23°C	2.9GPa
Tensile strength at 23°C	58MPa
Flexural strength at 23°C	107MPa
Elongation at break at 23°C	12
Water absorption	0.63% at 23°C for 10 days or 0.65% at 100°C for 30mins
Limiting oxygen index (LOI)	20%

Curing process is able to be done in room temperature at 23°C and pressure at 750mmHg for 24hours or in other particular conditions such as higher curing temperature and vacuum. The mixing ratio and curing method, which influence the number of crosslinks built in EP, are important to control the mechanical and physical properties of EP, such as stiffness, strength, toughness and glass transition temperature. In addition, different organic and inorganic additives were incorporated into epoxy enabling to modify the mechanical and physical properties of EP for achieving different objectives [Levchik et al., 2004; Sato et al., 2007].

3.2.5 Unsaturated Polyester Resin

The type of unsaturated polyester (UP) resin used in current experiments is LY191C. It a thermosetting plastic containing around 30-35% of styrene. UP LY191C was being used together with hardener, methyl ethyl ketone peroxide (MEKP) with code Trigonox V388. Its chemical structure is shown in ***Figure 3.3*** with its aromatic functional group containing dicarboxylic acis or anhydrides [Strong, 2000].

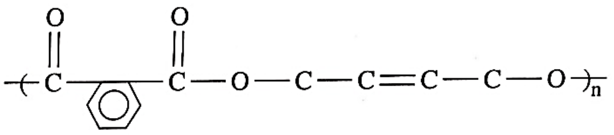

Figure 3.3 Schematic diagram of the repeating unit of unsaturated polyester [Strong, 2000]

A catalyst, cobalt (II) naphthenate, was added into the mixture for fastening the curing process under room temperature at 23℃ and pressure at 750mmHg. A coupling agent Vinyltriethoxysilane (VTES) with code KH151 was also added to modify the resin to be more compatible with E-glass fibres.

UP has moderate stiffness and strength, moderate chemical resistance and it cures easily. The mixing formula of UP is UP:MEKP:cobalt (II) naphthenate:KH151 in the ratio of 500:10:1:5. ***Table 3.5*** shows the properties of UP in room temperature [Dholakiya, 2012; Pepper, 2003; Lampman, 2003].

Table 3.5 Properties of UP [adopted from manufacturer]

Manufacturing properties of UP resin	
Mixing ratio	500:10:1:5 of UP:MEKP:cobalt (II) naphthenate:KH151
Viscosity at 23°C	0.4 -0.6Pa·s
Pot life	15mins at 23°C
Gel time	8-14mins at 23°C
Minimum curing time	24hours at 23°C
Properties of cured UP	
Density	1.13g/cm^3
Glass transition temperature	110°C
Thermal conductivity at 23°C	0.17-0.22W/(m·K)
Coefficient of thermal expansion	55-100 x 10^{-6}K^{-1}
Cure shrinkage	2.4%
Use temperature	120-150°C
Barcol hardness at 23°C	40
Poisson's ratio	0.3
Modulus of elasticity at 23°C	3.38GPa
Tensile strength at 23°C	75MPa
Flexural strength at 23°C	130MPa
Elongation at break at 23°C	3.3%
Water absorption	0.06-0.28% at 23°C for 24hours
Limiting oxygen index (LOI)	21%

3.2.6 Shape Memory Polymer

Two kinds of crosslinked shape memory polymers (SMPs) featuring thermosetting behaviour, epoxy-based SMP (EP-SMP) and styrene-based SMP (S-SMP), were studied with the implementation of ZnO nanoparticles on their UVR degradation and resistance. Both of them are provided by Centre for Composite Materials and Structures, Harbin Institute of Technology (HIT). The glass transition temperature of neat EP-SMP and S-SMP are claimed to be at 100°C and 85°C respectively. They have different fabrication methods and will be introduced in ***Chapter Six section 6.5***.

3.3 Methodology for Experimental Analysis

There are several physical and mechanical testing methods conducted to evaluate the UVR degradation and absorbability of testing samples. Accelerated UVA exposure chamber was used for exposing UVA onto the samples. UVR degradation is measured by the change of mechanical properties of samples without and after UVR exposure. Different evaluation methods will be talk over in the following sections.

3.3.1 Accelerated UVA Exposure Chamber

The accelerated UVA exposure chamber installed a mercury UV lamp emits major wavelength at 365nm within UVA region with the UVA intensity of 100mW/cm^2 at temperature of 50℃. The samples were placed right under the lamp inside the chamber at the distance of 250mm apart from the UVA source.

The accelerated UVA exposure was operated at laboratory condition with room temperature at 23℃, pressure at 750mmHg and humidity of 50% constantly for each operation. It is required to note that ozone (O_3) is produced during the operation of UVA exposure and accordingly the samples react more content of oxygen (O_2) for UVA degradation.

The accelerated cyclic UVA exposure was applied on samples referring to the exposure guideline set in ASTM D4329 standard, "Standard Practice for Fluorescent Ultraviolet (UV) Lamp Apparatus Exposure of Plastics". Fluorescent UV lamp emitting wavelength at 340nm within UVA region. Cyclic exposure procedure is specified in the test and cycle A has been chosen for most general applications which the samples are irradiated at 340nm with irradiance of 0.89W/(m^2•nm) for 8-hour UV irradiation at 60℃ and followed by 4-hour condensation at 50℃. All samples are placed on uninsulated black panel and they are repositioned horizontally and/or vertically to ensure each sample receives similar exposure condition.

3.3.2 UVR Absorbability Testing

UV-vis Spectrophotometers was used for measuring the UVR absorption or transmittance of a material in the form of solid or liquid. UV-vis Spectrophotometer Dynamica Halo DB-20 machine shown in ***Figure 3.4*** was the model used in current investigation. It is able to measure wavelength ranging from 190nm to 1100nm. The wavelength scanning speed was set to be 100nm/min with wavelength accuracy ±0.5nm.

Figure 3.4 UV-vis Spectrophotometer Dynamica Halo DB-20 machine

Light is generated by two lamp sources, tungsten lamp for producing visible region of the spectrum and deuterium for emitting the UVR range. The light is dispersed into its constituent wavelengths in a monochromator which contains diffraction grating and slit resulting a dispersed spectrum with a narrow band. In the diffraction process, several optics are placed in between to lead the light to reach the testing sample. The ray passed through the sample reaches a detector which is used for analyzing the level of light absorption or transmittance by the sample. ***Figure 3.5*** shows the light diffraction working principle of the spectrophotometer.

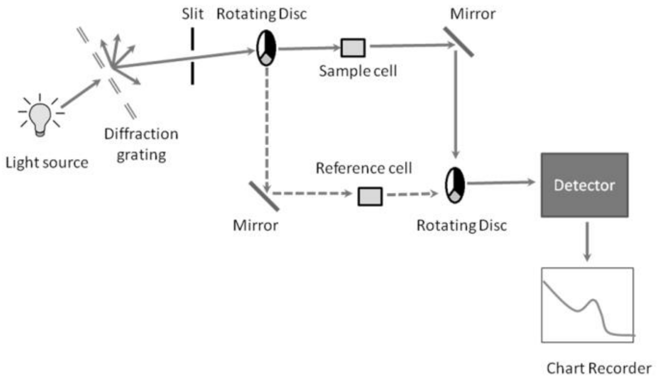

Figure 3.5 Visualization of the working principle of UV-vis Spectrophotometer

Beer-Lambert Law (***Equation 6***) is applied to determine the concentration of samples at a specific wavelength. It describes the linear relationship between absorbance and concentration. Furthermore, UVR absorbance and transmittance of a sample are correlated with and convertible to each other. An inverse logarithmic relationship between transmittance and concentration is found. ***Figure 3.6*** shows the relationship.

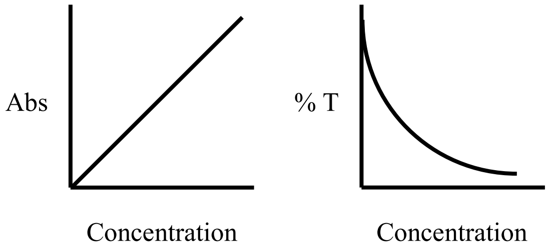

Figure 3.6 Absorbance (left) and transmittance (right) against concentration

Beer-Lambert Law is expressed as

$A = \varepsilon \times l \times c$ (***Equation 6***)

where at a specific wavelength, A is measured absorbance, ε is molar absorbance coefficient ($M^{-1}cm^{-1}$), l is sample path length (cm) and c is sample concentration (M).

Relationship between absorbance, A and transmittance, t is expressed as

$A = \log t$ (***Equation 7***)

Absorbance, A is expressed as

$\log 1/t = A$ (***Equation 8***)

Transmittance, t is expressed as

$I_t/I_o = t$ (***Equation 9***)

where I_t is intensity of light transmittance and I_o is intensity of light incidence.

3.3.3 Material Characterization

Material characterization is a typical process probing or measuring the materials for understanding their properties, structure and composition. It is a fundamental study in materials science and engineering. Material analysis including microscopic (x-ray crystallography and microscopy) and macroscopic (mechanical properties) studies will be introduced in the following sections.

3.3.3.1 Material Microscopic Characterization

3.3.3.1.1 X-ray Crystallography

X-ray diffraction (XRD) is the study of crystal structures and atomic spacing for minerals and inorganic compounds. It is calculated based on the constructive interference of monochromatic x-rays on a crystalline sample illustrated in ***Figure 3.7*** and the condition satisfies Bragg's Law (***Equation 10***).

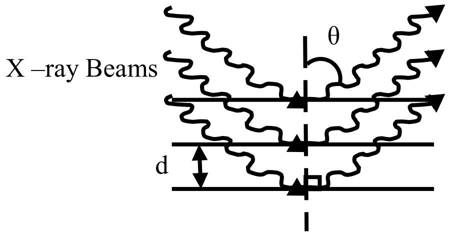

Figure 3.7 Schematic diagram of the Bragg equation

Bragg's Law is expressed as

$n\lambda = 2d \sin \theta$ (***Equation 10***)

where θ is x-ray beam is at certain angle of incidence, d is distance between atomic layers in a crystal, λ is wavelength of the incident X-ray beam and n is an integer.

XRD Rigaku SmartLab machine shown in ***Figure 3.8*** was used in present investigation for comparing the crystal structural changes between neat polymer and solvent and particle implemented polymer.

Figure 3.8 XRD Rigaku SmartLab machine

X-ray beam projects onto the sample and then detected, processed and counted. By scanning the sample through a range of 2θ angles, all possible diffracted directions of the lattice could be attained due to the random orientation of the sampling material. Conversion of the diffraction peak to d-spacing allows identification of the material because each material has a set of unique d-spacing. The phase analysis result of XRD measurement is a diffractogram, showing phase present (peak positions), phase concentration (peak heights), crystallite size (peak widths) and amorphous content (background hump). The width of the peak in a particular pattern provides an indication of the average crystallite size. Large crystallite gives rise to sharp peak, while crystallite size reduces as the peak height reduces and peak width increases. The area under the peak is related to the amount of each phase present in the sample.

3.3.3.1.2 Optical Microscopy

Optical microscope shown in ***Figure 3.9*** was used for imaging and evaluating materials. It is a light microscope using visible light and a system of lenses. It has a magnification of 2.5*x* to 1000*x*.

Figure 3.9 Optical Microscope Nikon Model Epiphot 200 machine

3.3.3.1.3 Scanning Electronic Microscopy

Scanning electron microscope (SEM) was used for surface morphology observation and elemental detection on samples. SEM JEOL Model JSM-6490 machine shown in ***Figure 3.10*** was the equipment used in current investigation.

Figure 3.10 SEM JEOL Model JSM-6490 machine

SEM uses a focused beam of high energy electrons to generate a variety of signals at the surface, top-down or cross section, of solid specimens. This is non-destructive analysis based on the signals derived from electron-sample interactions illustrated in ***Figure 3.11***.

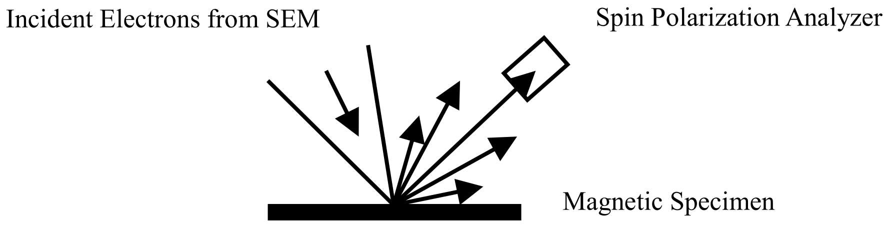

Figure 3.11 Schematic diagram of the working principle of SEM

The result obtained from SEM measurement, 2D imaging over a selected surface area of sample, shows the surface morphology, chemical composition, crystalline structure and orientation of materials integrating the sample. An area ranging from approximately 5μm to 1cm in width can be imaged in a scanning mode of conventional SEM techniques which are the magnification ranging from 20*x* to approximately 30,000*x* and the spatial resolution ranging from 50nm to 100nm. The chemical composition of a selected point or a specific area on the sample can be qualitatively determined using energy-dispersive X-ray spectroscopy (EDS) in SEM. The characterization capability of EDS is due to the fundamental principle that each element has a unique atomic structure allowing unique set of peaks on its X-ray emission spectrum which is similar to the working principle of XRD.

3.3.3.2 Material Macroscopic Characterization

3.3.3.2.1 Rheology Properties Testing

AR2000 EX Rotating Rheometer produced by TA Rheology Advantage Inc, USA shown in ***Figure 3.12*** was used for testing the rheology properties of polymeric fluid. The polymeric fluid sample was placed between two parallel stainless steel plates with diameter of 25mm. The testing was performed under controlled stress or shear rate at $10s^{-1}$ and in isothermal condition at 25℃. There are two major parameters, shear stress (yield stress) and viscosity, to determine the rheology properties of a fluid and their data were collected and plotted versus shear rate.

Figure 3.12 AR2000 EX Rotating Rheometer

At the starting point of shear stress curve is called the yield stress of a fluid. It is the minimum required stress to start the flow of the fluid. The viscosity is a measure of resistance, the intermolecular friction exerted within layers of fluid, to gradual deformation by shear stress. The rheology measurement was conducted to study the changes of fluid rheology properties after the implementation of ZnO particles with different concentration.

3.3.3.2.2 Thermal Analysis

Differential scanning calorimetry (DSC) is a technique for analyzing the thermal properties of polymeric material. A reference sample placed in the same temperature condition is required for measuring the sampling material to compare the difference in the amount of heat absorbed for the sampling material to increase its temperature. Differential Scanning Calorimeter Perkin Elmer DSC7 shown in ***Figure 3.13*** was used in present experiments. The testing temperature is available from -50 to 450℃. It can be used to determine the kinetics parameters expressed in Arrhenius' equation such as pre-exponential factor, activation energy and reaction order, to find out the specific heat, crystallization temperature, glass transition temperature, melting temperature, decomposition temperature and effects, phase transformations, phase diagrams, degree of crystallinity and purity of polymeric material.

Figure 3.13 Differential Scanning Calorimeter Perkin Elmer DSC7 machine

3.3.3.2.3 Microindentation Hardness Testing

Future-Tech Microhardness Tester shown in ***Figure 3.14*** was used in current investigation.

It is commonly used in mechanical engineering to determine the surface hardness of material by the method of deformation and indentation. There are various indentation tests, for example, Brinell hardness test (HB), Knoop hardness (HK), etc.

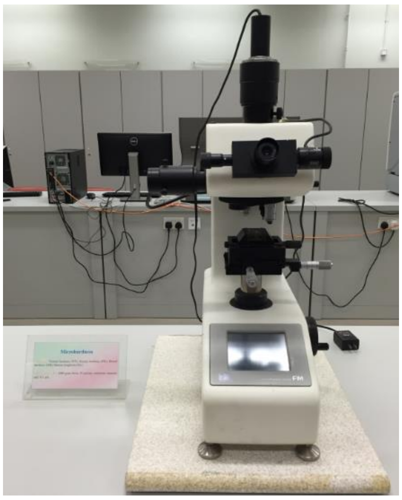

Figure 3.14 Hardness tester

Vickers hardness test (HV) which has one of the widest scales was conducted. A diamond indenter of specific geometry is impressed into the surface of testing specimen using a known applied load between 1gf to 1000gf. Typically, the test load is 200gf and the indentation is around 50μm for Microindentation test. The hardness is calculated based on the applied load, divide by the indented surface area, measuring both the diagonals to compute the Vickers pyramid number (***Equation 11***).

$$\mathrm{HV} = \frac{F}{A} \approx \frac{0.01819F}{d^2} \qquad \text{(}\textbf{\textit{Equation 11}}\text{)}$$

where F is the applied load in unit N and d is the average length of the diagonal left from the indentation in unit mm.

3.3.3.2.4 Shape Memory Effect Testing

Temperature-induced shape memory effects (SMEs) in shape memory polymers (SMPs) enable to be triggered by different stimulus, such as light, electric field, magnetic field and solution. Three conditions to quantify the SMEs of SMP are shape recovery ratio, recovery reaction time and full recovery time. Shape recovery ratio (R_r) is the determination of how much degree the shape can be recovered after the shape change. It is calculated by using ***Equation 12***. Recovery reaction time (T_r) is the time for a SMP to start the recovery and full recovery time (T_f) is the time for a SMP to complete the full recovery.

$$R_r = \frac{\theta_r}{180°} \qquad \text{(\textbf{\textit{Equation 12}})}$$

where θ_r is the recovery angle at room temperature.

SMP sample is cut into a rectangular strip, heated, bent into U shape and maintained the shape in room temperature at 23℃ and pressure at 750mmHg as indicated in ***Figure 3.15***. Dimethicone, a silicon based polymer with low chemical reactivity, is used as a heating bath for heating the deformed SMP and reshaping the SMP to its original shape. The recovered SMP is measured its shape recovery ratio (R_r) at room temperature. Video is taken for measuring the recovery reaction time (T_r) and full recovery time (T_f).

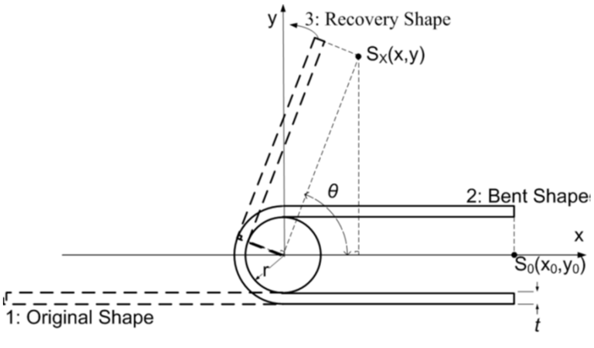

Figure 3.15 Schematic diagram of bending recovery test

3.3.3.2.5 Dynamic Mechanical Analysis

Dynamic mechanical analysis (DMA) is a useful technique used to understand the static and dynamic viscoelastic behaviour, to measure the creep and stress relaxation and to determine the complex modulus of polymers. A sinusoidal stress varying with temperature and frequency is applied on the sampling material and its dynamic and complex strain performance is measured accordingly. This technique also indicates the glass transition temperature, heat resistance and dampening intensity of the testing material which identifies the corresponding molecular transition of the polymer. Dynamic Mechanical Analyzer Perkin Elmer Diamond DMA Lab System shown in ***Figure 3.16*** is the machine used in the current experiments.

Figure 3.16 Dynamic Mechanical Analyzer Perkin Elmer Diamond DMA Lab System machine

3.3.3.2.6 Tensile Properties Testing

Tensile properties test is one of the fundamental mechanical properties test in materials engineering. The testing is universally conducted based on ASTM standard. Fibre polymer-based composites are required to comply the ASTM D3039 for tensile properties test. For polymeric materials, the standard is the ASTM D638. Useful data, such as the Young's modulus, the ultimate tensile strength and deformation strain, are obtained for analyzing the static material properties under tension load applied at a contact rate, and it shows the result of tension to failure. ***Figure 3.17*** shows the MTS universal testing machine for performing tensile test in current experiments.

Figure 3.17 MTS Universal Testing Machine

3.4 Methodology for Theoretical Analysis

Theoretical model is developed for analyzing the stress transfer ability of ZnO/HGF lamina under fibre pull-out action. It is a fundamental understanding for the fibre reinforced composite materials even for the layer in micron thickness. The bond between fibre and matrix was firstly described as the 'heart of the composite' by Piggott, one of the pioneers in the development of fibre pull out analysis, in 1986 [Piggott, 1986; Piggott, 1997]. The interface is notably crucial when the composite under environmental attacks, such as temperature, pressure and UVR.

There are extensive research on assessing the mechanical properties of single fibre composite by theoretical approach together with experimental analysis. Experimental analysis includes single fibre pull-out test [Gao et al., 2013; Heppenstall-Butler et al., 1996; Koyanagi et al., 2012; Martyniuk et al., 2013; Schuller et al., 2011; Thomason et al., 2014], single fibre fragmentation test [Zhao et al., 2000], single fibre push-out (indentation) test [Luethi et al., 1998], single fibre microbond (microdebond) test [Yang et al., 2010] and microfatigue test [Brodowsky et al., 2010]. Two major methodologies have been adopted for evaluating the mechanism of fibre pull-out in theoretical approach, fracture mechanics method [Chen et al., 2010; Francia et al., 1996; Francia et al., 1996; Liu et al., 2000; Wagner et al., 2013] and shear lag theory [Bannister et al., 1995; Fu et al., 2000; Nairn et al., 1997; Zhang, 1998; Zhang et al., 1999]. These two methods have been detailedly discussed by Kim et al. [1991]. Fracture mechanics method is based on energy criterion in terms of interfacial fracture toughness, G. It is more concerning to obtain the information of damage process of fibre inside a composite and a debonding zone is considered as an interfacial crack. Single fibre fragmentation technique has been used for determining the effects of surface treatment on fibre strength because of its convenient and reproducible test method. Shear lag theory is based on maximum shear stress criterion in terms of interfacial shear stress, τ. It is more concerning to obtain the information of maximum shear and axial strength of fibre and other elements inside a composite at the fibre debond initiation. An initiation of debond is considered to happen when the exerted interfacial shear stress exceeds the interfacial shear bonding strength. Single fibre pull-out test, which enables to reflect real failure situation of fibre composites among other tests, is commonly implemented.

Shear lag theory was first introduced by Hsueh [1990; 1990] and followed by Kim et al. [1991]. The Hsueh's model is defined as $\sigma_d^p \approx \sigma_0 + (\bar{\sigma} - \sigma_0)\left[1 - {B_1}/{(\lambda + B_2)}\right]$. Hsueh's model consists two components, the frictionless debonding stress component at the first part and the friction stress component at the second part. σ_0 is the frictionless debonding stress dependent to the embedded fibre length. $\bar{\sigma}$ is the asymptotic debonding stress for long embedded fibre length, L. B_1 and B_2 are a function of partial debonding length $(L - z)$. λ is the reciprocal length giving the effective shear stress transfer distance (or the coefficient of friction, μ). From the developed equation, Hsueh's model is a function of bonding length, z, and it approaches a constant value for long z as $tanh\beta z$ becomes unity.

Instead of considering the interfacial fracture energy, G, the frictionless debonding stress, σ_0, is controlled by the shear bonding strength, τ. Based on the Hsueh's model, Farhad et al. [1998] and Lau et al. [2001] developed theoretical models to analyze the effects of bonding characteristic between a single optical fibre and surrounding material inside a fibre-optic Bragg gating (FBG) sensor composite to the accuracy of strain measured by the FBG sensor. To a certain extent, the models from Farhad and Lau are similar, whereas, Lau considered one more adhesive layer in between the coated fibre and the base matrix. Lau's model is a four-cylindrical model, which is defined as $\varepsilon_c(z) = \varepsilon_0(1 - \frac{\sinh(\lambda z)}{\sinh(\lambda L_f)})$. Lau's model mainly concerns the change of axial strain of the base matrix to the core optical fibre. At different fibre distance from the centre, z, it is supposed that different strains are resulted. ε_0 is the axial strain of the base matrix at z=0. The axial strain distribution is dependent to the whole embedded fibre length, L_f, and is highly dominated by the constant parameter, λ, which is a function of the material properties and geometrical factors of the elements inside the composite system. Hsueh's model and Lau's model, which concern shear stress and shear strain respectively, are developed using the same analysis methodologies which are based on the shear strength criterion and regarding the force equilibrium of whole system at debond initiation or fully bonding state.

Chapter Four

UVR Degradation Mechanisms of Polymer-based Materials

Polyakov [1966] studied the effects of UVR towards the strength and failure of polymers under vacuum and air conditions. The study indicates the UVR degradation effects towards the mechanical properties of the polymer in vacuum condition of 10^{-6}mmHg (high vacuum) tend to cease after 80hours of exposure. Betteridge et al. [1977] set up a thermal degradation exposure chamber and tested the change of chemical compositions of polymers by using UV photoelectron spectroscopy (UVPS). The study points out the necessity to acquire analyzing techniques for monitoring the degradation products in the polymer.

Started from 1980, whereas the applications of polymer-based materials were expanding, the number of research papers concerning about the UVR effects in the materials were increasing at the same time. The UVR degradation mechanisms of polymer-based materials are reported in ***Chapter Four***.

4.1 Thermo Oxidation

UVR degrades polymer-based materials in two ways, one is thermal oxidation. The imparted UVR turns into thermal energy and accumulated in polymer-based materials which the heated materials become more vulnerable to the chemical reaction with oxygen (O_2) and water molecules (H_2O).

Polymers are sensitive to thermal changes which the changes are associated with the degree of crosslinking, crystallinity and entanglement of molecular chains in polymers. These characteristics are reflected by the thermal properties of polymers, such as glass transition temperature (T_g), melting temperature (T_m) and decomposition temperature (T_d). The common effects of thermal degradation are proven to be weight loss due to materials loss, mechanical properties loss and surface properties alternation in glossiness, wear resistance and water absorbability [Chawla, 2012]. Thermal energy starts breaking the weakest bonds in polymer-based composites. The interfacial bonds of particles–polymers and fibres–polymers are susceptive to the thermal energy attacks. The interfacial bonding strength is a determining factor for the degradability of polymer-based composites.

Elevated thermal degradation in polymer-based materials shows its effects in a relatively short time. Elevated temperature is defined as the temperature above room temperature, 25℃ [Chung, 2010]. Once the thermal energy over the bonding strength of polymer chains (covalent bond) and interfaces (particles–polymers and fibres–polymers) is applied, this subsequently losses the mechanical properties of the materials, this means thermal degradation occurs.

Generally, thermoplastics release gases and form crosslinks becoming thermosets while thermosets also release gases but they change colour, yellowing or blackening, under elevated temperature degradation. The yellowed or blackened layer resists thermal transfer [Strong, 2000]. Because of the existence of crosslinking system, thermosets acquire better thermal properties with higher glass transition temperature, melting temperature and decomposition temperature than thermoplastics. Therefore, thermosets are usually being utilized for structural materials. In particles filled and fibre reinforced polymer composites, dissimilar components inside a composite with different coefficient of thermal expansion (CTE) experience various degree of thermal expansion under a particular temperature, this leads to particle diffusion and fibre delamination or debond.

Thermal aging is defined as the materials treated by a relatively low amount of heat for a long period of time and the resulted effects in the materials are similar to that under elevated temperature degradation [Strong, 2000].

Thermal fatigue is the variation of temperature applied in the materials which the materials go through thermal expansion and contraction and consequently cyclic thermal stress is induced [Chung, 2010]. Polymers or dissimilar components in polymer-based composites with high CTE effectively enhance the endurance of the materials under thermal fatigue.

4.2 Photo Oxidation

Another UVR degradation mechanism in polymer-based materials is photo oxidation which is the major concern of present investigation for developing an UVR resistant GFRP by using ZnO nanoparticles and will be further discussed in ***Chapter Five***.

Photo oxidation in polymers occurs only when there is a present of photocatalyst, it is usually the metal oxide such as ZnO and TiO_2 nanoparticles. There are two ways of photo oxidation, photophysical and photochemical, which the mechanisms have been discussed [Emeline et al., 2007; Volodin, 2000]. Photophysical is the way that the metal oxides process physical absorption of UVR energy. The absorption of UVR energy is induced by the active reaction sites, the surface and the band gap of metal oxide. The absorbed UVR energy photogenerates charge carriers which are trapped and dissipated the energy between valance band and conduction band of the band gap inside metal oxide atom without producing harmful radicals. The surface absorption of UVR energy leads to the occurrence of reduction (electron trapping) with oxygen molecule and oxidation (hole trapping) with hydrogen dioxide molecule on the surface of metal oxide atom with the surrounding polymer which is the photochemical reaction. In addition, the interface of metal oxide nanoparticle with polymer, because of its relative weak bonding properties, creates an active reaction site for the reduction-oxidation (redox) chemical reaction. Photochemical reaction generates hydroxyl radical (OH^-) and superoxide radical (O_2^-) on metal oxide surface near the valance band (oxidation) and conduction band (reduction) respectively.

The reactivity of photo oxidation is determined by the band gap energy of metal oxide atom, the amount of reaction surface site at the surface of metal oxide and the interface between metal oxide and polymer and the restoration ability (relaxation and reconstruction) of the physical and chemical reaction sites. Besides the intrinsic properties of metal oxide to account its ability for photo oxidation, the acidity, alkalinity and temperature condition are also the effective factors to the reaction.

Chapter Five

UVR Absorption Mechanisms of Zinc Oxide and Zinc Oxide–Polymers

In recent years, researchers have started to discuss the methods to protect polymer-based materials against UVR attacks. ZnO nanoparticles are being commonly used for UVR resistance purpose because of its intrinsic and prominent physical UVR absorbability. Findings on the UVR absorption mechanisms of a ZnO atom and itself embedded in polymers are presented in ***Chapter Five***.

5.1 Physical UVR Absorption of Zinc Oxide

ZnO particle in nano size effectively achieves transparent properties [Jeeju et al., 2011; Kulyk et al., 2010]. And ZnO of larger size within nano scale up to 100nm is proven to obtain wider band gap width [Dutta et al., 2009]. Nano size allows ZnO to achieve better transparency, better physical UVR absorbability and broader UVR absorption spectrum.

UVR energy is absorbed by the band gap inside ZnO atom and excites the valance band to photogenerate charge carriers, the charge carriers dissipate their absorbed UVR energy between valance band and conduction band physically without the formation of harmful radials. ***Figure 5.1*** shows the physical photoreaction activities within the band gap inside a ZnO atom.

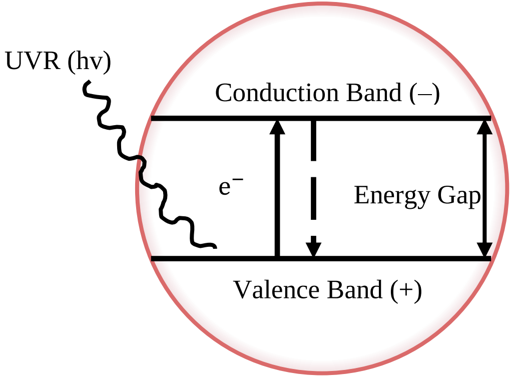

Figure 5.1 Schematic diagram of physical UVR absorption within the band gap inside a ZnO atom

A reaction expression is represented as

$$\mathrm{UV} + \mathrm{mo} \rightarrow \mathrm{mo}\ \ (\mathrm{h} + e^{-}) \qquad (\textbf{\textit{Equation 13}})$$

where mo represents metal oxide, h and e^{-} represent the hole and electron formed due to the exciton by UVR in valance band and conduction band respectively.

First step of UVR absorption happens on the surface of ZnO nanoparticle. UVR energy passes through the surface of ZnO nanoparticle which the transmittance of UVR entering into ZnO nanoparticle is dependent on the surface scattering properties, area and refractivity.

In general, ZnO surface has less scattering ability, unless a surfactant is doped on its surface. In ***Chapter Two section 2.6.5***, three types of silane coupling agents, APTES (KH550), GPTMS (KH560) and MPS (KH570), have been introduced which are the common surfactants for ZnO particle to enhance their compatibility with polymers. KH550 silane-doped ZnO particles embedded inside different polymers, thermoplastics: Poly(amide-imide) (PAI) [Mallakpour et al., 2012; Mallakpour et al., 2013; Mallakpour et al., 2014; Mallakpour et al., 2015], Poly(benzimidazole-amide) (PBIA) [Abdolmaleki et al., 2013], Poly(amide-ester-imide) (APEI) [Abdolmaleki et al., 2012] and thermosetting plastic: Polyurethane

(PU) [Hang et al., 2015], have been investigated regarding its intrinsic UVR absorbability.

Different chemicals incorporated into the backbone of polymers or different synthesis process incorporated with acid or alkaline medium interferes the UVR absorbability. Grasset et al. in 2003 [Grasset et al., 2003] studied the UVR absorbability of KH550 silane-doped ZnO by different grafting conditions. It proved KH550 silane-doped ZnO produced by acid process achieves a slightly higher UVR absorbability. Disregard the modification of chemical composition and the manufacturing process of KH550 silane-doped ZnO particle, in general, the implementation of different contents of KH550 silane-doped ZnO particle enables to enhance the UVR absorbability in different degrees. Higher content of KH550 silane-doped ZnO in biopolymers or thermoplastics achieves higher UVR absorbability. When comparing the UVR absorbability of pristine ZnO particle, KH550 silane-doped ZnO particle and KH550 silane-doped ZnO/thermoplastic, silane-doped ZnO obtain a lower UVR absorbability than pristine ZnO particle [Hang et al., 2015]. The degree of UVR absorbability of KH550 silane-doped ZnO/thermoplastic is different from KH550 silane-doped ZnO particle, it is dependent on the interfacial properties between the ZnO particle and the thermoplastic. KH560 silane-doped ZnO with various amount incorporated with epoxy has been examined their UVR absorbabilities [Hunag et al., 2014]. It indicates higher amount of KH560 silane-doped ZnO filled epoxy (EP) (a thermosetting plastic) has higher UVR absorbability. KH560 silane-doped ZnO and -TiO_2 have been compared [Zhang et al., 2015], KH560 silane-doped ZnO particle has a slightly higher UVR absorbability. Similar to KH550 silane, KH570 silane-doped ZnO particles embedded inside different polymers, thermoplastics: Poly(amide-imide) (PAI) [Mallakpour et al., 2012; Mallakpour et al., 2014], Poly(ester-amide) (PEA) [Abdolmaleki et al., 2011], Poly(amide-ester-imide) (APEI) [Abdolmaleki et al., 2012], Polystyrene (PS) [Tang et al., 2007], Poly(methyl methacrylate) (PMMA) [Wang et al., 2010] and thermosetting plastic: Polyurethane Acrylate (PUA) [Kim et al., 2012], have been investigated regarding its intrinsic UVR absorbability. Comparing the results done in the referred research, ZnO particles were more compatible in PAI and PS polymer than in PAEI and PEA, as noting that the UVR absorbability of the composite increases with the amount of ZnO particles increases. Furthermore, all the absorption peaks of polymer have a red shift towards the visible light spectrum after filling ZnO particles, the amount of ZnO particles shows no influences to the shift of wavelength absorption.

Similar to the work done by Hang et. al. [2015], Wang et. al. [2010] also discovered silane-doped ZnO has a lower UVR absorbability than pristine ZnO particle embedded inside a polymer. KH570 silane-doped ZnO with different amount incorporated in a thermosetting plastic, polyurethane Acrylate (PUA), have been tested their UVR absorbabilities [Kim et al., 2012], higher content of KH570 silane-doped ZnO/PUA achieve a higher and broader UVR absorbability. KH570 silane-doped ZnO particle at 5 wt.% has a slightly higher UVR absorbability than that at 2 wt.% and 10 wt.% according to the investigation by Musat et. al. [2014].

5.2 Chemical UVR Absorption of Zinc Oxide–Polymers

ZnO is classified as a photocatalyst which has the ability to induce the absorption of UVR energy. The absorbability is dependent to the strength of the reactive sites on ZnO atom which are the band gap inside the atom and the surface of the atom. Chemical photoreaction can be defined as the UVR absorption by photocatalyst induces reactive radicals and degrades polymer which happens at the interface of ZnO particle and surrounding polymer [Cockell et al., 1999; Serpone et al., 2007; Stiefel et al., 2015]. The UVR energy induced by ZnO reactive sites is reacted with the polymers surrounding ZnO particle resulting in reduction and oxidation reaction (redox reaction), harmful hydroxyl OH^- and superoxide O_2^- radicals were generated in the reaction which further degrade the polymer due to the presence of charge carriers. ***Figure 5.2*** shows the chemical photoreaction activities between ZnO particle and its surrounding polymer.

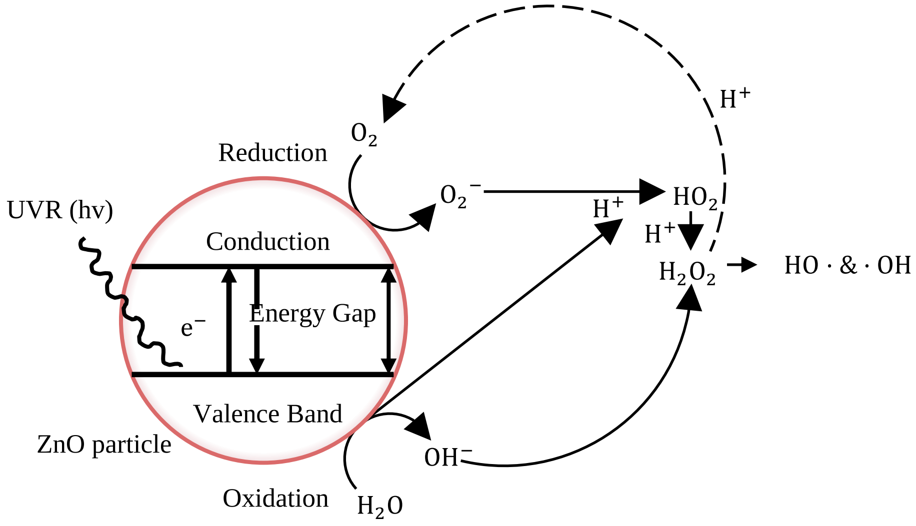

Figure 5.2 Schematic diagram of chemical UVR absorption between ZnO and its surrounding polymer

The ability of ZnO for inducing the UVR energy absorption has been implied in different journal papers [Chakrabarti et al., 2008; Kumar et al., 2009; Sil et al., 2010]. However, at the same time, the chemical absorption of UVR by the ZnO implemented polymer is also increased and this hastens the rate of UVR degradation. Although the purpose of implementing ZnO particle for UVR absorption is achieved and its effective absorbability is proved by different investigation [Cristea etal., 2010; Deka et al., 2012; Jeeju et al., 2011; Kulyk et al., 2010; Li et al., 2001; Li et al., 2006, Lowry et al., 2008; Sil et al., 2010; Tigges et al., 2010; Wang et al., 2013; Zhao et al., 2006; Zohdy et al., 2009], on another side, the UVR degradation has to be concerned for evaluating the function of implemented ZnO particle in lowering the harmful UVR effects and subsequent deterioration on the material's mechanical properties.

Two principle theoretical equations, Arrhenius equation (***Equation 14***) and Eyring equation (***Equation 15***), have been developed and adopted for analyzing the rate of chemical reaction in different applications.

Arrhenius equation is expressed as

$$\mathrm{k} = \mathrm{A}e^{-E_a/(RT)} \qquad \textbf{(}\textit{\textbf{Equation 14}}\textbf{)}$$

where k is the rate constant of chemical reaction at an absolute temperature T in K, A is the pre-exponential factor, E_a is the activation energy and R is the universal gas constant.

Eyring equation is expressed as

$$\mathrm{k} = \frac{k_B T}{h} e^{\frac{\Delta S}{R}} e^{\frac{-\Delta H}{RT}} \qquad \textbf{(}\textit{\textbf{Equation 15}}\textbf{)}$$

where k is the constant of reaction rate at an absolute temperature T in K, k_B is the Boltzmann constant, h is the Planck's constant, R is the gas constant, ΔS is the entropy of activation and ΔH is the enthalpy of activation.

Arrhenius equation was developed by Svante Arrhenius in 1889 for determining the rate of chemical reaction and calculating the energy of activation dependent to temperature. Supported by Arrhenius equation, it is claimed that every 10°C increase leads to a double rate of chemical reaction. Arrhenius equation was used to analyze the kinetic reaction in a polymer underwent UVR induced colour change [Yi et al., 2011], study the kinetic reaction of UV initiated polymerization [Voytekunas et al., 2008] and investigate the temperature and water absorption induced chemical changes in different polymers [Chou et al., 2000; El-Mossalamy et al., 2003; Patterson et al., 2015; Xian et al., 2012].

Eyring equation is able to associate one or more reactive intermediate parameters to understand the pre-exponential factor (A) and the activation energy (E_a). It was developed assuming chemical equilibrium (quasi-equilibrium) between reactants and activated transition state complexes. Similar to Arrhenius equation, Eyring equation, now is generally called transition-state theory, describes the rate of chemical kinetics in different variance of parameters involving in the reaction. It has been extensively applied to a wide variety of physical and chemical processes [Laidler, 1984] to study the photophysical properties of material which causes the transferring of charges [Rodrigues et al., 2012; Shimizu et al., 2011], analyze the breaking of polymer bonds under mechanical loads [Sebastian et al., 1999] and investigate the photo absorption and response of polymers [Canestraro et al., 2011; Phua et al., 2016; Xu et al., 2013].

Chapter Six

UVR Degradation of Zinc Oxide/Polymer Composites

Chapter Six reveals the effects of UVR degradation in ZnO/polymer composites from experimental analyses. Artificial UVR exposure was chosen in the experiment to effectively obtain the testing results and compare the effects of artificial continuous and cyclic UVR exposure in the polymer-based materials. Furthermore, four kinds of polymer-based materials, GF/EP composite, GF/UP composite, EP-SMP and S-SMP, filled with ZnO nanoparticles underwent artificial continuous UVR exposure were studied on their UVR degradation.

6.1 UVR Degradation Mechanism of Zinc Oxide/Glass Fibre/Polymer and Zinc Oxide/Polymer Composites

In ***Chapter Four***, two major UVR degradation mechanisms, thermo and photo oxidation, in polymer-based materials have been generally introduced. Present studies only concern the effects of photo oxidation to ZnO/GF/polymer and ZnO/polymer composites. Epoxy (EP), unsaturated polyester (UP), epoxy-based and styrene-based shape memory polymer (EP-SMP and S-SMP) have been investigated of their degradation under UVR attacks.

UVR degradation is significantly occurred in polymers compared with their implemented reinforcements, such as fibres and nanoparticles. Moreover, the existing common method for preventing polymers from UVR degradation is by implementing ZnO or TiO_2 nanoparticles. Based on the UVR absorption mechanism of ZnO nanoparticle and ZnO/polymer composite reviewed and stated in ***Chapter Five***, the UVR absorption rate of polymers was considered to be higher with the implementation of UVR absorbers. The reason is suggested as that UVR absorber acts as a catalyst or initiator to promote UVR absorption, UVR energy is absorbed into and onto the surface of ZnO nanoparticle which induces the desired physical UVR absorption, however the undesired chemical UVR absorption is also happened between the ZnO nanoparticle and its surrounding polymer. Chemical UVR absorption in polymer producing harmful radicals weakens the bonding between ZnO nanoparticle and surrounding polymer and leads a higher UVR degradation rate of the composite. In the case when physical UVR absorption of ZnO/polymer composite is not significant and dominate its chemical UVR absorption, the degradation rate of the composite is higher than the neat polymer.

The degradation rate of ZnO/GF/polymer or ZnO/polymer composite is considered to be dependent to the bonding strength between integrated elements which are discussed in next ***section 6.2*** and ***section 6.3***. Different degradation performances have been discovered between ZnO/GF/EP and ZnO/GF/UP composites and ZnO/EP-SMP and ZnO/S-SMP composites and compared in the following ***section 6.4*** and ***section 6.5***.

6.2 UVR against Bonding Strength of Polymer Composites

The attractive forces between integrated elements in polymer with two kinds of ZnO nanoparticles, 100nm ZnO and 20nm silane-doped ZnO, are explained in ***Figure 6.1***. The weakest attractive force is the electrostatic force appeared between two ZnO nanoparticles. The weaker attractive forces are Van de Waal’s force and hydrogen bond existed between 100nm ZnO–polymer and 20nm silane-doped ZnO–polymer respectively. The stronger attractive force happened between polymer chain–polymer chain and in crosslink.

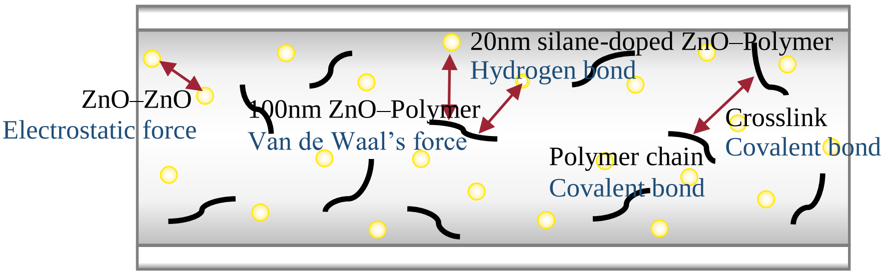

Figure 6.1 Schematic diagram of the attractive forces between integrated elements in ZnO/polymer

Types of bond are classified into two main categories, primary and secondary bonds. Primary bond is identified as having stronger bonding strength. They have higher attractions and are required higher energy to be broken down the linkage. Covalent bond is belonged to this group. In this bond, electrons are shared between elements integrating into a compound to stabilize the reactivity of elements. Single, double and triple bonds of Covalent bond are the configurations usually formed between polymer chains and in crosslinks which appear as C−C, C=C and C≡C bonds respectively. Triple covalent bond has the strongest bonding strength.

Secondary bond has weaker bonding strength than primary bond. Electrostatic force, Van der Waal's force and hydrogen bond are belonged to this category. Elements are bonded by these forces or bond in the presence of atomic or molecular dipoles with permanent or temporary attraction. Electrostatic force is the weakest force between stationary or slow-moving electric charges of two permanent dipoles. Each ZnO nanoparticle contains electron and proton which carry negative and positive charges. In between any neighbouring ZnO nanoparticles, they experience charged and discharged occasionally and the force between them experiences attractive or repulsive attraction which the movement is random and temporary. Van der Waal's force is formed between two temporary dipoles and is usually found in a symmetric molecule which the shared electronic charges are fluctuated with time. ZnO nanoparticle without silane-doped on its surface has this attractive force with surrounding polymer. Silane-doped ZnO nanoparticle has increased negative charging strength due to the presence of silane. It forms a hydrogen bond, the strongest bonding strength among the group of secondary bond, with surrounding polymer. Hydrogen bond is the bond between hydrogen atom and other atoms of the most electronegative charges having permanent polarity characteristic.

UVR degradation effects were revealed by the existence of cracks and delamination between reinforcement and polymer [Awaja et al., 2011; Chang et al., 2010; Yan et al., 2015]. However, the measure of damage on bonding strength caused by UVR was not extensively evaluated and reported. It is suggested that stronger bonding strength between integrated elements is able to alleviate the degradation effects in bonds and lower the degradation rate in mechanical properties of polymer composites by UVR attacks.

6.3 Accelerated Continuous versus Cyclic UVR Exposure Effects in Zinc Oxide/Glass Fibre/Unsaturated Polyester Composites

6.3.1 Background

There were investigations reported in previous ***section 2.4*** about the UVR degradation effects in polymer materials by using artificial accelerated continuous or cyclic UVR exposure method or comparing the effects between artificial and natural UVR exposures. Because of the time-consuming testing method of natural

UVR exposure, artificial accelerated UVR exposure has been implemented in many experiments for studying and comparing the UVR degradation effects between different kinds of polymer material. However, it is not reliable to determine the service life of different polymers used in ambient UVR exposure based on those experimental results. As there is no systematic research towards the UVR degradation test on different materials, different UVR exposure conditions were implemented, for instance, artificial UVR sources, exposure periods and UVR intensities. Furthermore, there is less research papers found which compare the effects of accelerated continuous and cyclic UVR exposure on the exposed materials in terms of their mechanical properties, such as tensile properties.

An experiment studying the difference between artificial accelerated continuous and cyclic UVR exposure effects in zinc oxide/glass fibre/unsaturated polyester (ZnO/GF/UP) composites was conducted and aimed at finding a differential factor between two exposure methods deteriorating the mechanical properties of the exposed composites.

6 wt.% of 100nm ZnO particle were implemented in between the first three layers of glass fabric with UP as polymer matrix to form a composite. 12 layers of plain woven E-glass fabric were used. A clear diagram showing the configuration is illustrated in ***Figure 6.2***.

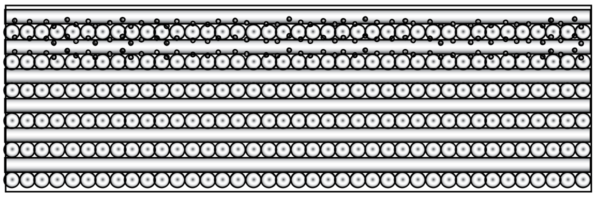

Figure 6.2 6 wt.% 100nm ZnO/GF/UP composite

The mixing formula of UP is UP:MEKP:cobalt (II) naphthenate:KH151 in the ratio of 500:10:1:5 referring to ***section 3.2.5***. 1 wt.% of silane coupling agent, Vinyltriethoxysilane (KH151), was mixed with the resin for enhancing the interfacial strength between glass fibre and resin. 6 wt.% ZnO/UP resin was ultrasonicated for 20mins and the resin mixture was mechanically mixed with hardener for another 5mins. Hand lay-up method was used in the fabrication. All composites were cured in laboratory with room temperature at 23℃, pressure at 750mmHg and humidity at 45%RH for 24hours followed by accelerated continuous or cyclic UVA exposure separately.

Cyclic UVA exposure was conducted referring to an international standard ASTM D4329 cycle A with 2.25hours of UVA exposure at 50℃ and 4hours of thermal condition at 50℃. Twenty-five samples underwent cyclic UVA exposure, one sample among them was taken out after every two cycles of UVA exposure for tensile test. One sample without UVA exposure was used as control sample. Three samples were exposed under UVA continuously and tested their tensile properties afterwards. The twenty-fifth sample underwent cyclic and the sample underwent continuous UVA exposure experienced the same total exposure time of 112.5hours. As UVA intensity emitted by the lamp in accelerated UVR chamber is 100mW/cm^2, which is approximately 11 times higher than terrestrial UVA intensity of 9.1105mW/cm^2 and natural UVA from the sun is generally alerted from 10am to 4pm for 6hours in every day, the 112.5-hour artificial accelerated UVA exposure is simulated as 208-day ambient sunlight exposure in terms of the accumulated UVA energy of 11250mW/cm^2 stored in the exposed materials. Details of the composites underwent both UVA exposure methods are shown in ***Table 6.1***.

Table 6.1 Details of ZnO/GF/UP composites underwent continuous or cyclic UVA exposure

	Accelerated Continuous UVA exposure	***Accelerated Cyclic UVA exposure***
Samples	100nm ZnO/GF/UP	100nm ZnO/GF/UP
Standard	-	ASTM D4329
Type of exposure	Continuous exposure under UVA	· 50cycles · 2h15mins UVA at 100mW/cm2 intensity at 50°C · 4h Thermal degradation at 50°C
No. of sample	3 samples for each types	25 samples, each sample underwent 2cycles
Hours of exposure	Total 112.5-hour UVA exposure	
Accumulated UVR intensity	Accumulated 11250mW/cm^2 UVA intensity in the composite	

6.3.2 Results and Discussion

6.3.2.1 Surface Morphology

The surfaces of two UVA degraded 6 wt.% ZnO/GF/UP composites underwent continuous and cyclic UVA exposure after 112.5hours pose similar degree of decolourization and yellowing. UVA energy breaks the bonds of polymers in the surface layers of the composites which leads the releasing of carbon elements. Carbon is black in nature, the surface of polymer if being continuously degraded by UVA is gradually changed to brownish colour. The surface glossiness are reduced and the surface roughness become noticeable on both samples. Characteristic of dehydration is observed in the cross section of both samples with UVA degradation. It is concluded that UVA energy removes moisture, this makes the surface to lose its glossy and become rough. No observable voids were found on both surfaces, 6 wt.% 100nm ZnO particle is effective to reinforce the polymer and prevent weight loss subjected to UVA degradation which is a common effect discovered in polymers associated with UVA exposure. ***Figure 6.3*** and ***Figure 6.4*** show the samples underwent continuous and cyclic UVA exposure respectively.

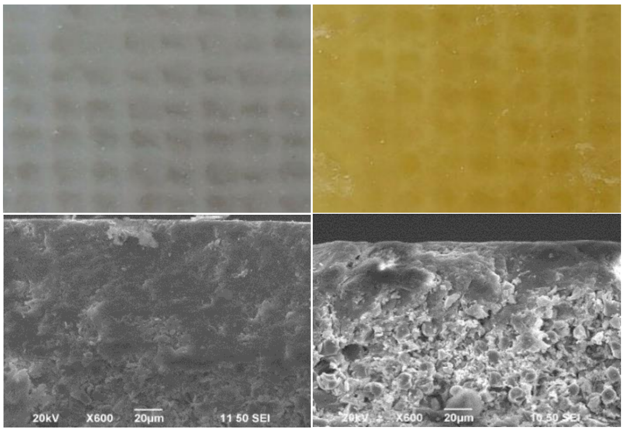

Figure 6.3 6 wt.% 100nm ZnO/GF/UP composite underwent continuous UVA exposure (left: before exposure, right: after exposure, top: surface and bottom: cross section)

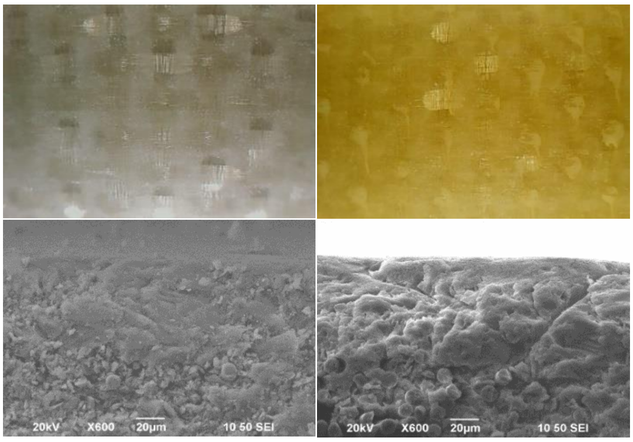

Figure 6.4 6 wt.% 100nm ZnO/GF/UP composite underwent cyclic UVA exposure (left: before exposure, right: after exposure, top: surface and bottom: cross section)

6.3.2.2 Tensile Properties

Tensile test is a universal testing method to determine the mechanical properties of a material. Tensile testing results of Young's modulus, ultimate tensile strength and strain deformation are obtained from experiments. All the tensile properties have an increasing trend within the testing period of 112.5hours. As the samples were cured under room condition, the reason of their increased tensile properties is explained by the occurrence of post curing process in the tested samples. Nevertheless, by comparing the degradation rate of samples underwent continuous and cyclic UVA exposure, a significant difference is found.

The differential factor between two exposure methods deteriorating the mechanical properties of the exposed composites is able to be obtained by this experimental data. In ***Figure 6.5***, figures on left hand side are the tensile properties of samples underwent continuous exposure and on the right hand side are those underwent cyclic exposure.

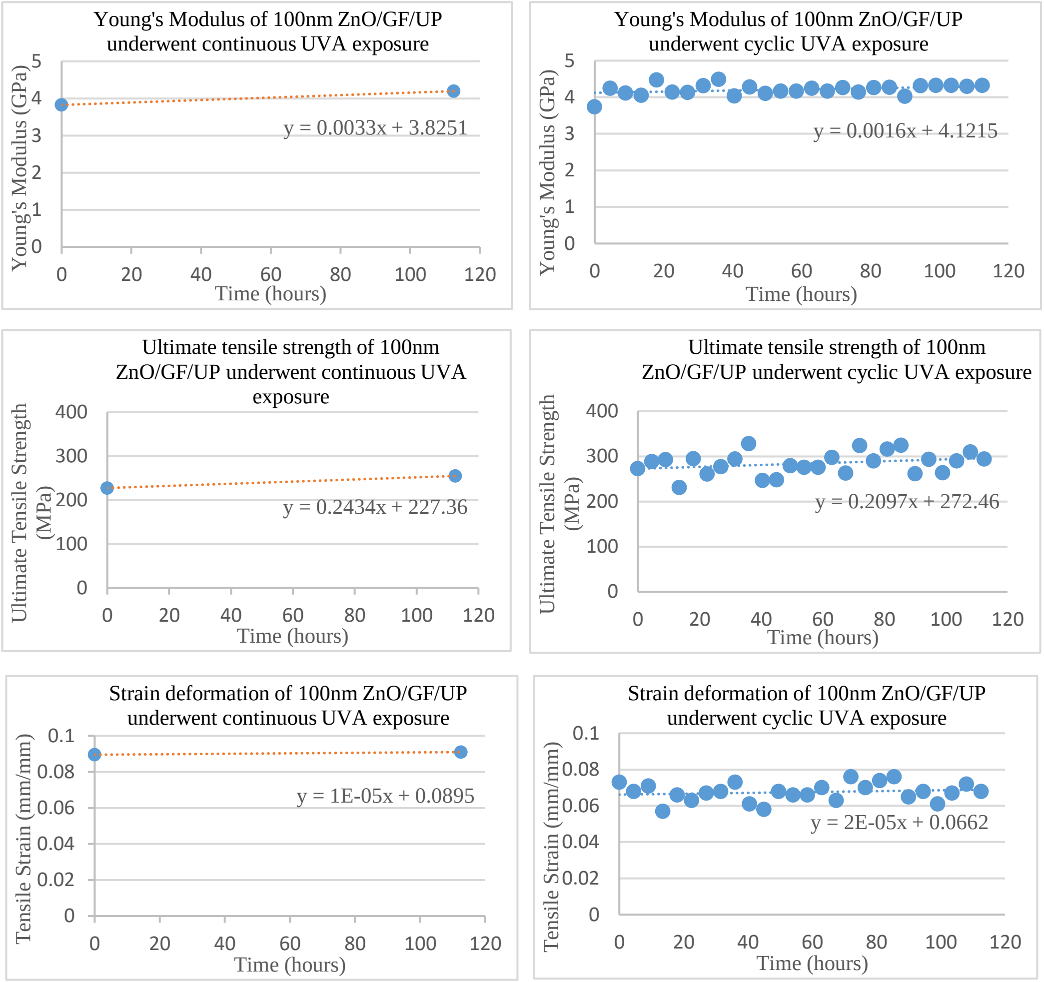

Figure 6.5 Degradation rate based on the change in tensile properties of 6 wt.% 100nm ZnO/GF/UP composites underwent continuous exposure (left) and cyclic exposure (right)

A trendline was drawn in every set of data and it is expressed by a mathematical equation. The degradation rate is represented by the slope parameter incorporated in the equation. Considering the result of Young's modulus, the degradation rate of the samples underwent continuous exposure is at 0.0033 which is 2 times faster than the samples underwent cyclic exposure having the degradation rate of 0.0016. Similarly, for the results of ultimate tensile strength and strain deformation, the degradation rates of the samples underwent continuous exposure are 1.16 and 0.5 times faster than the samples underwent cyclic exposure. Continuous UVA exposure employs a more aggressive manner to exert its harmful effects in the samples, as a consequence, the deterioration in mechanical properties of the samples underwent continuous exposure is greater than the samples underwent cyclic exposure and the difference is significant as it reaches 150% to 200% derived from the experimental results. In this experiment to compare the results of accelerated continuous and cyclic UVA exposure, no conclusion could be drawn on the reliability of accelerated exposure method which means the accelerated exposure method allows aligning closely with the natural UVA exposure by the sunlight regarding the UVA effects to a particular material.

Any absolute value of the tensile properties deteriorated by continuous or cyclic UVA exposure is not suggested to be an indicator for determining the UVA effects to the samples at a particular exposure time, it is because, first, no determination is made on which accelerated exposure method is more reliable to simulate the natural sunlight exposure; second, data collected from experiments are fluctuating within a range. Referring to ***Table 6.2***, for instance, data of strain deformation of the samples underwent cyclic exposure is not consistent with the increasing property of the trendline. Nonetheless, the degradation rate is more conservative to disclose the mechanical tolerance of a material exposed under UVA condition.

Table 6.2 Tensile properties of the samples underwent continuous and cyclic 112.5-hour UVA exposure

Tensile Properties	*Exposure*	*No UVA exposure*	*112.5-hour UVA exposure*
Young's modulus	***Continuous***	3.83	4.20
	Cyclic	3.74	4.33
Ultimate tensile strength	***Continuous***	227.36	254.74
	Cyclic	273.02	294.17
Strain deformation	***Continuous***	0.0895	0.0910
	Cyclic	0.073	0.068

6.4 UVR Effects in Zinc Oxide/Glass Fibre/Epoxy and Zinc Oxide/Glass Fibre/Unsaturated Polyester Composites

6.4.1 Background

Using artificial continuous UVA exposure method, GF/EP and GF/UP underwent the same degree of UVA exposure were tested and compared their tensile properties to understand their UVA degradability. With two different polymers, the composites react differently in UVA degradation. The degradability is contributed by the surface properties of polymer and ZnO nanoparticle, the interfacial bonding strength between fibres and polymer and ZnO and polymer.

6 wt.% of 100nm ZnO and 20nm silane-doped ZnO nanoparticles were implemented in GF/EP and GF/UP respectively to form composites. GF/EP and GF/UP composites without ZnO nanoparticles were fabricated as reference samples. The configuration is the same as mentioned in previous ***section 6.3***. Araldite GY251 and hardener HY956 in weight ratio 5:1 were used to fabricate the epoxy base. The mixing formula of UP is UP:MEKP:cobalt (II) naphthenate:KH151 in the ratio of 500:10:1:5 referring to ***section 3.2.5***. 6 wt.% ZnO nanoparticle in EP and 6 wt.% ZnO nanoparticle in UP resin were ultrasonicated for 20mins and the resin mixture were mechanically mixed with

hardener for another 5mins. All composites were fabricated by hand lay-up technique and cured in laboratory with room temperature at 23℃, pressure at 750mmHg and humidity at 45%RH for 24hours. Then all composites were treated by the same UVA exposure time of 112.5hours and their degree of deterioration as a result of UVA degradation were determined by tensile properties. Details of the composites underwent continuous UVA exposure method are shown in ***Table 6.3***.

Table 6.3 Details of ZnO/GF/EP and ZnO/GF/UP composites underwent continuous UVA exposure

	Accelerated CONTINUOUS UVA exposure		
Samples	Neat GF/EP	100nm ZnO/GF/EP	20nm silane-doped ZnO/GF/EP
	Neat GF/UP	100nm ZnO/GF/UP	20nm silane-doped ZnO/GF/UP
Type of exposure	Continuous exposure under UVA		
No. of sample	3 samples for each types		
Hours of exposure	Total 112.5-hour UVA exposure		
Accumulated UVR intensity	Accumulated 11250mW/cm^2 UVA intensity in the composite		

6.4.2 Results and Discussion

6.4.2.1 Surface Morphology

Voids are discovered on the surfaces of two UVA degraded GF/EP and GF/UP composites. The results are shown in ***Figure 6.6*** (top) and ***Figure 6.7*** (top). Without the reinforcement of ZnO nanoparticle on the surfaces, the energy of UVA led the results of shrinkage or chemical erosion in the polymers. The average size of void in UVA degraded GF/UP composite are found to be larger than in UVA degraded GF/EP composite. UP is resulted as more vulnerable under UVA degradation. It is reminded that additive of 30-35% styrene was mixed with UP for lowering the viscosity of resin and styrene is an organic oily based liquid with a vinyl functional group. Epoxy does not incorporate any additives. It is presumed that styrene negatively affects the chemical reaction of UP in UVA degradation.

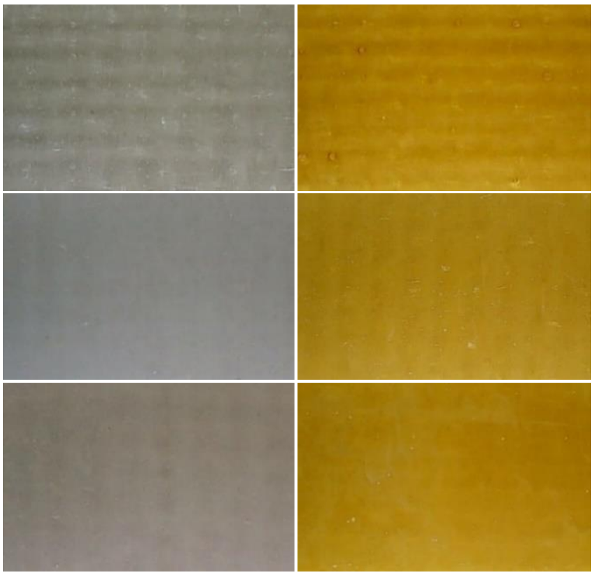

Figure 6.6 6 wt.% 100nm ZnO/GF/EP composite underwent continuous UVA exposure (left: before exposure, right: after exposure, top: neat, middle: 100nm ZnO and bottom: 20nm silane-doped ZnO)

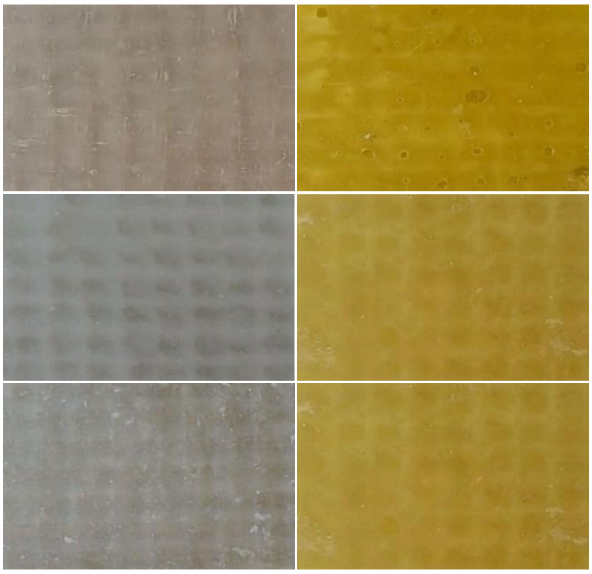

Figure 6.7 6 wt.% 100nm ZnO/GF/UP composite underwent continuous UVA exposure (left: before exposure, right: after exposure, top: neat, middle: 100nm ZnO and bottom: 20nm silane-doped ZnO)

No observable voids and smooth surfaces are found in the UVA degraded composites embedded with 6 wt.% 100nm and 6 wt.% 20nm silane-doped ZnO particles within the top three layers of glass fibres. The results are shown in ***Figure 6.6*** (middle and bottom) and ***Figure 6.7*** (middle and bottom). This shows that 6 wt. % ZnO is an effective amount to reinforce the surface of polymer under UVA degradation. Nanoparticle plays an important role to interrupt the entanglement of polymer chains which are able to lessen the density and reconstruct the arrangement of entangled polymer chains due to the effects of physical placement of nanoparticles between polymer chains and electrical charges presented on particles and polymers providing repulsive or attractive forces. ***Figure 6.8*** illustrates the idea. The implementation of ZnO nanoparticles makes well physical dispersion of themselves and polymer chains which results in a stronger bonding property between elements with each other inside the resin.

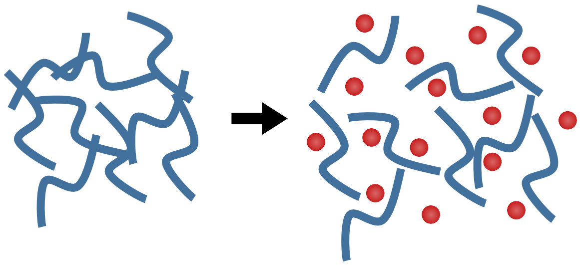

Figure 6.8 Schematic illustration of nanoparticles interplaying with polymer chains

White colour of ZnO nanoparticles is obviously noticed in UVA degraded GF/UP composites. It implies the ZnO nanoparticles are not compatible well in UP which consists of styrene than in EP resin.

Similar degree of decolourization and yellowing are observed individually in GF/EP and GF/UP composites with 6 wt.% 100nm ZnO and 20nm silane-doped

ZnO particles. Due to the whiteness of ZnO nanoparticle covering the composites, no conclusion could be made in the degree of decolourization between two kinds of composites, however, ZnO/GF/EP composites possess higher degree of yellowing. The reason for the decolourization of the samples under continuous and cyclic UVA exposure are the same which is the burn out of carbon found as a major element in polymer. The degree of decolourization is dependent to the amount of UVA intensity absorbed and measured in the unit of mW/cm^2. As mentioned in ***section 6.3.2.1***, UVA energy breaks the bonds of polymers which carbon is the major content, the degraded surface of polymer is gradually changed to brownish colour. The results are consistent with the previous investigations reported, the surface glossiness are reduced, the surface roughness become noticeable and the characteristic of dehydration is observed in all composites with UVA degradation. The same conclusion is made for that the UVA energy absorbed by the composites removes moisture which makes the surface to lose its glossy and become rough.

6.4.2.2 Tensile Properties

A large difference in tensile properties is resulted among the composites with different configurations, 6 wt.% 100nm ZnO or 20nm silane-doped ZnO particles embedded GF/EP or GF/UP, and the reference samples of GF/EP and GF/UP composites before and after UVA exposure. The results are listed in ***Table 6.4***. Comparing the variations of the tensile properties results of individual composites, the Young's Modulus and tensile strength of all composites were increased after UVA exposure. These imply the mechanical properties of the composites were still being strengthened under the amount of exposed UVA energy. Nevertheless, a large difference in the increased tensile properties indicates the reinforcement ability of ZnO nanoparticles in the polymers against UVA. 6 wt.% 100nm ZnO is found enabling to reinforce the GF/EP composite under UVA degradation which obtains a least variation in ultimate tensile strength after UVA exposure.

Table 6.4 Tensile properties of all composites

Composite	*UVA Exposure*	*E GPa*	*±%*	σ_{UTS} *MPa*	*±%*	*ε mm/mm*	*±%*
GF/EP	No	3.71	–	186.38	–	0.0755	–
	Yes	4.35	+17.25	241.42	+29.53	0.0835	+10.60
6 wt.% 100nm ZnO/GF/EP	No	3.24	–	**185.97**	**–**	0.0860	–
	Yes	4.11	+26.85	**192.53**	**+3.53**	0.0700	-18.60
6 wt.% 20nm silane-doped ZnO/GF/EP	No	3.64	–	193.63	–	0.0800	–
	Yes	4.22	+15.93	213.61	+10.32	0.0760	-5
GF/UP	No	3.73	–	236.09	–	0.0960	–
	Yes	4.32	+15.82	274.61	+16.32	0.0955	-0.52
6 wt.% 100nm ZnO/GF/UP	No	3.83	–	227.36	–	0.0895	–
	Yes	4.20	+9.66	254.74	+12.04	0.0910	+1.68
6 wt.% 20nm silane-doped ZnO/GF/UP	No	3.83	–	263.98	–	0.1055	–
	Yes	4.64	+21.15	299.84	+13.58	0.0970	-8.06

Although the same UVA energy was exerted onto the composites, the composites with different configurations receive and react with the same energy source differently. The reason is that different materials have their particular optical properties, such as, light scattering ability, light transmittance ability and light refractive index.

Light scattering ability is dependent on the surface properties of the materials and the way it reflects the light out to prevent the entry. Shiny and glossy surface of the composite has higher light scattering ability. However, the surface properties were altered, it was dehydrated and rough without shiny and glossy properties after

UVA exposure. The amount of light is increased to entre the material for UVA degradation and consequently further lowers the mechanical properties of the materials. In the microscopic view, the embedded ZnO nanoparticle with silane-doped on its surface was suspected to scatter the light away and prevent the ZnO nanoparticle to process its intrinsic UVA absorption for physically dissipating out the UVA energy to prevent chemical degradation of polymers. ***Figure 6.9*** explains the condition.

Once the energy is allowed to pass through the surface of the material, the amount of light transmitted out is dependent on the light transmittance ability of the material.

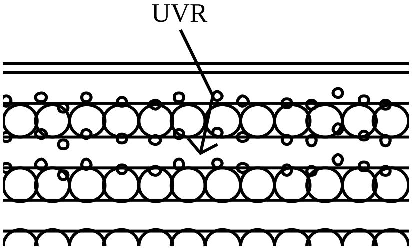

Figure 6.9 Schematic illustration of the ineffective UVR absorption of the composite embedded with silane-doped ZnO nanoparticles

Comparing two polymer layers with same thickness but different molecular densities, polymer with highly entangled polymer chains has lower light transmittance ability which means it has a stronger UVA energy absorbability and higher degradability under UVA exposure. In ZnO nanoparticles, their intrinsic UVR absorbability is various with the amount of UVR exposure energy and the band gap of the ZnO nanoparticles. If the ZnO nanoparticles are not able to fully absorb UVR energy, excess UVR energy is transmitted to surrounding polymer but the amount is lesser than direct UVR exposure in polymers without ZnO nanoparticles. If the ZnO nanoparticles are not densely packed, neat epoxy is barely exposed under UVA which makes the composites being not fully protected by the ZnO nanoparticles from UVA degradation. ***Figure 6.10*** illustrates the condition.

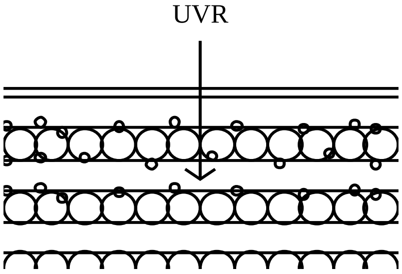

Figure 6.10 Schematic illustration of the composites without densely packed ZnO nanoparticles

Although the same fabrication method was used, there is still a difference in the dispersion of particles called layering. There are two conditions of uniformly dispersed particles in polymer, particles are uniformly dispersed in layer by layer vertically or uniformly dispersed horizontally. ***Figure 6.11*** indicates the conditions. The dispersion of ZnO nanoparticles is a critical factor influencing the absorbability or transmittability of the composites and also it is one of the reasons that the composites obtained a high variation of tensile properties results.

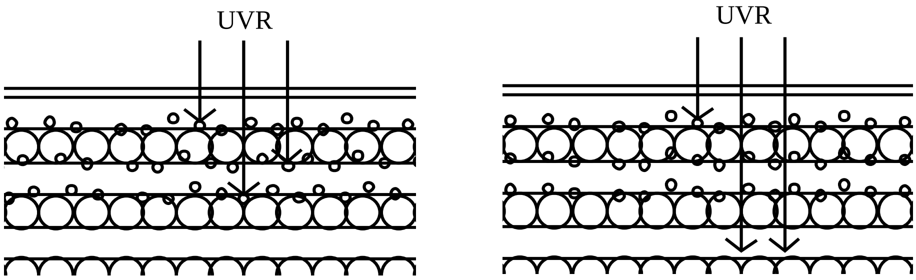

Figure 6.11 Schematic illustration of the dispersion condition of ZnO nanoparticles, vertical layering (left) and horizontal distribution (right)

6.5 UVR Effects in Zinc Oxide/Epoxy-based and Zinc Oxide/Styrene-based Shape Memory Polymers

6.5.1 Background

Besides studying the degradability of the ZnO/GF composites with EP and UP matrixes, two kinds of shape memory polymer (SMP), epoxy-based SMP (EP-SMP) and styrene-based SMP (S-SMP), were also studied on their surface morphology and mechanical properties in their UVA degradation condition.

SMP is an alternative material of shape memory alloy (SMA), although both possess shape memory effect (SME), SMP has higher tailorability and functionability by changing their compositions or implementing different fillers to alter, for example, the shape recovery temperature which is at the glass transition temperature, stiffness and bio-degradability. In addition, SMP has low density, low production cost, high recovery strain which can be achieved up to 400%, reliable recovery behaviour and convenient fabrication compared to SMA. SMP is able to be stimulated by thermo-, photo-, electrical-, magnetic- and chemo-stimulus. Crosslinking property is crucial for determining the mechanical properties of the SMPs. Chemically cross-linked structure, like EP-SMP and S-SMP, provides a more effective function of SME compared with physically cross-linked structure. In some applications, SMPs are utilized in different harsh environments which affect or even degrade their mechanical properties and lower their service life. UVA degradation is one of the environmental problem in SMP, so ZnO nanoparticles were implemented in the EP-SMP and S-SMP to study their UVA absorbability and degradability.

2 wt.%, 4 wt.%, 5 wt.% and 7 wt.% of 100nm ZnO particles were mixed with two SMPs precursor solutions respectively. The precursor solutions of EP-SMP and S-SMP were mixed according to the formula provided by Harbin Institute of

Technology (HIT). ZnO nanoparticles in EP-SMP and S-SMP resin were mechanically mixed for 20mins and then ultrasonicated for another 10mins. Afterwards, degas process was conducted until bubble-free resin mixtures were obtained. The resulting mixtures were poured into a two-plate mould. Thermal curing was performed on ZnO/EP-SMPs at 80℃ for 3hours, followed by 100℃ for 3hours and 150℃ for 5hours and on ZnO/S-SMPs at 75℃ for 36hours. All composites were cooled down at room temperature at 23°C and pressure at 750mmHg and then machined into a square shape in the dimension of 30mm (l)*30mm (w)*3mm (t). Neat EP-SMP and S-SMP without ZnO nanoparticles were fabricated as reference samples.

Using artificial continuous UVA exposure method described in ***section 7.3.3.1***, both EP-SMP and S-SMP underwent 12hours of UVA exposure and accumulated intensity of 1200mW/cm^2 were tested and compared their different surface morphology and mechanical properties in order to validate their UVR degradability. As UVA intensity emitted by the lamp in accelerated UVR chamber is 100mW/cm^2, which is approximately 11 times higher than terrestrial UVA intensity of 9.1105mW/cm^2 and natural UVA from the sun is generally alerted from 10am to 4pm for 6hours in every day, the 12-hour artificial accelerated UVA exposure is simulated as 22-day ambient sunlight exposure in terms of the accumulated UVA energy of 1200mW/cm^2 stored in the exposed materials. Details of the composites underwent continuous UVR exposure method are described in ***Table 6.5***.

Table 6.5 Details of 100nm ZnO/EP-SMP and 100nm ZnO/S-SMP composites underwent continuous UVA exposure

	Accelerated CONTINUOUS UVA exposure				
Samples	Neat EP-SMP	2 wt.% ZnO/EP-SMP	4 wt.% ZnO/EP-SMP	5 wt.% ZnO/EP-SMP	7 wt.% ZnO/EP-SMP
	Neat S-SMP	2 wt.% ZnO/S-SMP	4 wt.% ZnO/S-SMP	5 wt.% ZnO/S-SMP	7 wt.% ZnO/S-SMP
Type of exposure	Continuous exposure under UVA				
No. of sample	3 samples for each types				
Hours of exposure	Total 12-hour UVA exposure				
Accumulated UVR intensity	Accumulated 1200mW/cm^2 UVA intensity in the composite				

6.5.2 Results and Discussion

6.5.2.1 Surface Morphology

The surfaces of UVA degraded SMPs with and without ZnO nanoparticles underwent continuous UVA exposure after 12hours pose different degrees of decolourization or yellowing.

UVA degraded ZnO/S-SMPs have similar degree of decolourization among their samples and the yellowness are more severe than ZnO/EP-SMPs compared to their original form before UVA exposure. The results are shown in ***Figure 6.12*** and ***Figure 6.13***.

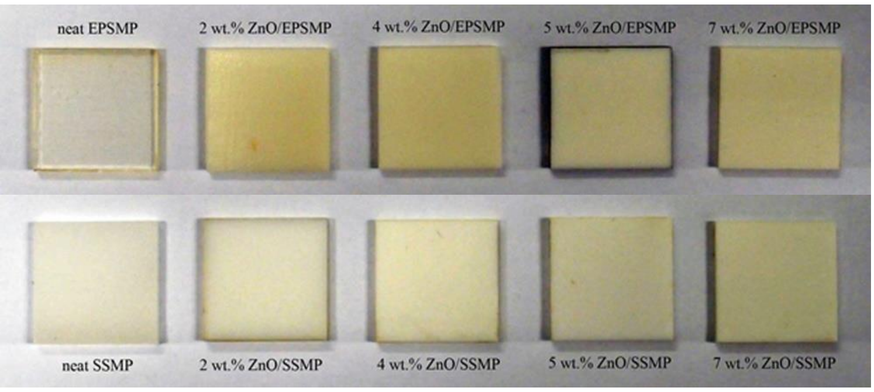

Figure 6.12 Surface colour of EP-SMP (top) and S-SMP (below) composites with and without 100nm ZnO particles before UVA exposure

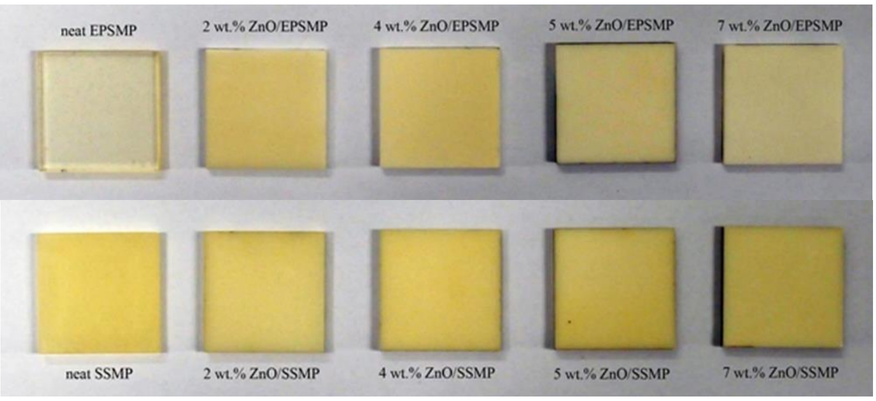

Figure 6.13 Surface colour of EP-SMP (top) and S-SMP (below) composites with and without 100nm ZnO particles after UVA exposure

This implies the ZnO nanoparticle is not able to alleviate the UVA degradation and has less compatibility in S-SMPs which the bonding strength between ZnO nanoparticle and S-SMP is not strong enough to tolerate the UVA energy attack. The yellowness is caused by the UVA energy attack which it breaks the bonds of polymers in the surface layers of the composites which leads the releasing of carbon elements. Carbon is black in nature, the surface of polymer if being continuously degraded by UVA is gradually changed to brownish colour.

UVA degraded ZnO/EP-SMPs have less observable changes in yellowing compared to their original form before UVA exposure and EP-SMP embedded with higher amount of ZnO nanoparticles obtains less yellowing which these indicate ZnO nanoparticle functions well in EP-SMP for preventing UVA degradation.

6.5.2.2 Surface Hardness

Parameters of test load was set as 100gf and dwell time was set as 15s for testing the surface hardness of the SMPs. ***Figure 6.14*** and ***Figure 6.15*** show the results of surface hardness of EP-SMPs and S-SMPs respectively before and after UVA exposure.

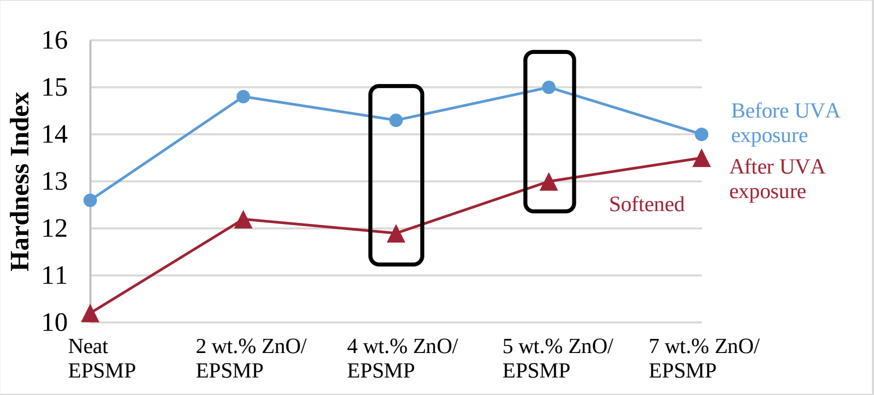

Figure 6.14 Surface hardness of EP-SMP with and without 100nm ZnO particles before and after UVA exposure

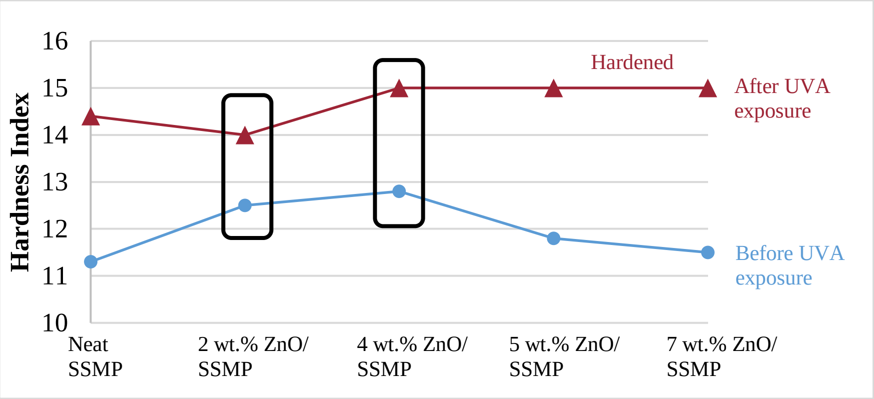

Figure 6.15 Surface hardness of S-SMP with and without 100nm ZnO particles before and after UVA exposure

Before UVA exposure, EP-SMP embedded only with 7 wt.% 100nm ZnO particle and S-SMPs embedded with higher amount of 5 wt.% and 7 wt.% 100nm ZnO particles obtain a lower surface hardness due to the occurrence of particles agglomeration. The problem of particle agglomeration happens even after undergoing an effective time of mechanical stirring and ultrasonication. Particles tend to agglomerate vigorously if they are in nano size and close to each other. The attraction is originated by the electrostatic charges inside each particle, so particles in nano size having a relatively high surface charge to weight ratio have a tendency to agglomerate with each other. The electrostatic forces are generated between the nanoparticles which the attractions exist when the distance between nanoparticles exceeds a critical point. Limitation of the distance or the content of nanoparticles in matrix is happened due to the existence of electrostatic attraction forces between nanoparticles. From the experimental results, 2 wt.%, 4 wt.% and 5 wt.% 100nm ZnO particles embedded EP-SMP and 2 wt.% and 4 wt. % 100nm ZnO particles embedded S-SMP obtain high surface hardness.

After UVA exposure, all the EP-SMPs were found to be softened and all the S-SMPs were found to be hardened. According to some reference books describing the general phenomenon of polymers after UVR treatment, thermoplastics become hardened because additional crosslinks are built by gaining the UVR energy and thermosetting plastics become softened because their inherent crosslinks are broken by the UVR energy attack. Comparing the surface hardness of SMPs before and after UVA exposure, the variation of surface hardness of 4 wt.% and 5 wt.% 100nm ZnO/EP-SMPs are 17% and 13% respectively and 2 wt.% and 4 wt.% 100nm ZnO/S-SMPs are 12% and 17% respectively. Embedding 4 wt.% and 5 wt.% 100nm ZnO particles are able to maintain the surface hardness of EP-SMP and 2 wt.% and 4 wt.% 100nm ZnO particles are able to maintain the surface hardness of S-SMP. Nevertheless, 4 wt.% 100nm ZnO particle is the prominent candidate to be implemented for UVR resistance in terms of surface hardness.

6.5.2.3 Thermal Properties

The glass transition temperature (T_g) of neat EP-SMP and 4 wt.% 100nm ZnO/EP-SMP are found to be at 61℃and 63℃ respectively and neat S-SMP and 4 wt.% 100nm ZnO/S-SMP are found to be at 66℃ and 56℃ respectively. DSC results are shown in ***Figure 6.16*** and ***Figure 6.17*** of all EP-SMPs and S-SMPs respectively.

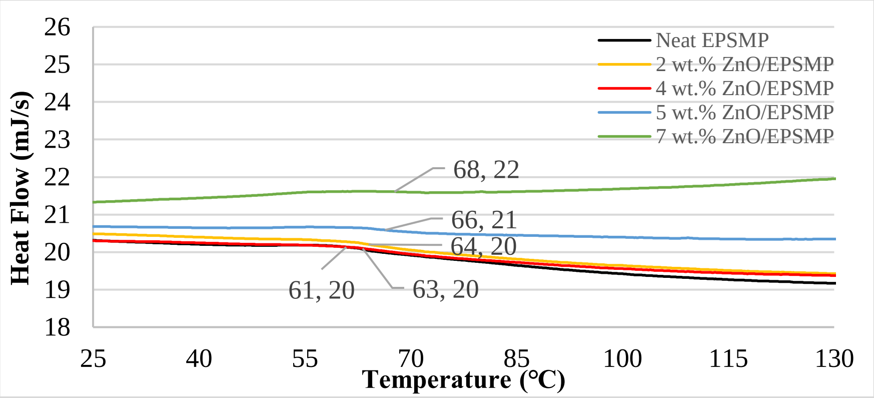

Figure 6.16 DSC results for all EP-SMPs

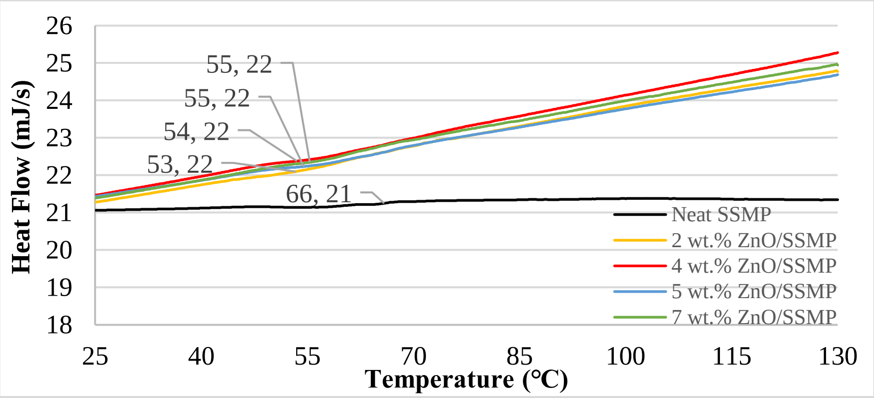

Figure 6.17 DSC results for all S-SMPs

The implementation of 100nm ZnO particles is not able to enhance the thermal stability of S-SMP. The reason has been stated in the observation of surface morphology as ZnO nanoparticle is found to be incompatible with UP and S-SMP because of the existence of styrene. Compatibility in material is a measure of the stability of a substance when mixed with another substance. It is also a measure of the bonding properties between ZnO nanoparticle and its surrounding polymer. It is worth noting that ZnO nanoparticle possesses high thermal capacity which is usually used for thermal stabilization in polymers. In this DSC analysis, ZnO nanoparticle is able to slightly enhance the thermal stability of EP-SMP. The T_g of 100nm ZnO/EP-SMPs are higher than neat EP-SMP and the thermal stability of EP-SMP is increased by increasing the amount of implemented ZnO nanoparticle. On the other hand, 100nm ZnO/S-SMPs obtain lower T_g than neat S-SMP, this further proves the weak bonding strength happened between ZnO and S-SMP. However, ZnO nanoparticles are still able to influence the thermal property of S-SMP that the thermal stability of S-SMP is increased by increasing the amount of implemented ZnO nanoparticle.

6.5.2.4 Dynamic Mechanical Properties

The shape changeability of SMP is highly dependent on the glass transition temperature (T_g) which is examined by DSC test. Furthermore, SMP has a good shape changeability when it has a large and sharp drop of its storage modulus at its T_g which the storage modulus is able to be determined by DMA test. The setting parameters for DMA test are shown in ***Table 6.6***. The parameters are set according to experimental experience as different materials have different response to stimulus.

Table 6.6 Setting parameters of DMA test for different SMPs

	Neat EP-SMP and 4 wt.% ZnO/EP-SMPs	***Neat S-SMP and 4 wt.% ZnO/S-SMPs***
Sample size	30 x 5 x 2mm^3	
Temperature range	-30 to 150℃	25 to 130℃
Testing rate	5℃min^{-1}	2℃min^{-1}
Testing frequency	1Hz	0.2Hz

Storage modulus is the dynamic modulus of a material. It is the measure of stored energy and represents the viscoelastic property of a material. Hardness is an engineering property of a material and enables to relate to yield strength. However, in this investigation, UVA degradation is only happened to the surface of the material which is not more than 0.5mm out of 3mm thickness, it is inaccurate to correlate the properties of surface hardness with the storage modulus which characterize the property of bulk material. Added that the surface hardness of the SMPs are tested under temperature at 25℃ and pressure at 750mmHg which is the starting temperature of DMA test, such that only at this temperature, under certain circumstances, the results of surface hardness are able to be related to that of storage modulus.

Referring to ***Figure 6.18***, at temperature of 25℃, UVA-degraded neat S-SMP and UVA-degraded 4 wt.% 100nm ZnO/S-SMP have 13% and 7% lower storage modulus than their individual non-UVA-degraded form. This proves UVA degradation has negative impacts to the storage modulus of S-SMPs which the materials react as having lower shape changeability after UVA exposure. However, the surface hardness of S-SMPs are proven to be hardened after UVA exposure. This specifies viscoelastic modulus is dependent on the mechanical properties of the bulk material, the mechanical properties of the material surface underwent the UVA degradation is not able to influence the structure of the material.

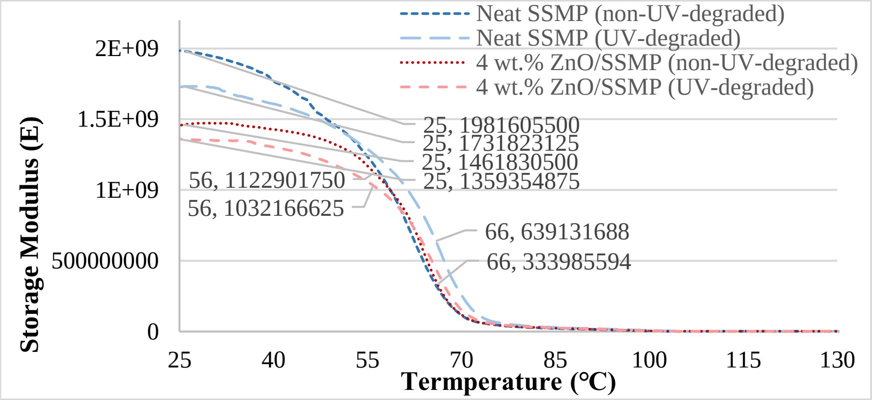

Figure 6.18 Storage modulus of S-SMP with and without 100nm ZnO particles before and after UVA exposure

Besides the influence of UVA degradation, the viscoelastic modulus is decreased by 26% after implementing ZnO nanoparticles. ZnO nanoparticles demonstrate to be incompatible with S-SMP and unable to reinforce the material. It is explained that they restrict the movement of polymer chains and negatively influence the viscoelasticity of the S-SMP.

At their individual T_g, non-UVA-degraded neat S-SMP has the largest drop of storage modulus but after the UVA exposure, its drop of storage modulus has been lessened, however, the storage modulus of UVA-degraded neat S-SMP is about a double higher compared to its non-UVA-degraded form. UVA-degraded S-SMPs have higher storage modulus and viscoelasticity at their T_g. With the reinforcement of ZnO nanoparticles, the storage modulus of UVA-degraded 4 wt.% 100nm ZnO/S-SMP has less deviation which is about 8% less from its non-UVA-degraded. The implementation of ZnO nanoparticles is capable to maintain the viscoelastic performance of S-SMP under the degree of UVA degradation applied.

Although the drop become lesser, the viscoelastic behaviour of non-UVA-degraded and UVA-degraded 4 wt.% 100nm ZnO/S-SMP are similar with that of non-UVA-degraded neat S-SMP during the transformation region. 100nm ZnO particles are proven to have less influence but enable to maintain the viscoelasticity of the S-SMP during the shape transformation.

According to ***Figure 6.19***, at temperature of 25℃, the storage modulus of all EP-SMPs are similar at around 2.00GPa which is similar to the result of non-UVA-degraded neat S-SMP having the highest storage modulus of 1.98GPa among the S-SMP samples. There are no significant influences of implemented 100nm ZnO particles and UVA-degraded surface to the viscoelastic of EP-SMP at 25℃. EP-SMP are less sensitive to UVA radiation than S-SMP.

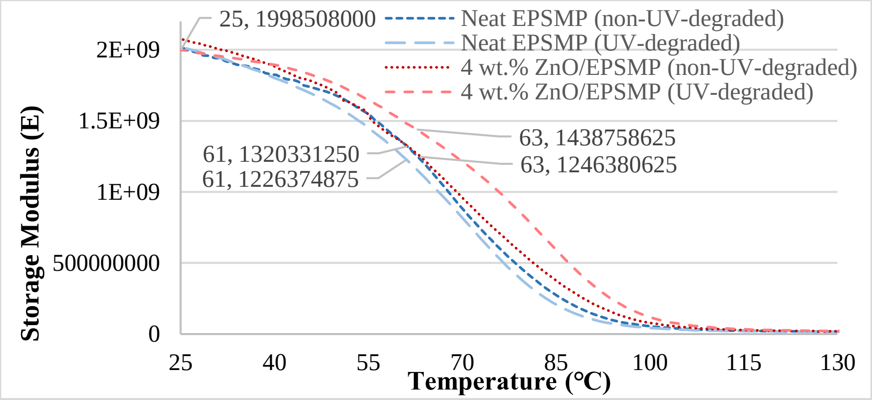

Figure 6.19 Storage modulus of EP-SMP with and without 100nm ZnO particles before and after UVA exposure

At their individual T_g, the drop of storage modulus is almost the same to all EP-SMPs. The rate of slope in the transformation region representing the shape changing behaviour are similar for all EP-SMPs. Only the UVA-degraded 4 wt.% 100nm ZnO/EP-SMP has slightly higher storage modulus at all the temperature within the region and it has 15% higher storage modulus than its non-UVA-degraded form at their T_g. EP-SMP implemented with 4 wt.% 100nm ZnO particle after UVA exposure obtains higher storage modulus and viscoelasticity. It has higher shape changeability than other EP-SMP samples at the same temperature.

100nm ZnO particles show that they have a good compatibility with EP-SMP and enable to reinforce the EP-SMP during the shape transformation.

UVA degradation has slight negative impact to the neat EP-SMP at its T_g. The storage modulus of UVA-degraded neat EP-SMP is 7% lower than its non-UVA-degraded form. Epoxy is being recognized as a promising material for structural usage. Using epoxy as the base matrix, EP-SMP is shown to be more tolerable than S-SMP under UVA degradation.

6.5.2.5 Shape Memory Effects

The shape memory effects (SMEs) of SMPs including the shape recovery ratio, full recovery time and recovery reaction time are examined by a series of steps. The setting parameters of SME tests for different SMPs are shown in ***Table 6.7***.

Table 6.7 Setting parameters of SME test for different SMPs

	Neat EP-SMP and all ZnO/EP-SMPs	***Neat S-SMP and all ZnO/S-SMPs***
Sample size	30 x 5 x 2mm^3	
Pre-heating temperature	120℃ (Tg+20℃)	105℃ (Tg+20℃)
Cooling temperature	0℃	0℃
Reheating temperature	120℃ (Tg+20℃)	105℃ (Tg+20℃)

The parameters are set according to experimental experience as different materials have different response to stimulus. Dimethicone was used as the isothermal medium for heat treatment and easy observation on the shape changing of SMPs since it has high transparency and high chemical stability. Each SMP was heated to a temperature of their T_g+20℃ in oven for 20mins. The softened SMP was immediately bent into U shape around an aluminum plate with 2mm radius arc at a bending rate of 10°s^{-1}. The U-shaped SMP was fixed on the plate and the whole pieces were put into cooling chamber at 0℃ for 20mins. The deformed SMP was then immersed into dimethicone bath at T_g+20℃. This is to investigate the shape recovery behaviour of the SMP and the process was recorded by video.

6.5.2.5.1 Shape Recovery Ratio

Shape recovery ratio is the ratio of the shape recovered angle of the tested SMP to 180°. The shape recovery ratio of all SMPs before and after UVA exposure are shown in ***Figure 6.20***. The shape recovery condition of 4 wt.% 100nm ZnO/EP-SMP and 4 wt.% 100nm ZnO/S-SMP before and after UVA exposure are shown in ***Figure 6.21***.

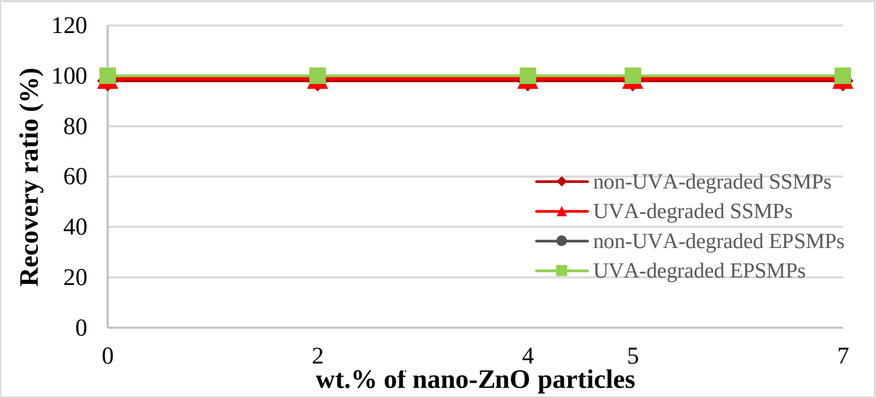

Figure 6.20 Shape recovery ratio of different SMPs before and after UVA exposure

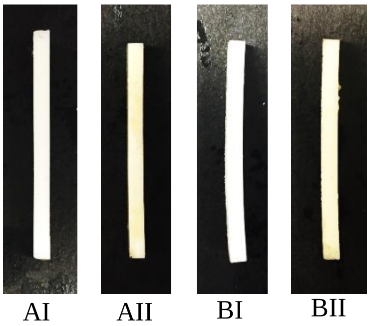

Figure 6.21 Shape recovery condition of 4 wt.% 100nm ZnO/EP-SMP (A) and 4 wt.% 100nm ZnO/S-SMPs (B) before (I) and after (II) UVA exposure

Non-UVA-degraded and UVA-degrade EP-SMPs obtain 100% shape recovery ratio. Although EP-SMPs are tested to be softened of their surface exposed under the degree of UVA applied, the DMA results show there are less variation in their storage modulus and viscoelasticity within the transformation region. EP-SMP demonstrates a higher shape changeability even after implementing 4 wt.% 100nm ZnO particle and after the degree of UVA applied. UVA-degraded S-SMPs have slightly higher shape recovery ratio of 99% than their non-UVA-degraded form of 98%. According to the tests of surface hardness and DMA, S-SMPs are hardened on their surface exposed under UVA and obtain higher storage modulus during the shape transformation, these testing results enable to explain the higher shape recovery ratio obtained in UVA-degraded S-SMPs.

100nm ZnO particles are shown to be independent to the shape recovery ratio as all the SMPs implemented with different weight percentages of 100nm ZnO particles demonstrate the same shape recovery ratio. In fact, UVA radiation imposes effects to the shape recovery ratio of S-SMPs as the shape recovery ratio of S-SMPs are changed after UVA exposure. The structure of S-SMP is constructed by building additional physical crosslinks between its polymer chains but that of EP-SMP is intrinsically in a linear monomer with built-in crosslinks. With these construction, the strength of viscoelasticity or shape changeability of EP-SMP is inherently stronger than S-SMP when under the impact of UVA energy which target to attack the weaker bonds in SMP, the bond between ZnO nanoparticle and surrounding polymer and the physical crosslink in S-SMP.

6.5.2.5.2 Recovery Reaction Time

Recovery reaction time was evaluated from the video which is to indicate the absolute time for initiating the shape recovery of SMP. The results are shown in

Figure 6.22. The evaluation compares the difference in shape changeability of non-UVA-degraded and UVA-degraded EP-SMP and S-SMP with or without the implementation of different weight percentages of 100nm ZnO particles.

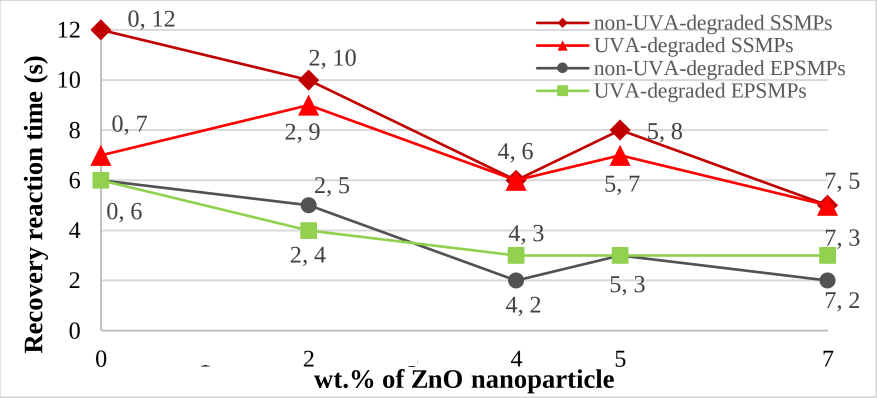

Figure 6.22 Recovery reaction time of different SMPs before and after UVA exposure

EP-SMPs achieve faster reaction time for initiating their shape changing than S-SMPs. From DMA testing results, the slope at the individual glass transition temperature represents the shape changeability of different SMPs which means a shape drop of slope represents the higher shape changeability of SMPs. This relationship is not true for the recovery reaction time of SMPs.

In addition, the larger amount of 100nm ZnO particle implemented in SMPs, the faster the recovery reaction time for initiating their shape change. This conclusion is straightforward obtained from the observation. The implementation of ZnO nanoparticles strengthens the bonding property of polymer.

The surface of EP-SMPs are softened and S-SMPs are hardened after UVA exposure. The recovery reaction time of EP-SMPs are slower and S-SMPs are faster after their UVA degradation compared with their original form. This phenomenon indicates the surface hardness property are correlated with the recovery reaction time of SMPs.

EP-SMP and S-SMP reinforced by 4 wt.% and 5 wt.% 100nm ZnO particles appear to have good sustainability in the recovery reaction time under the certain UVA degradation applied which their variations are within 0-2.38%.

6.5.2.5.3 Full Recovery Time

Full recovery time was evaluated from the video which is to indicate the absolute time for completing the shape recovery of SMP. The results are shown in ***Figure 6.23***. The evaluation compares the difference in shape changeability of non-UVA-degraded and UVA-degraded EP-SMP and S-SMP with or without the implementation of different weight percentages of 100nm ZnO particles.

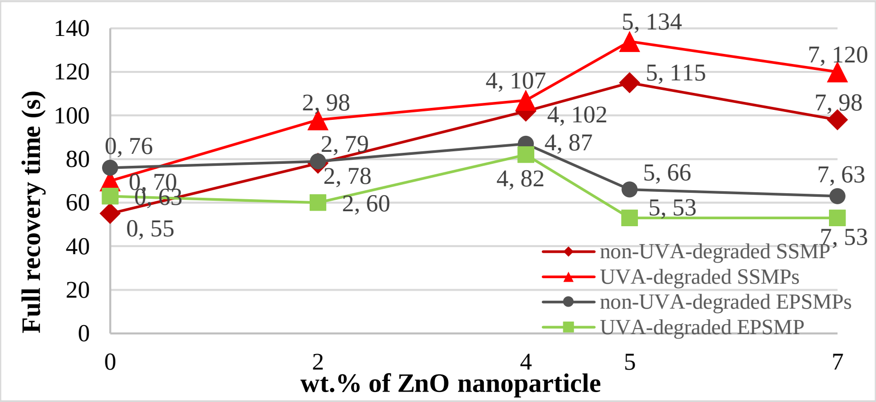

Figure 6.23 Full recovery time of different SMPs before and after UVA exposure

In general, EP-SMPs achieve faster reaction time for completing their shape changing than S-SMPs. From DMA testing results, the slope at the individual glass transition temperature represents the shape changeability of different SMPs which means a shape drop of slope represents the higher shape changeability of SMPs. This relationship is true for the full recovery time of SMPs.

The larger amount of 100nm ZnO particle implemented in S-SMP, the slower the full recovery time for completing its shape change. The implementation of 100nm ZnO particles does not impose significant changes to the full recovery time of EP-SMP compared with S-SMP. ZnO nanoparticles are able to stabilize EP-SMP with having good bonding strength, high shape recovery ratio which is proven in previous section and fast full recovery time of EP-SMP.

The surface of EP-SMPs are softened and S-SMPs are hardened after UVA exposure. The full recovery time of EP-SMPs are faster and S-SMPs are slower after their UVA degradation compared with their original form. This phenomenon indicates the surface hardness property are not correlated to the full recovery time of SMPs.

EP-SMP and S-SMP reinforced by 4 wt.% 100nm ZnO particle appear to have good sustainability in the full recovery time under the certain UVA degradation applied which their variations are within 0.12-1.03%.

ZnO nanoparticles strengthened the bonding property of SMPs favourably influences the recovery reaction time of both EP-SMP and S-SMP, however, it adversely affects the full recovery time of S-SMP. The full recovery time of EP-SMP is able to be maintained by ZnO nanoparticles. These results are obtained as ZnO nanoparticles have relatively high heat capacity and good bonding property with SMPs regulating the T_g of SMPs and reinforcing SMPs which are the key factors for their shape changeability.

UVA degradation softened the EP-SMP’s surface and hardened the S-SMP’s surface with not more than 0.5mm out of 3mm thickness. It enables to change the recovery ratio of SMPs, S-SMP has obvious change due to UVA degradation. EP-SMP has a stronger strength in shape changing, therefore, under the UVA exposure applied, the change is not obvious. There are two segments in a SMP, hard segment (UVA-degraded SMPs) dominates the recovery reaction time and soft segment (non-UVA-degraded SMPs) dominates the full recovery time of SMPs.

Under the circumstances of UVA exposure applied, the 4 wt.% 100nm ZnO particle implemented is able to maintain the shape changeability of both EP-SMP and S-SMP. 4 wt.% 100nm ZnO/EP-SMP obtains the higher performance in shape memory effects.

6.6 Summary of This Chapter

In this chapter, UVR effects to different polymer-based composites, ZnO/GF/EP, ZnO/GF/UP, ZnO/E-SMP and ZnO/S-SMP, were studied. Two accelerated UVA exposure methods, continuous and cyclic, using the same exposure time and accumulated intensity were conducted on 6 wt.% 100nm ZnO/GF/UP composite to understand the exposure effects impacted on the composite. Colour change is one of the indications showing the UVR degradation happened on material surface, no observable differences are found in the changed colour between two composites underwent continuous and cyclic UVA exposure. On the other hand, tensile properties of two composites have significant differences. The change of tensile properties is accounted the UVR degradation rate of the composite. According to the largest difference happened in the result of Young’s modulus, the degradation rate of the composite underwent continuous exposure is two times faster than the composite underwent cyclic exposure. Mechanical properties are the appropriate indication for determining the UVR degradation rate of composite material. Moreover, accelerated UVR testing has to be adopted for efficient evaluating the long term UVR effects to composite material. There is a question yet to be answered for which exposure method is appropriate for evaluating the life expectancy of composite material.

The UVR effects in neat GF/EP, neat GF/UP, 6 wt.% 100nm ZnO/GF/EP, 6 wt.% 100nm ZnO/GF/UP, 6 wt.% 20nm silane-doped ZnO/GF/EP and 6 wt.% 20nm silane-doped ZnO/GF/UP were compared. The investigation mainly focuses on the surface morphology and tensile properties of the composites to evaluate the degradation mechanism. With the implementation of ZnO nanoparticles, voids arose due to UVR are eliminated. Although various tensile properties are resulted, it is worth noting that 6 wt.% 100nm ZnO/GF/EP composite obtains the least variation in ultimate tensile strength after UVA exposure. 6 wt.% 100nm ZnO particle is at a satisfactory ratio to achieve a good collocation with epoxy polymer chains for reinforcing against UVR attack.

The UVR effects in ZnO/E-SMP and ZnO/S-SMP implemented with 2, 4, 5 and 7 wt.% of ZnO nanoparticles were also compared. The investigation focuses on the surface morphology, surface hardness, thermal properties, dynamic mechanical properties and shape memory effects including shape recovery ratio, recovery reaction time and full recovery time. Based on the bigger difference in colour change and the adverse thermal properties resulted of ZnO/S-SMP, S-SMP has less compatibility with ZnO nanoparticle due to the presence of styrene. 4 wt.% 100nm ZnO particle is at a satisfactory ratio to achieve a good collocation with SMP polymer chains for reinforcing against UVR attack as it obtains the least difference in surface hardness after UVA exposure. In addition, 4 wt.% 100nm ZnO/EP-SMP has higher storage modulus and viscoelasticity, higher shape recovery ratio, good recovery reaction time and good full recovery time compared as S-SMP.

Chapter Seven

UVR Resistance of Zinc Oxide/Polymer Composites

Chapter Seven discusses the UVR resistance of ZnO embedded in polymers and ZnO/polymer filled inside HGF. The dispersion of ZnO nanoparticle in epoxy and the rheology properties of ZnO/epoxy resin regarding the UVR resistance and manufacturing of the composite were concerned and discussed. The negative effect of silane-doped on ZnO nanoparticle for the UVR resistance of the composite was revealed in this chapter.

7.1 Dispersion of Zinc Oxide Nanoparticles in Epoxy

Particle dispersion is a critical parameter for particle filled composite towards the virtue of various mechanical and physical properties. There are three common methods for electrostatics dispersion of ZnO nanoparticles, the implementation of alcoholic solvent, the incorporation of mechanical stirring and ultrasonication. Another method is the steric stabilization of silane surface treatment on ZnO nanoparticle. In the following three sections, ***section 7.1.1***, ***section 7.1.2*** and ***section 7.1.3***, discuss the effects of solvent, mechanical stirring and ultrasonication to the dispersion of ZnO nanoparticles in polymer.

7.1.1 Solvent Effects in Zinc Oxide/Epoxy

7.1.1.1 Background

Isopropyl alcohol and ethanol were examined their effects in epoxy for the uniform dispersion of ZnO nanoparticles for which different alcoholic organic solvents have been investigated for their effectiveness on particle dispersion in a medium [Diallo et al., 2016; Hashmi, 2012; Li et al., 2014; Parveen et al., 2013; Rhodes et al., 2010; Sato et al., 2007; Yan et al., 2015]. The dispersion properties and morphological condition of ZnO nanoparticles are strongly dependent on the specific functional groups, for example hydroxyl group (OH), of solvent media. Both isopropyl alcohol and ethanol contain OH in their polymer chains as the functional group. However, they have different behaviour with polymers because of their slightly different physical properties, such as boiling point, density and hydrogen bonding properties. ***Table 7.1*** shows different physical properties of the two solvents.

Table 7.1 Physical properties of isopropyl alcohol and ethanol

	Isopropyl alcohol	***Ethanol***
Appearance	Colourless	Colourless
Viscosity	1.96mPa·s at 25℃	1.074mPa·s at 25℃
Density	0.785g/cm^3 at 25℃	0.789g/cm^3 at 25℃
Molecular formula	$(CH_3)_2CHOH$	CH_3CH_2OH
Molecular weight	60.10	46.07
Boiling point	82℃	78℃
Refractive index	1.380	1.361
Flash point	12℃	14℃
Solubility	Soluble in water	Soluble in water

The chemical structures of isopropyl alcohol and ethanol are shown in ***Figure 7.1*** and ***Figure 7.2***. Their chemical formula are $(CH_3)_2CHOH$ and CH_3CH_2OH

respectively.

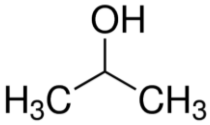

Figure 7.1 Chemical structure of isopropyl alcohol [www.sigmaaldrich.com]

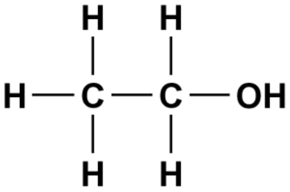

Figure 7.2 Chemical structure of ethanol [www.sigmaaldrich.com]

Before implementing ZnO nanoparticles into the solvent-modified epoxy, it is necessary to test the chemical reaction of solvents with the epoxy. Araldite GY251 and hardener HY956 in weight ratio 5:1 were used to fabricate the epoxy base. Epoxy and hardener were mechanically mixed for 10mins and the resin mixture was mechanically mixed with each solvent for another 5mins. All samples were cured in laboratory with room temperature at 23℃, pressure at 750mmHg and humidity at 45%RH for 24hours prior to characterization and analyses. Nine samples with different combination of solvents and weight contents mixed with epoxy were shown in ***Table 7.2***.

Table 7.2 Combinations of nine samples being tested

Sample Group	*Solvent*	*Weight Content (wt.%)*
0	None	0
1	Ethanol	10
2	Ethanol	20
3	Ethanol	40
4	Ethanol	60
5	Isopropyl alcohol	10
6	Isopropyl alcohol	20
7	Isopropyl alcohol	40
8	Isopropyl alcohol	60

After the XRD test on solvent-modified epoxy, ZnO nanoparticles were mixed with isopropyl alcohol modified epoxy to be the second last matrix layer of glass fibre epoxy (GF/EP) composite laminated with five layers of plain woven E-glass fabric. All samples were made by hand lay-up fabrication technique and were also cured in laboratory with room temperature at 23°C, pressure at 750mmHg and humidity at 45%RH for 24hours prior to characterization and analysis. Nine samples with different combination of solvents and ZnO nanoparticle weight contents mixed with epoxy were shown in ***Table 7.3***.

Table 7.3 Combinations of nine samples being tested

Sample Group	*Solvent*	*Weight Content of ZnO nanoparticle (wt.%)*
0	None	0
1	20 wt.% Isopropyl alcohol	4
2	20 wt.% Isopropyl alcohol	12
3	20 wt.% Isopropyl alcohol	20
4	20 wt.% Isopropyl alcohol	40
5	None	4
6	None	12
7	None	20
8	None	40

7.1.1.2 Results and Discussion

7.1.1.2.1 Crystallography

Based on ***Figure 7.3*** and ***Figure 7.4*** representing the XRD diffractograms of neat epoxy and 20 wt.% isopropyl alcohol/epoxy respectively, second excitation peak of epoxy without solvent modification is located at the diffraction angle of 17.84degree with intensity of 6360cps. Comparing that of 20 wt.% isopropyl alcohol/epoxy is not varied much which is located at 19.84degree but its intensity is two times lower. First and third excitation peak of neat epoxy are located at 3.6degree and 43.32degree with intensity of 2500cps and 1461cps.

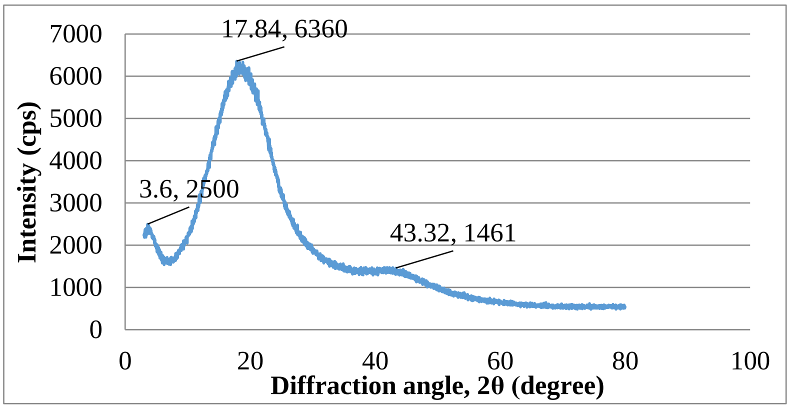

Figure 7.3 XRD diffractogram of neat epoxy

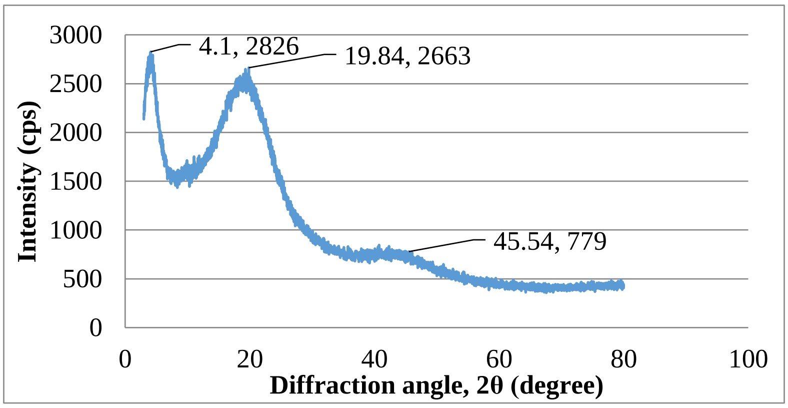

Figure 7.4 XRD diffractogram of 20 wt.% isopropyl alcohol/epoxy

All the excitation peaks of 20 wt.% isopropyl alcohol/epoxy are slightly shifted towards higher degree with 0.5 to 2.22degree or 5-14% variation. The variation percentage is increasing from the first to the third excitation peak. The characteristic of epoxy is being modified by isopropyl alcohol according to the change of intensity value and peak position. However, the change of 20 wt.% isopropyl alcohol/epoxy is the least among all samples being tested. Therefore, 20 wt.% isopropyl alcohol is the appropriate amount for modifying epoxy without influencing much of its crystalline structure which interfere its physical and mechanical properties. This amount is implemented into epoxy and filled into glass fibre epoxy composite for testing its dispersion condition and UVR absorbability subsequently.

7.1.1.2.2 Surface Morphology

SEM images with 500x magnification shown in ***Figure 7.5*** and ***Figure 7.6*** were captured from the fractured surface of neat GF/EP composite and 20 wt.% ZnO/20 wt.% isopropyl alcohol/GF/EP composite.

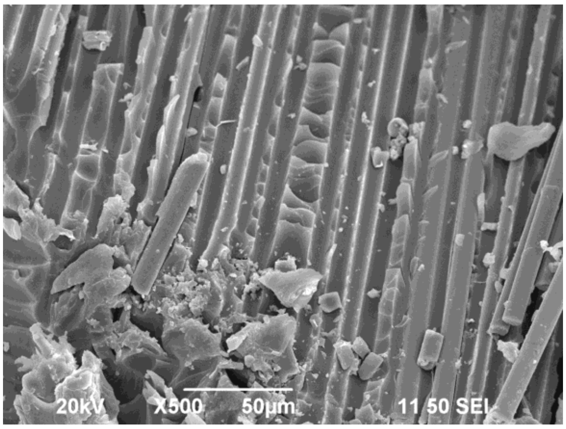

Figure 7.5 SEM image of the neat GF/EP composite

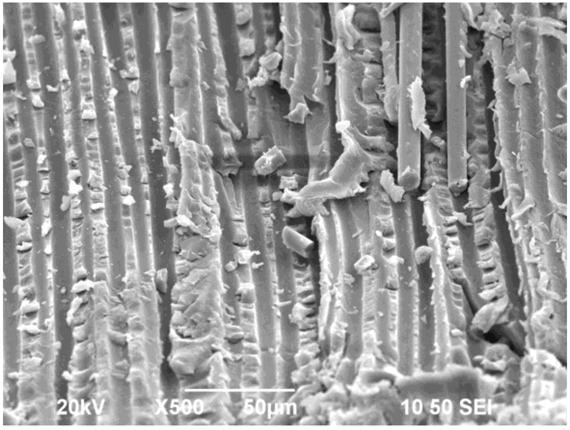

Figure 7.6 SEM image of 20 wt.% 100nm ZnO/20 wt.% isopropyl alcohol/GF/EP composite

From the observation, the stripped pattern, which is created from the shear of matrix by the pull out of fibres under loads, represents the strength of adhesive and fracture of the fibre polymer composite. Comparing the two figures, more uniform stripped patterns are observed on the fracture surface of epoxy of GF/EP composite with 20 wt.% ZnO nanoparticle and 20 wt.% isopropyl alcohol than the neat GF/EP composite. These indicate the reinforcement and the uniform dispersion of ZnO nanoparticles were effectively proceeded.

The fractured cross section of GF/EP composite with 20 wt.% ZnO nanoparticle and 20 wt.% isopropyl alcohol is shown in ***Figure 7.7***. The bonding behaviour between the glass fibres and the epoxy resin is good as the epoxy resin is fully filled between glass fibres and the fibre fracture is obviously seen. ZnO nanoparticles are uniformly dispersed in epoxy and make a good bonding property between fibre and epoxy.

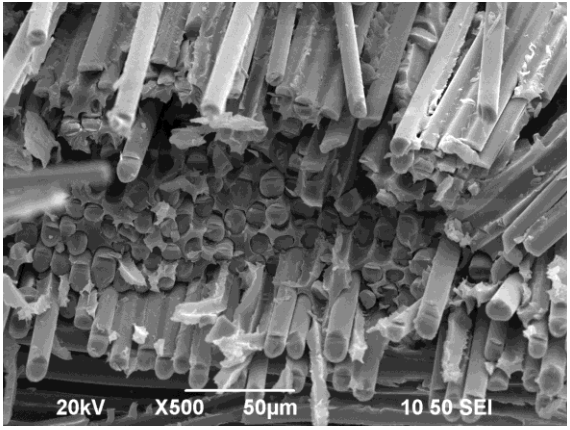

Figure 7.7 SEM image of 20 wt.% 100nm ZnO/20 wt.% isopropyl alcohol/GF/EP composite

7.1.2 Mechanical Mixing Effects in Zinc Oxide/Epoxy

7.1.2.1 Background

Each HGF with outer and inner diameters of 125µm and 100µm respectively were filled with epoxy mixed with different weight contents, 2 wt.%, 4 wt.%, 5 wt.% and 7 wt.%, of ZnO nanoparticle. Araldite GY251 and hardener HY956 in weight ratio 5:1 were used to fabricate the epoxy base. ZnO nanoparticles and epoxy resin were mechanically mixed for 10mins and the resin mixture were mechanically mixed with hardener for another 5mins. No solvent was used and only mechanical stirring, the primitive mixing method, was utilized in the particle dispersion process.

Vacuum infiltration technique was used to fill the matrix inside the HGFs and the HGFs were placed at different intervals in epoxy to form a lamina. The setup of vacuum infiltration is shown in ***Figure 7.8***, one end of the samples was immersed in a resin solution and the other end is exposed to a vacuum chamber to create a negative pressure to take in the solution into the HGF.

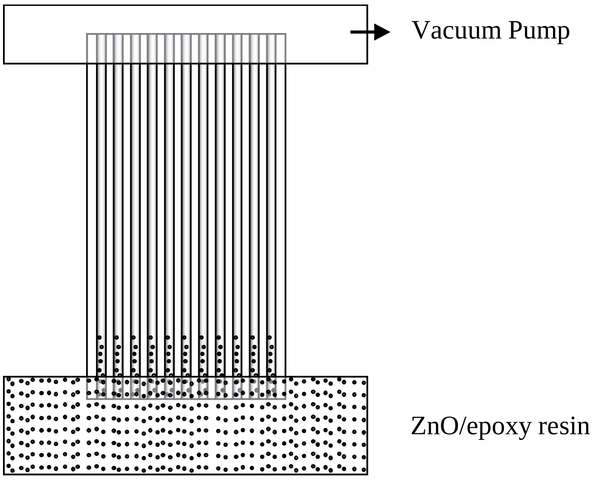

Figure 7.8 Set up of vacuum infiltration technique

Vacuum pump with the total ultimate vacuum pressure of 2Pa was applied constantly for 10mins to ensure a full infiltration in the HGF. All samples were cured in laboratory with room temperature at 23℃, pressure at 750mmHg and humidity at 45%RH for 24hours prior to characterization and analysis. The sample size was made into a dimension of 50mm (l)*30mm (w)*2mm (t). All samples shown in ***Table 7.4*** were broken into two halves and were characterized the fractured cross section of ZnO/epoxy filled inside the HGFs.

Table 7.4 Combinations of fifteen samples being tested

		Interval of HGFs		
		0.2 mm	***0.5 mm***	***1.5 mm***
Weight content of ZnO nanoparticle	–	Control sample 1	Control sample 2	Control sample 3
	2 wt.%	Sample 4	Sample 5	Sample 6
	4 wt.%	Sample 7	Sample 8	Sample 9
	5 wt.%	Sample 10	Sample 11	Sample 12
	7 wt.%	Sample 13	Sample 14	Sample 15

7.1.2.2 Results and Discussion

7.1.2.2.1 Surface Morphology

SEM images with 70x magnification of the cross section of 4 wt.% ZnO/HGF and 7 wt.% ZnO/HGF laminas at 0.5mm interval of HGFs are shown in ***Figure 7.9*** and ***Figure 7.10***. A smooth surface is found on the fracture surface of 4 wt.% ZnO/epoxy inside the HGFs but a rough surface is found on the fracture surface of 7 wt.% ZnO/epoxy inside the HGFs. Particle agglomeration is happened in 7 wt.% ZnO/epoxy at the upstream section inside the HGFs.

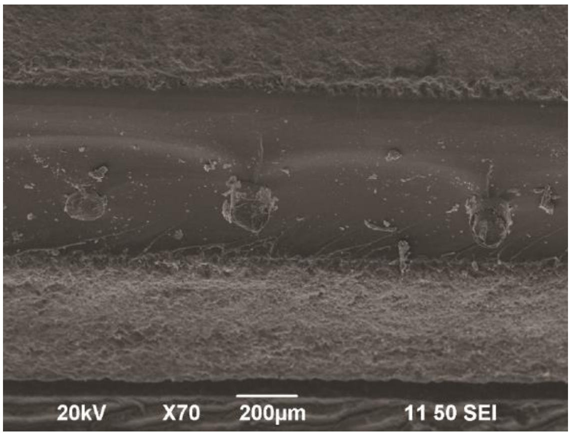

Figure 7.9 SEM image of the cross section 4 wt.% 100nm ZnO/HGF lamina at 0.5mm interval of HGFs

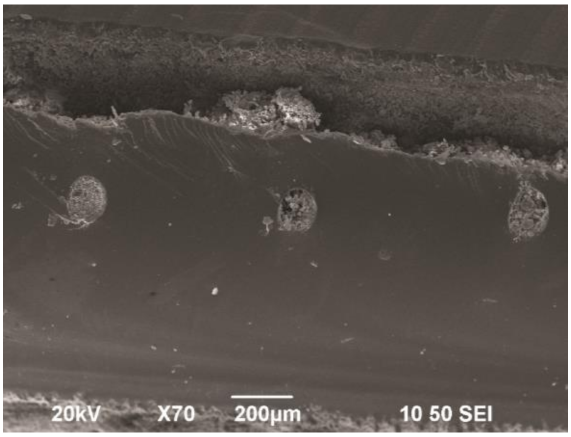

Figure 7.10 SEM image of the cross section of 7 wt.% 100nm ZnO/HGF lamina at 0.5mm interval of HGFs

An EDX examination was conducted to test the chemical content of both resin matrices inside the HGFs. Zn element was not found on the fracture surface of 7 wt.% ZnO/epoxy inside the HGFs. This happened is because ZnO nanoparticles formed into clusters and prevented the flow of ZnO/epoxy resin to be fully filled the HGFs. ***Figure 7.11*** illustrates the phenomenon.

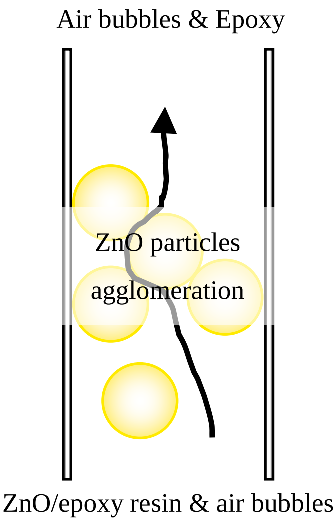

Figure 7.11 Schematic diagram of the infiltration condition of ZnO/epoxy resin in HGF with particle agglomeration occurred

The spaces between ZnO clusters allow only air bubbles and epoxy resin to pass through. Since the resin solution was not in laminar flow after passing through the ZnO clusters, therefore after curing a rough surface was found on the fracture surface of 7 wt.% ZnO/epoxy inside the HGFs.

7.1.3 Ultrasonication Effects in Zinc Oxide/Epoxy and Silane-doped Zinc Oxide/Epoxy

7.1.3.1 Background

Two types of ZnO nanoparticles were tested, one was in a diameter of 100nm and one was in a diameter of 20nm with a surfactant of silane coupling agent. Their crystal structures and apparent densities, 0.560g/cm^3 of 100nm ZnO particle and 0.532g/cm^3 of 20nm silane-doped ZnO particle, which present their deformability, are similar. Both of them are in spherical shape and in white colour. The surface area of a 100nm ZnO particle is 31.42fm^2 which is 25 times larger than a 20nm silane-doped ZnO particle. A 100nm ZnO particle has 25 times larger contact surface area with epoxy molecules during processing. A 20nm ZnO particles is coated with silane coupling agent (KH550) with the weight ratio of 99:1.

Each HGF with outer and inner diameters of 125µm and 100µm respectively were filled with epoxy mixed with different weight contents, 2 wt.%, 4 wt.% and 7 wt.%, of ZnO nanoparticle**.** Araldite GY251 and hardener HY956 in weight ratio 5:1 were used to fabricate the epoxy base. ZnO nanoparticles and epoxy resin were ultrasonicated for 20mins and the resin mixture were mechanically mixed with hardened for another 5mins. No solvent was used in the dispersion process.

Vacuum infiltration technique was used to fill the matrix inside the HGF. The set up of vacuum infiltration is the same as described in ***section 7.1.2.1***. Vacuum pump with the total ultimate vacuum pressure of 2Pa was applied constantly for 10mins to ensure a full infiltration in the HGF of 100mm long. All samples were cured in laboratory with room temperature at 23°C, pressure at 750mmHg and humidity at 45%RH for 24hours prior to characterization and analysis. ***Table 7.5*** shows the seven samples being tested.

Table 7.5 Combinations of seven samples being tested

		Type of ZnO nanoparticle	
		100nm ZnO	***20nm silane-doped ZnO***
Weight content of ZnO nanoparticle	–	Control sample 1	
	2 wt.%	Sample 2	Sample 3
	4 wt.%	Sample 4	Sample 5
	7 wt.%	Sample 6	Sample 7

7.1.3.2 Results and Discussion

7.1.3.2.1 Surface Morphology

Particle dispersion is the reciprocation of the intermolecular strength between nanoparticle–nanoparticle, nanoparticle–epoxy molecular and epoxy molecule–epoxy molecule. Two major mechanisms for particle dispersion in a medium are electrostatics and steric stabilization which are physical and kind of chemical reaction respectively.

Ultrasonication is the physical electrostatic technique and it is commonly used for particle dispersion. Ultrasound induces high frequency in the medium to interact with the bonding strength between elements and separate the elements apart once the frequency is high enough to break the electrostatic bonds. The intensity and time is the determinants for the effectiveness of dispersion by using ultrasonication. Silane surface treatment of ZnO particle is the steric stabilization. Common silane coupling agents on ZnO were introduced in ***section 2.6.5*** and there are more different capping agents on ZnO were studied for the dispersion behaviour in polymer [Diallo et al., 2016; Nguyen et al., 2015; Tang et al., 2006; Yan et al., 2015; Zhang et al., 2013]. Silane-doped on ZnO particle is proven to be capable to reduce particle agglomeration because it increases negative charges, OH^-, on the surface of ZnO particle which increases the magnitude of repulsive force between ZnO particle–ZnO particle to overcome their hydrogen bond and improves the bonding strength between ZnO particle–epoxy molecule simultaneously. ***Figure 7.12*** indicates how silane works on ZnO particles for particle dispersion. The concentration and doping method of silane coupling agent-doped on the ZnO particle is the determinant for the effectiveness of particle dispersion.

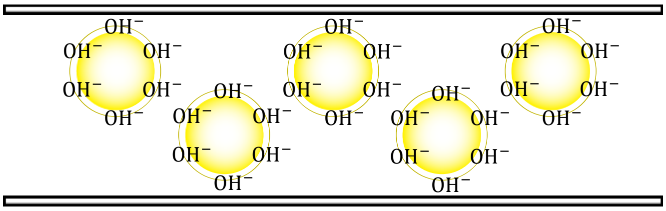

Figure 7.12 Schematic diagram shows the function of silane surfactant on ZnO particle

The dispersion characteristics of different contents of 100nm ZnO particle and 20nm silane-doped ZnO particle in epoxy inside the HGF are shown in ***Figure 7.13, Figure 7.14, Figure 7.15 and Figure 7.16***. Epoxy mixed with different contents of 100nm ZnO particle and 20nm silane-doped ZnO particle inside the HGF are opaque. 4 wt.% 100nm ZnO and 20nm silane-doped ZnO particles have the same degree of uniform and dense dispersion in epoxy inside the HGF. Contrarily, 2 wt.% 100nm ZnO and 20nm silane-doped ZnO particles are loosely dispersed in epoxy inside the HGF at the same degree. Particle agglomeration are occurred in 7 wt.% 100nm ZnO/epoxy and 7 wt.% 20nm silane-doped ZnO/epoxy. However, the particle agglomeration in 7 wt.% 100nm ZnO/epoxy is severer than 7 wt.% 20nm silane-doped ZnO/epoxy.

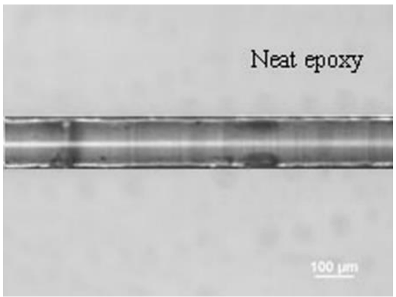

Figure 7.13 Particle dispersion of neat epoxy inside micron HGF

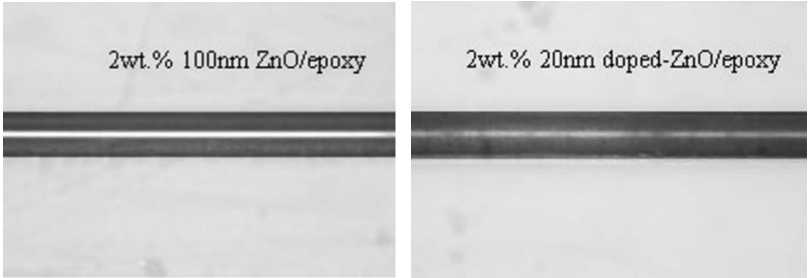

Figure 7.14 Particle dispersion of 2 wt.% 100nm ZnO/epoxy (left) and 2 wt.% 20nm silane-doped ZnO/epoxy (right) inside micron HGF

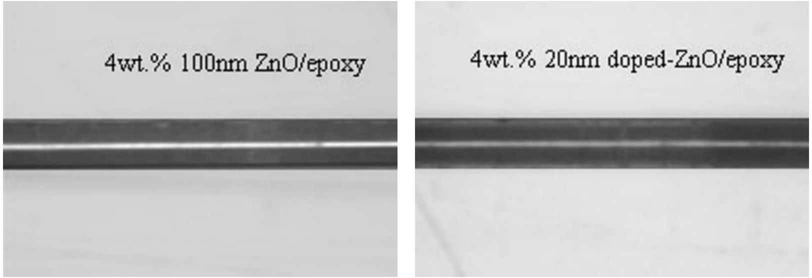

Figure 7.15 Particle dispersion of 4 wt.% 100nm ZnO/epoxy (left) and 4 wt.% 20nm silane-doped ZnO/epoxy (right) inside micron HGF

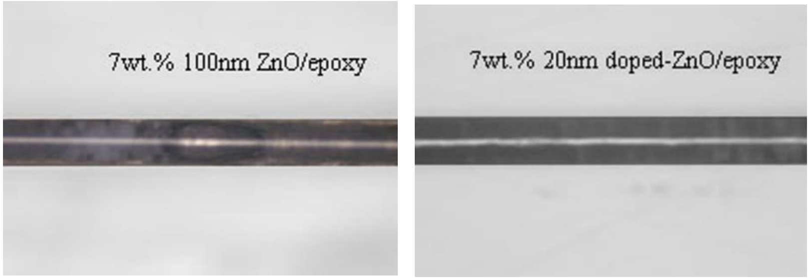

Figure 7.16 Particle dispersion of 7 wt.% 100nm ZnO/epoxy (left) and 7 wt.% 20nm silane-doped ZnO/epoxy (right) inside micron HGF

After the same intensity and time of ultrasonication of ZnO nanoparticles in epoxy, the fluid mixture was filled into the HGF subsequently under the same vacuum pressure and flowed against the wall fraction of the HGF. The weight ratio of ZnO nanoparticle:epoxy molecule is the only factor changed making alternation to the dispersion of particles. 2 wt.% ZnO/epoxy, 4 wt.% ZnO/epoxy and 7 wt.% ZnO/epoxy are in the ratio of 1:49, 1:24 and 1:13 respectively. It is suggested that the ratio of ZnO nanoparticle:epoxy at the ratio around 1:24 is good for particle dispersion in the HGF. The size effect of spherical ZnO nanoparticle is not a critical factor in this case. Silane surfactant shows its effect in the resin fluid at high content of ZnO nanoparticles. At 7 wt.% ZnO/epoxy inside the HGF, the 100nm ZnO particle without silane surfactant has severer agglomeration than the 20nm ZnO particle doped with silane surfactant.

7.2 Processing of Zinc Oxide Nanoparticles in Epoxy

In fabricating ZnO/HGF lamina, besides particle dispersion, the process of resin infiltration and curing are implemented. The factors along with the two processes are concerned including the rheology properties of ZnO/epoxy resin infiltrated into HGF and polymerization shrinkage of ZnO/epoxy cured inside HGF which are discussed in the following two sections, ***section 7.2.1*** and ***section 7.2.2***.

7.2.1 Rheology Properties of Zinc Oxide/Epoxy

7.2.1.1 Background

Two types of ZnO nanoparticle with different weight contents, 2 wt.%, 4 wt.% and 7 wt.%, mixed with epoxy and neat epoxy resin were prepared for studying their rheology properties. Two types of ZnO nanoparticles were described in ***section 7.1.3.1***. Araldite GY251 and hardener HY956 in weight ratio 5:1 were used to fabricate the epoxy base. ZnO nanoparticles were mixed with epoxy resin by using ultrasonication for 20mins and the resin mixture were mixed with hardened for another 5mins by using mechanical stirring at the same period of time, room temperature at 23℃ and pressure at 750mmHg. All samples were kept at 0-3℃ after mixing to ensure the rheology tests were conducted within their pot life. ***Table 7.6*** shows the seven samples being tested.

Table 7.6 Combinations of seven samples being tested

		Type of ZnO nanoparticle	
		100nm ZnO	***20nm silane-doped ZnO***
Weight content of ZnO nanoparticle	–	Control sample 1	
	2 wt.%	Sample 2	Sample 3
	4 wt.%	Sample 4	Sample 5
	7 wt.%	Sample 6	Sample 7

Each sample was placed between two parallel plane plates with circular geometry, the diameter of 25mm and the gap distance of 1mm under isothermal condition at the temperature of 25℃.

Polymer rheology is the study of the deformation and the flow of polymeric fluid. Shear stress and shear viscosity are the two major characteristics to be obtained in the rheology tests for understanding the rheology properties of polymeric fluid. Yield stress is obtained at zero or low applied shear stress which the yield stress of a fluid exhibits solid or gel-like behaviour and starts flowing in plastic deformation once exceeding a certain threshold of shear stress. Shear viscosity of a fluid is the measurement of resistance that is the intermolecular friction exerted within layers of fluid to gradual deformation by the applied shear stress. Initial, plateau and critical viscosities are concerned from the analysis. Initial viscosity is the viscosity at zero shear rate. Critical viscosity is the viscosity right before the large The concentration of ZnO nanoparticle alters the intermolecular forces between nanoparticle–nanoparticle, nanoparticle–epoxy molecule and epoxy molecule–epoxy molecule in the fluid. The interaction between elements in the fluid has significant effects on the flowing characteristics of the fluid especially inside the micron HGF. The shear stress and shear viscosity of all fluid samples were evaluated along the shear rate from 0 to 250s^{-1} and the shear rate is in log scale for easy evaluation.

7.2.1.2 Results and Discussion

Rheology properties of different ZnO/epoxy resins were studied to understand the disturbance of infiltration in the dispersion of ZnO nanoparticle in epoxy inside the 100µm HGF. Since vacuum infiltration imposes a shear stress on the resin to fully filled inside the HGF whilst rheology test also uses shearing technique for the analysis of fluid flow. ***Figure 7.17*** and ***Figure 7.18*** show the shear stress and shear viscosity against shear rate in log scale of different resin.

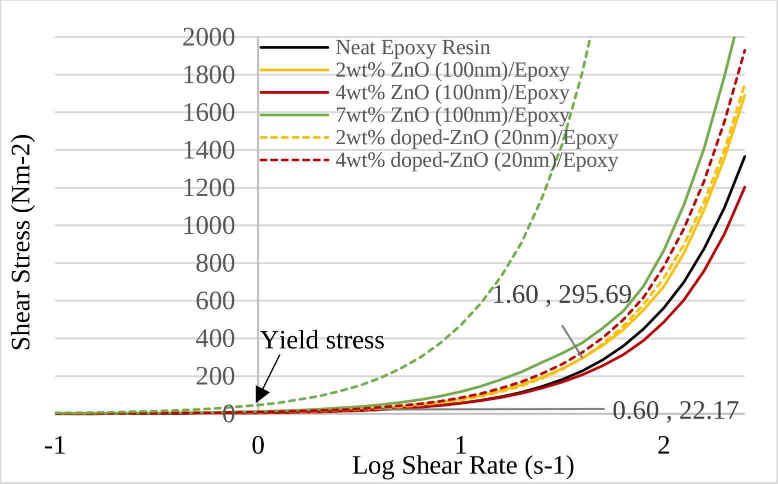

Figure 7.17 Shear stress against shear rate of different resin

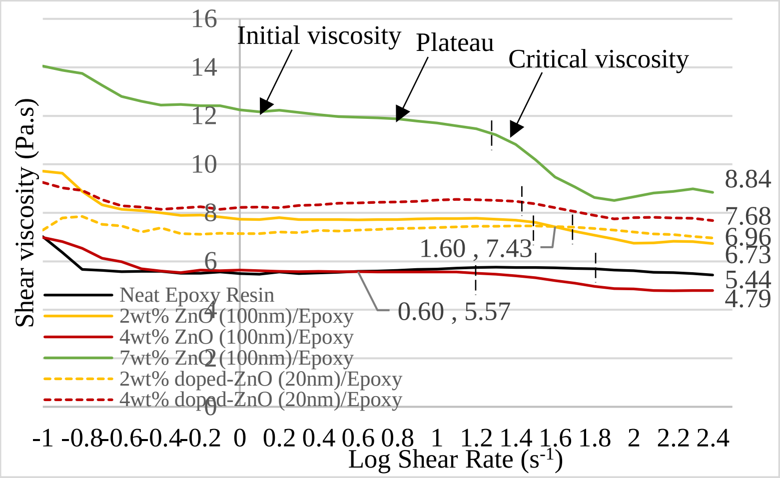

Figure 7.18 Shear viscosity against shear rate of different resin (without showing 7 wt.% 20nm silane-doped ZnO/epoxy resin)

Yield stress and best-fit exponential curve of each resin are presented in ***Table 7.7***. Initial and critical viscosities of all resin are presented in ***Table 7.8***. It is also required to refer the information provided in ***section 6.2*** about the attractive forces between integrated elements in ZnO/polymer resin inside HGF.

Table 7.7 Yield stress and best-fit exponential curve of all resin

		Type of ZnO nanoparticle	
		100nm ZnO	***20nm silane-doped ZnO***
Weight content of ZnO nanoparticle	–	5.7138Nm^{-2} $y = 5.7138e^{2.2892x}$ $(R^2 = 0.9997)$	
	2 wt.%	8.1078Nm^{-2} $y = 8.1078e^{2.2298x}$ $(R^2 = 0.9997)$	7.3531Nm^{-2} $y = 7.3531e^{2.2942x}$ $(R^2 = 0.9999)$
	4 wt.%	5.8189Nm^{-2} $y = 5.8189e^{2.2225x}$ $(R^2 = 0.9997)$	8.4474Nm^{-2} $y = 8.4474e^{2.275x}$ $(R^2 = 0.9998)$
	7 wt.%	12.384Nm^{-2} $y = 12.384e^{2.1623x}$ $(R^2 = 0.9994)$	46.2Nm^{-2} $y = 46.2e^{2.2744x}$ $(R^2 = 0.9994)$

Table 7.8 Initial and critical viscosities of all resin

		Type of ZnO nanoparticle	
		100nm ZnO	***20nm silane-doped ZnO***
Weight content of ZnO nanoparticle	–	5.49Pa·s (initial) 5.71Pa·s (critical)	
	2 wt.%	7.73Pa·s (initial) 7.61Pa·s (critical)	7.15Pa·s (initial) 7.40Pa·s (critical)
	4 wt.%	5.64Pa·s (initial) 5.51Pa·s (critical)	8.23Pa·s (initial) 8.51Pa·s (critical)
	7 wt.%	12.25Pa·s (initial) 11.46Pa·s (critical)	46.27Pa·s (initial) 47.57Pa·s (critical)

In general, epoxy resin mixed with silane-doped ZnO nanoparticles requires higher yield stress to start the fluid flow and higher shear stress to move the resin for continuous flow. At lower content of 2 wt.% ZnO nanoparticle, epoxy resin mixed with silane-doped ZnO nanoparticles requires lower shear stress to move the resin for continuous flow but it requires higher shear stress after the shear rate at $1.6s^{-1}$ compared to the epoxy resin mixed with undoped ZnO nanoparticles. This indicates silane surfactant on ZnO nanoparticle is able to help achieving a good dispersion of ZnO nanoparticles in epoxy resin and slightly lower shear stress is required to move the resin for continuous flow. Undoped ZnO nanoparticle is able to meet a stable and lower shear stress requirement in epoxy resin for continuous flow compared to all the ZnO/epoxy resin.

4 wt.% ZnO nanoparticle without silane surfactant mixed with epoxy resin requires the lowest shear stress for continuous flow compare to all the ZnO/epoxy resin. Low shear stress requirement of 4 wt.% ZnO/epoxy resin is comparable to neat epoxy resin. 4 wt.% ZnO/epoxy resin achieves the lowest shear stress after the shear rate at $0.6s^{-1}$ among all resin.

7 wt.% ZnO nanoparticle with or without silane surfactant mixed with epoxy resin

requires the highest shear stress for continuous flow among all resin. Particle agglomeration is suggested to be happened and alters the resin flow to become more difficult.

Concerning the 4 wt.% ZnO/epoxy resin, ***Figure 7.19*** shows their shear stress against shear rate without log scale. 4 wt.% 20nm silane-doped ZnO/epoxy and 4 wt.% 100nm undoped ZnO/epoxy resin are classified as Pseudo plastic fluid which exhibits shear thinning behaviour under shear strain as indicated in ***Figure 7.20*** since their flow are increasing vigorously at low shear rate and increasing gradually along the increasing shear rate. At higher shear rate, the fluid flow is nearly linear and best-fit linear curve are drawn from 4 wt.% 20nm silane-doped ZnO/epoxy and 4 wt.% 100nm undoped ZnO/epoxy resin. The initial shear stress of 4 wt.% 20nm silane-doped ZnO/epoxy resin is around 45% higher than 4 wt.% 100nm undoped ZnO/epoxy resin which are 8.4474Nm^{-2} and 5.8189Nm^{-2} respectively. Their grow of shear stress is further apart along the increasing shear rate. At higher shear rate of 100s^{-1} (102s^{-1}), 4 wt.% 20nm silane-doped ZnO/epoxy resin requires higher shear stress of 780.84Nm^{-2} which is around 60% higher than 4 wt.% 100nm undoped ZnO/epoxy resin that requires lower shear stress of 486.03Nm^{-2} for fluid flow. At the highest shear rate of 250s^{-1} (10$^{2.4}$s^{-1}) in this rheology test, the required shear stress of 4 wt.% 20nm silane-doped ZnO/epoxy resin is also around 60% higher than 4 wt.% 100nm undoped ZnO/epoxy resin which are 1929.58Nm^{-2} and 1202.93Nm^{-2} respectively. Silane surfactant on ZnO nanoparticles contributes at around 45 to 60% higher of required shear stress for the fluid flow of epoxy resin along higher shear rate from 0 to 250s^{-1}.

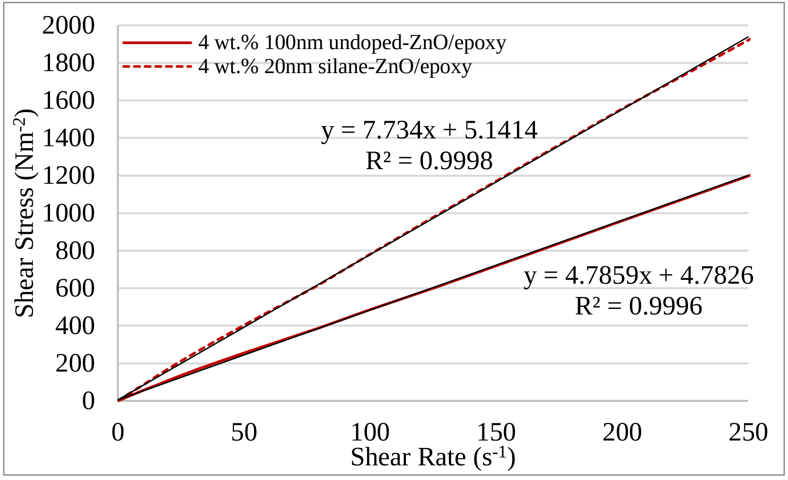

Figure 7.19 Shear stress against shear rate of 4 wt.% ZnO/epoxy resin

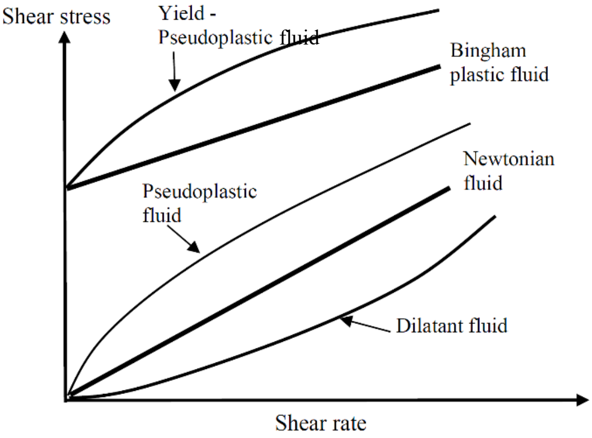

Figure 7.20 Different types of time independent non-Newtonian fluid

According to ***Figure 7.18*** and ***Table 7.8***, on the whole, the grow of viscosity of epoxy resin mixed with 20nm silane-doped ZnO nanoparticles is increasing which behave similar to the neat epoxy resin. The increasing slope is steeper with the increasing of weight content of ZnO nanoparticles. Contrarily, the grow of viscosity of epoxy resin mixed with 100nm undoped ZnO nanoparticles is decreasing. The decreasing slope is steeper with the increasing of weight content of ZnO nanoparticles. Furthermore, after critical viscosity, the drop of viscosity of 100nm undoped ZnO/epoxy resin is sharper than 20nm silane-doped ZnO/epoxy resin at the same weight content of ZnO nanoparticle. Silane surfactant on ZnO nanoparticles is able to stabilize the characteristics of fluid flow of epoxy resin with the implementation of ZnO nanoparticles.

High shear viscosity of ZnO/epoxy resin is contributed by the higher intermolecular friction within fluid layers as the friction surface is increased and intermolecular bond is stronger between ZnO nanoparticles and epoxy molecules in the presence of high content of ZnO nanoparticle and silane surfactant on ZnO nanoparticles. High shear stress is required to overcome the yield stress and start the flow of ZnO/epoxy resin with high viscosity. Resin fluid with low viscosity is preferable for saving energy use and offering cost effectiveness in manufacturing. In addition, ZnO/epoxy resin with viscosity along the plateau of curve is favourable for manipulating as the change of viscosity is steady along the plateau. However, the range of plateau is shortened when the weight content of ZnO nanoparticle mixed with epoxy resin is increasing.

The variation of the results of viscosity is similar to the results of shear stress. As mentioned in ***section 7.1.3.1***, a 100nm ZnO particle has 25 times larger contact surface area with epoxy molecules during processing than a 20nm silane-doped ZnO particle. They have similar densities of 0.560g/cm^3 and 0.532g/cm^3 of 100nm ZnO and 20nm silane-doped ZnO particle respectively and the volume ratio of 100nm ZnO:20nm silane-doped ZnO is 125:1. Under the same weight content of ZnO nanoparticle in epoxy resin, the total surface area ratio of 100nm undoped ZnO:20nm silane-doped ZnO in contact with epoxy molecule is 1:5. And referring to the results obtained from shear stress, silane surfactant on ZnO nanoparticles contributes at around 45 to 60% higher of required shear stress for the fluid flow of epoxy resin along higher shear rate from 0 to 250s^{-1}. This indicates that the silane surfactant on ZnO nanoparticle restricts the fluid flow at 1.6 times higher than the ZnO nanoparticle without silane. At the same weight content of 2 wt.%

ZnO nanoparticle, the viscosity of 20nm silane-doped ZnO/epoxy resin is slightly lower than 100nm undoped ZnO/epoxy resin which are 7.15-7.40Pa·s and 7.73-7.61Pa·s respectively as shown in ***Table 7.8***. This implies that the weight content of 2 wt.% ZnO nanoparticle or the weight ratio of 1:49 of ZnO:epoxy causing the surface friction or intermolecular force between silane surfactant or ZnO nanoparticles and epoxy molecule is insufficient to have negative influence in the shearing flow of 2 wt.% silane-doped ZnO/epoxy resin. At 4 wt.% ZnO nanoparticle, the viscosity of 20nm silane-doped ZnO/epoxy resin is around 0.5 times higher than 100nm undoped ZnO/epoxy resin which are 8.23-8.51Pa·s and 5.64-5.51Pa·s listed in ***Table 7.8***. At 7 wt.% ZnO nanoparticle, the difference of viscosity of 20nm silane-doped ZnO/epoxy resin is even higher which is around 4 times higher than 100nm undoped ZnO/epoxy resin. the viscosities of 20nm silane-doped ZnO/epoxy resin and 100nm undoped ZnO/epoxy resin range from 46.27-47.57Pa·s and 12.25-11.46Pa·s respectively referred to ***Table 7.8***.

The implementation of silane surfactant is able to stabilize the fluid flow of ZnO/epoxy resin, the ZnO/epoxy resin with the lowest viscosity is the flavour of the infiltration into HGFs. Comparing two types of ZnO nanoparticles mixed with epoxy resin, 100nm undoped ZnO/epoxy resin is more favourable to achieve lower viscosity and implies that it obtains better dispersion of ZnO nanoparticles in epoxy resin. In infiltration process, vacuum pump with the total ultimate vacuum pressure of 2Pa was applied constantly for 10mins to ensure a full infiltration of resin into the HGF of 100mm long. The applied shear stress of 2Pa·s does not exceed the shear viscosity of 4 wt.% 100nm undoped ZnO/epoxy resin of 6Pa·s. The bonding strength between elements in the resin with lowest viscosity is higher than the applied shear stress. The vacuum infiltration is not able to influence the bonding properties between elements in the resin being tested.

7.2.2 Dimensional Stability of Zinc Oxide/Epoxy in Hollow Glass Fibre

7.2.2.1 Background

Two types of ZnO nanoparticle with different weight contents, 2 wt.%, 4 wt.% and 7 wt.%, mixed with epoxy and neat epoxy resin were prepared for studying their dimensional stability inside HGF. Two types of ZnO nanoparticles were described in ***section 7.1.3.1***. Araldite GY251 and hardener HY956 in weight ratio 5:1 were used to fabricate the epoxy base. ZnO nanoparticles were mixed with epoxy resin by using ultrasonication for 20mins and the resin mixture was mixed with hardened for another 5mins by using mechanical stirring. No solvent was used in the dispersion process.

Each HGF with outer and inner diameters of 125μm and 100μm respectively were filled with ZnO/epoxy resin**.** Vacuum infiltration technique was used to fill the resin mixture inside HGF. The setup of vacuum infiltration is the same as described in ***section 7.1.2.1***. Vacuum pump with the total ultimate vacuum pressure of 2Pa was applied constantly for 10mins to ensure a full infiltration in the HGF of 100mm long. All samples were cured in laboratory with room temperature at 23°C, pressure at 750mmHg and humidity at 45%RH for 24hours prior to characterization and analysis. ***Table 7.9*** shows the seven samples being tested.

Table 7.9 Combinations of seven samples being tested

		Type of ZnO nanoparticle	
		100nm ZnO	***20nm silane-doped ZnO***
Weight content of ZnO nanoparticle	–	Control sample 1	
	2 wt.%	Sample 2	Sample 3
	4 wt.%	Sample 4	Sample 5
	7 wt.%	Sample 6	Sample 7

7.2.2.2 Results and Discussion

7.2.2.2.1 Surface Morphology

Microscopic observation discloses the evidence that the vacuum pressure draws the resin inside the HGF in a convex shape which the middle layer of resin experiences less frictional force and the layers of resin contacting with the inner wall of HGF are greatly exerted by wall friction against their fluid flow. In curing process, resin shrinks, the wall friction helps reducing the shrinkage of resin, however, with less frictional force exerted, the middle layer of resin shrinks in a higher degree. ***Figure 7.21*** shows a schematic diagram describing the infiltration process and curing process of the resin in HGF.

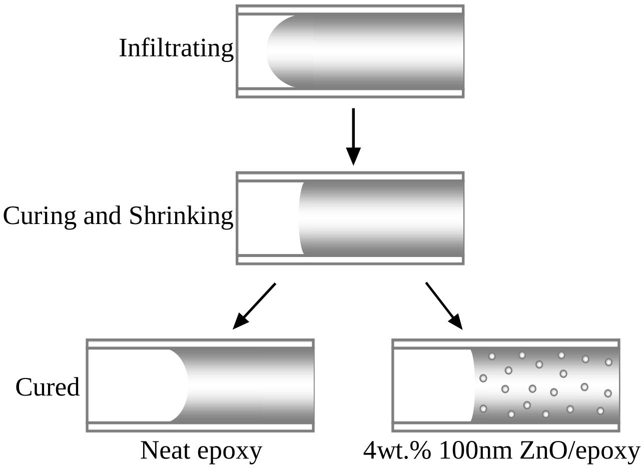

Figure 7.21 Schematic diagram showing the polymerization shrinkage of neat epoxy and 4 wt.% 100nm ZnO/epoxy in micron HGF during curing process

Different degrees of polymerization shrinkage are observed at the end of epoxy resin mixed with difference contents of ZnO nanoparticles inside HGF. The results are shown in ***Figure 7.22, Figure 7.23, Figure 7.24 and Figure 7.25***. The degree of polymerization shrinkage of neat epoxy inside HGF is 45°, 2 wt.% ZnO/epoxy inside HGF is 53°, 4 wt% ZnO/epoxy inside HGF is 55° and 7 wt.% ZnO/epoxy inside HGF is 57°. Without ZnO particles, neat epoxy resin is at 45° with the inner wall surface of HGF. After implementing 2 wt.% ZnO nanoparticle, the polymerization shrinkage of epoxy resin inside HGF is largely reduced of around 18%. 4 wt.% ZnO nanoparticle contribute around 22% enhancement of the dimensional stabilization in epoxy resin inside HGF and 7 wt.% ZnO nanoparticle have the enhancement at around 27%. The implementation of ZnO nanoparticles induces a higher frictional force to infiltration process but it exerts a frictional force on resin against the polymerization shrinkage and this is the dimensional stability of ZnO nanoparticle in polymers during curing process. ZnO nanoparticles in large amount allows to effectively enhance its dimensional stability in polymers, even the particle agglomeration is occurred.

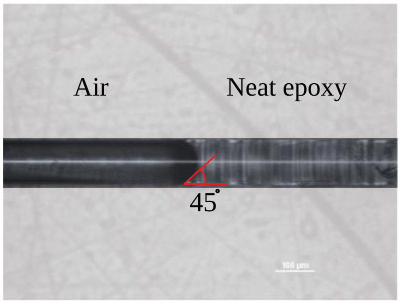

Figure 7.22 Polymerization shrinkage of neat epoxy in micron HGF

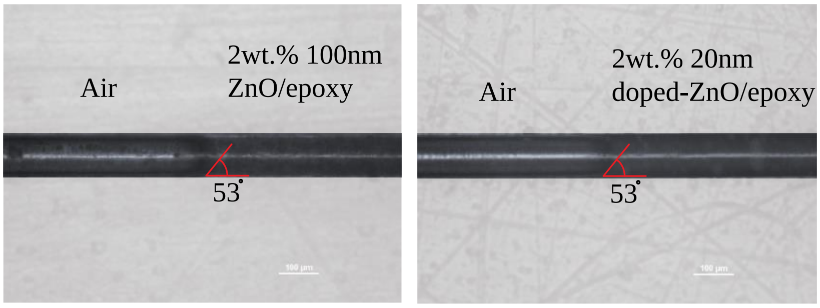

Figure 7.23 Polymerization shrinkage of 2 wt.% 100nm ZnO/epoxy (left) and 2 wt.% 20nm silane-doped ZnO/epoxy (right) in micron HGF

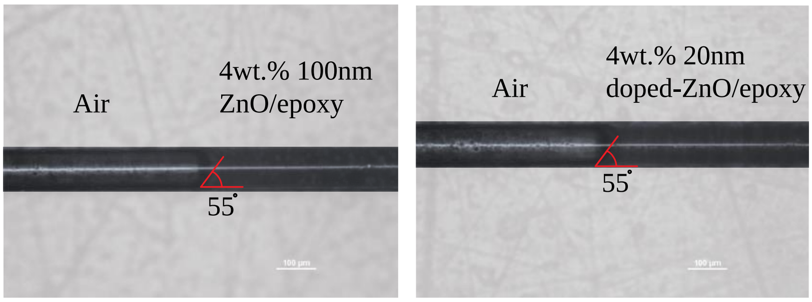

Figure 7.24 Polymerization shrinkage of 4 wt.% 100nm ZnO/epoxy (left) and 4 wt.% 20nm silane-doped ZnO/epoxy (right) in micron HGF

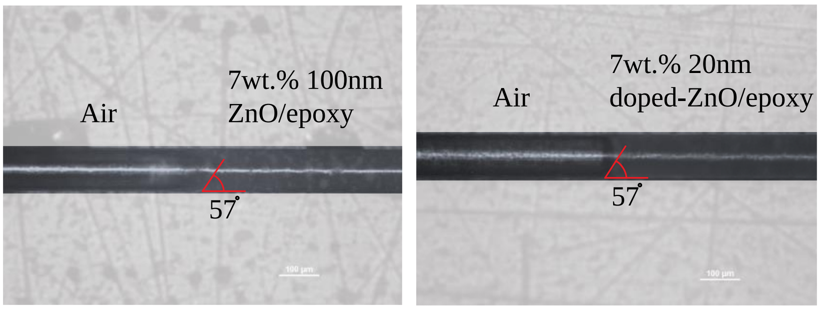

Figure 7.25 Polymerization shrinkage of 7 wt.% 100nm ZnO/epoxy (left) and 7 wt.% 20nm silane-doped ZnO/epoxy (right) in micron HGF

7.3 UVR Absorbability of Zinc Oxide/Polymer Composites

7.3.1 UVR Absorbability of Zinc Oxide/Glass Fibre/Epoxy Composite Using Solvent and Ultrasonication for Zinc Oxide Nanoparticle Dispersion

7.3.1.1 Background

The UVR energy absorbability of zinc oxide/glass fibre/epoxy (ZnO/GF/EP) composites using solvent and ultrasonication for ZnO nanoparticle dispersion were discussed in the following.

100nm ZnO nanoparticle with different contents of 4 wt.%, 12 wt.%, 20 wt.% and 40 wt.% were mixed with 20 wt.% isopropyl alcohol modified epoxy to be the second last matrix layer of GF/EP composite laminated with five layers of plain woven E-glass fabric. 20 wt.% isopropyl alcohol was used for the particle dispersion because it has been tested that it has less influence to the crystalline structure of epoxy which has less influence to the physical and mechanical properties of the composite. Araldite GY251 and hardener HY956 in weight ratio 5:1 were used to fabricate the epoxy base. ZnO nanoparticles and isopropyl alcohol were mixed with epoxy resin by using mechanical stirring for 15mins. All composites were fabricated by hand lay-up technique and cured in laboratory with room temperature at 23℃, pressure at 750mmHg and humidity at 45%RH for 24hours prior to characterization and analysis. ***Figure 7.26*** shows the configuration of the sample. A five layered GF/EP composite without ZnO nanoparticles was the reference sample.

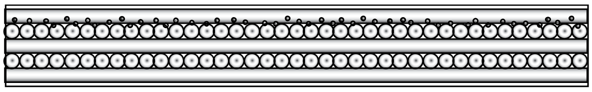

Figure 7.26 ZnO/five-layered GF/EP composite

Another set of composite is 6 wt.% 100nm ZnO/epoxy implemented in between the first three layers of glass fabric of GF/EP composite laminated with twelve layers of plain woven E-glass fabric. Araldite GY251 and hardener HY956 in weight ratio 5:1 were used to fabricate the epoxy base. ZnO nanoparticles in epoxy were ultrasonicated for 20mins and the resin mixture were mechanically mixed with hardener for another 5mins. All composites were also fabricated by hand lay-up technique and cured in laboratory with room temperature at 23℃, pressure at 750mmHg and humidity at 45%RH for 24hours prior to characterization and analysis. ***Figure 7.27*** shows the configuration of the sample. A twelve layered GF/EP composite without ZnO nanoparticles was the reference sample.

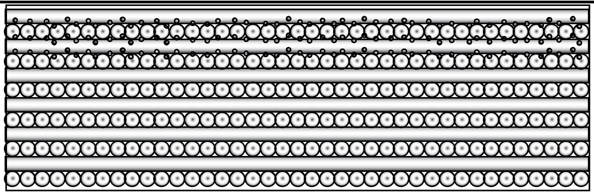

Figure 7.27 ZnO/twelve-layered GF/EP composite

7.3.1.2 Results and Discussion

Referring to ***Figure 2.28***, five layered GF/EP composite has a full UVR energy absorbability in the wavelength range of 190nm to 328.5nm. A sudden drop of UVR energy absorbability at the wavelength of 328.5nm, and it has a gradual declination between the wavelength range of 328.5nm to 400nm with the UVR energy absorbability of around index 2. Without the implementation of ZnO nanoparticles, five layered GF/EP composite has no full UVR absorption in the wavelength range of UVA. Showing in ***Figure 2.29***, after implementing 20 wt.% or 40 wt.% 100nm ZnO nanoparticles using 20 wt.% isopropyl alcohol as solvent for particle dispersion, the ZnO/GF/EP composite has a full UVR energy absorbability for the whole range of UVA, UVB and UVC.

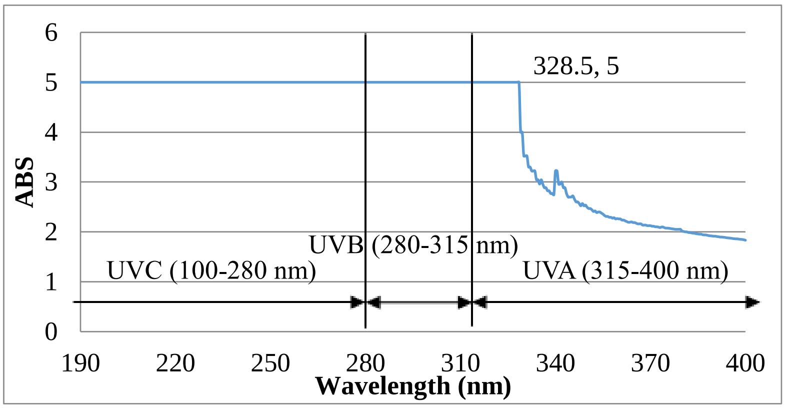

Figure 7.28 UVR energy absorbability of five-layered GF/EP composite without ZnO nanoparticles

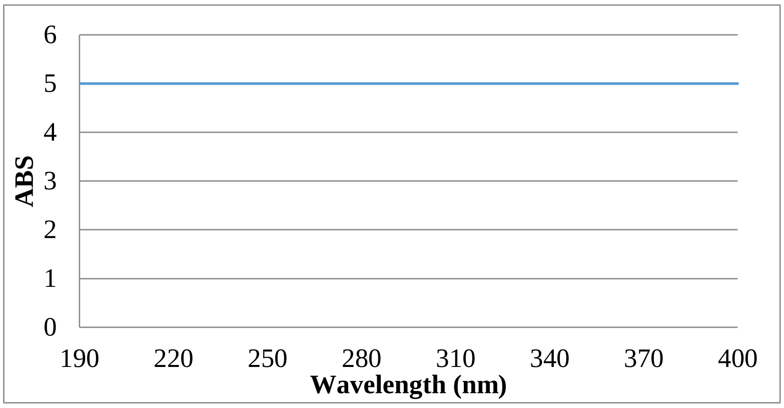

Figure 7.29 UVR energy absorbability of 20 wt.% or 40 wt.% 100nm ZnO/five-layered GF/EP using 20 wt.% of isopropyl alcohol for ZnO nanoparticle dispersion

Figure 7.30 shows a full UVR energy absorbability of twelve layered GF/EP composite without ZnO nanoparticles in the wavelength range of 190nm to 379.5nm. Without the implementation of ZnO nanoparticles, five layered GF/EP composite has no full UVR absorption in the wavelength range of UVA. However, by stacking seven more layers of glass fibres compared to five layered GF/EP composite without ZnO nanoparticles, the UVR energy absorbability of twelve layered GF/EP composite without ZnO nanoparticles is enhanced for around 15%. E-glass fabric has certain UVR energy absorbability and the interface between glass fibre and epoxy resin is attacked by the UVR energy which it absorbs certain amount of UVR energy and less UVR energy is allowed being transmitted through the composite.

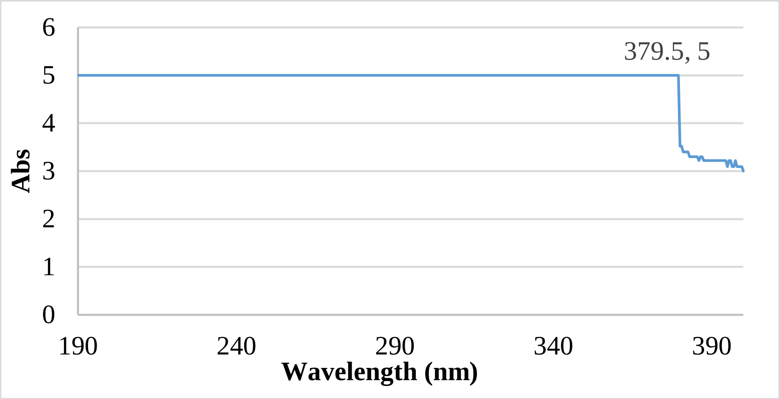

Figure 7.30 UVR energy absorbability of twelve-layered GF/EP composite without ZnO nanoparticles

6 wt.% 100nm ZnO nanoparticle using ultrasonication for particle dispersion is able to achieve a full UVR energy absorbability of the ZnO/GF/EP composite for the whole range of UVA, UVB and UVC. The result is shown in ***Figure 7.31***. By utilizing ultrasonication, uniform dispersion of particles is able to be achieved and a largely reduced amount of ZnO nanoparticle is sufficient for the whole range of full UVR energy absorption.

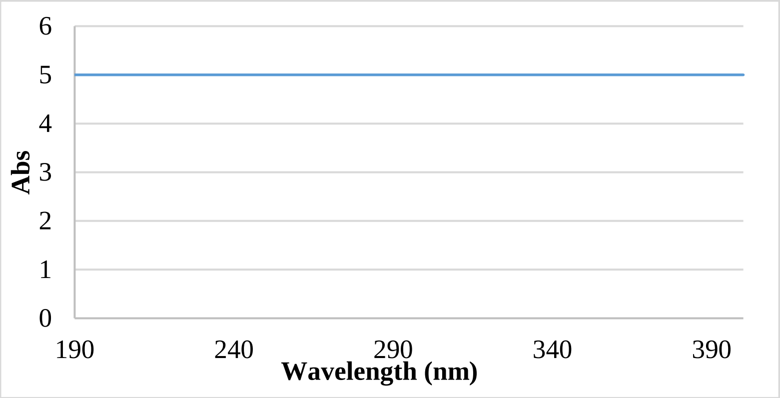

Figure 7.31 UVR energy absorbability of 6 wt.% 100nm ZnO/twelve-layered GF/EP composite using ultrasonication for ZnO nanoparticle dispersion

No full UVA absorption is obtained in silane-doped ZnO/GF/EP composite. The result is shown in ***Figure 7.32***. Although ultrasonication is utilized for particle dispersion and silane surfactant is doped on ZnO nanoparticles, particle agglomeration is still occurred for the small sized nanoparticles. Uniform dispersion of ZnO nanoparticles is one of the crucial factors for achieving a whole range of full UVR energy absorbability of ZnO/GF/EP composite.

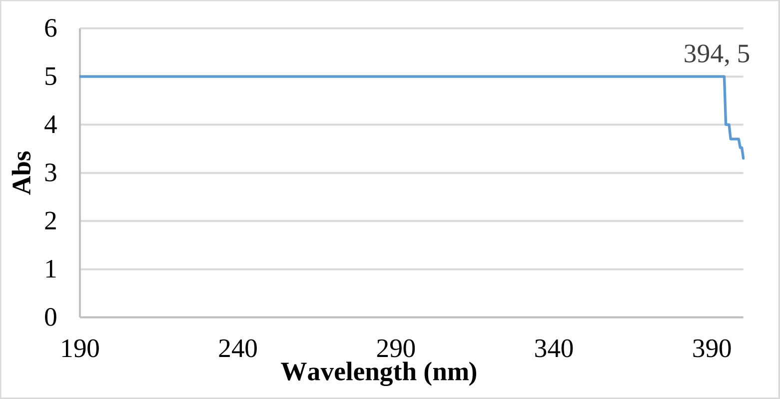

Figure 7.32 UVR energy absorbability of 6 wt.% 20nm silane-doped ZnO/twelve-layered GF/EP composite using ultrasonication for ZnO nanoparticle dispersion

Comparing the physical UVR energy absorption between 100nm ZnO nanoparticle and 20nm silane-doped ZnO nanoparticle and their implementation in GF/EP composite, there are few factors differentiate their UVR absorbabilities. The band gap energy responsible for the physical UVR energy absorption of 100nm ZnO nanoparticle and 20nm silane-doped ZnO nanoparticle are 3.22eV and 3.14eV respectively.100nm ZnO nanoparticle having higher band gap energy contributes higher physical UVR energy absorbability. At the same content of ZnO, the total surface area of 20nm silane-doped ZnO nanoparticles is five times more than 100nm ZnO nanoparticles referring to the calculation discussed in ***section 7.2.1.2***. Moreover, the surface of 20nm ZnO nanoparticle is doped with 1% silane coupling agent. The surface of ZnO nanoparticle delivering scattering effect prevents UVR energy to entre and physically dissipate the energy within the band gap of ZnO atom. The interpretation is further discussed in ***section 7.3.2.2***.

7.3.2 UVR Absorbability of Zinc Oxide/Hollow Glass Fibre Lamina Using Mechanical Mixing and Ultrasonication for Zinc Oxide Nanoparticle Dispersion

7.3.2.1 Background

The UVR energy absorbability of zinc oxide/hollow glass fibre (ZnO/HGF) lamina using mechanical mixing and ultrasonication for ZnO nanoparticle dispersion were discussed in the following.

100nm ZnO nanoparticle with different weight contents of 2 wt.%, 4 wt.%, 5 wt.% and 7 wt.% were mixed with epoxy and each resin mixture was filled into HGFs to form a lamina. Araldite GY251 and hardener HY956 in weight ratio 5:1 were used to fabricate the epoxy base. ZnO nanoparticles and epoxy resin were mechanically mixed with epoxy for 10mins and the resin mixture were mechanically mixed with hardener for another 5mins. Different ZnO/epoxy resin was filled into HGF by using vacuum infiltration technique. Each ZnO/HGF lamina was fabricated at different intervals of HGFs and in 2mm thickness. ***Table 7.10*** shows the fifteen samples being tested. ***Figure 7.33*** shows the configuration of the sample. A neat epoxy/HGF lamina without ZnO nanoparticles was the reference sample.

Table 7.10 Combinations of fifteen samples being tested

		Interval of HGFs		
		0.2 mm	***0.5 mm***	***1.5 mm***
Weight content of ZnO nanoparticles in epoxy filled into HGFs	–	Control sample 1	Control sample 2	Control sample 3
	2 wt.%	Sample 4	Sample 8	Sample 12
	4 wt.%	Sample 5	Sample 9	Sample 13
	5 wt.%	Sample 6	Sample 10	Sample 14
	7 wt.%	Sample 7	Sample 11	Sample 15

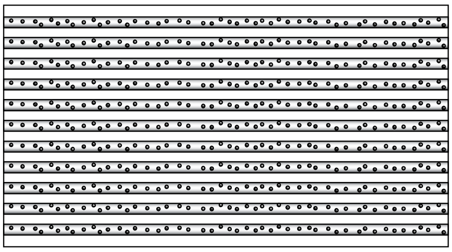

Figure 7.33 ZnO/HGF lamina with 2mm thickness

Another set of composite is two types of 100nm undoped ZnO and 20nm silane-doped ZnO particle with different weight contents of 2 wt.%, 4 wt.% and 7 wt.% were mixed with epoxy and each resin mixture was filled into HGFs to form a lamina. Araldite GY251 and hardener HY956 in weight ratio 5:1 were used to fabricate the epoxy base. ZnO nanoparticles and epoxy resin were ultrasonicated for 20mins and the resin mixture were mechanically mixed with hardener for another 5mins. Different ZnO/epoxy resin was filled into HGF by using vacuum infiltration technique. Each ZnO/HGF lamina was fabricated in 0.2mm interval of HGFs and in 2mm thickness. ***Table 7.11*** shows the seven samples being tested. The configuration of the sample is the same as shown in ***Figure 7.33***. A neat epoxy/HGF lamina without ZnO nanoparticles was the reference sample.

Table 7.11 Combinations of seven samples being tested at 0.2mm interval of HGFs

		Type of ZnO nanoparticle	
		100nm undoped ZnO	***20nm silane-doped ZnO***
Weight content of ZnO nanoparticles in epoxy filled into HGFs	–	Control sample 1	
	2 wt.%	Sample 2	Sample 3
	4 wt.%	Sample 4	Sample 5
	7 wt.%	Sample 6	Sample 7

7.3.2.2 Results and Discussion

Every ZnO/HGF lamina obtains a full UVR absorbability in the wavelength range of 190nm to around 330nm with little variation according to the amount of implemented ZnO nanoparticles.

Figure 7.34, ***Figure 7.35*** and ***Figure 7.36*** show the UVR energy absorbability of all 100nm ZnO/HGF laminas using mechanical mixing for ZnO nanoparticle dispersion. The y-axis represents the index of UVR absorption and five is the maximum UVR absorption. In general, 2 wt.% ZnO/HGF, 4 wt.% ZnO/HGF and 5 wt.% 100nm ZnO/HGF laminas at every interval of HGFs have higher UVR energy absorbability in the wavelength range of 330nm to 400nm. Their UVR energy absorbability are around 25% to 50 % higher than neat epoxy/HGF and 7 wt.% 100nm ZnO/HGF laminas. Nevertheless, their highest UVR energy absorbability is capable to achieve around 30% of the maximum UVR absorption.

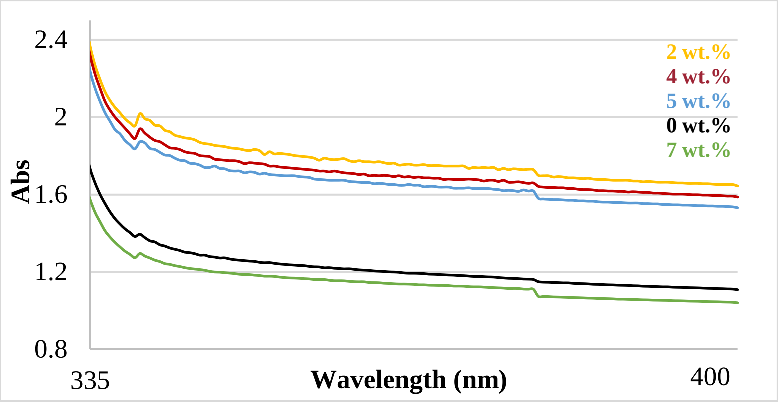

Figure 7.34 UVR energy absorbability of different laminas at 0.2mm interval of HGFs

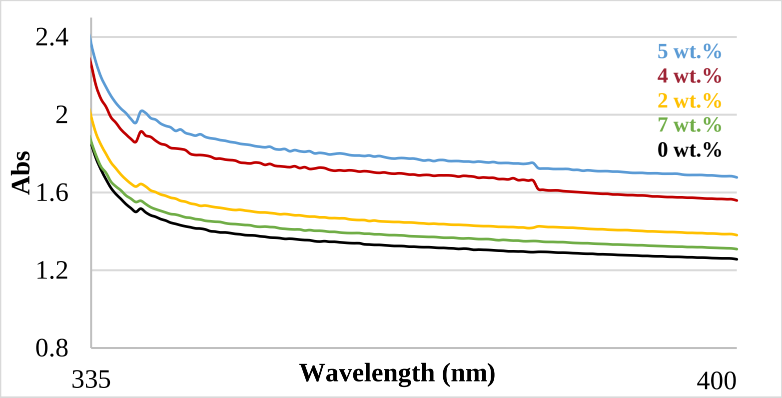

Figure 7.35 UVR energy absorbability of different laminas at 0.5mm interval of HGFs

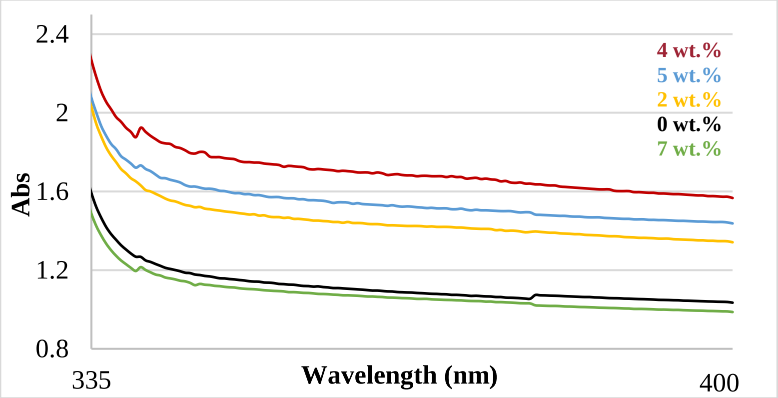

Figure 7.36 UVR energy absorbability of different laminas at 1.5mm interval of HGFs

The UVR energy absorbability of all samples have a steady declination from the wavelength range of 330nm to 400nm. The lowest UVR energy absorbability of all samples are at 400nm wavelength and they are around 20% of the maximum UVR absorption. The results are shown in ***Table 7.12***.

Table 7.12 Lowest UVR energy absorbability at 400nm wavelength of all samples

		Interval of HGFs		
		0.2 mm	***0.5 mm***	***1.5 mm***
Weight content of ZnO nanoparticles in epoxy filled into HGFs	**–**	1.1079	1.2564	1.0347
	2 wt.%	1.6439	1.3809	1.3419
	4 wt.%	1.5867	1.559	1.567
	5 wt.%	1.5316	1.6777	1.4377
	7 wt.%	1.04	1.3089	0.9871

4 wt.% 100nm ZnO/HGF lamina demonstrates a consistent result of having the highest UVR energy absorbability while 7 wt.% 100nm ZnO/HGF lamina shows a consistent result of having the lowest UVR absorbability among other laminas at every interval of HGFs.

The UVR energy absorbability of ZnO/HGF lamina has a relationship with the surface morphology of epoxy mixed with different contents of ZnO nanoparticles which have been characterized and discussed in ***section 7.1.2***. Particle agglomeration is found in 7 wt.% 100nm ZnO/epoxy resin inside HGF. This produces many tiny spaces in between ZnO/epoxy resin which makes it difficult to be fully filled with epoxy resin and results in air gaps. Moreover, there are no Zn elements detected from the EDX examination on the fracture surface of 7 wt.% 100nm ZnO/epoxy resin inside HGF. These explain ZnO nanoparticles in 7 wt.% 100nm ZnO/epoxy resin inside HGF is not uniformly dispersed and air gaps happens in between the resin which these allow UVR energy to directly penetrate through HGF, neat epoxy or air as they carry low or none UVR energy absorbability. Therefore, 7 wt.% 100nm ZnO/HGF lamina reaches the lowest UVR energy absorbability among other laminas. ***Figure 7.37*** explains the problem.

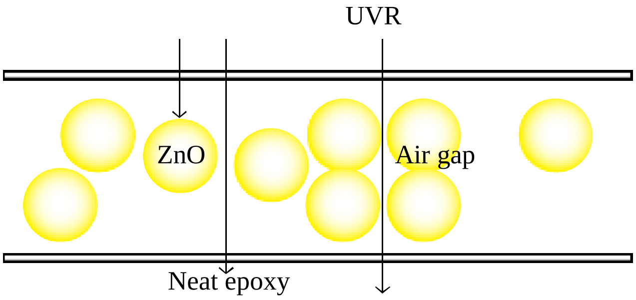

Figure 7.37 Relationship between UVR energy absorbability and particle dispersion of ZnO/epoxy in HGF

The UVR energy absorbability of ZnO nanoparticles in epoxy resin is an active reaction. With the reflection benefited from the HGF, the amount of UVR energy fell into ZnO nanoparticles for physical UVR absorption is increased. ***Figure 7.38*** explains the idea. Active UVR energy absorption is defined when UVR energy falls on ZnO/HGF lamina, the UVR energy is attracted and absorbed by ZnO nanoparticle with the band gap inside its atom. 4 wt.% 100nm ZnO/HGF lamina has a consistent result having the highest UVR energy absorbability at every interval, 0.2mm, 0.5mm and 1.5mm, of HGFs. In addition, it has been mentioned in last section that the UVR energy absorbability of ZnO/HGF lamina has a relationship with the surface morphology and smooth surface is found in 4 wt.% 100nm ZnO/epoxy resin inside HGF which indicates it carries an uniform dispersion of ZnO nanoparticles. These explains different intervals of HGFs tested in the experiment has less influence on the UVR energy absorbability of 4 wt.% 100nm ZnO/HGF lamina provided that ZnO nanoparticles in epoxy resin have active UVR energy absorbability with uniform dispersion and high density.

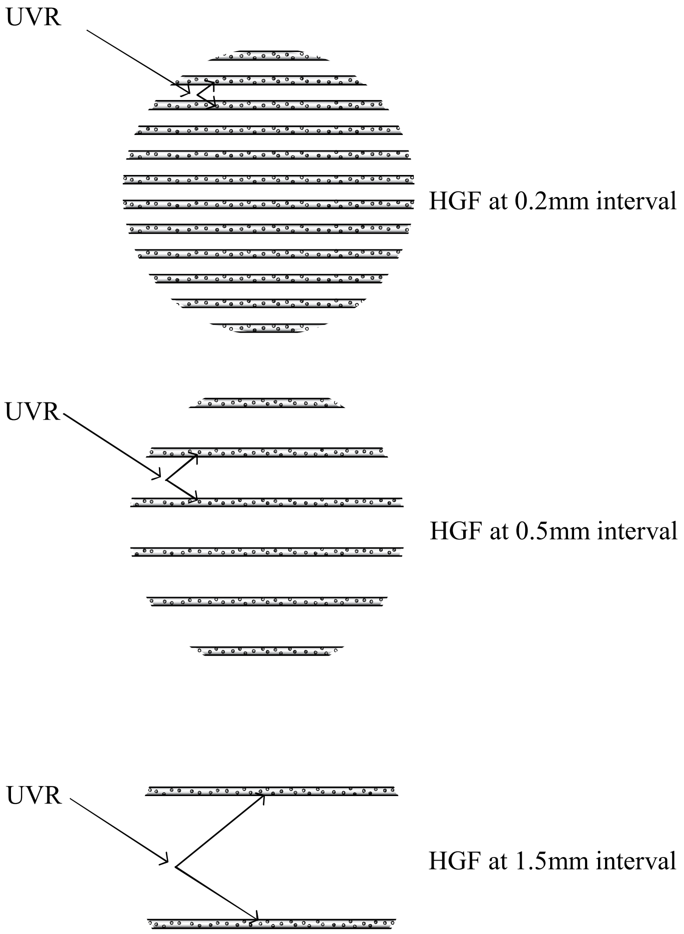

Figure 7.38 Relationship between UVR energy absorbability and different intervals of HGFs of 4 wt.% 100nm ZnO/HGF lamina

The UVR energy absorbability of all 100nm ZnO/HGF and 20nm silane-doped ZnO/HGF laminas using ultrasonication for ZnO nanoparticle dispersion are shown in ***Figure 7.39***. The y-axis represents the index of UVR absorption and five is the maximum UVR absorption

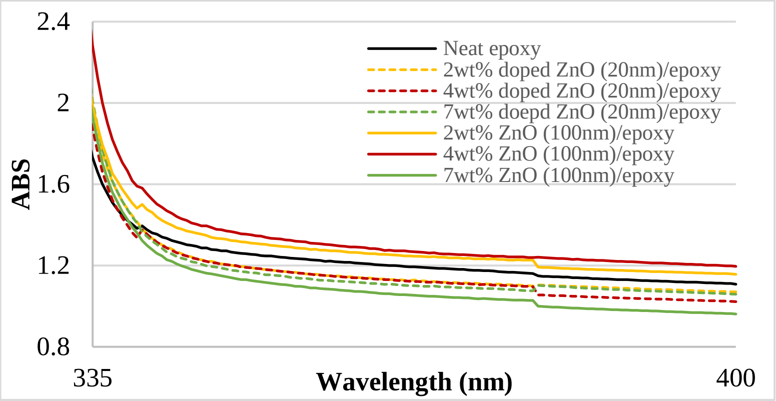

Figure 7.39 UVR energy absorbability of different laminas at 0.2mm interval of HGFs

Comparing the results shown in ***Figure 7.34*** to ***Figure 7.35***, ***Figure 7.36*** and ***Figure 7.39***, all 100nm ZnO/HGF laminas using ultrasonication for particle dispersion obtain lower UVR energy absorbability than all laminas using mechanical mixing although uniform dispersion of 100nm ZnO particles in epoxy using both dispersion methods were found. Ultrasonication dispersion method poses a negative effect to the physical UVR energy absorbability of ZnO nanoparticle. It is suggested that ZnO nanoparticle is somewhat damaged by ultrasonication applying high frequency at 20kHz or more, which is higher than the upper audible limit of human hearing, or energy on the nanoparticles in a fluid for agitation.

All 20nm silane-doped ZnO/HGF laminas using ultrasonication for particle dispersion have lower UVR energy absorbability than all 100nm ZnO/HGF laminas shown in ***Figure 7.39***. Besides the difference in particle size providing a slightly difference in band gap energy which 20nm milled ZnO particle has band gap energy of around 3.14eV and 100nm milled ZnO particle has band gap energy of around 3.22eV, silane surfactant is applied on 20nm ZnO particles. The surface of 100nm ZnO particle without silane coupling agent is favourable for interacting with UVR energy as the surface of undoped ZnO nanoparticle is more hydrophilic compare with the one doped with silane surfactant and polymeric materials, the chemical UVR energy absorption of ZnO nanoparticle requires the presence of water and oxygen. Chemical UVR energy absorption has to be inhibited and physical UVR energy absorption has to be encouraged. However, it is suggested that the silane surfactant has negative impacts on the incidence of UVR energy into ZnO and dissipate UVR energy physically within the band gap of the nanoparticle. In other words, the silane surfactant increases the reflection of UVR energy to epoxy resin for chemical UVR energy absorption while inhibits the active physical UVR energy absorption of ZnO nanoparticle. ***Figure 7.40*** illustrates the idea.

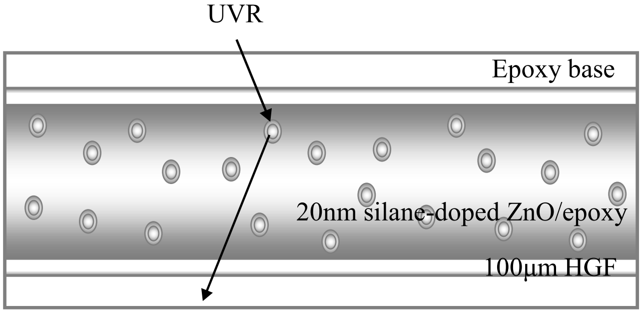

Figure 7.40 Negative effects of silane surfactant on ZnO nanoparticle to the UVR energy absorption

The UVR energy absorbability of all 20nm silane-doped ZnO/HGF laminas are even lower than neat epoxy/HGF lamina. Air gaps presented in between 20nm silane-doped ZnO/epoxy resin is suggested to be one of the reason. It is supposed that air bubbles are capable to pass out through ZnO/epoxy resin and HGF during vacuum infiltration process. However, under the higher amount of 20nm silane-doped ZnO particles at the same weight content as 100nm ZnO particles, the gas bubbles are difficult to be infiltrated out of the ZnO/epoxy resin and HGF. Moreover, tiny gas bubbles are generated 20nm ZnO particles are not easily observed under optical microscope but it is revealed its effect in UVR energy absorbability of the lamina.

Nevertheless, 4 wt.% 100nm ZnO/HGF lamina has the best UVR energy absorbability among all laminas although it is suggested that the nanoparticle is defected by the ultrasonication dispersion method. The presence of less air gaps in between the ZnO/epoxy resin, the uniform dispersion of ZnO nanoparticles and the favourable surface properties providing active physical UVR energy absorption are suggested to be the reason.

7.3.3 UVR Absorbability of Zinc Oxide/Glass Fibre/Unsaturated Polyester Composite underwent Continuous and Cyclic UVR Exposure

7.3.3.1 Background

6 wt.% 100nm ZnO/UP were implemented in between the first three layers of glass fabric of GF/UP composite laminated with twelve layers of plain woven E-glass fabric. The mixing formula of UP is UP:MEKP:cobalt (II) naphthenate:KH151 in the ratio of 500:10:1:5 referring to ***section 3.2.5***. ZnO nanoparticles in UP were ultrasonicated for 20mins and the resin mixture were mechanically mixed with hardener for another 5mins. All composites were fabricated by hand lay-up technique and cured in laboratory with room temperature at 23℃, pressure at 750mmHg and humidity at 45%RH for 24hours prior to characterization and analysis. ***Figure 7.41*** shows the configuration of the sample. A twelve layered GF/UP composite without ZnO nanoparticles was the reference sample.

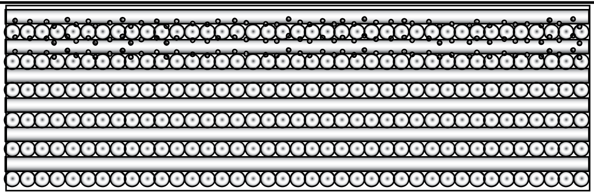

Figure 7.41 ZnO/twelve-layered GF/UP composite

Cyclic and continuous UVR exposure methods were conducted on 6 wt.% 100nm ZnO/GF/UP composite. Details of the composites underwent both UVR exposure methods are described in ***Table 7.13*** and ***section 6.3.1***. As UVA intensity emitted by the lamp in accelerated UVR chamber is 100mW/cm^2, which is approximately 11 times higher than terrestrial UVA intensity of 9.1105mW/cm^2 and natural UVA from the sun is generally alerted from 10am to 4pm for 6hours in every day, the 112.5-hour artificial accelerated UVA exposure is simulated as 208-day ambient sunlight exposure in terms of the accumulated UVA energy of 11250mW/cm^2 stored in the exposed materials.

Table 7.13 Details of ZnO/GF/UP composites underwent continuous or cyclic UVA exposure

	Accelerated Continuous UVA exposure	***Accelerated Cyclic UVA exposure***
Samples	6 wt.% 100nm ZnO/GF/UP	6 wt.% 100nm ZnO/GF/UP
Standard	-	ASTM D4329
Type of exposure	Continuous exposure under UVA	· 50cycles · 2h15mins UVA at 100mW/cm2 intensity at 50℃ · 4h Thermal degradation at 50℃
No. of sample	3 samples for each type	25 samples, each sample underwent 2cycles
Hours of exposure	Total 112.5-hour UVA exposure	
Accumulated UVR intensity	Accumulated 11250mW/cm^2 UVA intensity in the composite samples	

7.3.3.2 Results and Discussion

With the first three layers of 6 wt.% 100nm ZnO/GF/UP, ZnO nanoparticle is responsible for physical UVR absorption in the surface layers which subsequently alleviate the UVR degradation problem in the core of the composite. The UVR degradability of the composite is assessed by surface morphology characterization and tensile properties test revealing its degradation condition under different degrees of UVA exposure which were presented in ***section 6.3***. The UVR absorbability of the composite is a factor of the degradability and it is a measure of the amount of absorbance or transmittance of light at different wavelength reacting with the composite. The first three layers of 6 wt.% 100nm ZnO/GF/UP with higher UVR absorbability is able to lower the UVR degradability of the bulk composite.

The UVR absorbability of 6 wt.% 100nm ZnO/GF/UP composite achieves full UVR absorption spectrum before and after continuous and 25 cyclic UVA exposure. The results are shown in ***Figure 7.42*** and ***Figure 7.43***. This explains 6 wt.% 100nm ZnO particle has an uniform dispersion in GF/UP and 6 wt.% is a good content of the particle to be implemented in between the first three layers of glass fabric for the full UVR absorption of bulk GF/UP composite. 6 wt.% 100nm ZnO particle is able to maintain the molecular density of the composite under the degree of UVR exposure, 112.5hours of artificial accelerated UVA exposure simulated as 208days of ambient sunlight exposure, applied in the composite which the molecular density of the composite has influence to the UVR absorbability.

Combining the results of UVR absorbability and tensile properties discussed in ***section 6.3*** of the composite, a large variation is found in the tensile properties of the composite after the exposure of continuous UVA compared with cyclic UVA under the same accumulated UVA intensity in the composite. However, there is no difference between the UVR absorbability in the composite underwent the exposure of continuous UVA and cyclic UVA. Therefore, the UVR degradability of the composite represented by the change of tensile properties of the composite somehow is not able to be explained by the changes of molecular density and the UVR absorbability of the composite. The UVR degradability of the composite is a crucial factor to evaluate the serviceability, furthermore, continuous and cyclic UVA exposure have different negative effects to the composite and the alternation in the tensile properties of the composite underwent continuous UVA exposure is severer than cyclic UVA exposure. It is important to consider which exposure method has to be chosen for testing the serviceability of the composite in order to avoid overestimation or underestimation.

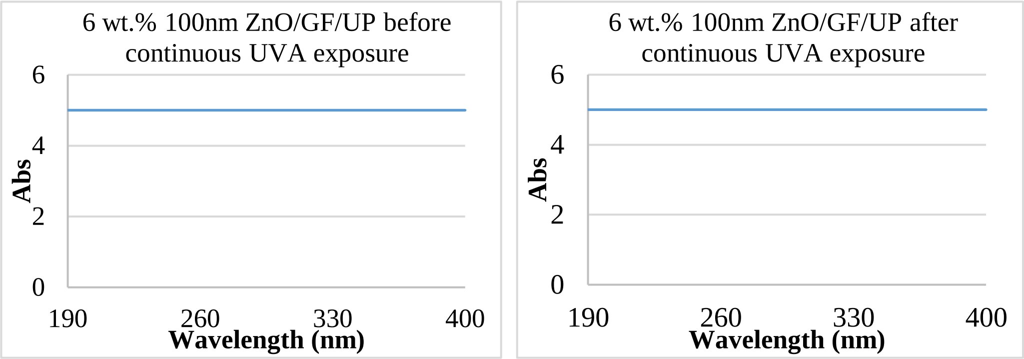

Figure 7.42 UVR absorbability of 6 wt.% 100nm ZnO/GF/UP composites before and after continuous UVA exposure

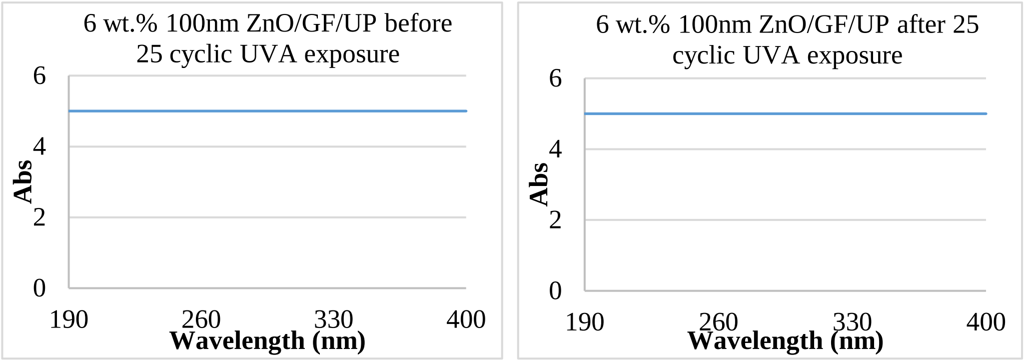

Figure 7.43 UVR absorbability of 6 wt.% 100nm ZnO/GF/UP composites before and after 25 cyclic UVA exposure

7.3.4 UVR Absorbability of Zinc Oxide/Glass Fibre/Epoxy and Zinc Oxide/Glass Fibre/Unsaturated Polyester Composites

7.3.4.1 Background

Using artificial continuous UVA exposure method described in ***section 7.3.3.1***, the GF/polymer composites with two different matrixes underwent the same degree of UVA exposure were tested and compared their UVR absorbability. With two different polymer matrixes, the composites react differently in UVA degradation. The absorbability is contributed by the amount and dispersion of ZnO nanoparticle, the optical properties of ZnO nanoparticle and polymer matrix and the molecular density of polymer matrix.

6 wt.% of 100nm ZnO and 20nm silane-doped ZnO nanoparticles were implemented in GF/EP and GF/UP respectively to form composites. GF/EP and GF/UP composites without ZnO nanoparticles were fabricated as reference samples. The configuration is the same as mentioned in ***section 7.3.3.1***. Araldite GY251 and hardener HY956 in weight ratio 5:1 were used to fabricate the epoxy base. The mixing formula of UP is UP:MEKP:cobalt (II) naphthenate:KH151 in the ratio of 500:10:1:5 referring to ***section 3.2.5***. ZnO nanoparticles in EP and UP resin were ultrasonicated for 20mins and the resin mixture were mechanically

mixed with hardener for another 5mins. All composites were fabricated by hand lay-up technique and cured in laboratory with room temperature at 23℃, pressure at 750mmHg and humidity at 45%RH for 24hours prior to characterization and analysis. Details of the composites underwent continuous UVR exposure method are described in ***Table 7.14*** and ***section 6.4.1***.

Table 7.14 Details of ZnO/GF/EP and ZnO/GF/UP composites underwent continuous UVA exposure

	Accelerated CONTINUOUS UVA exposure		
Samples	Neat GF/EP	6 wt.% 100nm ZnO/GF/EP	6 wt.% 20nm silane-doped ZnO/GF/EP
	Neat GF/UP	6 wt.% 100nm ZnO/GF/UP	6 wt.% 20nm silane-doped ZnO/GF/UP
Type of exposure	Continuous exposure under UVA		
No. of sample	3 samples for each types		
Hours of exposure	Total 112.5-hour UVA exposure		
Accumulated UVR intensity	Accumulated 11250mW/cm^2 UVA intensity in composite samples		

7.3.4.2 Results and Discussion

Similar to the previous experiment, 6 wt.% 100nm ZnO and 6 wt.% 20nm silane-doped ZnO particles were implemented in the first three layers of GF/EP and GF/UP composites which the implementation of ZnO nanoparticles is responsible for physical UVR absorption in the surface layers in order to mitigate the UVR degradation problem in the core of the composite. The UVR absorbability of the composite is a factor of the degradability and it is a measure of the amount of absorbance or transmittance of light at different wavelength reacting with the composite. The first three layers of GF/EP and GF/UP implemented with 6 wt.% 100nm ZnO and 6 wt.% 20nm silane-doped ZnO particles possessing higher UVR absorbability is able to lower the UVR degradability of the bulk composite.

EP and UP resins have slightly different reactivity in UVR absorption because of the intrinsic optical property and molecular density of the polymers. Both of the polymers are transparent in nature and the molecular density of EP resin is slightly lower than UP resin which explains EP contributing lower UVR absorbability. Neat GF/EP and neat GF/UP composites without ZnO nanoparticles is not able to achieve a full UVR absorption spectrum and demonstrate low UVA absorbability. 6 wt.% of 100nm ZnO and 6 wt.% 20nm silane-doped ZnO particles are able to enhance and maintain the molecular density of GF/EP and GF/UP composites underwent the same degree of UVR exposure, 112.5hours of artificial accelerated UVA exposure simulated as 208days of ambient sunlight exposure, applied in the composites which the molecular density of the composites has influence to the UVR absorbability. The results are shown in ***Figure 7.44***, ***Figure 7.45***, ***Figure 7.46 and Figure 7.47***. Together with the uniform particle dispersion, therefore, the composites are able to achieve a full UVR absorption spectrum before and after UVA exposure.

Meanwhile, EP and UP resins have different compatibility with ZnO nanoparticles having two different surface properties, 100nm ZnO without surface treatment and 20nm silane-doped ZnO with silane surfactant. This difference has no significant effects in the UVR absorbability of the composites, however, the effects are found in the surface morphology and the tensile properties discussed in ***section 6.4***.

Although silane surfactant is presented on ZnO nanoparticles, the particle of 20nm in diameter is relatively small and particle agglomeration or non-uniform particle dispersion is happened which prevents the composites to achieve a full UVA absorption. Otherwise, the silane surfactant on 20nm ZnO particle having high reflectivity prevents UVR energy to entre the particle and reach the band gap of

ZnO atom which lowers the occurrence of physical UVR absorption. Contradictorily, the silane surfactant on 20nm ZnO also lowers the occurrence of chemical UVR absorption with surrounding polymer and reduces a high number of harmful radicals to be produced and further degrade the polymer.

After accelerated continuous UVA exposure, all GF/polymers composites with or without ZnO nanoparticles are able to achieve a full UVR absorption spectrum. The results are shown in ***Figure 7.47***. Combining the results of tensile properties of the composites after UVA exposure, this indicates the molecular density of polymer chains is enhanced, the UVA energy attacked into the composites provides energy for the polymer chains to further polymerize and the molecular density of polymer chains is correlated with the UVR absorbability of the polymer composites. All fully cured composites with higher molecular density demonstrate a better or a full UVR absorption spectrum.

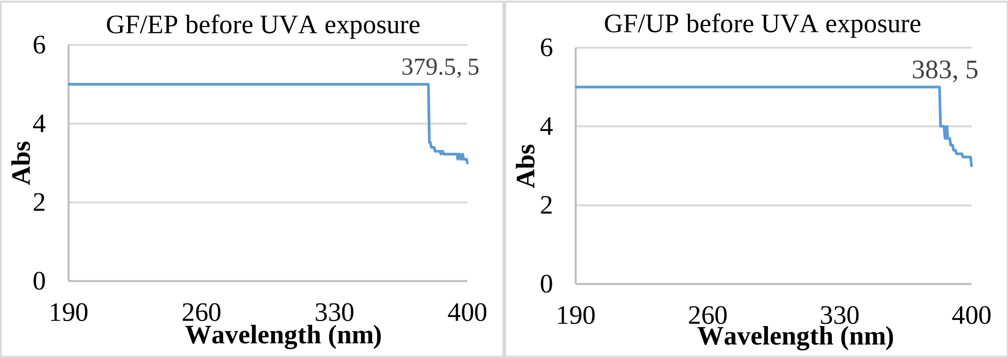

Figure 7.44 UVR energy absorbability of neat GF/EP and GF/UP composites without UVA exposure

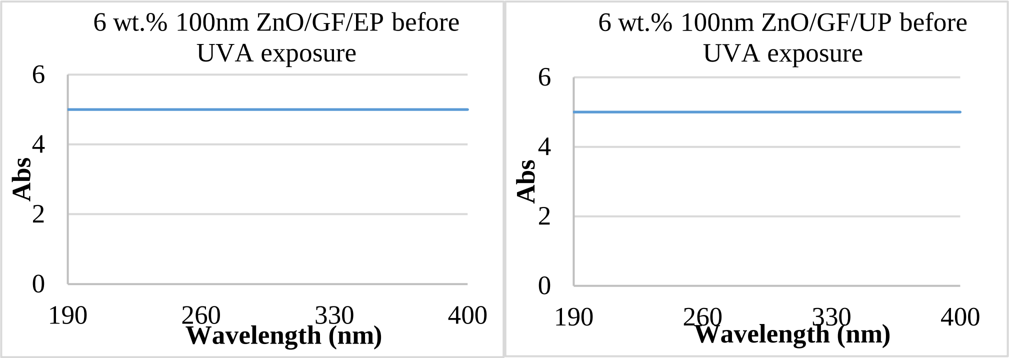

Figure 7.45 UVR energy absorbability of 6 wt.% 100nn ZnO/GF/EP and 6 wt.% 100nm ZnO/GF/UP composites without UVA exposure

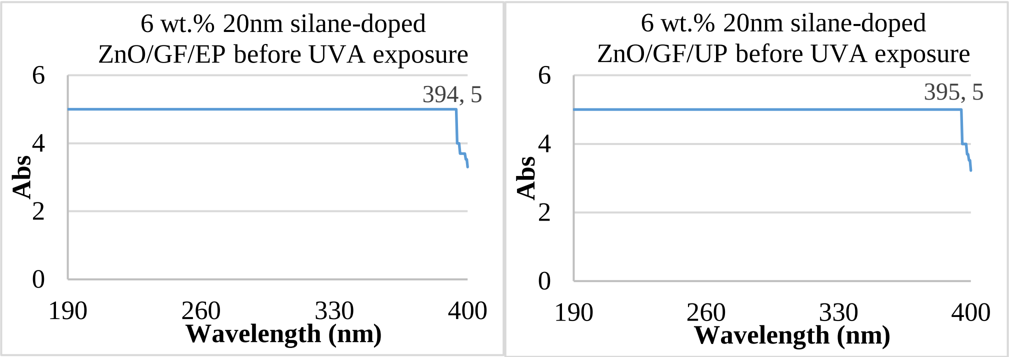

Figure 7.46 UVR energy absorbability of 6 wt.% 20nm silane-doped ZnO/GF/EP and 6 wt.% 20nm silane-doped ZnO/GF/UP composites without UVA exposure

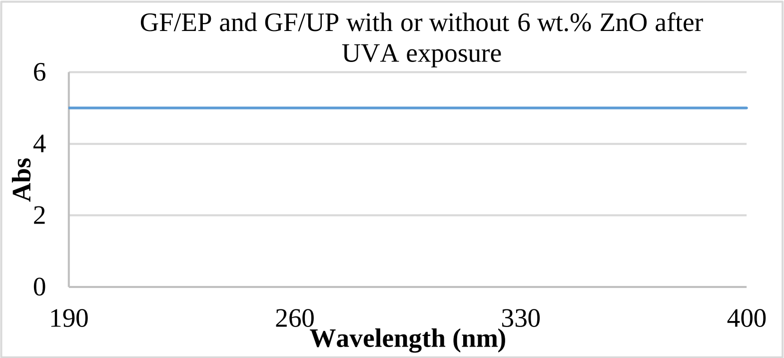

Figure 7.47 Full UVR absorption of GF/polymers composites with or without 6 wt.% ZnO nanoparticle after UVA exposure

7.3.5 UVR Absorbability of Zinc Oxide/Epoxy-based and Styrene-based Shape Memory Polymer

7.3.5.1 Background

2 wt.%, 4 wt.%, 5 wt.% and 7 wt.% of 100nm ZnO particles were mixed with two shape memory polymers (SMPs) precursor solutions, epoxy-based SMP (EP-SMP) and styrene-based SMP (S-SMP), respectively. The precursor solutions of EP-SMP and S-SMP were mixed according to the formula provided by Harbin Institute of Technology (HIT). ZnO nanoparticles in EP-SMP and S-SMP resin were mechanically mixed for 20mins and then ultrasonicated for another 10mins. Afterwards, degas process was conducted until bubble-free resin mixtures were obtained. The resulting mixtures were poured into a two-plate mould. Thermal curing was performed on ZnO/EP-SMPs at 80°C for 3hours, followed by 100°C for 3hours and 150°C for 5hours and on ZnO/S-SMPs at 75°C for 36hours. All composites were cooled down at room temperature at 23°C and pressure at 750mmHg and then machined into a square shape in the dimension of 30mm (l)*30mm (w)*3mm (t). Neat EP-SMP and S-SMP without ZnO nanoparticles were fabricated as reference samples.

Using artificial continuous UVA exposure method described in ***section 7.3.3.1***, both EP-SMP and S-SMP underwent 12hours of UVA exposure and accumulated intensity of 1200mW/cm^2 were tested and compared their UVR absorbability. As UVA intensity emitted by the lamp in accelerated UVR chamber is 100mW/cm^2, which is approximately 11 times higher than terrestrial UVA intensity of 9.1105mW/cm^2 and natural UVA from the sun is generally alerted from 10am to 4pm for 6hours in every day, the 12-hour artificial accelerated UVA exposure is simulated as 22-day ambient sunlight exposure in terms of the accumulated UVA energy of 1200mW/cm^2 stored in the exposed materials. Details of the composites underwent continuous UVR exposure method are described in ***Table 7.15*** and ***section 6.5.1***.

Table 7.15 Details of ZnO/EP-SMP and ZnO/S-SMP composites underwent continuous UVA exposure

	Accelerated CONTINUOUS UVA exposure				
Samples	Neat EP-SMP	2 wt.% ZnO/EP-SMP	4 wt.% ZnO/EP-SMP	5 wt.% ZnO/EP-SMP	7 wt.% ZnO/EP-SMP
	Neat S-SMP	2 wt.% ZnO/S-SMP	4 wt.% ZnO/S-SMP	5 wt.% ZnO/S-SMP	7 wt.% ZnO/S-SMP
Type of exposure	Continuous exposure under UVA				
No. of sample	3 samples for each types				
Hours of exposure	Total 12-hour UVA exposure				
Accumulated UVR intensity	Accumulated 1200mW/cm^2 UVA intensity in composite samples				

With two different polymer matrixes, the composites react differently in UVA degradation. The absorbability is contributed by the amount and dispersion of ZnO nanoparticle, the optical properties of ZnO nanoparticle and polymer matrix and the molecular density of polymer matrix.

7.3.5.2 Results and Discussion

2 wt.%, 4 wt.%, 5 wt.% and 7 wt.% 100nm ZnO particles in EP-SMP and S-SMP are able to obtain full UVR absorption before and after UVA exposure. The results are shown in ***Figure 7.48***. This indicates the ZnO nanoparticles is uniformly dispersed in the SMPs.

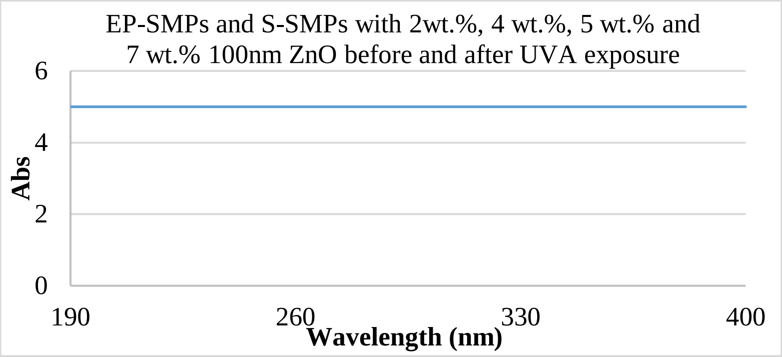

Figure 7.48 UVR absorbability of 2 wt.%, 4 wt.%, 5 wt.% and 7 wt.% 100nm ZnO/EP-SMPs and S-SMPs before and after UVA exposure

Neat EP-SMP and neat S-SMP are able to obtain full UVC (100nm-280nm), full UVB (280nm-315nm) and part of UVA (315nm-400nm) absorption spectrum up to 387.5nm and 311.5nm shown in ***Figure 7.49*** and ***Figure 7.50*** respectively. The UVA absorbability of the neat SMPs drops accordingly without the contribution of the UVA absorption of ZnO nanoparticles.

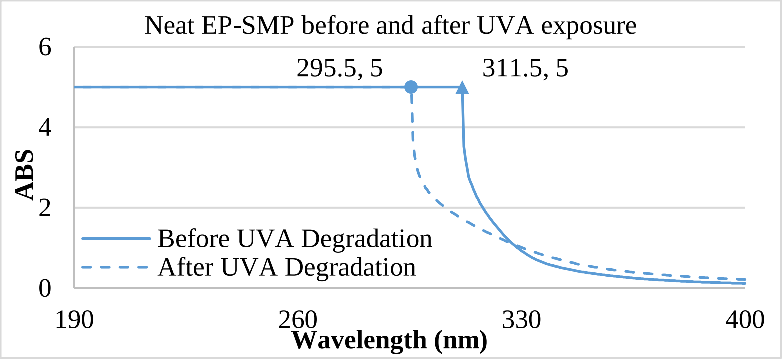

Figure 7.49 UVR absorbability of neat EP-SMP before and after UVA exposure

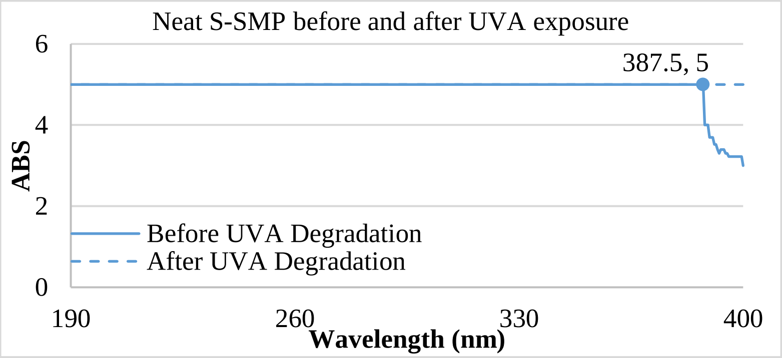

Figure 7.50 UVR absorbability of neat S-SMP before and after UVA exposure

Neat EP-SMP is not able to achieve a full UVR absorption before UVA exposure, moreover, its UVR absorbability is even lowered after UVA exposure. Regarding the lowered surface hardness of neat EP-SMP discussed in ***section 6.5.2.2***, the softened surface obtains a lower molecular density which allows UVR energy penetrating into the core of EP-SMP and transmitting through the bulk EP-SMP easily. In the flavour of EP-SMP having higher molecular density after the implementation of ZnO nanoparticles, the shape memory effects and the UVR absorbability are maintained under the applied UVA exposure.

Neat S-SMP is not able to achieve a full UVR absorption before UVA exposure, whilst, its full UVR absorbability is obtained after UVA exposure. Regarding the increased surface hardness of neat S-SMP discussed in ***section 6.5.2.2***, the hardened surface delivers a higher molecular density of polymer which impedes UVR energy to transmit through the UVA degraded layer and penetrate the core polymer. Molecular density is contributed by the bonding strength of ZnO–polymer and polymer–polymer. In turn, the hardened surface is formed as a protection surface to prevent UVR absorption of the core polymer and lower the UVR degradation rate of the bulk polymer.

7.4 Summary of This Chapter

In this chapter, UVR energy absorbability of ZnO/HGF lamina and different polymer-based composites, ZnO/GF/EP, ZnO/GF/UP, ZnO/E-SMP and ZnO/S-SMP, were studied. Particle dispersion, rheology properties and polymerization shrinkage of ZnO/epoxy resin were investigated as they are the factors influencing UVR energy absorbability of the composite.

Alcoholic solvent, mechanical mixing and ultrasonication are the common methods for particle dispersion. 20 wt.% Isopropyl alcohol has less alteration to the crystalline structure of epoxy but still poses influence to the properties of epoxy, therefore, alcoholic solvent is not considered for dispersing ZnO nanoparticles in epoxy since it is difficult for the solvent to evaporate out during curing process but remains inside HGF. Mechanical mixing is the ordinary method for stirring mixture using different frequency and duration according to the rheology properties of the mixture. It is still demanding for using mechanical mixing to achieve good particle dispersion at room temperature once the weight content of particle is getting larger. The dispersion property of the mixture is even significant inside micron HGF. 4 wt.% 100nm ZnO/epoxy obtains a good particle dispersion but 7 wt.% 100nm ZnO/epoxy shows particle agglomeration in HGF. Two types of ZnO nanoparticle, 100nm ZnO and 20nm silane-doped ZnO, were dispersed in epoxy by using ultrasonication and filled into HGF. Similar particle dispersion conditions of two types of ZnO nanoparticle at the same amount are obtained which demonstrates silane has a limited effectiveness to the particle dispersion. 7 wt.% ZnO/epoxy shows particle agglomeration in HGF no matter using mechanical mixing or ultrasonication methods for particle dispersion which this indicates mechanical mixing and ultrasonication have similar effectiveness to the particle dispersion.

Besides, silane coupling agent was investigated for the purposes of good particle dispersion and mechanical properties. However, regarding the results of rheology properties of ZnO/epoxy resin and UVR energy absorbability of ZnO/HFG lamina, silane coupling agent has negative impact on the incidence of UVR energy into ZnO for physical UVR absorption and it increases the reflection of UVR energy to surrounding epoxy resin for chemical UVR energy absorption.

Vacuum infiltration and curing condition are associated with the rheology and polymerization shrinkage properties of ZnO/epoxy resin in HGF. Rheology test reveals silane surfactant is able to stabilize the fluid flow, however, it increases viscosity and requires higher shear stress for fluid flow. 4 wt.% 100nm ZnO/epoxy resin classified as pseudo plastic fluid obtains the lowest yield stress and viscosity for fluid flow comparable to neat epoxy resin. Polymerization shrinkage is a common problem in the curing process of polymer material. The shrinkage is even significant in HGF. Nanoparticles enables to stabilize the dimension of cured resin. Two types of ZnO implemented in epoxy, 100nm ZnO/epoxy and 20nm silane-doped ZnO/epoxy, and filled into HGF with 100μm inner diameter were evaluated the angle of shrinkage. The results explain that the type of ZnO nanoparticle contributes no difference to the polymerization shrinkage of ZnO/epoxy resin in HGF and having higher weight content of ZnO nanoparticle, ZnO/epoxy resin obtains lower degree of polymerization shrinkage in HGF.

Comparing the UVR energy absorbability of ZnO/GF/EP composite using solvent and ultrasonication for ZnO nanoparticle dispersion, GF/EP layer is capable to chemically absorb UVR energy, seven more layers contribute 13% higher in UVR absorbability. Solvent dispersed 20 wt.% 100nm ZnO particle is required to increase 18% for achieving full UVR energy absorbability of five-layered GF/EP whilst ultrasonicated 6 wt.% 100nm ZnO particle is required to increase 5% for achieving full UVR energy absorbability of twelve-layered GF/EP. Ultrasonicated 6 wt.% 20nm silane-doped ZnO particle implemented in the first three layers of twelve-layered GF/EP has no full UVR absorption due to particle agglomeration and silane surfactant impeding the entry of UVR energy into ZnO atom for physical UVR absorption.

From the UVR energy absorbability results of ZnO/HGF lamina investigating the differences between two types of ZnO nanoparticle at different weight contents, different intervals of HGFs and two particle dispersion methods, 4 wt.% 100nm

ZnO/HGF lamina obtains the highest UVR energy absorbability because 1. the UVR energy absorption of ZnO is an active reaction and disregards different intervals of HGF and 2. the reflection of HGF increases the incidence of UVR energy into ZnO. Other composites with different configurations obtain lower UVR energy absorbability because 1. the content of ZnO nanoparticle is insufficient for physical UVR absorption, 2. particle agglomeration occurs and produces air gap in between of particles and 3. silane surfactant impedes the entry of UVR energy into ZnO atom for physical UVR absorption.

Based on the UVR energy absorbability results of 6 wt.% 100nm ZnO/GF/UP composite underwent continuous and cyclic UVR exposure, all composites obtain full UVR absorption before and after UVA exposure which indicates 6 wt.% 100nm ZnO particle is at a satisfactory ratio to reinforce the polymer against UVR attack at the same exposure time and accumulated intensity while maintain the UVR absorbability.

According to the UVR energy absorbability results of ZnO/GF/EP and ZnO/GF/UP, 6 wt.% 100nm ZnO particle obtains a full UVR absorbability in GF/EP and GF/UP before and after UVA exposure. Before UVA exposure, neat GF/EP, neat GF/UP, 6 wt.% 20nm ZnO/GF/EP and 6 wt.% 20nm ZnO/GF/UP are not able to obtain full UVR absorption due to the absence of ZnO nanoparticle and the presence of particle agglomeration with silane surfactant impeding the entry of UVR energy into ZnO atom for physical UVR absorption respectively. After UVA exposure, all composites are able to obtain full UVR absorption and this explains the molecular density of polymer chains is enhanced through the further polymerization by UVA energy. The molecular density of polymer chains is accounted the UVR absorbability of the composites.

Comparing the UVR energy absorbability results of ZnO/EP-SMP and ZnO/S-SMP, 2 wt.% 100nm ZnO particle is sufficient for obtaining full UVR absorption in both SMPs using 20mins mechanical mixing followed by 10mins ultrasonication for particle dispersion. UVA degraded S-SMP results in hardened surface hardness whilst UVA degraded EP-SMP results in softened surface hardness, subsequently, the UVR absorbability of UVA degraded S-SMP is enhanced to have full UVR absorption whist the UVR absorbability of UVA degraded EP-SMP is weakened. This denotes that the hardened surface delivering a higher polymer molecular density enables to impede UVR energy for penetrating through and reaching the core polymer. In other words, the hardened surface is formed as a ‘protection layer’ to prevent UVR absorption of the core polymer and lower the UVR degradation rate of the bulk polymer. It is worth noting that the polymer molecular density of ZnO/polymer composite is contributed by the bonding strength of ZnO–polymer and polymer–polymer.

Chapter Eight

Theoretical Analysis for Parameters Optimization

Theoretical analysis of ZnO/HGF lamina, a five-cylindrical system, is deliberated in ***Chapter Eight***. The developed mathematical model provides a theoretical principle to evaluate and optimize the design parameter of a system constructed in similar way based on its stress transfer ability. In addition, the model provides a theoretical concept for the configuration of the lamina regarding the content of ZnO in the core, the length and the thickness of HGF, the shear strength and the thickness of adhesive layers in relation to the mechanical and geometric properties of all elements in the system.

8.1 Stress Transfer Ability of Zinc Oxide/Hollow Glass Fibre Lamina

The mechanical properties of ZnO/epoxy core, HGF and epoxy base and the interfacial strength of HGF-epoxy are the parameters controlling the stress transfer ability of the ZnO/HGF lamina. The bonding property between fiber-polymer is described as the ‘heart of the composite’ [Piggott, 1986; Piggott, 1997]. Silane surfactant is commonly doped on glass fibre and ZnO nanoparticle to enhance the compatibility of glass fiber-polymer and ZnO-polymer by introducing the hydrogen functional group turning the hydrophilic glass fiber surface to hydrophobic and increasing negative ions on the surface of ZnO nanoparticle. The compatibility of glass fibre-polymer and ZnO-polymer determines the adhesion strength between the elements and the mechanical properties of the bulk composite. Fibre pull-out action describes the whole process of fiber delamination including fiber debond initiation, fiber debond propagation and fiber sliding which is highly dependent on the interfacial shear strength of hollow glass fibre-polymer. Jiang et al. [1999] discussed the contact state of fibre-polymer in a composite and divided into three conditions, the adhesive contact state, slipping contact state, and non-contact state indicated by different corresponding mechanical parameters considering the relationship between the normal stress, shear stress and the contact boundary.

Force equilibrium approach is adopted for analyzing the adhesive contact state of fibre-polymer which normal stress and shear stress are the two major force components applied on the composite system under the fiber pull-out action. ***Figure 8.1*** shows a sectional diagram of a ZnO/HGF lamina. ***Figure 8.2*** shows the five-cylinder model for analyzing the stress transfer ability between the elements of the composite. The composite system is symmetric about r-axis and x-axis, therefore, a quarter of the system is significant for analysis. The axial direction along x-axis indicates the instantaneous displacement of fiber movement counted from the centre of ZnO/epoxy core $(x = 0)$ under being pulled out. The radial direction, $r_b,\ r_{A_{bf}},\ r_f,\ r_{A_{fc}}\ and\ r_c$ represents the outer radii of epoxy base, adhesive layer, A_{bf}, HGF, adhesive layer A_{fc} and ZnO/epoxy core counted from the centre of ZnO/epoxy core $(r = 0)$. The total length of HGF is defined as $2L_f$.

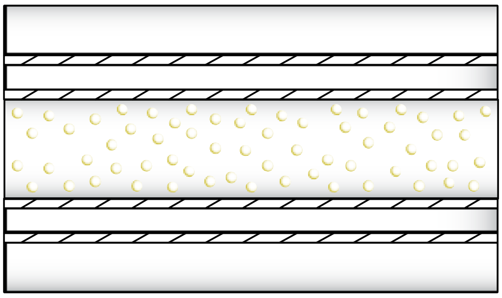

Figure 8.1 Sectional diagram of ZnO/HGF lamina

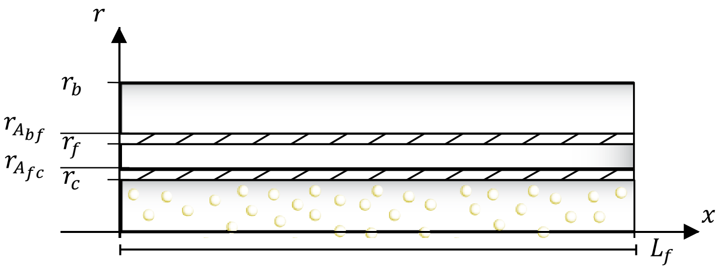

Figure 8.2 Five-cylinder model of ZnO/HGF lamina for stress transfer analysis

Referring to ***Figure 8.3***, the indexes of b, A_{bf}, f, A_{fc} *and* c denote as epoxy base, adhesive layer between epoxy base and HGF, HGF, adhesive layer between HGF and ZnO/epoxy core and ZnO/epoxy core respectively. E_b, E_f and E_c represent the Young's moduli of epoxy base, HGF and ZnO/epoxy core. G_A represents the shear modulus of adhesive layers, A_{bf} and A_{fc}. The thickness of two adhesive layers is much smaller comparing to the whole ZnO/HGF lamina. Having small differences between $r_{A_{bf}}$ and r_f and $r_{A_{fc}}$ and r_c, $r_{A_{bf}}\tau_{bA_{bf}}\left(x, r_{A_{bf}}\right) = r_{A_f}\tau_{A_{bf}f}(x, r_f)$ *and* $r_{A_{fc}}\tau_{fA_{fc}}\left(x, r_{A_{fc}}\right) = r_c\tau_{A_{fc}c}(x, r_c)$ is allowed to be expressed as $\tau_{bA_{bf}}\left(x, r_{A_{bf}}\right) = \tau_{A_{bf}f}(x, r_f)$ *and* $\tau_{fA_{fc}}\left(x, r_{A_{fc}}\right) = \tau_{A_{fc}c}(x, r_c)$. Tensile forces are applied on each element, $N_b, N_{A_{bf}}, N_f, N_{A_{fc}}$ and N_c denote as tensile forces applied on epoxy base, adhesive layer, A_{bf}, HGF, adhesive layer A_{fc} and ZnO/epoxy core. $\tau_{A_{bf}f}(x, r_f)$

is the shear stress along the axial direction at the outer and inner interface of adhesive layer, A_{bf} whilst $\tau_{A_{fc}C}(x, r_c)$ is the shear stress along the axial direction at the outer and inner interface of adhesive layer, A_{fc}. Two adhesive layers of ZnO/epoxy core-HGF and HGF-epoxy base are the interface in contact with the adjacent relatively rigid elements which are subjected to interfacial shear stress whilst the relatively rigid elements of ZnO/epoxy core, HGF and epoxy base are subjected to normal tensile stress under fiber pull-out action experiencing a tensile load applied on the bulk composite. All elements in the composite are dependent on one another under stress transfer process.

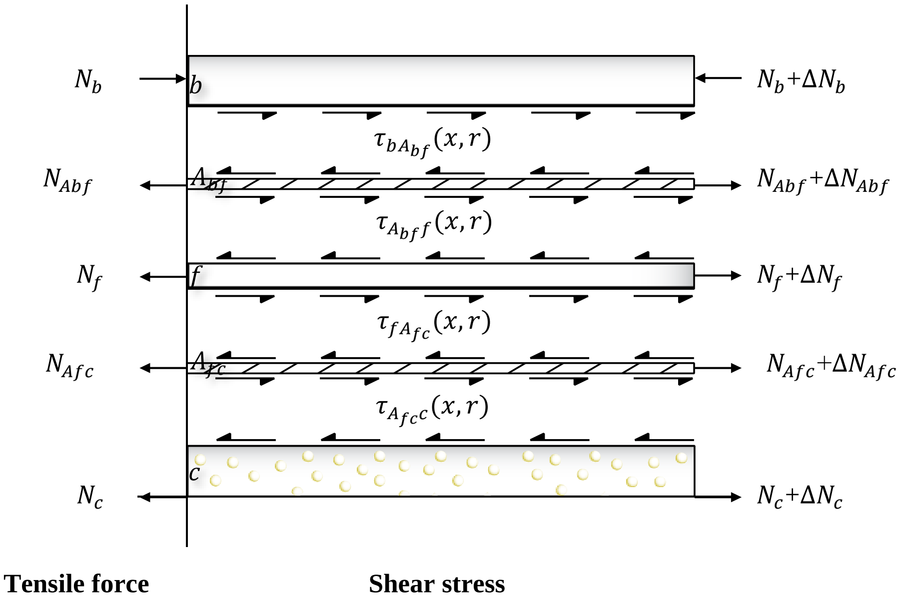

Figure 8.3 Force diagram of ZnO/HGF lamina

According to ***Figure 8.4***, $\mathrm{U_b}, U_f$ and U_c represent the axial displacement of epoxy base, HGF and ZnO/epoxy core while $\delta_{A_{bf}}$ *and* $\delta_{A_{fc}}$ represent the relative displacement of two adhesive layers, A_{bf} *and* A_{fc}. Details of the mechanical and geometrical properties of the elements in the composite system under a fundamental configuration are listed in ***Table 8.1***.

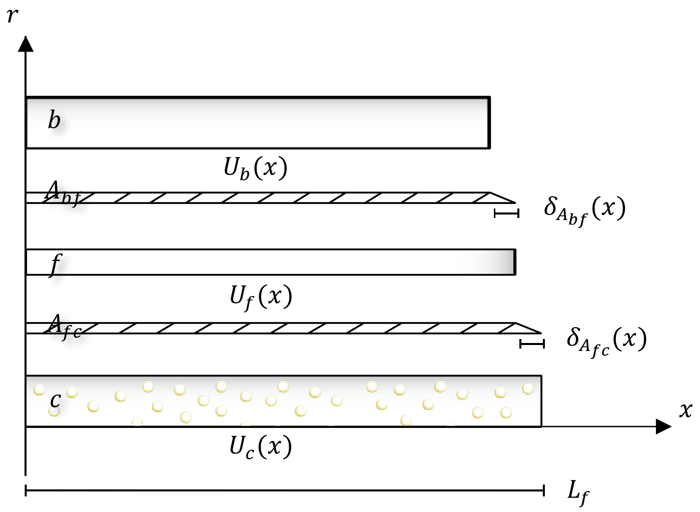

Figure 8.4 Axial displacement diagram of ZnO/HGF lamina

Table 8.1 Mechanical and geometrical properties of the elements in the lamina system under a fundamental configuration

Elements	Symbols	Values
Outer diameter		
Epoxy base	r_b	208µm
Adhesive layer	$r_{A_{bf}}$	158µm
HGF	r_f	149µm
Adhesive layer	$r_{A_{fc}}$	99µm
ZnO/epoxy core	r_c	90µm
Young's Modulus		
Epoxy	E_b	3GPa
HGF	E_f	68.5GPa
Adhesive layer	E_A	3.3GPa
ZnO	E_{ZnO}	111.2GPa
Shear Modulus		
Adhesive layer	G_A	1.2GPa
Thickness of adhesive layer	t_A	4.5µm

Several assumptions were made to simplify the current theoretical analysis. All elements are perfectly bonded; mechanical properties of ZnO/epoxy core, HGF and epoxy base are linear, elastic and isotropic; no thermal load is applied to the system; the applied load is only concerned along the axial direction and the applied force is uniformly exerted on ZnO/epoxy core. During fibre pull-out process under a tensile load applied on the bulk composite, ZnO/epoxy core, HGF and epoxy base possessing relatively high tensile moduli experience normal tensile loads whilst two adhesive layers possessing relatively low shear moduli experience shearing loads. Considering the reverse direction of fibre pull-out action from epoxy base to ZnO/epoxy core, theoretically, all elements in the composite system under the same configuration is considered to experience the same axial strain deformation condition.

All elements in the composite are dependent on one another for stress transfer under fibre pull-out action. Each element shifts to a relative displacement associating with adjacent elements. The axial displacement condition of epoxy base which link up the mechanical and physical properties of all elements in the composite system is able to be obtained by considering

$$U_c(x) = U_b(x) + \delta_{A_{bf}}(x) + \delta_{A_{fc}}(x) \qquad \text{(\textbf{\textit{Equation 16}})}$$

and

$$U_c(x) = U_f(x) + \delta_{A_{fc}}(x) \qquad \text{(\textbf{\textit{Equation 17}})}$$

or

$$U_b(x) = \delta_{A_{bf}}(x) + \delta_{A_{fc}}(x) + U_c(x) \qquad \text{(\textbf{\textit{Equation 18}})}$$

and

$$U_b(x) = \delta_{A_{bf}}(x) + U_f(x) \qquad \text{(\textbf{\textit{Equation 19}})}$$

In which the axial displacement of ZnO/epoxy core, HGF and epoxy base are determined by

$$U_b(x) = \frac{1}{E_b}\int_0^x \sigma_b(x)dx \qquad \textbf{(\textit{Equation 20})}$$

and

$$U_f(x) = \frac{1}{E_f}\int_0^x \sigma_f(x)dx \qquad \textbf{(\textit{Equation 21})}$$

and

$$U_c(x) = \frac{1}{E_c}\int_0^x \sigma_c(x)dx \qquad \textbf{(\textit{Equation 22})}$$

And the relative displacement of two adhesive layers are determined by

$$\delta_{A_{bf}} = \frac{1}{G_A}\int_{r_f}^{r_{A_{bf}}} \frac{r_{A_{bf}}}{r}\tau_{A_{bf}f}(x,r)dr \qquad \textbf{(\textit{Equation 23})}$$

and

$$\delta_{A_{fc}} = \frac{1}{G_A}\int_{r_c}^{r_{A_{fc}}} \frac{r_{A_{fc}}}{r}\tau_{A_{fc}c}(x,r)dr \qquad \textbf{(\textit{Equation 24})}$$

The tensile force of ZnO/epoxy core, HGF and epoxy base are given by

$$N_c(x) = \pi {r_c}^2\sigma_c - 2\pi r_c \int_0^x \tau_{A_{fc}c}(x,r_c)dx \qquad \textbf{(\textit{Equation 25})}$$

and

$$N_f(x) = \pi\left(r_f - r_{A_{fc}}\right)^2 \sigma_f - 2\pi r_f \int_0^x \tau_{A_{bf}f}(x,r_f)dx + 2\pi r_c \int_0^x \tau_{A_{fc}c}(x,r_c)dx$$

$$\textbf{(\textit{Equation 26})}$$

and

$$N_b(x) = \pi\left(r_b - r_{A_{bf}}\right)^2 \sigma_b - 2\pi r_f \int_0^x \tau_{A_{bf}f}(x,r_f)dx \qquad \textbf{(\textit{Equation 27})}$$

The $\sigma_c(x), \sigma_f(x)$ and $\sigma_b(x)$ are the axial tensile stress of ZnO/epoxy core, HGF and epoxy base respectively which they are changed with respect to their pull-out displacement, x. While σ_c, σ_f and σ_b represent the maximum axial tensile stress, at $x = 0$, of ZnO/epoxy core, HGF and epoxy base respectively.

Letting $u = \tau_{A_{fc}c}(x, r_c)$ and $v = \tau_{A_{bf}f}(x, r_f)$

and

$$① = E_c {r_c}^2 \ln(\frac{r_{A_{fc}}}{r_c})$$

$$② = E_b (r_b - r_{A_{bf}})^2 \ln(\frac{r_{A_{bf}}}{r_f})$$

$$③ = E_f (r_f - r_{A_{fc}})^2 \ln\left(\frac{r_{A_{fc}}}{r_c}\right)$$

$$④ = E_f (r_f - r_{A_{fc}})^2 \ln\left(\frac{r_{A_{bf}}}{r_f}\right)$$

Considering $\tau_{A_{fc}c}(x, r_c), u$. Substituting ***Equation 20*** to ***Equation 24*** into ***Equation 16*** and ***Equation 17***, it gives the following equations

$$\frac{1}{E_c \pi {r_c}^2} \int_0^x \left[\pi {r_c}^2 \sigma_c - 2\pi r_c \int_0^\xi \tau_{A_{fc}c}(\xi, r_c) d\xi\right] dx = \frac{1}{E_b \pi (r_b - r_{A_{bf}})^2} \int_0^x \left[\pi (r_b - r_{A_{bf}})^2 \sigma_b - 2\pi r_f \int_0^\xi \tau_{A_{bf}f}(\xi, r_f) d\xi\right] dx + \frac{r_f}{G_{A_{bf}}} \tau_{A_{bf}f}(x, r_f) \ln(\frac{r_{A_{bf}}}{r_f}) + \frac{r_c}{G_{A_{fc}}} \tau_{A_{fc}c}(x, r_c) \ln(\frac{r_{A_{fc}}}{r_c})$$

(***Equation 28***)

and

$$\frac{1}{E_b \pi (r_b - r_{A_{bf}})^2} \int_0^x \left[\pi (r_b - r_{A_{bf}})^2 \sigma_b - 2\pi r_f \int_0^\xi \tau_{A_{bf}f}(\xi, r_f) d\xi\right] dx = \frac{r_f}{G_{A_{bf}}} \tau_{A_{bf}f}(x, r_f) \ln(\frac{r_{A_{bf}}}{r_f}) + \frac{r_c}{G_{A_{fc}}} \tau_{A_{fc}c}(x, r_c) \ln(\frac{r_{A_{fc}}}{r_c}) + \frac{1}{E_c \pi {r_c}^2} \int_0^x \left[\pi {r_c}^2 \sigma_c - 2\pi r_c \int_0^\xi \tau_{A_{fc}c}(\xi, r_c) d\xi\right] dx$$

(***Equation 29***)

Differentiating ***Equation 28*** and ***Equation 29*** twice, the equations become

$$\frac{r_f}{G_{A_{bf}}} \ln(\frac{r_{A_{bf}}}{r_f}) \frac{d^2 v}{dx^2} - \frac{2 r_f}{E_b (r_b - r_{A_{bf}})^2} v + \frac{r_c}{G_{A_{fc}}} \ln(\frac{r_{A_{fc}}}{r_c}) \frac{d^2 u}{dx^2} + \frac{2 r_c}{E_c {r_c}^2} u = 0$$

(***Equation 30***)

and

$$\frac{r_c}{G_{A_{fc}}} \ln(\frac{r_{A_{fc}}}{r_c}) \frac{d^2 u}{dx^2} + \left[\frac{2 r_c}{E_c {r_c}^2} + \frac{2 r_c}{E_f (r_f - r_{A_{fc}})^2}\right] u - \frac{2 r_f}{E_f (r_f - r_{A_{fc}})^2} v = 0$$

(***Equation 31***)

Differentiating ***Equation 31*** twice and substituting it into ***Equation 30***, the result becomes

$$\left[E_c {r_c}^2 E_f (r_f - r_{A_{fc}})^2 E_b (r_b - r_{A_{bf}})^2 \ln(\frac{r_{A_{bf}}}{r_f}) \ln(\frac{r_{A_{fc}}}{r_c})\right] \frac{d^4 u}{dx^4} +$$

$$2G \left[\begin{array}{c} E_f (r_f - r_{A_{fc}})^2 E_b (r_b - r_{A_{bf}})^2 \ln\left(\frac{r_{A_{bf}}}{r_f}\right) - E_c {r_c}^2 E_f (r_f - r_{A_{fc}})^2 \ln\left(\frac{r_{A_{fc}}}{r_c}\right) \\ + E_c {r_c}^2 E_b (r_b - r_{A_{bf}})^2 \ln\left(\frac{r_{A_{bf}}}{r_f}\right) + E_c {r_c}^2 E_b (r_b - r_{A_{bf}})^2 \ln(\frac{r_{A_{fc}}}{r_c}) \end{array}\right] \frac{d^2 u}{dx^2} -$$

$$4G^2 \left[E_c {r_c}^2 + E_f (r_f - r_{A_{fc}})^2 - E_b (r_b - r_{A_{bf}})^2\right] u = 0 \qquad \textbf{(\textit{Equation 32})}$$

The real positive roots of $\tau_{A_{fc}c}(x, r_c)$ are

$u =$

$$\sqrt{G_A \left[\left[\frac{1}{②} - \frac{1}{①} - \frac{1}{③} - \frac{1}{④}\right] \pm \sqrt{\left[-\frac{1}{②} + \frac{1}{①} + \frac{1}{③} + \frac{1}{④}\right]^2 + 4\left[\frac{1}{①②} - \frac{1}{①④} + \frac{1}{②③}\right]}\right]}$$

(***Equation 33***)

Considering $\tau_{A_{bf}f}(x, r_f)$, v. Substituting ***Equation 20*** to ***Equation 24*** into ***Equation 18*** and ***Equation 19***, it gives the following equations

$$\int_0^x \left[\frac{\sigma_b}{E_b} - \frac{2r_f}{E_b (r_b - r_{A_{bf}})^2} \int_0^\xi \tau_{A_{bf}f}(\xi, r_f) d\xi\right] dx = \frac{r_f}{G_{A_{bf}}} \tau_{A_{bf}f}(x, r_f) \ln(\frac{r_{A_{bf}}}{r_f}) +$$

$$\frac{r_c}{G_{A_{fc}}} \tau_{A_{fc}c}(x, r_c) \ln(\frac{r_{A_{fc}}}{r_c}) + \int_0^x \left[\frac{\sigma_c}{E_c} - \frac{2r_c}{E_c {r_c}^2} \int_0^\xi \tau_{A_{fc}c}(\xi, r_c) d\xi\right] dx \qquad \textbf{(\textit{Equation 34})}$$

and

$$\int_0^x \left[\frac{\sigma_b}{E_b} - \frac{2r_f}{E_b (r_b - r_{A_{bf}})^2} \int_0^\xi \tau_{A_{bf}f}(\xi, r_f) d\xi\right] dx = \frac{r_f}{G_{A_{bf}}} \tau_{A_{bf}f}(x, r_f) \ln(\frac{r_{A_{bf}}}{r_f}) +$$

$$\int_0^x \left[\frac{\sigma_f}{E_f} - \frac{2r_f}{E_f (r_f - r_{A_{fc}})^2} \int_0^\xi \tau_{A_{bf}f}(\xi, r_f) d\xi + \frac{2r_c}{E_f (r_f - r_{A_{fc}})^2} \int_0^\xi \tau_{A_{fc}c}(\xi, r_c) d\xi\right] dx$$

(***Equation 35***)

Differentiating ***Equation 34*** and ***Equation 35*** twice, the equations become

$$\frac{r_f}{G_{A_{bf}}} \ln(\frac{r_{A_{bf}}}{r_f}) \frac{d^2 v}{dx^2} + \frac{2r_f}{E_b (r_b - r_{A_{bf}})^2} v + \frac{r_c}{G_{A_{fc}}} \ln(\frac{r_{A_{fc}}}{r_c}) \frac{d^2 u}{dx^2} - \frac{2r_c}{E_c {r_c}^2} u = 0$$

(***Equation 36***)

and

$$\frac{r_f}{G_{A_{bf}}}\ln(\frac{r_{A_{bf}}}{r_f})\frac{d^2v}{dx^2}+\left[\frac{2r_f}{E_b(r_b-r_{A_{bf}})^2}-\frac{2r_f}{E_f(r_f-r_{A_{fc}})^2}\right]v+\frac{2r_c}{E_f(r_f-r_{A_{fc}})^2}u=0$$

(***Equation 37***)

Differentiating ***Equation 37*** twice and substituting it into ***Equation 36***, the result becomes

$$\left[E_c{r_c}^2E_f(r_f-r_{A_{fc}})^2E_b(r_b-r_{A_{bf}})^2\ln\left(\frac{r_{A_{bf}}}{r_f}\right)\ln\left(\frac{r_{A_{fc}}}{r_c}\right)\right]\frac{d^4v}{dx^4}+$$

$$2G\left[\begin{array}{c}E_c{r_c}^2E_f(r_f-r_{A_{fc}})^2\ln\left(\frac{r_{A_{fc}}}{r_c}\right)-E_c{r_c}^2E_b(r_b-r_{A_{bf}})^2\ln\left(\frac{r_{A_{fc}}}{r_c}\right)\\-E_c{r_c}^2E_b(r_b-r_{A_{bf}})^2\ln\left(\frac{r_{A_{bf}}}{r_f}\right)-E_f(r_f-r_{A_{fc}})^2E_b(r_b-r_{A_{bf}})^2\ln\left(\frac{r_{A_{bf}}}{r_f}\right)\end{array}\right]\frac{d^2v}{dx^2}-$$

$$4G^2\left[E_f(r_f-r_{A_{fc}})^2-E_b(r_b-r_{A_{bf}})^2+E_c{r_c}^2\right]v=0$$

(***Equation 38***)

The real positive roots of $\tau_{A_{bff}}(x,r_f)$ are

$$v=$$

$$\sqrt{G_A\left[\left[-\frac{1}{\text{②}}+\frac{1}{\text{①}}+\frac{1}{\text{③}}+\frac{1}{\text{④}}\right]\pm\sqrt{\left[\frac{1}{\text{②}}-\frac{1}{\text{①}}-\frac{1}{\text{③}}-\frac{1}{\text{④}}\right]^2+4\left[\frac{1}{\text{①②}}-\frac{1}{\text{①④}}+\frac{1}{\text{②③}}\right]}\right]}$$

(***Equation 39***)

Considering the pull-out action from ZnO/epoxy core, the general solution for ***Equation 38*** is expressed as

$$\tau_{A_{bff}}(x,r_f)=C_1\cosh(ux)+C_2\sinh(ux)+C_3\cosh(vx)+C_4\sinh(vx)$$

(***Equation 40***)

Four unknowns of C_1, C_2, C_3 and C_4 are determined by the four boundary conditions as shown below in ***Equation 41***.

1. $N_b(0)=\pi\left(r_b-r_{A_{bf}}\right)^2\sigma_b=C_1$
2. $N_b(L_f)=0=C_2$
3. $\int_0^{L_f}\tau_{A_{bff}}(x,r_f)dx=\frac{\left(r_b-r_{A_{bf}}\right)^2\sigma_b}{2r_f}=C_3$
4. $\int_0^{0}\tau_{A_{bff}}(x,r_f)dx=0=C_4$ (***Equation 41***)

At the centre of the whole composite, $x = 0$, the normal tensile force acting on the epoxy base is at its maximum value as the force is supposed to be fully transferred from the ZnO/epoxy core to the epoxy base and the axial shear stress acting on the adhesive layer of A_{bf} is zero as it is considered to have no friction or no contact surface area between the elements. At the edge of HGF, L_f, the normal tensile force acting on the epoxy base is zero as the force is supposed to be fully transferred from the ZnO/epoxy core to the epoxy base and the axial shear stress acting on the adhesive layer of A_{bf} is maximum as it is considered to experience the maximum friction or maximum contact surface area between the elements.

Combining ***Equation 41*** into the integration of ***Equation 40***, the solution would become

$$\int_0^x \tau_{A_{bf}f}(x, r_f)dx = \left(r_b - r_{A_{bf}}\right)^2 \sigma_b \left[\frac{v\sinh(ux) - u\sinh(vx)}{2r_f\left(vsinh(uL_f) - usinh(vL_f)\right)}\right] \quad \text{(\textbf{\textit{Equation 42}})}$$

And using ***Equation 27***, the final form for the axial strain deformation condition of ZnO/HGF lamina would be

$$\varepsilon_b(x) = \varepsilon_c\left[1 - \frac{vsinh(ux) - usinh(vx)}{vsinh(uL_f) - usinh(vL_f)}\right] \quad \text{(\textbf{\textit{Equation 43}})}$$

where ε_c is the maximum axial strain of ZnO/epoxy core.

Equation 43 shows the axial strain deformation condition is dominated by the constant variables, u and v, and he length of HGF, L_f. The parameters are integrated by factors of the mechanical and geometrical properties of all elements in the composite system, ZnO/epoxy core, HGF, epoxy base and two adhesive layers.

Every change of factors representing the mechanical and geometrical properties of all elements in the composite system influences the axial strain deformation at the bonding end of the composite system, which this phenomenon is represented by the presence of hyperbolic function, $\sinh(ux)$, in the mathematical expression. Moreover, according to the mathematical equation, the axial strain deformation of epoxy base is equal to the maximum axial strain of ZnO/epoxy core at $x = 0$ which this explains the applied stress is fully transferred from ZnO/epoxy core to epoxy base.

Five conditions of ZnO/HGF lamina are concerned to study the change of single factor representing the mechanical or geometrical property of each element in the composite to the stress transfer ability of the bulk composite under fibre pull-out action. Five conditions are the change of ZnO content in ZnO/epoxy core; hollowness of HGF; length of HGF; thickness of HGF; shear strength and thickness of adhesive layers.

8.1.1 Condition One Content of Zinc Oxide in the Core, E_c

The content of ZnO nanoparticle in ZnO/epoxy core is changed to investigate its effect to the stress transfer ability of the bulk composite. The change of ZnO content yields different stiffness and UVR absorbabilities of the ZnO/epoxy core. There are three major approaches of Rule of Mixtures (ROM) to predict the elasticity of fibre or particle reinforced composite based on the mechanical and geometrical properties of the filler and polymer matrix. Voigt model (upper bound) [Joshy et al., 2013; Kim et al., 2001; Olmos et al., 2014] and Reuss model (lower bound) [Kim et al., 2001], which correspond to the longitudinal and transverse loading respectively, are commonly used. Halpin-Tsai equation is another method formulated by experimental measurements for the prediction [Shenoi et al., 2002]. Since HGF in the composite is arranged in unidirectional direction and placed parallel to the applied axial tensile load in the present investigation, Voigt model, which is commonly used, is chosen for the analysis of the elasticity of ZnO/HGF lamina and it is formulated as

$$E_{c\,(upper\ bound)} = E_m V_m + E_p V_p \qquad \textbf{(\textit{Equation 44})}$$

where c is the ZnO/epoxy core, m is epoxy resin and p is ZnO nanoparticle.

Young’s Modulus of ZnO/epoxy core with different ZnO contents are calculated. The Young’s Modulus of neat epoxy core, 2 wt.%, 4 wt.%, 5 wt.% and 7 wt.% of ZnO/epoxy core ($E_{0\%}, E_{2\%}, E_{4\%}, E_{5\%}$ and $E_{7\%}$) are 3GPa, 5.2GPa, 7.3GPa, 8.4GPa and 10.6GPa respectively. ZnO content changes the Young’s modulus of ZnO/epoxy core accordingly that larger ZnO content contributes higher stiffness of ZnO/epoxy core.

The curves showing in ***Figure 8.5*** demonstrate the axial strain deformation of epoxy base in the composite which represent the stress transfer ability of the bulk composite. The composite with larger ZnO content providing higher stiffness of ZnO/epoxy core possesses stronger stress energy absorption per unit length where the dissipation of stress energy transferred to the last epoxy base layer is completed earlier. 7 wt.% ZnO/HGF lamina completes the stress energy dissipation at its original length of around 0.1440m from the centre which is faster compared to the neat epoxy/HGF lamina completes the stress energy dissipation at its original length of around 0.1418m from the center. 4 wt.% ZnO/HGF lamina completes the stress energy dissipation at its length of around 0.1436m obtaining a similar stress transfer ability to 7 wt.% ZnO/HGF lamina.

According to the surface morphology characterization discussed in ***section 7.1.2.2.1***, 7 wt.% ZnO nanoparticle appears to be agglomerated inside 100μm HGF. In this theoretical analysis, ZnO/epoxy core is considered as isotropic, therefore, the elasticity of ZnO/epoxy core in real case is not accurately predicted. Moreover, with the agglomeration of ZnO nanoparticles in epoxy, the elasticity and stress transfer ability of ZnO/epoxy core are lowered and unpredictable. Nevertheless, 4 wt.% ZnO/epoxy core has proven having a satisfactory stress transfer ability of the lamina, for this reason, this parameter is adopted for the following analyses.

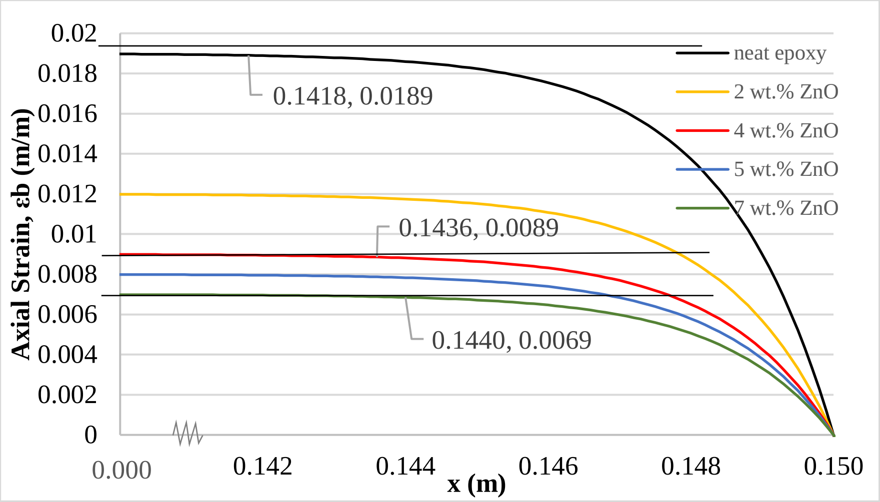

Figure 8.5 Strain deformation of epoxy base with different contents of ZnO nanoparticle in core under fibre pull-out action

8.1.2 Condition Two Length of Hollow Glass Fibre, L_f

The length of HGF is determined as an important factor for the stress transfer ability of fibre composite [Fu et al., 2000; Gao et al., 2013; Hata et al., 2010; Koyanagi et al., 2012; Luethi et al., 1998; Martyniuk et al., 2013; Pietrzak et al., 1984; Thomason et al., 2014]. It is changed to investigate its effect to the stress transfer ability of the bulk composite. The change of HGF length yields different load carrying capabilities of ZnO/HGF. HGF length of 5cm, 10cm, 15cm, 20cm and 25cm were selected to be analyzed.

Figure 8.6 shows the axial strain deformation of the last epoxy base layer when the axial tensile stress is transferred to this layer from ZnO/epoxy core. The composite with longer HGF length providing longer time for stress energy dissipation possesses higher load carrying capability where the occurrence of failure is delayed. Therefore, failure is likely happened first in the composite with shorter HGF provided that all composites experience the same axial tensile load. The change of HGF length influences the maximum load carrying capability but does not vary the stress transfer ability. All curves showing in the figure present to have the same shape indicating there is no difference in the stress transfer ability among all samples.

Furthermore, the critical HGF length for the composite to be failure is determined as 2cm with the fundamental configuration of the composite listed in ***Table 8.1*** and under the same axial tensile load applied to the composite with other samples. Since at the HGF length of 2cm, no solution is resulted from the mathematical formula constructed in the present theoretical analysis. HGF length shorter than 2cm is not considered having load carrying capability in the composite. Accordingly, HGF longer than 2cm is required to provide load carrying capability for the composite. As 25cm is the length of HGF obtaining satisfactory stress transfer ability of the composite, this factor is utilized for other analyses.

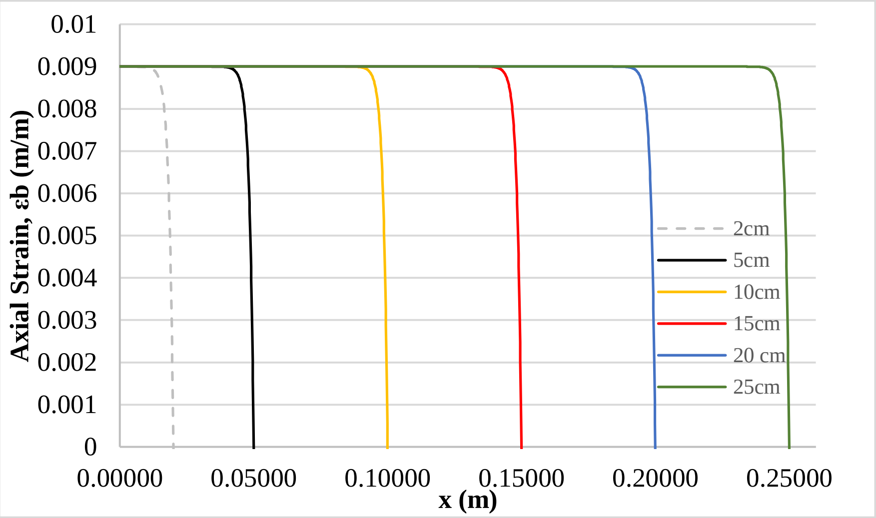

Figure 8.6 Strain deformation of epoxy base with different lengths of HGF under fibre pull-out action

8.1.3 Condition Three Thickness of Hollow Glass Fibre, t_f

The thickness of HGF is changed to investigate its effect to the stress transfer ability of the bulk composite. The change of HGF thickness yields different cross-sectional areas per unit length of HGF. HGF thickness of 15µm, 20µm, 25µm, 30µm and 35µm ($HGF_{15\mu m}$, $HGF_{20\mu m}$, $HGF_{25\mu m}$, $HGF_{30\mu m}$ and $HGF_{35\mu m}$) were taken to be analyzed.

The composite with larger HGF thickness providing larger cross-sectional area of HGF possesses stronger stress energy absorption per unit length where the dissipation of stress energy transferred to the last epoxy base layer is completed earlier. From ***Figure 8.7***, 4 wt.% ZnO/$HGF_{35\mu m}$ lamina completes the stress energy dissipation slightly faster compared to the 4 wt.% ZnO/$HGF_{15\mu m}$ lamina. 4 wt.% ZnO/$HGF_{25\mu m}$ lamina completes the stress energy dissipation at a point similar to 7 wt.% ZnO/$HGF_{35\mu m}$ lamina. As 25µm is the thickness having a satisfactory stress transfer ability of the composite, this factor is implemented in other analyses.

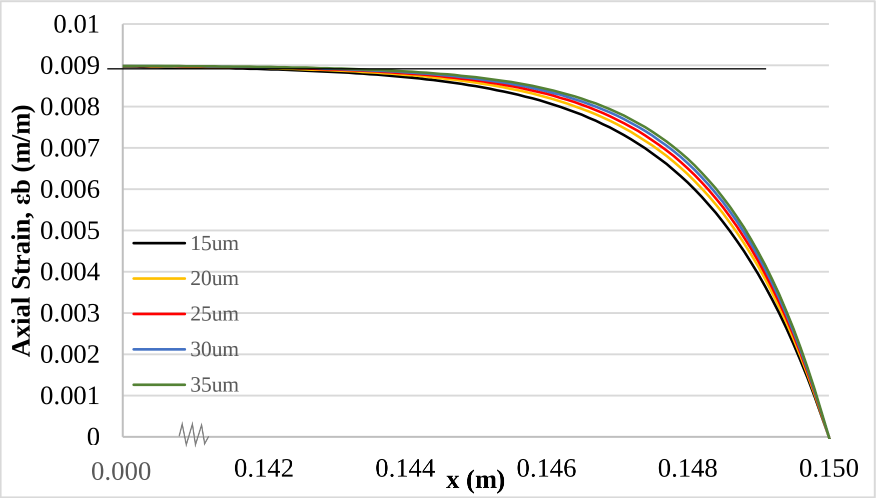

Figure 8.7 Strain deformation of epoxy base with different thicknesses of HGF under fibre pull-out action

8.1.4 Condition Four Shear Strength of Adhesive Layer, G_A

The shear strength of adhesive layer is changed to investigate its effect to the stress transfer ability of the bulk composite. The change of shear strength yields different shear carrying capabilities of the adhesive layer and stress transfer abilities of the bulk composite. Two adhesive layers, A_{fc} and A_{bf}, with the same configuration is incorporated in the composite. Adhesive layer shear strength of 1.2GPa, 1.4GPa, 1.6GPa, 1.8GPa and 2.0GPa were chosen to be analyzed.

Figure 8.8 shows there is a difference among all laminas in the stress transfer ability. With the mathematical equation of shear modulus, $G = \frac{\tau}{\gamma}$ where τ is the shear stress and γ is the shear deformation, the composite with lower adhesive layer shear strength providing higher axial shear deformation of adhesive layer under the same shearing load applied possesses stronger stress energy absorption where most of the stress energy is dissipated before transferring to the last epoxy base layer. 4 wt.% ZnO/HGF lamina with adhesive layer of 1.2GPa shear strength completes the stress energy dissipation at its original length of around 0.1442m from the centre which is faster compared to the 4 wt.% ZnO/HGF lamina with adhesive layer of 2.0GPa shear strength completes the stress energy dissipation at its original length of around 0.1424m from the centre. 4 wt.% ZnO/HGF lamina with adhesive layer of 1.2GPa shear strength has proven having a satisfactory stress transfer ability of the composite and this parameter is utilized in other analyses.

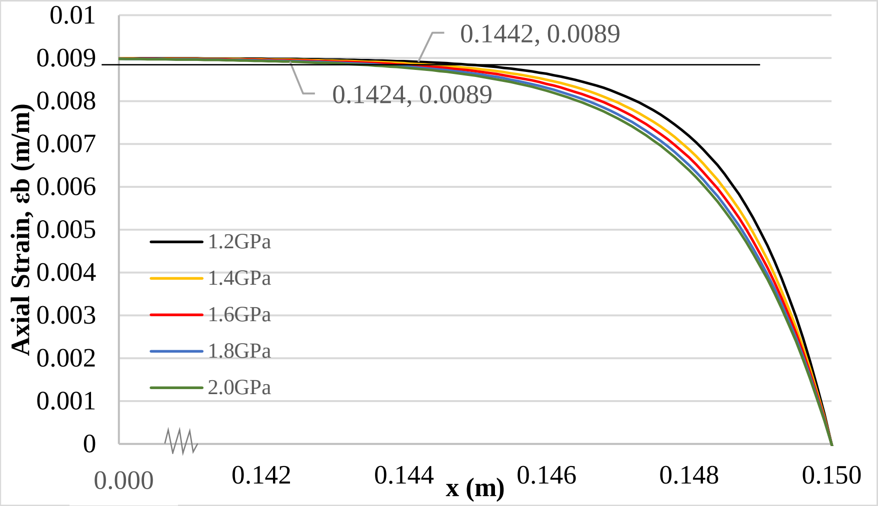

Figure 8.8 Strain deformation of epoxy base with different shear strengths of adhesive layers under fibre pull-out action

8.1.5 Condition Five Thickness of Adhesive Layer, t_A

The thickness of adhesive layer is changed to investigate its effect to the stress transfer ability of the bulk composite. The change of thickness yields different shear carrying capabilities of the adhesive layer and stress transfer abilities of the bulk composite. Two adhesive layers, A_{fc} and A_{bf}, with the same configuration is incorporated in the composite. In real situation, adhesive layer is an additive treated on the surface of fibre implemented in polymer or the interface between two elements, fibre and polymer, in the composite. However, the mechanical and geometric properties of the interface between two elements is difficult to be controlled by controlling the curing process of the composite. Additive produced the adhesive layer between HGF and epoxy or called as the surfactant on HGF is considered of a few percentages of polymer resin. In this analysis, the surfactant weight percentages of 0.4%, 0.6%, 0.8%, 1% and 1.2% yield the adhesive layer thickness of 2.8μm, 3.5μm, 4.0μm, 4.5μm and 4.9μm respectively were chosen to be analyzed.

By comparing the results shown in ***Figure 8.8*** and ***Figure 8.9***, the stress transfer behaviour of composite obtained by changing the thickness of adhesive layer and the shear strength of adhesive layer are almost the same. keeping the same shear modulus of adhesive layer, with the mathematical equation of shear modulus, $G = \frac{\tau}{\gamma}$ where τ is the shear stress and γ is the shear deformation, the composite with lower adhesive layer thickness providing higher axial shear deformation of adhesive layer under the same shearing load applied possesses stronger stress energy absorption where most of the stress energy is dissipated before transferring to the last epoxy base layer. 4 wt.% ZnO/HGF lamina with adhesive layer of 2.8μm thickness completes the stress energy dissipation at its original length of around 0.1446m from the centre which is faster compared to the 4 wt.% ZnO/HGF lamina with adhesive layer of 2.8μm thickness completes the stress energy dissipation at its original length of around 0.1429m from the centre. 4 wt.% ZnO/HGF lamina with adhesive layer of 2.8μm thickness has proven having a satisfactory stress transfer ability of the composite, nevertheless, adhesive layer of 4.5μm thickness considered as 1% of polymer of surfactant which is commonly adopted in manufacturing process of doped-fibre or nanoparticle for enhancing the compatibility is utilized in other analyses.

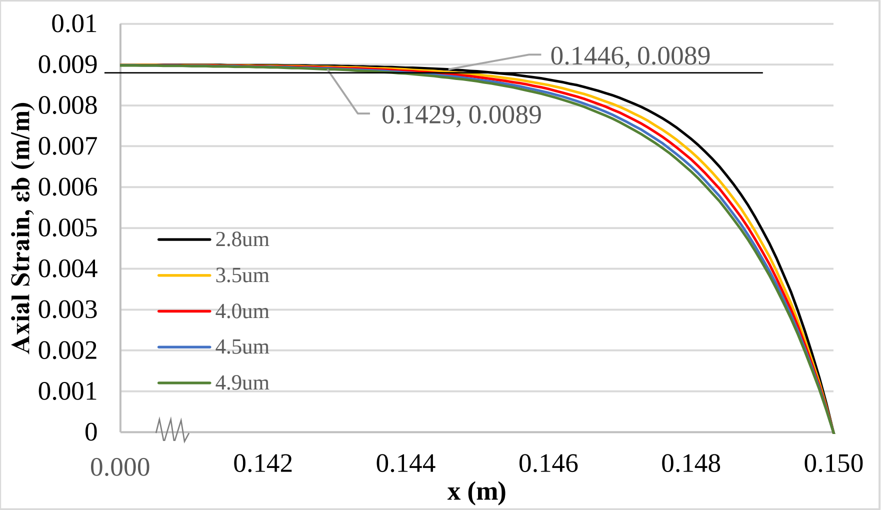

Figure 8.9 Strain deformation of epoxy base with different thicknesses of adhesive layers under fibre pull-out action

8.2 Summary of This Chapter

A theoretical model, $\varepsilon_b(x) = \varepsilon_c\left[1 - \frac{v\sinh(ux) - u\sinh(vx)}{v\sinh(uL_f) - u\sinh(vL_f)}\right]$, was developed for the analyses of stress transfer ability of ZnO/HGF lamina, a five-cylinder model, with five different conditions. Although the lamina is about hundreds micrometer thin on top of FRP stacks, it is required to understand its stress transfer ability as different mechanical actions, like scratching and shearing, might be happened to this top lamina. The analyses of five conditions include the change of ZnO content in ZnO/epoxy core; length of HGF; thickness of HGF; shear strength and thickness of adhesive layers. Combined with the experimental analyses, 4 wt.% ZnO/HGF$_{25\mu m\ \text{thickness}}$ lamina has an optimal result in stress transfer with the absence of particle agglomeration. HGF with larger thickness and longer fibre length have higher load taking or carrying capability. At the fundamental configuration shown in *Table 8.1*, 2mm is the critical HGF length of 4 wt.% ZnO/HGF lamina for load carrying. Adhesive layer with lower shear strength and smaller thickness are effective of ZnO/HGF lamina for stress transfer.

Chapter Nine

Concluding Remarks and Suggestions for Future Development

A summarized conclusion for the present research is made in ***Chapter Nine*** which is the last chapter of this thesis. The investigation documented in this thesis is not the completion for the research on UVR degradation and resistance in polymer-based composites. Future potential development of the research on this subject is also suggested in this chapter indicating there are plenty of room to be exploited for the integrity of polymer-based composites.

This research aims at providing a feasible and durable solution for the UVR protection of FRPs employed in aircraft and civil construction exposing constantly under UVR during their service.

9.1 Concluding Remarks

Up to the moment in present research, few significant findings have been confirmed regarding the development of ultraviolet radiation (UVR) resistant polymer-based materials. Zinc oxide (ZnO) particle with 100nm diameter is found to be performing optimized results in UVR absorption due to its good dispersion properties in polymers, epoxy, unsaturated polyester, epoxy-base and styrene-based shape memory polymers (EP- and S-SMPs). 100nm ZnO particle at 4 wt.% has the best dispersion properties in hollow glass fibre (HGF) and therefore the best UVR absorption of its 4 wt.% 100nm ZnO/HGF lamina among the tested samples including epoxy, 2 wt.% and 7 wt.% 100nm ZnO/HGF laminas. In different intervals of HGF, 4 wt.% 100nm ZnO/HGF lamina still achieves a steady UVR absorbability which is 1.5x higher than neat epoxy/HGF lamina. This indicates ZnO particle is active in UVR absorption. Furthermore, 4 wt.% 100nm ZnO particle also exhibits good particle dispersion and UVR absorption which enable it to maintain the surface hardness and shape memory effects in EP- and S-SMPs after UVA exposure.

20nm silane-doped ZnO and 100nm ZnO particles are compared for their particle dispersion and polymerization shrinkage properties with epoxy in HGF. Silane surface on ZnO particle and the diameter of particle do not exhibit any effects to the properties, but the ratio of ZnO particle to epoxy leads to the variations. The investigations reveal that ZnO:epoxy at 1:24 is an optimal ratio for achieving even particle dispersion, good dimension stability and rheology properties. 4 wt.% 100nm ZnO/epoxy exhibits the lowest viscosity similar to neat epoxy. Particle agglomeration occurs when the ZnO particle content is increased to 7 wt.%. Subsequently, 7 wt.% 100nm ZnO/epoxy poses the highest viscosity and 7 wt.% 100nm ZnO/HGF lamina poses the lowest UVR absorption.

Besides the influence of particle dispersion property to the UVR absorbability of ZnO particle in HGF, other determinants are the particle dispersion method and surface property on ZnO particle. ZnO dispersed by mechanical stirring achieves better UVR absorption embedded in epoxy. In addition, ZnO particle with silane surfactant performs lower UVR absorption than ZnO particle without silane surfactant. These two phenomena are required to be confirmed in later experiments.

The surface morphology and tensile properties of glass fibre unsaturated polyester composite with 6 wt.% 100nm ZnO particles embedded in the first three layers of glass fabric underwent accelerated continuous and cyclic UVA exposure are compared. Significant changes occur in the tensile properties but not in the surface morphology. The rate of change of the Young's modulus of the composite that has undergone continuous UVA exposure is 2 times higher than that with cyclic UVA exposure. It has similar result in the tensile strength which is 1.16 times higher. Experimental methodology for the investigation of UVR effects in polymer-based materials should be unified and mechanical properties should be the determinant for the degradation rate of polymer-based composites and estimation on their service life.

Formation of void is observed on the polymer surface of glass fibre epoxy and unsaturated polyester composites without the implementation of ZnO particles in the layers exposed under UVR. ZnO particles are able to reinforce the polymer surface from void formation against UVR attacks since the particles entangle with polymer chains and they are interconnected when they are well dispersed. Whenever the particles-polymer chains system is under stress, the particles in between decrease the latitude of movement of polymer chains. This phenomenon is also revealed in another experiment on SMPs. EP-SMP exhibits stronger surface hardness and better recovery characteristics than S-SMP. However, after UVA exposure, surface hardness of EP-SMP is lower than S-SMP. By Implementing 4 wt.% 100nm ZnO particles, the surface hardness is able to be maintained to a certain level. With different contents of ZnO particles, the full recovery ratio of EP-SMP is still able to achieve full recovery. ZnO particles increase the polymer molecular density and bonding strength between polymer chains results in less deterioration against UVR attacks.

Theoretical model, $\varepsilon_b(x) = \varepsilon_c \left[1 - \frac{vsinh(ux) - usinh(vx)}{vsinh(uL_f) - usinh(vL_f)}\right]$, was developed for the parameter optimization in designing the configuration of ZnO/HGF lamina considering stress transfer ability. Combining the results obtained from experimental analysis, 4 wt.% 100nm ZnO/HGF lamina with longer length of HGF poses good stress transfer ability, load carrying capability, particle dispersion and UVR resistibility.

To summarize, with the increasing utilization of FRPs in aerospace and civil engineering applications, UVR protection is an essential criterion where the materials are inevitably used under cyclic UVR exposure and dynamic load. Together with other environmental conditions, for instance, extreme temperature, moisture and vacuum, the damaging effects in polymer-based materials would be more severe and unpredictable. 100nm ZnO/HGF lamina on top of core polymer-based materials is desirable for UVR resistance which allows to enhance the physical UVR absorption by ZnO particles with high density and uniform dispersion and suppresses the chemical UVR absorption in polymer while protecting the ZnO particles from dissolution out of the polymer and enhancing the wearability of the polymer surface by HGF.

9.2 Suggestions for Future Development

Summary of present research has been made in the previous section and followed by the discussion below on the potential developments for UVR resistant polymer-based materials. The following discussion is divided into three sections, systematic investigation on the UVR degradation in polymer-based materials, further development and possible applications of ZnO/HGF lamina on polymer-based materials for UVR resistance and potential multifunctional applications of ZnO particle in polymer-based materials.

9.2.1 Systematic Investigation on the UVR Degradation in Polymer-based Materials

9.2.1.1 UVR Exposure Method

Taking the advantage of time-cost efficiency, accelerated continuous and cyclic UVR exposure are widely adopted for simulating natural sunlight exposure to study UVR degradation in polymer-based materials. However, from the experiment conducted in present research, 0.5 to 2 times difference are found between the tensile properties of the FRPs with continuous and cyclic exposure. In real situation, materials are randomly utilized under continuous and/or cyclic UVR exposure. In this case, both exposures are essentially implemented to investigate the UVR degradability of polymer-based materials. The continuous exposure is considered as the upper boundary while the cyclic exposure is considered as the lower boundary towards the life expectancy of materials.

Important criteria for UVR exposure are the energy intensity and exposure period which determine the accumulated UVR energy, a determinant of degradation, experienced in the exposed materials. Moreover, trend analysis is preferred as the response of polymer-based composites against UVR attacks is dynamic and therefore the absolute value of the mechanical properties of exposed materials is fluctuated with time.

9.2.1.2 Failure Imaging Technique

Non-destructive and online testing techniques are suggested to be used for characterizing the degree of damages caused by UVR exposure or other environmental effects in FRPs in terms of the cost and time efficiency. Infrared Thermography (IRT) and Shearography [Lai et al., 2009] demonstrated their effectiveness in characterizing the flaws embedded in CFRP-strengthened concrete. Damages, such as cracks and delamination, causing deterioration of mechanical properties of FRPs are possible to be observed under specific kinds of imaging techniques. Undoubtedly, mechanical property tests should be conducted together with efficient imaging techniques to evaluate the deterioration and determine the life prediction of FRPs under various environmental exposures.

9.2.1.3 Theoretical Analysis

Arrhenius and Eyring equations mentioned in ***section 5.2*** are developed to analyze the chemical reaction rate of polymer-based materials under thermal degradation. Theoretical analysis of the physical and chemical reaction rate of polymer-based composites under UVR degradation delivers a direction for investigation as little research has been done on this issue. In addition, the theoretical model would consist elements of the reaction rate in terms of mechanical properties changes of polymer-based composites against UVR attacks.

9.2.2 Further Development and Possible Applications of ZnO/HGF Lamina on Polymer-based Materials for UVR Resistance

9.2.2.1 Combined Environmental Effects (UVR, Extreme Temperature (±150°C) and Vacuum in Space)

Section 2.2 has mentioned the nature of UVR in space and on the Earth. Ozone is the atmospheric layer capable of scattering a part of UVB and almost all UVC to prevent them from entering the Earth. Scientists keep working to find out the UVR condition in space which is more complicated than that on the Earth. It has been found that clouds of gas or particles containing newly formed stars are many times more massive than the Sun and glowing strongly in UVR which contains a considerable amount of UVA, UVB and UVC at around 10^{-3}mW/(cm^2•nm) [NASA, 2001].

NASA in Composite Conference 2012 addressed the increasing utilization of polymer-based composite in space applications. Extreme temperature (±150°C) and vacuum conditions in space should impose effects in polymer-based materials besides UVR. The related studies are required to be investigated to understand the behaviour of polymer-based materials under different environments.

According to some literatures and the present research, oxygen is one of the necessities for processing the chemical UVR degradation in polymers. The UVR degradation mechanism of polymer-based materials under vacuum condition is not well understood which opens a direction for investigation.

9.2.2.2 Combined Environmental Effects (UVR, High Temperature, Moisture and Chemicals on the Earth)

Polymer-based materials are intrinsically susceptive to UVR, temperature, moisture and chemicals. The effects of combined environmental condition would result in unexpected impacts in the exposed materials unless we understand the imposed effect of each condition in the materials.

Polymer-based materials applied in civil buildings are constantly in contact with different degrees of UVR, temperature and moisture and the materials applied in medical applications have to contact with different chemicals and radiations together with temperature and moisture. Polymer-based materials are mandatorily examined with various environmental effects before being used in various applications.

9.2.2.3 Combined Mechanical Effects (Static and Dynamic)

Combining the effects of static and dynamic stress applied on the materials, the deterioration of the mechanical properties of polymer-based materials is the most critical if they are used for structural applications. Especially, the latest commercial aircrafts are implementing FRPs in their fuselage and the development of using FRPs is expected to grow increasingly. Materials used in fuselage experience thermal changes, expansion and contraction during takeoff and landing of the aircraft. However, during the flight in lower stratospheric level, fuselage material constantly expands due to the lower pressure outside of the aircraft. The temperature and pressure of the atmosphere induce static and dynamic mechanical stresses in FRPs.

9.2.2.4 Applications of ZnO/HGF Lamina (Aircraft, Civil Building, Automobile, Eyeglass and Clothing Industries)

The purpose of developing ZnO/HGF lamina is to protect the core materials from UVR degradation and deterioration of mechanical properties. The lamina is proposed to be the outermost lamina of FRPs or other polymer-based materials utilized on aircraft fuselage and building façade.

Aircraft fuselage not only has to be UVR resistant but also electrical conductive. The existing coating consists of many layers which a clearcoat has to be on top of the UVR resistant and coloured coating layers with around 200μm thickness for protecting underneath layers from wearing. Between the UVR resistant and coloured coating layers and the core FRP is an electrical conducting film for conducting electrical charges out of the aircraft regarding safety issue. ZnO is a promising substance implemented to be multifunction lamina, since ZnO possess electrical conductivity as well as UVR resistance.

Building façades are usually decolourized after long-term UVR exposure from sunlight and chemical wash from rainwater. ZnO/HGF lamina is able to prevent ZnO particles from dissolution out of the polymer and allows the lamina to provide long-term UVR resistant in coloured core building materials.

The UVR resistance and transparent properties of ZnO/HGF lamina could comparable with windows over the strength and brittleness for aircraft, civil building and automobile. The lamina also has potential to be applied in eyeglass and clothing industries to protect human bodies from prolonged UVR exposure which causes irreversible heath damages and, at the same time, to provide safe, durable and flexible materials for use on human.

Appendices

(Copies of Publications)

Composites: Part B 54 (2013) 41–43

Contents lists available at SciVerse ScienceDirect

Composites: Part B

journal homepage: www.elsevier.com/locate/compositesb

Property enhancement of polymer-based composites at cryogenic environment by using tailored carbon nanotubes

Kin-tak Lau [a,*], Tsz-ting Wong [a], Jinsong Leng [b], David Hui [c,d], Kyong Yop Rhee [d]

[a] Department of Mechanical Engineering, The Hong Kong Polytechnic University, Kowloon, Hung Hom, Hong Kong Special Administrative Region
[b] Centre for Composite Materials and Structures, Harbin Institute of Technology (HIT), Harbin 150080, PR China
[c] Department of Mechanical Engineering, University of New Orleans, LA 70148, USA
[d] Department of Mechanical Engineering, Kyung Hee University, Yongin, Republic of korea

ARTICLE INFO

Article history:
Received 2 February 2013
Accepted 26 March 2013
Available online 10 April 2013

Keywords:
B. Mechanical property
B. Delamination
B. Hardness
A. Nano-structures

ABSTRACT

At high attitude, all polymer-based materials would suffer from degradation at very low temperature in the range between 220 and 77 K (commonly called “at cryogenic environment”) and low atmospheric pressure. Within this temperature range, polymer-based composites behave very brittle and many micro-cracks are formed due to differential thermal coefficients of expansion (CTEs) between polymer matrix and high strength reinforcements. An anti-cracking mechanism in the composites is necessary and can be tailored by using nano-particles. Many studies have addressed that the use of single-walled (SWNTs) and multi-walled carbon (MWNTs) nanotubes could enhance the mechanical properties of polymer-based composites. However, interfacial bonding properties are always an issue as it would affect the efficiency and effectiveness of stress transfer in the composites. This paper addresses the viability of using coiled carbon nanotubes (CCNTs) and randomly-oriented nanoclay-supported nanotubes (NSCNTs) to enhance the mechanical properties of epoxy resin at the cryogenic environment.

1. Introduction

In the outer space, composite structures are always subject to cyclic thermal stress in which one surface of the structures facing to the Sun experiences temperature over 393 K while an opposite side is 173 K. Besides, the structures may also suffer from damages due to meteoroid attack, in which many tiny particles left over from the formation of the solar system and they are travelling at very high speed to cause serious impact and abrasion onto the structures. In the new Ares V Cargo Launch Vehicle (for the Mar’s mission) designed by National Aeronautics and Space Administration (NASA), the core fuel storage tank will be made by using polymer-based composites and many materials science and engineering research have been conducted to better understand the behavior of these materials at cryogenic condition [1]. In view of all aforementioned problems, composites used at the high attitude (at the level above the Troposphere) should be able to maintain high strength at low temperature environment. Epoxy-based composites are very popular for making advanced composites due to their high strength and chemically-inert properties, making them excellent to be used as aircraft and aerospace structural materials. However, epoxy normally behaves very brittle and therefore, loss of its toughness and impact performance at low temperature. Besides, due to their low energy dissipatability at low temperature, any impact imposed onto its structures would cause delamination and debond at an interface between reinforced fibre and matrix [2].

Carbon nanotubes (CNTs) have been proved as very promising tiny reinforcements to improve the mechanical properties of polymer-based materials due to their ultra-high mechanical strength and aspect ratio. However, for bare CNTs without being chemically reacted with surface’s functional groups, bonding is always an issue to allow stress transfer from the polymer matrix to the CNTs. Debonding followed by bare CNT pull-outs were observed by many research groups worldwide. Lu et al. [3,4] have developed coiled CNTs (CCNTs) and also nanoclay-supported nanotubes (NSCNT) (Figs. 1 and 2) and observed that the bonding properties of composites serving at room temperature (RT) were improved due to their unique surface morphologies.

2. Experimental study and discussion

As aforementioned, epoxy-based composites always suffer from failure due to the brittleness and low energy dissipation ability at the cryogenic environment when the composites are subject to dynamic loadings or foreign object impacts. By using straight CNTs somehow may not be appropriated due to their ultra-high strength

---

* Corresponding author. Tel.: +852 2766 ; fax: +852 2365 4703.
E-mail address: mmktlau@

1359-8368/$ - see front matter © 2013 Elsevier Ltd. All rights reserved.
http://dx.doi.org/10.1016/j.compositesb.2013.03.044

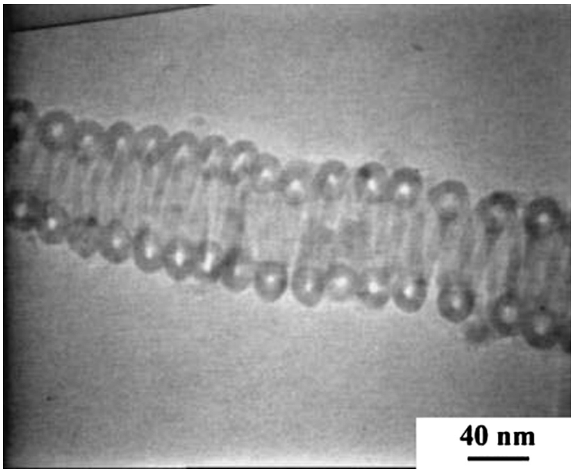

Fig. 1. SEM image of CCNT.

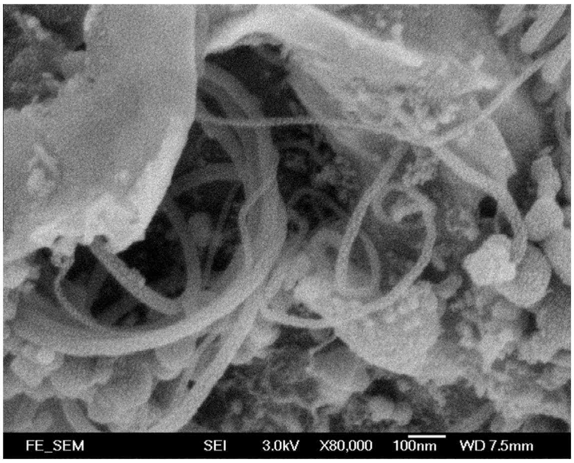

Fig. 2. SEM image of NSCNT.

and poor bonding characteristics between the CNT and matrix. Many studies have shown that pullout of nanotubes happened in polymer-based composites due to poor bonding at the interface. For multi-walled nanotubes (MWNTs), more severe as slipping between inter-walls of the nanotubes exists, which substantially lowers their mechanical strength due to the decrease of effective cross sectional area. To compare the result obtained from MWNT, CCNT and NSCNT reinforced epoxy composites, Table 1 shows that the properties of the composites are enhanced with the use of 2 wt% of CCNTs and NSCNTs as reinforcement at room temperature condition as compared with the one reinforced by 2 wt% MWNTs.

To study the performance of these composites at space environment, CCNTs and NSCNT were therefore used to mix with the epoxy to study their mechanical performance at low temperature (~93 K). All composite samples were tested immediately after they had been submerged into liquid nitrogen for 15 min. The samples were made in the diameter of 25 mm and 10 mm thick. The fabrication process was followed by the instruction as addressed in [5]. For both CCNT/epoxy and NSCNT/epoxy samples, CCNT and NSCNT were added from 0 up to 3 wt%. Hardness and Young's modulus of CCNT/epoxy samples were measured while only hardness test was conducted for NSCNT/epoxy samples.

Table 1
Comparison of the properties of epoxy reinforced by 2 wt% of MWNTs, CCNTs and NCNTs.

	MWNTs	CCNTs	NCNTs
Micro-hardness	0.26	0.31	0.32
Young's modulus	5	5.9	6.2

Table 2
Mechanical properties of CCNT reinforced epoxy composites at room temperature and 77 K.

Wt% of CCNT	Vicker's hardness			Young's modulus		
	RT	77 K	% increase	RT	77 K	% increase
0	0.23	0.31	35	5.0	7.1	42
1	0.28	0.36	28	5.3	7.5	41
2	0.31	0.38	23	5.9	7.9	34
3	0.35	0.41	17	7	8.9	27

In Table 2, it is found that both Vicker's hardness and Young's modulus of CCNT/epoxy samples increase with increasing the CCNT content at both RT and 77 K environments. The increase of strength has no surprise as the geometry of the CCNTs could enhance the strength and resilience of CCNT/epoxy samples. Spring-like CCNT can induce mechanical interlocking in the samples. Besides, this pattern can also increase the energy absorbability of the samples at both static and dynamic loading conditions. According to the Spring's theory, the energy absorption (E) of a spring subject to a compressive load is equal to the half of spring constant of CCNT (k) times the square of the amount of compression (x) ($E = ½kx^2$). As compared with the straight CNT, CCNT obviously has a relatively low mechanical strength along its coil's direction (i.e. coil's longitudinal axis). However, its coiled geometry can secure the bonding between CCNT and surrounding matrix so as enhance the stiffness and hardness of its composites. From the hardness reading, it also shows that the wear properties can also be improved through the use of CCNT as reinforcement in the epoxy. As a low temperature condition, epoxy experiences thermal contraction which induces high compressive strength toward the surface of CCNT. Thus, high clamping strength is resulted and thereby, better mechanical strength of CCNT/epoxy composites can be achieved.

In Table 3, the NSCNT provides similar property enhancement in the epoxy at both RT and 77 K environments. By growing CNT between clay layers can ensure an exfoliated nanoclay structure

Table 3
Hardness of NSCNT reinforced epoxy composites at room temperature and 77 K.

Wt% of NCNTs	Vicker's hardness		
	RT	77 K	% increase
0	0.23	0.31	34
0.5	0.25	0.38	53
1	0.26	0.41	54
2	0.32	0.39	23
3	0.31	0.48	52

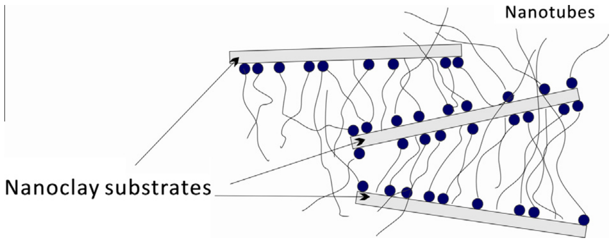

Fig. 3. Schematic of NSCNT (patent: CN 100432009C).

is achieved (Fig. 3). The grown CNTs can also be used as reinforcements for epoxy resin. As NSCNT is a structure combining both exfoliated nanoclay linked by CNTs, agglomeration of NSCNTs would not normally happen which provides the resultant composites with good dispersion properties, and thereby high mechanical strength. As cryogenic environment, although the hardness of a pristine epoxy sample is enhanced, the use of NSCNT can maintain better strength and keep the hardness 30% more as compared with the samples measured at RT condition. This result was firstly governed by the contraction of epoxy which additionally generated strong clamping forces to the NSCNTs, and thus enhanced the bonding strength between NSCNT and epoxy matrix. The uniform dispersion properties of NSCNTs also provided homogenous mechanical strength of the whole NSCNT/epoxy samples. Theoretically, these nano-reinforcements not only enhance the mechanical properties of polymer-based composites, but also minimize their crack-formation.

3. Conclusion

As a conclusion, the CCNTs and NSCNTs can enhance the strength of polymer-based composites due to their tailored geometrical patterns. Although few research works have reported that the use of straight-type of CNTs can enhance the strength of polymers, agglomeration is still an issue when their content exceeds 2 wt%. Compared with straight-type of CNTs, CCNT and NSCNT can compensate many problems arising from poor interfacial bonding properties, brittleness of polymers and agglomeration of CNTs.

Acknowledgment

This project is funded by The Hong Kong Polytechnic University.

References

[1] Human exploration of mars design reference architecture 5.0. NASA-SP-2009-566, July 2009.

[2] Zhang YH, Wu JT, Fu SY, Yang SY, Li Y, Fan L, et al. Studies on characterization and cryogenic mechanical properties of polyimide-layered silicate nanocomposite films. Polymer 2004;45:7579–87.

[3] Mei Lu, Lau KT, Xu JC, Li HL. Coiled carbon nanotubes growth and DSC study in epoxy-based composites. Colloids Surf, A 2005;257-258:339–43.

[4] Lu M, Lau KT, Tam WY, Liao K. Enhancement of vicker's hardness of nanoclay-supported nanotube reinforced novel polymer composites. Carbon 2005;44:381–92.

[5] Yang JP, Chen ZK, Feng QP, Deng YH, Liu Y, Ni QQ, et al. Cryogenic mechanical behaviors of carbon nanotube reinforced composites based on modified epoxy by poly(ethersulfone). Composites: Part B 2012;43(1):22–6.

Materials and Design 56 (2014) 254–257

Contents lists available at ScienceDirect

Materials and Design

journal homepage: www.elsevier.com/locate/matdes

Technical Report

UV resistibility of a nano-ZnO/glass fibre reinforced epoxy composite

Tsz-ting Wong [a], Kin-tak Lau [a,*], Wai-yin Tam [a], Jinsong Leng [b], Julie A. Etches [c]

[a] Department of Mechanical Engineering, The Hong Kong Polytechnic University, Hung Hom, Kowloon, Hong Kong
[b] Centre for Composite Materials and Structures, Harbin Institute of Technology, Harbin, China
[c] Faculty of Engineering, University of Bristol, United Kingdom

ARTICLE INFO

Article history:
Received 19 August 2013
Accepted 7 November 2013
Available online 20 November 2013

ABSTRACT

The harmfulness of ultraviolet (UV) radiation (UVR) to human health and polymer degradation has been the focus recently in all engineering industries. A polymer-based composite filled with nano-ZnO particles can enhance its UV resistibility. It has been found that the use of appropriate amount of nano-ZnO/Isopropyl alcohol solvent to prepare a UV resistant nano-ZnO/glass fibre reinforced epoxy (ZGFRE) composite can effectively block the UV transmission with negligible influence on the crystal structure of its resin system. This paper aims at investigating the interfacial bonding behaviour and UV resistibility of a ZGFRE composite. The solvent effect in relation to the dispersion properties of ZnO in the composite is also discussed. XRD results indicated that 20 wt% Isopropyl alcohol was an effective solvent for filling nano-ZnO particles into an epoxy. SEM examination also showed that the bonding behaviour between glass fibre and matrix was enhanced after filling 20 wt% nano-ZnO particles with 20 wt% Isopropyl alcohol into the composite. Samples filled with 20 wt% nano-ZnO/Isopropyl alcohol and 40 wt% nano-ZnO/Isopropyl alcohol has full absorption of UVA (315–400 nm), UVB (280–315 nm) and a part of UVC (190–280 nm).

1. Introduction

Laminated glass fibre reinforced polymer (GFRP) composites possess high strength and stiffness relative to their weight ratio when compare with conventional metallic materials [1]. These materials are popularly used in the aerospace and civil construction industries. Recently, many researches have focused on exploiting extraordinary functions of composite structures by utilizing hollow glass fibres (HGFs). An investigation on magnetic fibre composites by filling ferromagnetic substances into HGFs has offered a great potential for the development of various functional composites with unique characteristics [2]. Nowadays, a great concern is placed on the harmfulness of ultraviolet radiation (UVR) which attacks human bodies [4,5] and degrades polymer-based composites, particular for all public transportation systems [21]. UVA and UVB are the main sources of UVR in the atmosphere. UVC, which could generate severe damage to human, is mostly absorbed by an ozone layer before reaching to the Earth's surface [3–5]. Once both UVA and UVB reach to human's skin and eyes, it would cause an acute effect of sunburn and chronic effect of skin cancer and cataract [4,5]. Due to an increasing use of composite structures in different transportation vehicles, it is therefore an urgent need to explore UV resistant composites to minimize the harmful effects to human body and polymer-based composite materials.

It is known that zinc oxide (ZnO) is an effective inorganic UVA and UVB radiation absorbent. Unlike other inorganic metal oxides such as titanium oxides (TiO_2), iron oxide (FeO), cerium oxide (CeO_2) and indium tin oxide (ITO), ZnO is abundant, inexpensive, broad spectrum UV resistant, chemically stable and highly transparent in visible light [1,6,7]. By filling ZnO particles into the HGFs to form an integral part of a resultant composite for transportation vehicles, an UV resistant composite structure can be produced for protecting the passengers' health of skin and eyes together with protecting the polymer-based composite structures away from crack formation [21].

2. Experimental approach

In the current study, X-ray Diffraction (XRD) was used to study the solvent effect of Isopropyl alcohol and ethanol inside the epoxy. Scanning Electron Microscope (SEM) was used to investigate the bonding behaviour between glass fibre and matrix and UV–Vis Spectrophotometer was used to investigate the UV resistibility of nano-zinc/glass fibre reinforced epoxy composites (ZGFRECs).

2.1. Materials and samples preparation

5:1 Ratio of Araldite GY251 and hardener HY956 were used to produce epoxy resin as a base for the solvents in the XRD test. The resultant epoxy was then used with plain woven E-glass

---

* Corresponding author. Tel.: +852 2766 ; fax: +852 2365 4703.
E-mail address: mmktlau@.

0261-3069/$ - see front matter © 2013 Elsevier Ltd. All rights reserved.
http://dx.doi.org/10.1016/j.matdes.2013.11.014

fabrics as matrix and reinforcement respectively for producing composites for the SEM and UVR tests. Nano-ZnO particles with Isopropyl alcohol were mixed with the epoxy to be one of the matrix layers for UV protection.

2.2. XRD examination

Nine samples including one control sample (0–8, Table 1) were prepared. One group of epoxy samples (1–4) were mixed with ethanol while another group of epoxy samples (5–8) were mixed with Isopropyl alcohol. Solvents in both sets of samples were tested with different weight contents of 10 wt%, 20 wt%, 40 wt% and 60 wt%. One control sample (0) of epoxy without any solvent was prepared for a comparison purpose. The samples were cured under an ambient condition for 24 h prior to the test. The examination by using XRD (Rigaku Smart Lab) was conducted to investigate the solvent effect inside the epoxy samples.

2.3. SEM and UVR resistibility examinations

Another nine samples including one control sample (0–8, Table 2) were prepared. Each composite sample was fabricated using five layers of plain woven E-glass fabric with epoxy by the hand lay-up process. One group of composite samples (1–4) consisted of one epoxy layer with nano-ZnO particles and 20 wt% Isopropyl alcohol while another group of epoxy sample (5–8) consisted of one epoxy layer with nano-ZnO particles but without Isopropyl alcohol. Nano-ZnO particles in both sets of samples were filled with different weight contents of 4 wt%, 12 wt%, 20 wt% and 40 wt%. Similar to the XRD examination, one control sample (0) of composite without nano-ZnO particles was prepared for a comparison purpose. The composite samples were cured under an ambient condition for 24 h prior to the examination. Examination by using SEM (Jeol 6490) was conducted to investigate the bonding behaviour between glass fibre and matrix (pure epoxy and nano-ZnO/epoxy). UV–Vis spectrophotometer (Dynamica DB-20, 190–1100 nm) was used to investigate the UV absorbability of the samples.

3. Results and discussions

3.1. Solvent effect

Alcoholic organic solvents are commonly used to control the dispersion properties of nano-particles in a solution [14–20]. Ma et al. [16] and Liu and Zeng [17] have stated that the dispersion properties and morphological condition of ZnO crystals are strongly depended on the specific functional groups of solvent media, such as hydroxyl group (OH), in which Isopropyl alcohol and ethanol both have OH in their chemical chains but they have slightly different in physical properties, such as boiling point, density and hydrogen bonding behaviour. In the current investigation, Isopropyl alcohol and ethanol were examined their effect in epoxy matrix for the purpose of dispersing nano-ZnO particles. Diffractograms extracted from the XRD test of the control sample and the sample with 20 wt% Isopropyl alcohol are shown in Figs. 1 and 2 respectively. The control sample has the peak value located at 17.84° (diffraction angle, 2θ) while the sample with 20 wt% Isopropyl alcohol has it at 19.84°. The diffractograms also show that the peak values of the two samples are close to each others. The control sample has the intensity at the peak of 6360 while the sample with 20 wt% Isopropyl alcohol has it at 2663. The intensity of the sample with 20 wt% Isopropyl alcohol is lower than that of the control sample. The diffraction pattern varies the least of the sample with 20 wt% Isopropyl alcohol to the control sample when comparing with the other samples. This implies that the sample with 20 wt% Isopropyl alcohol has the least influence to the epoxy which is a good quantity to be used as solvent.

Table 1
Detail of epoxy samples mixed with different solvents.

Sample group	Solvent	Weight content (wt%)
0	None	0
1	Ethanol	10
2	Ethanol	20
3	Ethanol	40
4	Ethanol	60
5	Isopropyl alcohol	10
6	Isopropyl alcohol	20
7	Isopropyl alcohol	40
8	Isopropyl alcohol	60

Table 2
Detail of GFRE composite samples filled with nano-ZnO particles.

Sample group	Solvent	Weight content (wt% of nano-ZnO particles)
0	None	0
1	20 wt% Isopropyl alcohol	4
2	20 wt% Isopropyl alcohol	12
3	20 wt% Isopropyl alcohol	20
4	20 wt% Isopropyl alcohol	40
5	None	4
6	None	12
7	None	20
8	None	40

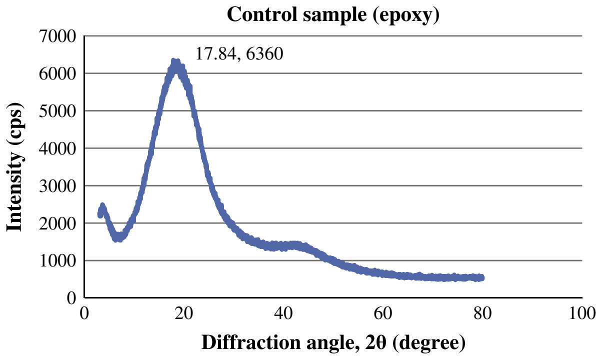

Fig. 1. XRD result of the control sample (epoxy).

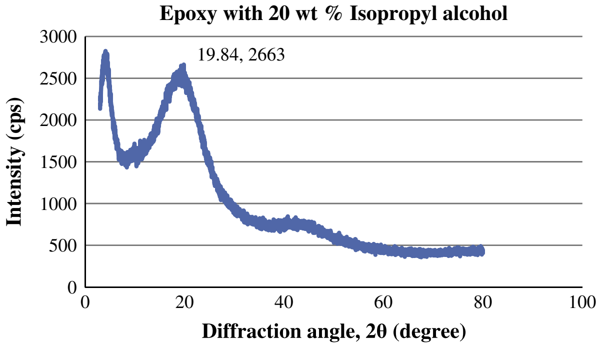

Fig. 2. XRD result of the epoxy sample with 20 wt% Isopropyl alcohol.

3.2. Bonding behaviour

SEM images with 500x magnification of the control sample and the sample with 20 wt% nano-ZnO particles and 20 wt% Isopropyl

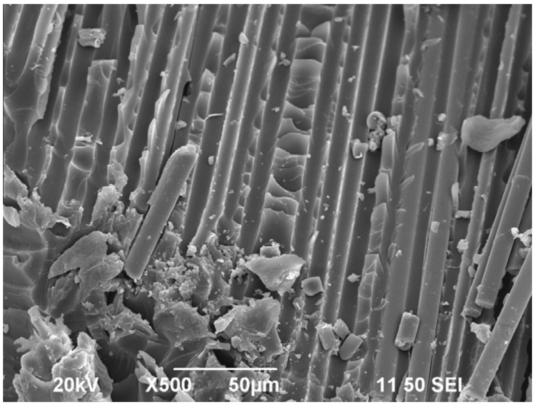

Fig. 3. SEM image of the control sample (GFRE composite).

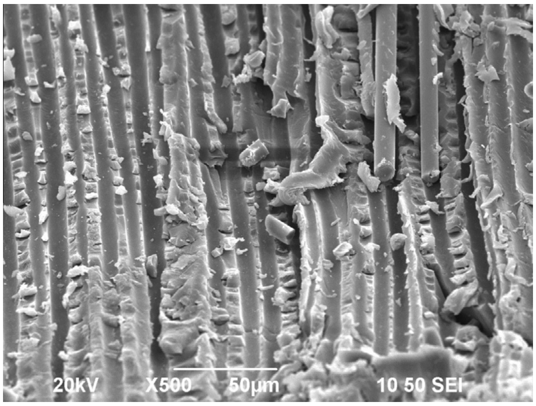

Fig. 4. SEM image of the composite with 20 wt% nano-ZnO particles and 20 wt% Isopropyl alcohol.

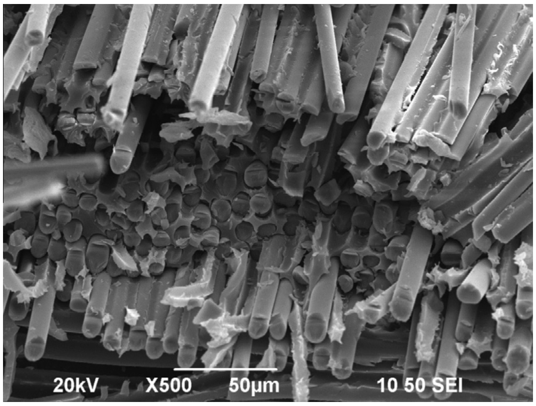

Fig. 5. SEM image of the composite with 20 wt% nano-ZnO particles and 20 wt% Isopropyl alcohol.

alcohol are shown in Figs. 3–5. Zhai et al. [12] and Alamri and Low [13] have proved that nanoparticles could improve the epoxy adhesive strength and fracture strength. In their finding, stripped patterns as shown in Fig. 3 appear in the control sample and it might be resulted from the shear of matrix in the sample subjected to loading. By comparing Figs. 3 and 4, more stripped patterns are observed in the samples with 20 wt% nano-ZnO particles and 20 wt% Isopropyl alcohol. The stronger the bonding behaviour between glass fibre and matrix, the more the stripped pattern appear. It implies that the 20 wt% nano-ZnO particles with Isopropyl alcohol as the solvent can enhance the bonding behaviour between glass fibres and epoxy. In Fig. 5, it shows the fractured surface of the sample with 20 wt% nano-ZnO particles and 20 wt% Isopropyl alcohol. The bonding behaviour between the glass fibre and the epoxy is good as fibre fracture is obviously seen. Esthappan et al. [8] have proved that a smooth surface morphology could be obtained even after the addition of nanoparticles in polymer matrix which is similar to the effect obtained in the current study.

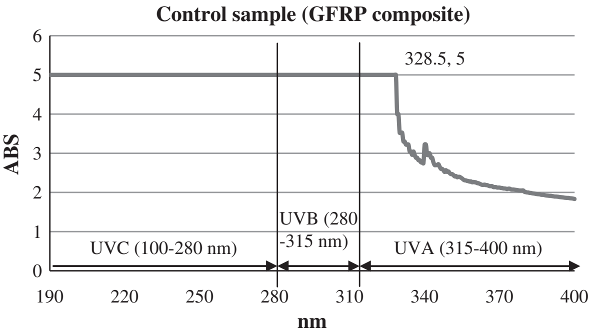

Fig. 6. UV absorbability of the control GFRE sample.

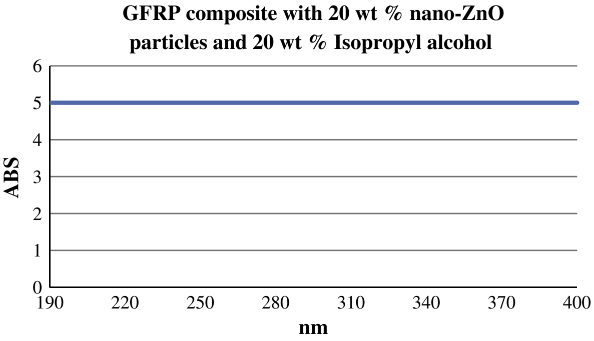

Fig. 7. UV absorbability of the GFRE composite with 20 wt% nano-ZnO particles and 20 wt% Isopropyl alcohol.

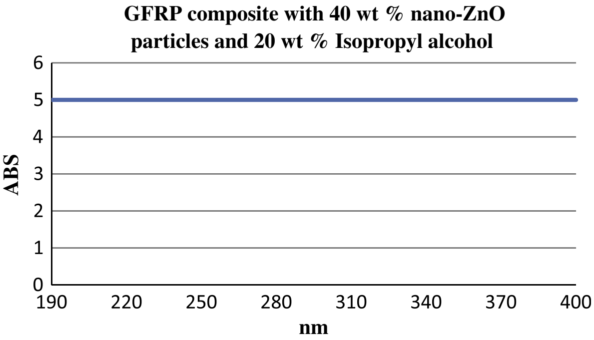

Fig. 8. UV absorbability of the GFRE composite with 40 wt% nano-ZnO particles and 20 wt% Isopropyl alcohol.

3.3. UV resistibility

The UV absorbability of ZnO particles varies with the content of ZnO particles in the polymer matrix [7,9–11,21]. Different weight percentages of nanoparticles were tested in different researches.

Ding et al. [9] discovered epoxy composite with 5 wt% of ZnO particles had optimal mechanical properties, Siddhartha et al. [11] have suggested that a composite with 20 wt% fillers had an improved flexural strength and impact strength and Lowry et al. [7] have also indicated that 7 wt% of ZnO outperforms 4 wt% of ZnO in terms of UV absorption. In the current finding, 4 wt%, 12 wt%, 20 wt% and 40 wt% of ZnO particles were chosen for investigation. The UV absorbability of the control sample, the sample with 20 wt% nano-ZnO particles and 20 wt% Isopropyl alcohol and the sample with 40 wt% nano-ZnO particles and 20 wt% Isopropyl alcohol are shown in Figs. 6–8 respectively. In Fig. 6, it shows that the control sample has an excellent absorption of UV radiation in the wavelength ranges from 190 to 328.5 nm, however, it has no fully absorption of UV radiation in the wavelength ranges from 328.5 to 400 nm which the UV absorbability increases with the decrease of wavelength. This result implies that the UV absorbability of the control sample is not excellent enough in the range of UVA (315–400 nm). By comparing with the Figs. 6–8 and the other samples, the sample with 20 wt% nano-ZnO particles and 20 wt% Isopropyl alcohol and the sample with 40 wt% nano-ZnO particles and 20 wt% Isopropyl alcohol show an excellent UV absorption through the whole range of wavelength from 190 to 400 nm. Lowry et al. [7] have stated that the criterion for complete UV protection is defined as less than 1% UV transmission (more than 99% absorption). It implies they have complete absorption (reaches 100% absorption) in the whole range of UVA (315–400 nm) and UVB (280–315 nm).

4. Conclusions

According to the XRD examination, 20 wt% Isopropyl alcohol has the least influence to the properties of epoxy and is shown to be an effective solvent for dispersing nano-ZnO particles inside the epoxy. The SEM images also showed that the bonding behaviour between glass fibre and matrix is enhanced after filling up with 20 wt% nano-ZnO particles with 20 wt% Isopropyl alcohol into the composite. From the UV absorption measurements, both samples of 20 wt% nano-ZnO particles with 20 wt% Isopropyl alcohol and 40 wt% nano-ZnO particles with 20 wt% Isopropyl alcohol had full UVA (315–400 nm) and UVB (280–315 nm) absorbability. These measurements indicated that 20 wt% Isopropyl alcohol is effective for the dispersion of nano-ZnO particles with negligible influence to the composition of epoxy. 20 wt% nano-ZnO particles are effective for absorption of UVA and UVB with the bonding behaviour enhanced between glass fibre and epoxy inside the composite.

Acknowledgement

The Project is supported by the Hong Kong Polytechnic University Grant (G-YK84).

References

[1] Krishan K, Chawla. Composite materials, science and engineering. 3 ed. New York Heidelberg Dordrecht London: Springer; 2012.

[2] Etches JA. Exploiting functional fibers in advanced composite materials. J Intell Mater Syst Struct 2006;18:449–58.

[3] Cockell CS, Knowland J. Ultraviolet radiation screening compounds. Biol Rev Cambridge Philos Soc 1999;74:311–45.

[4] Paul ND, Gwynn-Jones D. Ecological roles of solar UV radiation: towards an integrated approach. Trends Ecol Evol 2003;18:48–55.

[5] Diffey BL. Solar ultraviolet radiation effects on biological systems. Phys Med Biol 1991;36:299–328.

[6] Moezzi A, McDonagh AM, Cortie MB. Zinc oxide particles – Synthesis, properties and applications. Chem Eng J 2012;185–186:1–22.

[7] Lowry M, Hubble D, Wressell A, Vratsanos M, Pepe F, Hegedus C. Assessment of UV-permeability in nano-ZnO filled coatings via high throughput experimentation. J Coat Technol Res 2008;5(2):233–9.

[8] Esthappan SK, Kuttappan SK, Joseph R. Thermal and mechanical properties of polypropylene/titanium dioxide nanocomposite fibers. Mater Des 2012;37:537–42.

[9] Ding Ke Hong, Wang Gen Lin, Zhang Ming. Characterization of mechanical properties of epoxy resin reinforced with submicron-sized ZnO prepared via in situ synthesis method. Mater Des 2011;32(7):3986–91.

[10] Meguid SA, Sun Y. On the tensile and shear strength of nano-reinforced composite interfaces. Mater Des 2004;25:289–96.

[11] Siddhartha Amar, Patnaik Amba D, Bhatt Amba D. Mechanical and dry sliding wear characterization of epoxy–TiO_2 particulate filled functionally graded composites materials using Taguchi design of experiment. Mater Des 2011;32(2):615–27.

[12] Zhai LL, Ling GP, Li J, Wang YW. The effect of nanoparticles on the adhesion of epoxy adhesive. Mater Lett 2006;60:3031–3.

[13] Alamri H, Low IM. Effect of water absorption on the mechanical properties of nano-filler reinforced epoxy nanocomposites. Mater Des 2012;42:214–22.

[14] Juan Xie, Ping Li, Yanting Li, Yanji Wang, Wei Yu. Solvent-induced growth of ZnO particles at low temperature. Mater Lett 2008;62(17):2814–6.

[15] Hu Zeshan, Oskam Gerko, Searson Peter C. Influence of solvent on the growth of ZnO nanoparticles. J Colloid Interface Sci 2003;263(2):454–60.

[16] Ma Jianjun, Jiang Cairong, Xiong Ying, Xu Guangliang. Solvent-induced growth of ZnO microcrystals. Powder Technol 2006;167(1):49–53.

[17] Liu B, Zeng HC. Room temperature solution synthesis of monodispersed single-crystalline ZnO nanorods and derived hierarchical nanostructures. Langmuir 2004;20:4196–204.

[18] Zhang J, Sun LD, Yin JL, Su HL, Liao CS, Yan CH. Control of ZnO morphology via a simple solution route. Chem Mater 2002;14:4172–7.

[19] Sato K, Kondo S, Tsukada M, Ishigaki T, Kamiya H. Influence of solid fraction on the optimum molecular weight of polymer dispersants in aqueous TiO_2 nanoparticle suspensions. J Am Ceram Soc 2007;90:3401–6.

[20] Sarita Kango, Susheel Kalia, Annamaria Celli, James Njuguna, Youssef Habibi, Rajesh Kumar. Surface modification of inorganic nanoparticles for development of organic–inorganic nanocomposites – A review. Prog Polym Sci 2013;38(8):1232–61.

[21] Hongxia Zhao, Li Robert KY. A study on the photo-degradation of zinc oxide (ZnO) filled polypropylene nanocomposites. Polymer 2006;47(9):3207–17.

Materials Letters 128 (2014) 220–223

Contents lists available at ScienceDirect

Materials Letters

journal homepage: www.elsevier.com/locate/matlet

Feasibility of using ZnO/epoxy filled hollowed glass fibres (HGFs) for UV resistant polymer composites

Tsz-ting Wong [a], Wai-yin Tam [a], Julie A. Etches [b], Wen-xin Wang [c], Jinsong Leng [c], Kin-tak Lau [a,*]

[a] Department of Mechanical Engineering, The Hong Kong Polytechnic University, Hung Hom, Kowloon, Hong Kong
[b] Faculty of Engineering, University of Bristol, Bristol, United Kingdom
[c] Centre for Composite Materials and Structures, Harbin Institute of Technology, Harbin, China

ARTICLE INFO

Article history:
Received 26 March 2014
Accepted 16 April 2014
Available online 23 April 2014

Keywords:
Composite
Hollow glass fibre
Zinc oxide
Ultraviolet

ABSTRACT

Protecting human skin and structural polymers away from an ultraviolet radiation (UVR) attack is a serious concern in all engineering industries at present. In the meanwhile, hollow glass fibres (HGFs) could provide an opportunity to develop a variety of functions for advanced composites. They could be made good use of their advantages by filling up with zinc oxide (ZnO)/epoxy to create an inherent UV absorption property. This paper experimentally investigates the desirable amount of ZnO particles filled into HGFs and their interval inside a composite to maximize its UV absorbability. UV–vis Spectrophotometer was used to investigate the UV absorption property of samples with different ZnO/epoxy compositions. It was found that the HGFs filled by 4 wt% and 5 wt% ZnO with their intervals of 0.2 mm and 0.5 mm had excellent UVB and high UVA absorbability. With continuously increasing the interval between the HGFs, only a 4 wt% ZnO sample can keep the same UV absorption property.

1. Introduction

Ultraviolet radiation (UVR) attack is a serious concern in all engineering industries as it has been proven to be harmful on human skin and structural polymers. It would cause skin cancer and polymer degradation by changing their atomic properties, respectively [1,2,7,14,20,23,28]. In the atmosphere, human bodies and polymer materials are severely exposed under 95% of UVA directly from the sun. UVA (315–400 nm) has the highest level of intensity to reach the earth and it has a long wavelength which can penetrate deeper from the surface of both human skin and polymer materials [11,13,17,24]. As in recent research, hollow glass fibre (HGF) has been mostly exploited its extraordinary functions in composite structures. Julie et al. [9] developed various functional polymer-based composites with unique magnetic characteristics by filling ferromagnetic substances into HGFs. Williams et al. [25] introduced HGFs into a carbon fibre reinforced polymer (CFRP) composite and identified the flexural strength and ply disruption can be enhanced after the incorporation of HGFs within a CFRP composite. It is believed that if UV resistant particles filled into HGFs to form a new class of composites could be a unique solution to protect human bodies and polymer materials, particular for the design of an UV shield body shell for airplanes and car bodies.

ZnO particle is a promising candidate for different combinations and applications because of its intrinsic properties. ZnO shows a highly ionic character due to the large difference in electronegativity between Zn and O atoms. Non-centrol symmetric tetrahedral coordination in ZnO results in piezoelectric properties and crystallographic polarity [27,29]. ZnO doped with different transition metals to produce electrical and magnetic properties were intensively studied by many researchers. Boris et al. [4–6] indicated Iron (Fe)-doped ZnO, Manganese (Mn)-doped ZnO and Cobalt (Co)-doped ZnO possess Room Temperature (RT) Ferromagnetic (FM) behaviour which is influenced by the grain boundary (GB) specific area S_{GB} on the ferromagnetism of the three doped ZnOs (the three doped ZnOs are ferromagnetic if they contain enough GBs). In addition, it is well known that ZnO particle at nano-scale is an effective inorganic UVA (315–400 nm) and UVB (280–315 nm) radiation absorbent [15,16,22,26,28,30]. However, composites with different weight percentages of ZnO particles filled into HGFs and intervals would affect their UV absorbability. Different weight percentages of ZnO particles were investigated by different researchers [8,12]. Lowry et al. [12] has indicated that an epoxy composite with 7 wt% ZnO particles outperformed 4 wt% in terms of the UV absorbability. Moreover, in the last experimental study, 4 wt%, 12 wt%, 20 wt% and 40 wt% ZnO particles were chosen to be the fillers in glass fibre reinforced epoxy composites (GFRECs). 20 wt% and 40 wt % ZnO were found to be desirable amounts of nano-ZnO particles filled into GFRECs to exhibit better UV shielding effect [22].

---

* Corresponding author. Tel.: +852 2766
E-mail address: mmktlau@.

http://dx.doi.org/10.1016/j.matlet.2014.04.083
0167-577X/© 2014 Elsevier B.V. All rights reserved.

Table 1
Fifteen samples including three control samples were prepared.

		Spacing of HGFs		
		0.2 mm	0.5 mm	1.5 mm
Weight percentages of ZnO particles in the epoxy filled in the HGFs	–	Control sample 1	Control sample 2	Control sample 3
	2 wt%	Sample 4	Sample 8	Sample 12
	4 wt%	Sample 5	Sample 9	Sample 13
	5 wt%	Sample 6	Sample 10	Sample 14
	7 wt%	Sample 7	Sample 11	Sample 15

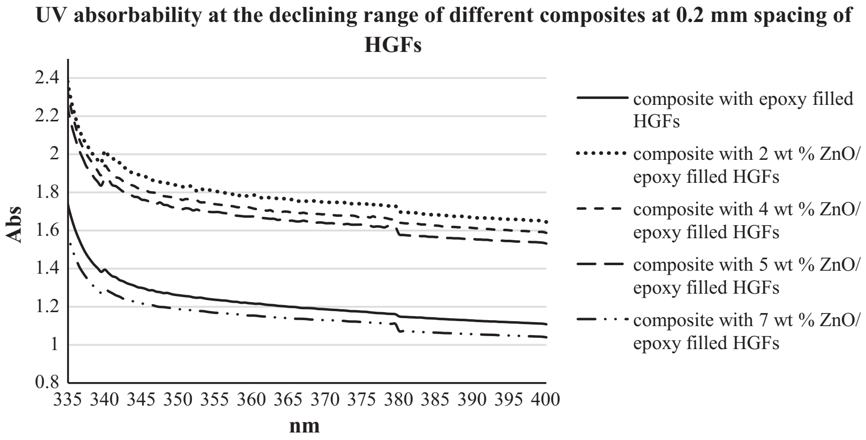

Fig. 1. UV absorbability at the declining range of composites with different weight percentages of nano-ZnO particles at 0.2 mm spacing of HGFs.

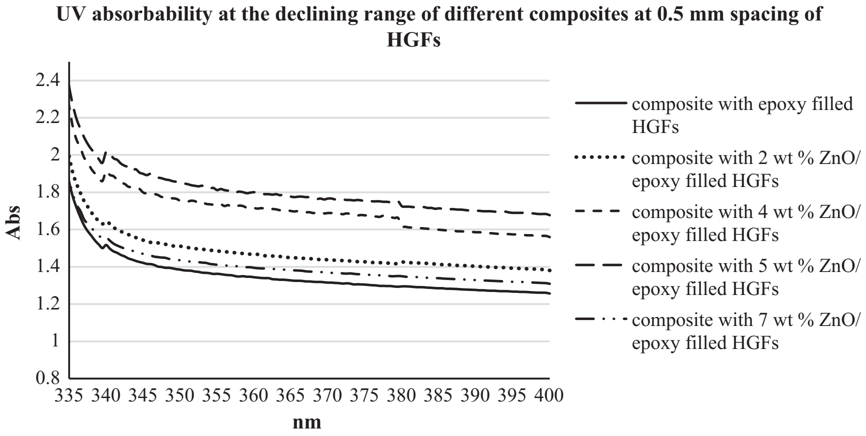

Fig. 2. UV absorbability at the declining range of composites with different weight percentages of nano-ZnO particles at 0.5 mm spacing of HGFs.

2. Experimental approach

In this study, different weight percentages of ZnO particles, at nano-scale mixed with epoxy resin to form ZnO/epoxy mixtures were fabricated and then filled into HGFs to create an UV absorption media inside polymer-based composites. The UV absorbability of the composites was measured by using an UV–vis spectrophotometer. The bonding property between the HGF and ZnO/epoxy inside the composites was visually examined by using Scanning Electron Microscope (SEM).

Materials and samples preparation: The HGFs with outer and inner diameters of 125 μm and 100 μm respectively were produced by the Department of Aerospace Engineering of the University of Bristol [12]. Araldite GY251 and hardener HY956 were mixed in the ratio of 5:1 to produce epoxy plate samples with the dimension of 50 mm (l) × 30 mm (w) × 2 mm (t). HGFs were embedded in the middle of the samples with different pre-determined intervals, which were 0.2 mm, 0.5 mm and 1.5 mm. All plate samples were cured under ambient condition for 24 h prior to the infiltration of ZnO/epoxy into the HGFs.

Vacuum infiltration technique was adopted to fill the ZnO/epoxy into the HGFs. Similar method was shown to be effective for preparing resin filled HGFs in self-healing composites [3,9,10,18,19]. For the set up of vacuum infiltration, one end of the samples was immersed in a homogenous mixture of ZnO/epoxy mixture while another end is exposed to a vacuum chamber to create a negative pressure to take the mixture into the HGFs.

UV absorbability examination: A total of 15 samples were fabricated and their information are listed in Table 1. Different weight percentages of ZnO particles (2 wt%, 4 wt%, 5 wt% and 7 wt%) were used to make the ZnO/epoxy mixtures for filling up into HGFs for different samples. All filled samples were cured under ambient condition for 24 h prior to the UV absorption examination. UV–vis Spectrophotometer (Dynamica DB-20, 190–1100 nm) was used to investigate the UV absorbability of the samples.

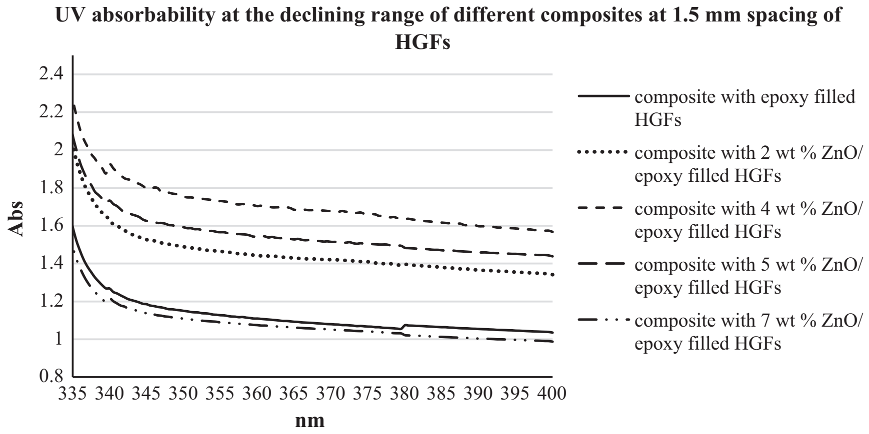

Fig. 3. UV absorbability at the declining range of composites with different weight percentages of nano-ZnO particles at 1.5 mm spacing of HGFs.

Table 2
Comparing the UV absorbability level at the declining range of different composites.

Comparing the UV absorbability level at the declining range of different composites (UV absorbability at 400 nm)				
		Spacing of HGFs		
		0.2 mm	0.5 mm	1.5 mm
Weight percentages of ZnO particles in the epoxy filled in the HGFs	–	Low Level (1.1079)	Low Level (1.2564)	Low Level (1.0347)
	2 wt%	High Level (1.6439)	Medium Level (1.3809)	Medium Level (1.3419)
	4 wt%	High Level (1.5867)	High Level (1.559)	High Level (1.567)
	5 wt%	High Level (1.5316)	High Level (1.6777)	Medium Level (1.4377)
	7 wt%	Low Level (1.04)	Medium Level (1.3089)	Low Level (0.9871)

Remarks:
Low level: UV absorbability < 1.3.
Medium level: $1.3 <$ UV absorbability < 1.5.
High level: UV absorbability > 1.5.

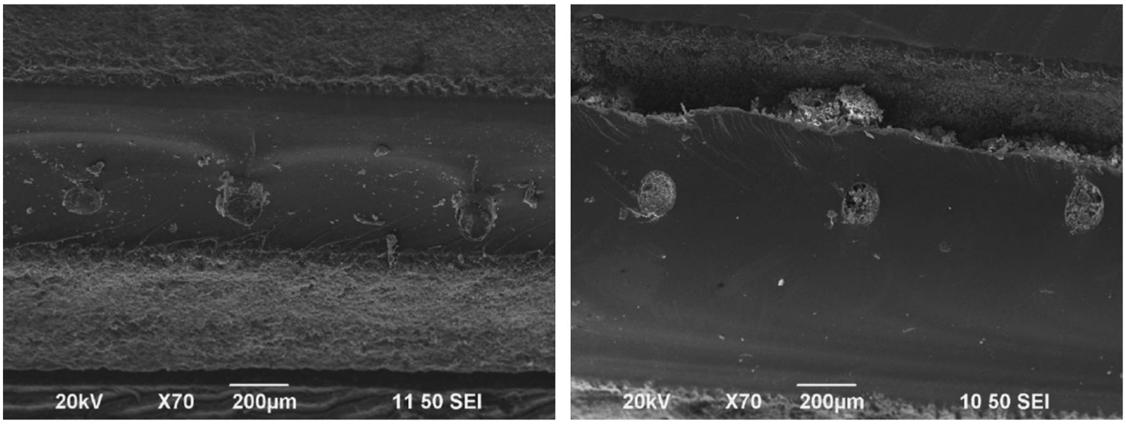

Fig. 4. SEM images of composites with 4 wt% (left) and 7 wt% (right) ZnO/epoxy filled HGFs at 0.5 mm spacing.

SEM examination: All the samples were broken into two half and followed by the SEM examination using SEM (Jeol 6490) to study the bonding behavior between the HGFs and the ZnO/epoxy particles.

3. Results and discussions

UV absorbability: In the current study, 2 wt%, 4 wt%, 5 wt% and 7 wt% ZnO particles mixed with epoxy resin were chosen to be infiltrated into HGFs. Based on the result found, the UV absorbability of samples were similar. All samples indicated that the maximum intensity occurred within the wavelength of 190 nm and 333 nm and started dropping in the range inside UVA. A sample with 4 wt% ZnO inside the HGFs and their interval of 0.2 mm obtained a good UV absorption property in the range of UVA.

Figs. 1–3 show the trend of UV absorption of sample with different weight percentages of ZnO particles in HGFs and their intervals of 0.2 mm, 0.5 mm and 1.5 mm at the declining range. In Table 2, it is discovered that when the intervals between HGFs are small (0.2 mm and 0.5 mm) and the content of ZnO particles in the HGFs are 4 wt% and 5 wt%, the samples exhibit the highest UVA absorption. When the interval between HGFs continues increasing to 1.5 mm, only 4 wt% ZnO sample can exhibit highest UVA absorption. Samples with pure epoxy and 7 wt% ZnO/epoxy filled HGFs exhibit lowest UVA absorption whenever their intervals

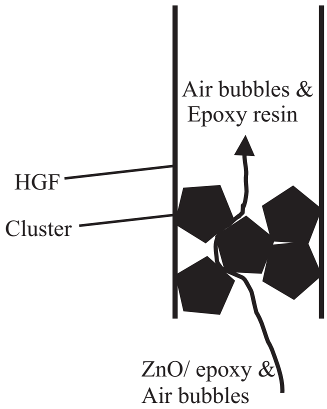

Fig. 5. Schematic illustration of the ZnO/epoxy infiltration process in a HGF with clusters formed inside.

were 0.2 mm, 0.5 mm and 1.5 mm. Last but not the least, by comparing the UV absorbability at 400 nm in Table 2, it can be concluded that the UV absorbability of different samples decreases when the interval between HGFs increases.

Fig. 4 shows SEM images of samples with 4 wt% (left) and 7 wt% (right) ZnO/epoxy filled HGFs with the embedment interval of 0.5 mm. Clusters were formed inside the 7 wt% ZnO/epoxy filled HGFs while no observable clusters existed in the sample of 4 wt% ZnO/epoxy filled HGFs. An EDX examination was conducted to analyze the chemical content inside the HGFs. It was discovered that Zn element appeared inside 4 wt% ZnO/epoxy filled HGFs while none was detected inside 7 wt% ZnO/epoxy filled HGFs. This phenomenon may be due to the ZnO clusters were formed during the infiltration process and blocked the flow of the mixture into the HGFs. Particles agglomeration in the epoxy resin occurred seriously when the weight percentage of ZnO particles increased. Fig. 5 shows the schematic illustration of the ZnO/epoxy infiltration process in a HGF with the formation of clusters at the upstream section of the HGF. It therefore results in lowering the UV resistance properties of the sample.

Due to the formation of ZnO particle agglomeration, poor bonding behaviour between ZnO and epoxy inside the HGFs appeared. Whether this bonding behaviour would have ferromagnetic effects, are worthy for further study.

4. Conclusions

Based on the result from EDX examination, Zn element was not seen inside HGFs filled with 7 wt% ZnO/epoxy, it was probably because of the formation of ZnO clusters at the upstream of the HFGs and blocked the infiltration of the particles into the HGFs successfully. Nevertheless, samples with 2 wt%, 4 wt% and 5 wt% of ZnO particles were observed as the desirable amount to be filled into HGFs to achieve maximal UV absorption property. For the interval between HFGs as 0.2 mm, HGFs with filled 4 wt% and 5 wt % of ZnO particles also exhibited better UV absorbability than the interval of 0.5 mm was used. For the interval of 1.5 mm, 4 wt% of ZnO particles provided the best UV absorbability.

Acknowledgement

This project is supported by the Hong Kong Polytechnic University Grant (G-YK84).

References

[1] Andrady AL, Hamid SH, Hu X, Torikai A. Effects of increased solar ultraviolet radiation on materials. J Photochem Photobiol, B 1998;46(1):96–103.

[2] Awaja Firas, Nguyen Minh-Tam, Zhang Shengnan, Arhatari Benedicta. The investigation of inner structural damage of UV and heat degraded polymer composites using X-ray micro CT. Composites Part A 2011;42(2):408–18.

[3] Bleay SM, Loader CB, Hawyes VJ, Humberstone L, Curtis PT. A smart repair system for polymer matrix composites. Composites Part A 2001;32:1767–76.

[4] Straumal Boris B, Protasova Svetlana G, Mazilkin Andrei A, Tietze Thomas, Goering Eberhard, Schutz Gisela, et al. Ferromagnetic behaviour of Fe-doped ZnO nanograined films. Beilstein J Nanotechnol 2013;4:361–9.

[5] Straumal Boris B, Mazilkin Andrei A, Protasova Svetlana G, Myatiev Ata A, Straumal Petr B, Schutz Gisela, et al. Magnetic study of nanograined pure and Mn-doped ZnO films: formation of a ferromagnetic grain-boundary foam. Phys Rev B: Condens Matter 2009;79:205206.

[6] Straumal Boris B, Mazilkin Andrei A, Protasova Svetlana G, Straumal Petr B, Myatiev Ata A, Schutz Gisela, et al. Grain boundaries as the controlling factor for the ferromagnetic behaviour of Co-doped ZnO. Philos Mag 2013;93(10–12):1371–83.

[7] Diffey BL. Solar ultraviolet radiation effects on biological systems. Phys Med Biol 1991;36:299–328.

[8] Hong Ding Ke, Lin Wang Gen, Ming Zhang. Characterization of mechanical properties of epoxy resin reinforced with submicron-sized ZnO prepared via in situ synthesis method. Mater Des 2011;32(7):3986–91.

[9] Etches JA, Scholey JJ, Williams GJ, Bond IP, Mellor PH, Friswell MI, et al. Exploiting functional fibers in advanced composite materials. J Intell Mater Syst Struct 2007;18:449 (-58).

[10] Etches J, Bond I, Mellor P. Manufacture and applications of magnetically active fibre reinforced composites. Smart Mater Struct 2006;15:288–94.

[11] FDA. Ultraviolet (UV) radiation. [cited 07/09/2012]. Available from: 〈http://www.fda.gov/RadiationEmittingProducts/RadiationEmittingProductsandProcedures/Tanning/ucm116425.htm〉.

[12] Hucker M, Bond I, Bleay S, Haq S. Experimental evaluation of unidirectional hollow glass fibre/epoxy composites under compressive loading. Composites Part A 2003;34:927–32.

[13] Karentz D. Ozone Layer. Reference module in earth systems and environmental sciences, from encyclopedia of ecology 2008:2615–21.

[14] Kumar AP, Depan D, Tomer NS, Singh RP. Nanoscale particles for polymer degradation and stabilization—trends and future perspectives. Prog Polym Sci 2009;34:479–515.

[15] Lowry M, Hubble D, Wressell A, Vratsanos M, Pepe F, Hegedus C. Assessment of UV-permeability in nano-ZnO filled coatings via high throughput experimentation. J Coat Technol Res 2008;5(2):233–9.

[16] Moezzi A, McDonagh AM, Cortie MB. Zinc oxide particles—synthesis, properties and applications. Chem Eng J 2012;185–186:1–22.

[17] Oliva Matthew S, Taylor Hugh. Ultraviolet radiation and the eye. Int Ophthalmol Clin 2005;45(1):1–17.

[18] Pang JWC, Bond IP. A hollow fibre reinforced polymer composite encompassing self-healing and enhanced damage visibility. Compos Sci Technol 2005;65:1791–9.

[19] Pang JWC, Bond IP. 'Bleeding composites'—damage detection and self-repair using a biomimetic approach. Composites Part A 2005;36:183–8.

[20] Paul ND, Gwynn-Jones D. Ecological roles of solar UV radiation: towards an integrated approach. Trends Ecol Evol 2003;18:48–55.

[22] Tsz-ting Wong, Kin-tak Lau, Wai-yin Tam, Leng Jinsing, Julie A. Etches. UV resistability of a nano-ZnO/glass fibre reinforced epoxy composite. Mater Des 2013.

[23] UNEP (United Nations Environment Programme). Environmental effects of ozone depletion and its interactions with climate change: 2010 assessment. United Nations Environment Programme, Nairobi, Kenya. 2010.

[24] WHO. Global solar UV index: a practical guide. World Health Organization (WHO), World Meteorological Organization (WMO), United Nations Environment Program (UNEP), and International Commission on Non-Ionising Radiation Protection (ICNRP). Geneva, Switzerland. 2002.

[25] Williams G, Trask R, Bond I. A self-healing carbon fibre reinforced polymer for aerospace applications. Composites Part A 2007;38(6):1525–32.

[26] Ting Cao Hua-Jie Wang, Cao Cui, Sun Yuan-Yuan, Yang Lin, Ya-Nan Zhang. Synthesis and anti-ultraviolet properties of monodisperse BSA-conjugated zinc oxide nanoparticles. Mater Lett 2011;65:340–2.

[27] Yuanjie Li Development of ZnO-based thin film transistors and phosphorus-doped ZnO and (Zn,Mg)O by pulsed laser deposition. 2006.

[28] Zhao Hongxia, Li Robert KY. A study on the photo-degradation of zinc oxide (ZnO) filled polypropylene nanocomposites. Polymer 2006;47(9):3207–17.

[29] Wang ZL. Zinc oxide nanostructures: growth, properties and applications. J Phys Condens Matter 2004;16(25):R829.

[30] NanoMarkets. Zinc oxide (ZnO)—material, properties, applications and market opportunities of zinc oxide. [updated 11/06/2013]. Available from: 〈http://www.azom.com/article.aspx?ArticleID=4522〉.

Composite Structures 132 (2015) 1056–1064

Contents lists available at ScienceDirect

Composite Structures

journal homepage: www.elsevier.com/locate/compstruct

Degradation of nano-ZnO particles filled styrene-based and epoxy-based SMPs under UVA exposure

Tsz-ting Wong [a], Kin-tak Lau [a,*], Wai-yin Tam [a], Jinsong Leng [b,*], Wenxin Wang [b], Wenbing Li [b], Hongqiu Wei [b]

[a] *Department of Mechanical Engineering, The Hong Kong Polytechnic University, Hung Hom, Kowloon, Hong Kong*
[b] *Centre for Composite Materials and Structures, Harbin Institute of Technology, Harbin, China*

ARTICLE INFO

Article history:
Available online 15 July 2015

Keywords:
Shape memory polymer
Zinc oxide
Ultraviolet radiation
Surface hardness
Dynamic mechanical properties
Shape memory effects

ABSTRACT

Styrene-based and epoxy-based SMPs (SSMPs and EPSMPs) filled with different contents of nano-ZnO particles were fabricated, their decolouration, UVR absorbabilities, surface hardness, dynamic mechanical properties and shape memory effects under UVA degradation test were then investigated. Experimental results showed that all samples subjected to the UVA degradation were yellowish with different degree. By adding 2 wt.% of nano-ZnO particles, all SMPs achieved full UVR blockage. 2 and 4 wt.% nano-ZnO/SSMP and 5 and 7 wt.% nano-ZnO/EPSMP could maintain their surface hardness at moderate level after the UVA degradation. Storage modulus of 4 wt.% nano-ZnO/SSMP and EPSMP before and after UVA degradation obtained satisfactory results compared with their pure forms. It was proven that shape recovery ratio was not affected by nano-ZnO particles inside SMPs. Treated EPSMPs could obtain 100% shape recovery. However, UVA degradation was proven to have effects on the shape memory effect in SSMPs. UVA-degraded SSMPs had better recovery than non-UVA-degraded SSMPs, this could be explained by the degraded surface which was changed to be hardened. 4 wt.% of nano-ZnO particles filled into SSMP and EPSMP could maintain a similar full recovery time before and after UVA degradation and could significantly reduce the recovery reaction time.

1. Introduction

Traditionally, shape memory alloy (SMA), which is a kind of metal alloys, has been recognised the only material that possesses the shape memory effect (SME) based on its twinned and de-twinned phase transformation characteristics. Until recently, smart memory polymer (SMP), like Polyurethane-based (PU-based) polymers [26], styrene-based (S-based) polymers [27] and epoxy-based (EP-based) polymers [10] have been discovered to also possess the SME. PU-based SMP, which is physically cross-linked, has been proven to increase residual stress and decreased shape recovery rate, which cannot provide an effective function for the SME when compared with that of chemically cross-linked structures [26,27]. Therefore, to popularise the SMP for SME applications, chemically cross-linked S-based and EP-based SMPs are investigated in this study.

SMPs have been broadly investigated by integrating them with different fillers to become a new class of composites that are thermo- [10,25,27], photo- [18], electrical- [12,29], magnetic- [3] and chemo- [14] sensitive. These composites have many advantages over traditional SMAs, for examples, they have high tailorability and functionability by changing their compositions or adding different fillers to alter their shape recovery temperature, stiffness and bio-degradability. Low density, low cost, high shape recovery strain (can be achieved up to 400%), reliable recovery behaviour and convenient fabrication technique (compared with SMA which requires over 100 °C and high pressure) make it to become more attractive in recent years. Because of these advantages, SMP composites are widely applicable in aerospace [1,11], textiles [30], automobiles [2] and biomedicine [3,9] areas.

In some applications, SMPs are utilised at different harsh environments, which may affect or even degrade their mechanical properties and lower their service lifetime. UV (100–400 nm) degradation is always a critical problem for polymer-based materials including SMPs, especially when they are used as primary structures that are exposed to sunlight. Around 95% UVA (315–400 nm), out of 9% UVR from the sun, entered onto the Earth surface has the highest average intensity of 1.37 mW/cm^2 and the highest penetration ability into human bodies and

---

* Corresponding authors.
E-mail addresses: mmktlau@ , lengjs@.

http://dx.doi.org/10.1016/j.compstruct.2015.07.023
0263-8223/

polymers [4,24]. UVA usually attacks human bodies [7] and polymers [16,27] under ageing (a long period of time) in physical and chemical ways. The degradation of polymers results in yellowing on materials' surface and alternation in their mechanical properties. Xu et al. [27] have discovered that the exposed surfaces of SMPs were discoloured under UVR in the air. Their compressive strength and ductility were also severely decreased as compared with their tensile strength. Generally speaking, UV degradation in polymers is a combination of physical movements and chemical reactions between chains of polymer molecules. UV degradation requires oxygen to proceed and produces water molecules and several types of free radicals, so it is also said to be photo-oxidation. UVR also induces thermal degradation, which speeds up the damage in polymers. The damage is commonly seen as depolymerization [17].

Kumar et al. [8] have discussed that nano-scaled inorganic particles would be a new trend for polymer-based materials to improve their UV resistibility. ZnO and TiO_2 are semiconductors, metal oxides and inorganic UVR absorbers, this kind of substances has intrinsic ability of UVR absorption. TiO_2 has been extensively investigated for its UVR absorbability. In fact, ZnO particle has relatively wider band gap energy of 3.37 eV at room temperature so as it has a broader range of UVR absorption of 290–400 nm (a full UVA and UVB absorption) than TiO_2. TiO_2 has band gap energy of 3.02 eV at room temperature and has a UVR absorption within the range of 290–350 nm. The refractive index of ZnO in visible light is 1.9 while TiO_2 is 2.6 so as ZnO possesses better light transmissibility [5,15,20,22]. In general, nano-sized (less than or equal to 100 nm) ZnO particles have relatively high UVR absorbability and transparency. In addition, ZnO is inexpensive, relatively abundant and chemically stable making it suitable for many applications, such as an ingredient of cosmetics and clothing [20,23]. Some researchers have integrated ZnO particles into different polymer materials for UVR protection [13,19,22]. Lowry et al. [13] have studied the UVR permeability in nano-ZnO filled coating and discovered a low dose of 7 wt.% of ZnO layer was sufficient to block UVA and UVB and outperformed 4 wt.% of ZnO in terms of UVR protection. In this study, different weight percentages of nano-ZnO particles were introduced into S-based and E-based SMPs. Their influences in terms of UV degradation, decolourisation, UVR absorbability and surface hardness were investigated.

2. Experimental setup

2.1. Raw materials

Styrene-based SMP (SSMP) and Epoxy-based SMP (EPSMP) were thermoset plastics in the analytical grade and used without further purification. Both SMP matrices were fabricated in Harbin Institute of Technology (HIT) [10,28]. The glass transition temperatures (Tg) of neat SSMP and neat EPSMP were claimed to be 85 °C and 100 °C respectively. Nano-ZnO particles with a diameter of approximate 100 nm and white in colour, were purchased commercially.

2.2. Specimen preparations

Precursor solutions of SSMP and EPSMP were mixed with 2, 4, 5 and 7 wt.% of nano-ZnO particles. The resins were firstly mechanically stirred for 20 min and then sonicated for another 10 min. Afterwards, they were degassed until bubble-free mixtures were obtained. The resulting mixtures were poured into a two-plate glass mould with a thickness of 3 mm. Thermal curing of ZnO/SSMPs was performed at 75 °C for 36 h while that of ZnO/EPSMPs was at 80 °C for 3 h, followed by100 °C for 3 h and 150 °C for 5 h. All samples were cooled down at room temperature and then machined into a square shape with the dimension of 30 mm × 30 mm × 3 mm for investigations. For the comparison purpose, neat SSMP and neat EPSMP samples were also prepared.

2.3. Accelerated UVA ageing

The effects of nano-ZnO particles in SSMPs and EPSMPs under UVA degradation were investigated. Two groups of samples and their pure forms were exposed under UVA with 250 mm apart from the source for 12 h inside an UVA chamber. The intensity of UVA from the lamp (100 mW/cm^2) was approximately 11 times higher than that of terrestrial UVA (9.1105 mW/cm^2 in average) [4]. Generally, UVR is alerted from 10 am to 4 pm (6 h) in every day [24]. For a 12-h exposure under the UVA lamp, it could simulate the effect similar to 22-day exposure under the sunlight. In addition, the samples were experienced at a temperature (80 °C) 3 times higher than that on the Earth's surface at sea level (25 °C), this further accelerated the effect of UVA degradation. The exposed temperature (80 °C) was slightly lower than the Tgs of neat SSMP (85 °C) and neat EPSMP (100 °C).

2.4. UVR absorption test

The UVR absorbabilities of ZnO/SMPs before and after UVA degradation were tested and compared. UV–vis Spectrophotometer (Dynamica DB-20, 190–1100 nm) was used to test the absorbabilities of UVA (315–400 nm), UVB (280–315 nm) and UVC (190–280 nm) of all samples. Absorbance displays along the *Y*-axis with maximum absorbance index of 5 while UVR displays along the *X*-axis with wavelength ranging from 190 nm to 400 nm. For the comparison purpose, UVR absorption tests on neat SSMP and neat EPSMP were also conducted.

2.5. Yellowing of neat SMPs and ZnO/SMPs by UVA degradation

Different degrees and rates of yellowing of neat SMPs and ZnO/SMPs before and after UVA degradation were observed and compared.

2.6. Surface hardness test

The surface hardness of ZnO/SMPs were measured before and after the UVA degradation by using Microhardness Tester (Future-Tech) with test load of 100 gf and dwell time of 15 s. For the comparison purpose, the surface hardness tests on neat SSMP and neat EPSMP samples were also conducted.

2.7. Dynamic mechanical analysis (DMA)

DMA testing is commonly used to determine the dynamic molecular motion changes of SMP. DMA (Perkin Elmer Diamond DMA Lab System) was used to conduct the tensile test mode with the different setting parameters as shown in Table 1 for non-UVA-degraded and UVA-degraded SSMP and EPSMP samples with and without 4 wt.% nano-ZnO particles.

Table 1
Setting parameters of DMA test for neat SMP and 4 wt.% ZnO/SMP samples.

	Neat SSMP and 4 wt.% ZnO/SSMPs	Neat EPSMP and 4 wt.% ZnO/EPSMPs
Sample size		$30 \times 5 \times 2$ mm^3
Temperature range	25–130 °C	−30 to 150 °C
Testing rate	2°C min^{-1}	5°C min^{-1}
Testing frequency	0.2 Hz	1 Hz

2.8. Shape memory effects (SMEs)

SMEs including the shape recovery ratio, full recovery time and recovery reaction time of SMP were determined by a series of steps. Different set parameters of the SME test for SSMP and EPSMP samples with and without nano-ZnO particles are shown in Table 2. Dimethicone was used to be the isothermal medium for heat treatment on SMPs because it has high transparency and high chemical stability. SMPs were heated to a temperature of their Tgs + 20 °C in an oven for 20 min. Then the soften SMPs were immediately bent into U-shape around an aluminium plate with 2 mm radius arc at a bending rate of $10°s^{-1}$. U-shape SMPs were fixed on the plate and the whole pieces were put into cooling chamber at 0 °C for 20mins. Deformed SMPs were immersed into Dimenthicone bath at Tgs + 20 °C to investigate their shape recovery behaviour which the processes were recorded by video. The shape recovery ratio is the ratio of shape recovery angle to 180°. Full recovery time and recovery reaction time were evaluated from the video to distinguish the differences in SME of non-UVA-degraded and UVA-degraded SSMP and EPSMP with and without nano-ZnO particles.

Table 2
Setting parameters of SME tests for neat SMP and all ZnO/SMP samples.

	Neat SSMP and all ZnO/SSMPs	Neat EPSMP and all ZnO/EPSMPs
Sample size		$30 \times 5 \times 2$ mm^3
Pre-heating temperature	105 °C (Tg + 20 °C)	120 °C (Tg + 20 °C)
Cooling temperature	0 °C	0 °C
Reheating temperature	105 °C (Tg + 20 °C)	120 °C (Tg + 20 °C)

3. Results and discussions

3.1. UVR absorbability of nano-ZnO particle

ZnO particle is an inorganic UVR absorber, which enables to absorb UVR in the range of 290–400 nm (a whole range of UVA and UVB). A ZnO atom absorbs UVR and deteriorates the energy physically. The reaction is dependent on the ability of a ZnO atom having its band gap energy (~3.22 eV for a ZnO atom with particle size of 100 nm) to create an electron–hole (e^-–h^+) pair. A schematic diagram is shown in Fig. 1, electrons present in the valence band (+ve) are excited by UVR having an energy greater than the band gap of a ZnO atom and jump to the conduction band (−ve). These electronic transitions occur between the two bands as long as the ZnO atom exposed to UVR. It was suggested that the electrons are fluctuated in an excitonic system between the internal field [5,6] and it is believed that the energies of electrons decay with travelled distance and time and become exhausted.

The intensity energy of UVR can be calculated by Eqs. (1) and (2):

$$E = hf \tag{1}$$

where E is the intensity energy of light, h is Planck's constant $= 6.626 \times 10^{-34}$ J s and f is the frequency of the light vibration and

$$\lambda = \frac{v}{f} \tag{2}$$

where λ is the wavelength of light, v is the speed of the light $= 3 \times 10^8$ m/s and f is the frequency of the light vibration.

In this experiment, only UVA (318–400 nm) degradation was considered. The intensity energy of light is 6.251×10^{-19} J at wavelength of 318 nm while the intensity energy of light is 4.903×10^{-19} J at wavelength of 400 nm. The smaller the wavelength of light, the higher of its energy. The band gap energy of a ZnO atom with particle size of 100 nm is about 3.22 eV which is equal to 1.602×10^{-19} J. The intensity energy of UVA is 3 times more than the band gap energy of a 100 nm ZnO atom which it is large enough to excite electrons from the valence band of a ZnO atom and they iterate between the band gap until their energies are exhausted.

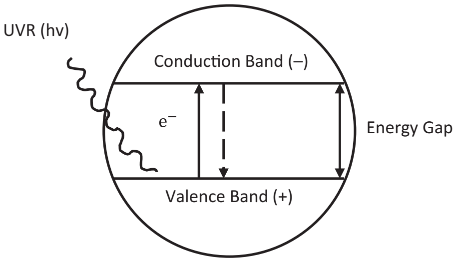

Fig. 1. A schematic diagram shows the UVR absorption of band gap inside a ZnO atom.

3.2. UVR absorption tests of neat SMPs and ZnO/SMPs

Before the UVA degradation test, the neat SSMP had full UVB and UVC absorptions and most part of UVA but not for UVA from 387.5 nm to 400 nm (Fig. 2) while the neat EPSMP had a full UVC and most part of UVB absorptions but not for UVB from 311.5 nm to 315 nm and the whole range of UVA (Fig. 3). After the accelerated UVA ageing, the neat SSMP had a full UVR absorption (Fig. 2) while the neat EPSMP had a full UVC and less part of UVB absorptions but not for UVB from 295.5 nm to 315 nm and the whole range of UVA (Fig. 3).

The UVR absorbability of the neat SSMP was strengthened while that of the neat EPSMP was weakened after the test. These phenomena were resulted from the difference of UV degradation mechanisms of styrene and epoxy and will be explained in the following session. Additionally, both SSMP and EPSMP with 2, 4, 5 and 7 wt.% of nano-ZnO particles could achieve a full UVR absorption (Fig. 4). 2 wt.% of nano-ZnO particles inside SSMP and EPSMP were enough to achieve a full UVR absorbability.

3.3. UV degradation mechanisms in polymer materials (styrene and epoxy)

Polymer absorbs UVR chemically and it degrades as a result of energy accumulation. Even a low energy of UVR is applied to the polymer for over a long period of time, the cumulative degradation effect is significant. There are two ways of UVR absorption on polymers, one way is that the UVR excites the electrons in the bonds between polymer chains. Another way is the UV produces thermal energy to cause thermal degradation on polymers. The degree and the rate of UV degradation on polymers depends on the intensity and thermal energy of UVR absorbed by polymers. To further explain, the amount of UVR energy required to degrade a polymer is determined by the molecular structures of polymers, such as amorphous or crystalline, and the bonding characteristics, such as secondary bonds (Van der Waals bonds and hydrogen bonds) or crosslinks or covalent bonds, between polymer chains.

Styrene is an amorphous thermoplastic and epoxy is a thermoset plastic. Theoretically, if the energy of UVR is large enough, it is able to break firstly the secondary bonds between the polymer chains and then the covalent bonds of the primary polymer chains because the secondary bond is much weaker than the covalent bond. Generally, amorphous thermoplastic has no crosslinks between polymer chains and low density, so it is more susceptible

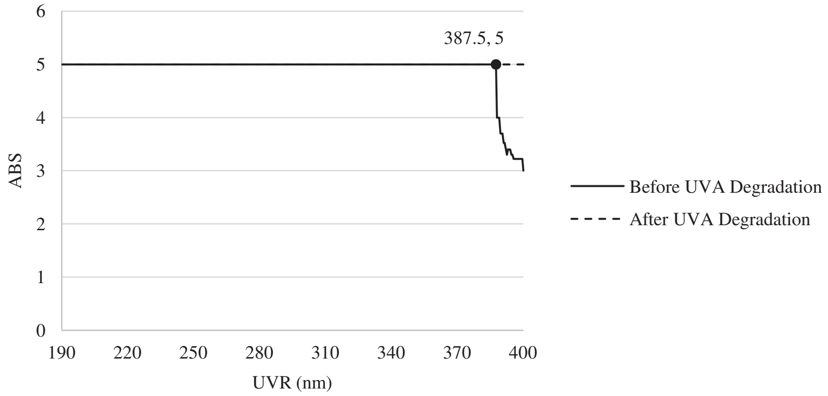

Fig. 2. The UV absorbability of neat SSMP before and after UVA degradation.

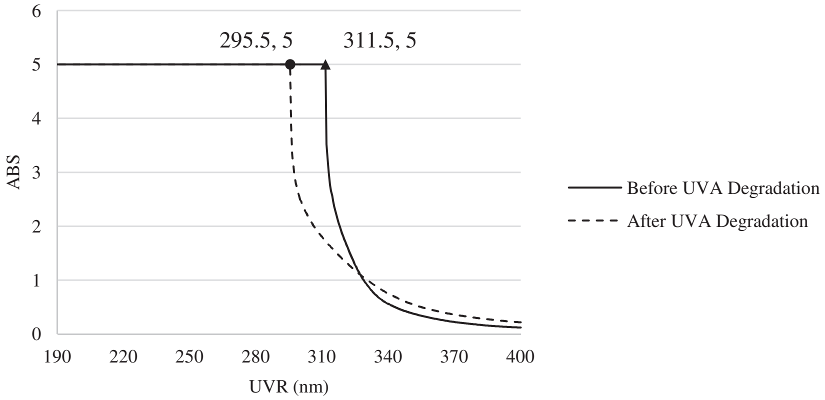

Fig. 3. The UV absorbability of neat EPSMP before and after UVA degradation.

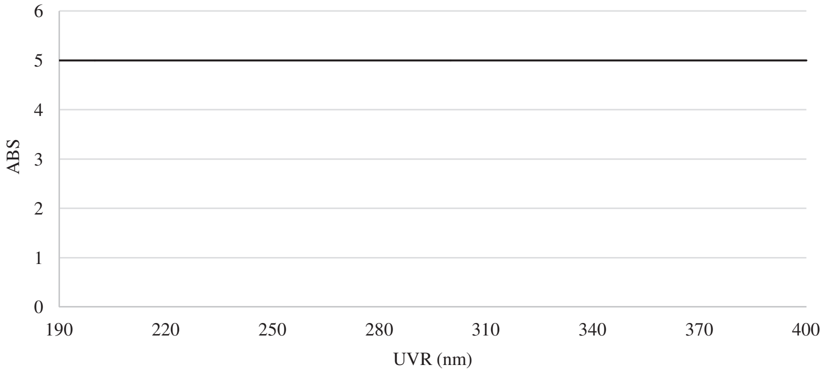

Fig. 4. The UV absorbabilities of 2, 4, 5, 7 wt.% ZnO/SSMPs and 2, 4, 5, 7 wt.% ZnO/EPSMPs before and after UVA degradation.

to UVR. It has been proven that it forms crosslinks and releases a gas under UV degradation with a temperature a little below its Tg. As a result, the degraded amorphous thermoplastic becomes a thermoset plastic. On the contrary, thermoset plastic has crosslinks between polymer chains and high density, therefore, more energy is needed to break the bonds, so it is more resistant to UVR.

The intensity energy of UVA lies between 4.903×10^{-19} J and 6.251×10^{-19} J. The rate of degradation on polymers various with the thermal energy they exposed, it can be calculated by *Arrhenius Equation* in Eq. (3),

$$\text{Rate} = Ae^{-(E/RT)} \tag{3}$$

where A is the collision factor, E is the energy required to make the reaction occur, R is the gas constant and T is the temperature in Kelvin the polymer exposed [21].

3.4. Yellowing of neat SMPs and ZnO/SMPs by UVA degradation

Before the UVA degradation (Fig. 5), the neat SSMP was opaque in white and the neat EPSMP was transparent in white. All ZnO/SSMPs and ZnO/EPSMPs were opaque in nearly the same degree of white because the white nano-ZnO particles were added. After accelerated UVA ageing (Fig. 6), all samples were yellowish with different degrees. The neat SSMP and all ZnO/SSMPs were at

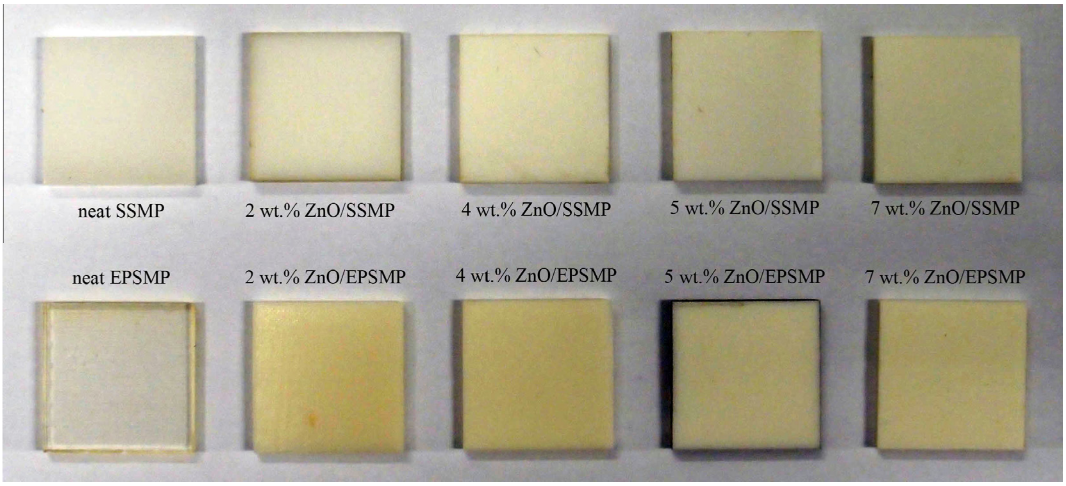

Fig. 5. The neat SSMP, all ZnO/SSMPs, the neat EPSMP and all ZnO/EPSMPs before UVA degradation.

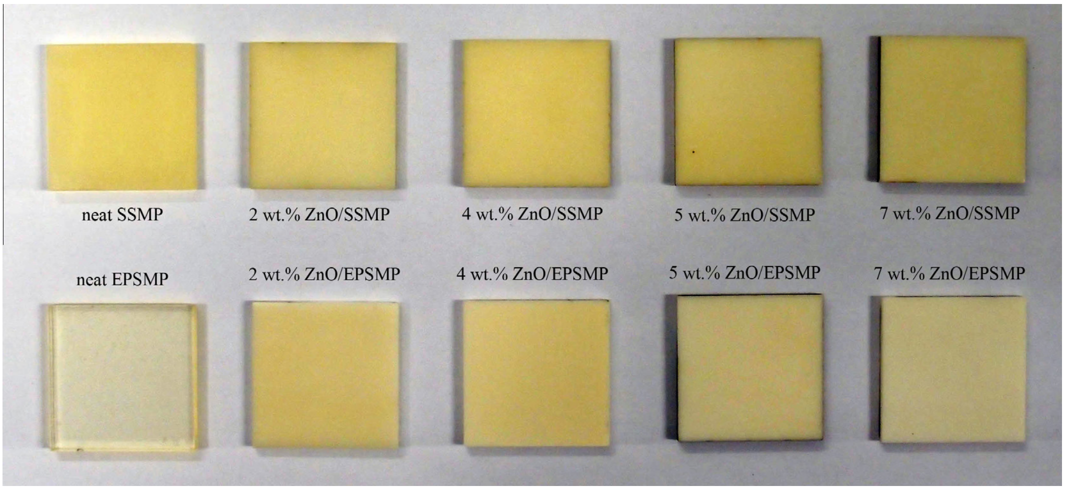

Fig. 6. The neat SSMP, all ZnO/SSMPs, the neat EPSMP and all ZnO/EPSMPs after UVA degradation.

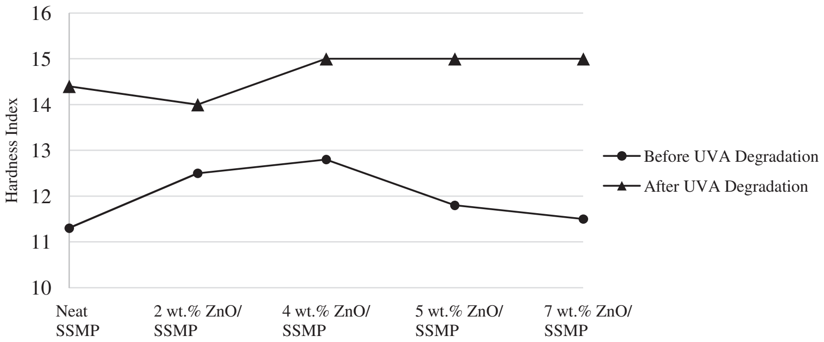

Fig. 7. Hardness of neat SSMP and all ZnO/SSMPs before and after UVA degradation.

nearly the same degree and rate of yellowing and they were much yellower than the neat E-SMP and all ZnO/E-SMPs. The neat EPSMP was transparent in yellow. And it is worth to notice that ESMPs with larger amount of nano-ZnO particles resulted in lower degree and rate of yellowing which this result could not be found in SSMPs.

These phenomena implied that the bonds between polymer chains in SSMP were weaker and more susceptible to UVA than that in EPSMP. Also, nano-ZnO particles were more compatible in EPSMP than in SSMP in terms of UVR absorbability.

3.5. Surface hardness tests of neat SMPs and ZnO/SMPs

Two kinds of SMPs, SSMP and EPSMP in their pure form and with 2, 4, 5 and 7 wt.% ZnO were tested for the surface hardness before and after the UVA degradation and their results were shown

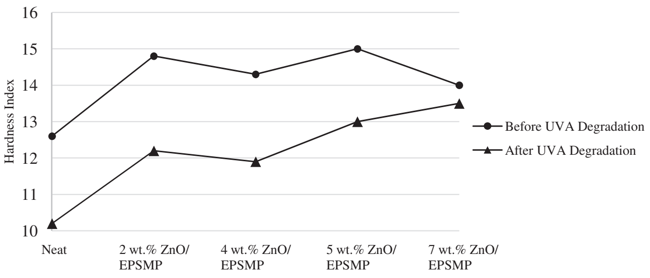

Fig. 8. Hardness of neat EPSMP and all ZnO/EPSMPs before and after UVA degradation.

in Figs. 7 and 8. Before the UVA degradation test, the surface hardness of S-SMPs with 5 and 7 wt.% of nano-ZnO particles had a tendency of decreasing. This might be resulted from the shrinkage of the SSMPs during the curing process that caused the agglomeration of nano-ZnO particles to occur although they were evenly dispersed inside the SSMPs. After accelerated UVA ageing, the surface hardness of all SSMP samples were hardened while that of all EPSMP samples were softened. These implied all SSMP samples behaved more alike amorphous thermoplastics which they formed crosslinks and became a thermoset plastic while all EPSMP samples behaved alike thermoset plastics which their crosslinks were broken and became more flexible and tough but less strong and stiff after UVA degradation.

It could be concluded that 2 and 4 wt.% of nano-ZnO particles in SSMPs and 5 and 7 wt.% of nano-ZnO particles in EPSMPs could maintain their surface hardness at a moderate level after UVA degradation.

3.6. Dynamic mechanical analysis (DMA)

A good shape memory material depends on a large and sharp drop in the storage modulus around its Tg. From Figs. 9 and 10, the rate of drop of neat SMPs and ZnO/SMPs at their Tg were similar. The most significant deviation appear on UVA-degraded neat SSMP and UVA-degraded 4 wt.% ZnO/EPSMP. Their rate of drop keep similar to other SMP samples but the response in drop is delayed to a higher temperature. The storage modulus is accounted for the hardness of the polymer. The harder the polymer, the larger the storage modulus. It is noted that SSMP would become hardened while EPSMP would become softened of their UVA-degraded surface. From the DMA result, it proved that the storage modulus of UVA-degraded neat SSMP was dominated by the hardened UVA-degraded surface and that of UVA-degraded 4 wt.% ZnO/EPSMP was dominated by the 4 wt.% nano-ZnO particles. The softened UVA-degraded surface of EPSMP was suppressed its effect on storage modulus by the reinforced particles.

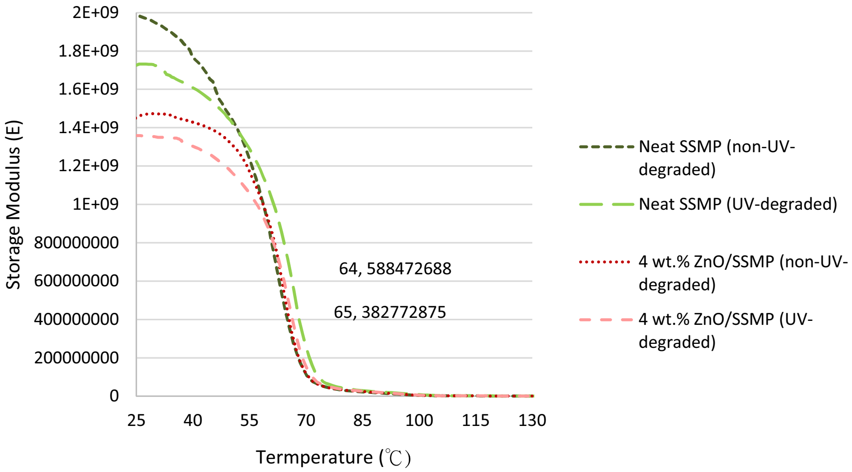

Fig. 9. Storage modulus of neat SSMPs and 4 wt.% SSMPs before and after UVA degradation.

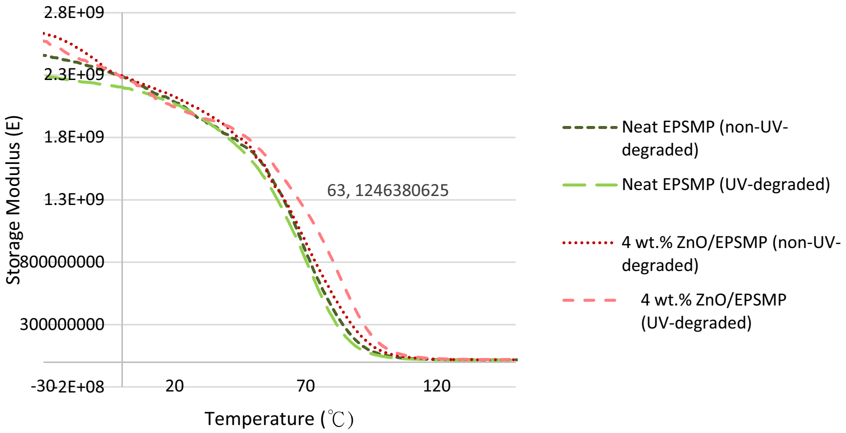

Fig. 10. Storage modulus of neat EPSMPs and 4 wt.% EPSMPs before and after UVA degradation.

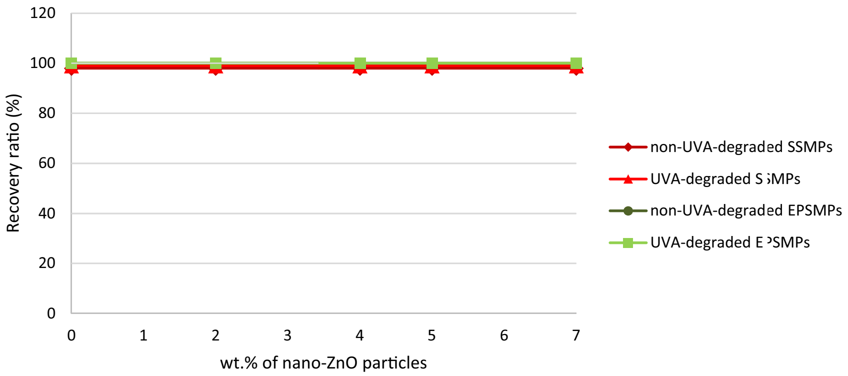

Fig. 11. Shape recovery ratio of different SMPs before and after UVA degradation.

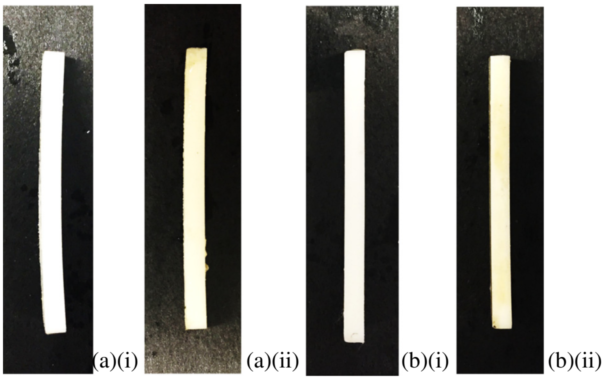

Fig. 12. Shape recovery for non-UVA-degraded (i) and UVA-degraded (ii) 4 wt.% ZnO/SSMP (a) and 4 wt.% ZnO/EPSMP (b).

The deviation of temperature at the same storage modulus for the UVA-degraded neat SSMP was +5.2 °C (5.9%) and for the UVA-degraded 4 wt.% ZnO/EPSMP was +4.3 °C (4.3%) from their non-UVA-degraded samples. It could also concluded that nano-ZnO particles, at the amount enough for obtaining a full UVR absorption, would not significantly affect the dynamic mechanical property of SMPs but UVA degradation would have more effects on the property.

It is assumed that by implementing appropriate amount of ZnO particles into SMPs for the UVA absorption, the drop of storage modulus could be maintained at the nearest temperature to their non-UVA degraded samples after UVA degradation.

3.7. Shape memory effects (SMEs)

3.7.1. Shape recovery ratio

Fig. 11 shows the shape recovery ratio of all neat SMPs and all ZnO/SMPs. Fig. 12 shows the final shape after recovery for non-UVA degraded and UVA-degraded 4 wt.% ZnO/SSMP and 4 wt.% ZnO/EPSMP. UVA-degraded SSMPs had slightly higher recovery ratio than non-UVA-degraded SMPs. Non-UVA-degraded and UVA-degraded EPSMPs had full recovery ratio. Under the same circumstance, SSMP was more sensitive to UVA degradation. Nano-ZnO particles, at the amount enough for obtaining a full UVR absorption, would not alter the recovery ratio but UVA degradation would have effect on the property. The shape recovery ratio depended mostly on the base shape memory polymer, its cross linking agent content of SSMP or linear monomer content of EPSMP.

3.7.2. Recovery reaction time and full recovery time

Besides counting the full recovery time, reaction time for starting the recovery is also an important factor to be considered. From Figs. 13 and 14, EPSMPs showed having the faster recovery reaction time and full recovery time than SSMPs. This could be explained by the linking network structure of polymer molecular chains of base shape memory matrix. SSMP and EPSMP have two-phases (soft and hard) or a cross-linked structure to exhibit the SME. EPSMP has long linear monomer chain of C–O bonds and two epoxy groups at the chain ends which crosslink points are far more linked together with higher flexible segment mobility.

For non-UVA-degraded and UVA-degraded SSMPs and EPSMPs, the larger the content of nano-ZnO particles, the higher the hardness of SMPs, the faster their recovery reaction time. Hard segment of SMP dominated the recovery reaction time.

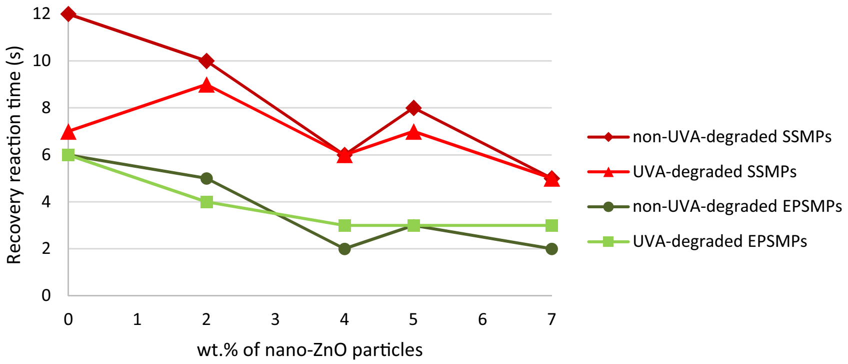

Fig. 13. Recovery reaction time of different SMPs before and after UVA degradation.

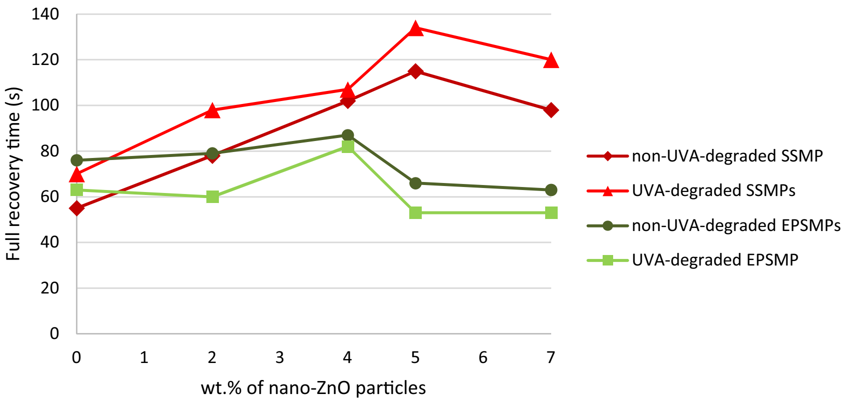

Fig. 14. Full recovery time of different SMPs before and after UVA degradation.

For non-UVA-degraded and UVA-degraded EPSMPs, the larger the content of nano-ZnO particles, the faster their full recovery time but it was contrary to that of SSMPs and at 7 wt.% of nano-ZnO particles, SSMP showed a reduced full recovery time. Although implementing nano-ZnO particles would increase the hardness of SMPs, it did not show significant changes as the same as the results in recovery reaction time. The soft segment of SMP dominated the full recovery reaction time.

It is more preferable for the SMP having the less variation of recovery reaction time before and after UVA degradation. In general, 4 wt.% ZnO/SSMP and 5 wt.% ZnO/EPSMP had less variation and time for recovery reaction and full recovery before and after UVA degradation. And the hardened and softened UVA-degraded surface of SSMPs and EPSMPs respectively agreed with the conclusion stated: the hard segment of SMP dominated the recovery reaction time and the soft segment of SMP dominated the full recovery reaction time.

4. Conclusions

Different weight percentages of nano-ZnO particles were introduced into styrene-based (SSMP) and epoxy-based (EPSMP) shape memory polymers respectively. Their decolouration, UVR absorbabilities, surface hardness, dynamic mechanical properties and shape memory effects under UVA degradation test were then investigated. They were under accelerated UVA ageing at intensity 11 times higher and a temperature 3 times higher than that of the ambient environment. It is equivalent to a situation that the samples were exposed to 22 days under the Sunlight in terms of UVA intensity. The purpose of adding nano-ZnO particles into a polymer was to absorb UVR between 290 and 400 nm (whole range of UVA and UVB) to protect the polymer from full UV degradation.

The UVR absorption tests showed that 2 wt.% of nano-ZnO particles was enough to absorb the whole range of UVR (190–400 nm) for SSMP and EPSMP samples. Besides nano-ZnO particles, shape memory matrix which is in polymer base would also absorb part of the UVR and this showed in the yellowish of all neat SMP and ZnO/SMP samples after UVA degradation test.

All SSMP samples had nearly the same degree of yellowing, but they were much yellower than EPSMP samples. EPSMP samples with large amount of nano-ZnO particles could achieve lower degree and rate of yellowing. This implied that nano-ZnO particles could effectively resist the UVA degradation for EPSMP samples as compared with SSMP samples.

Apart from examining the functionality of nano-ZnO particles in SMPs, it is worth to mention that neat SSMP and neat EPSMP had different behaviours under UVA degradation. Surface hardness tests showed that the neat SSMP was harder while neat EPSMP was relatively softener after UVA degradation. This could be explained that SSMP had more alike amorphous thermoplastic in which crosslinks were formed between the polymer chains inside it and became thermoset plastic after the degradation test. EPSMP was alike a typical thermoset plastic in which the crosslinks between the polymer chains inside EPSMP were broken by the incident UVA energy and become more flexible and tough but less strong and stiff after UVA degradation.

From the surface hardness test, 2 and 4 wt.% ZnO/SSMPs and 5 and 7 wt.% ZnO/EPSMPs could maintain their surface hardness at a moderate level after UVA degradation.

For the shape memory behaviour, 4 wt.% ZnO/SSMP and 5 wt.% ZnO/EPSMP would be the good candidate to achieve fast recovery reaction time and full recovery time while minimising the effects of UVA degradation on the shape memory effects of SMPs.

Nano-ZnO particles at the tested weight percentages had no significant variation to the dynamic mechanical properties and recovery ratio of SSMP and EPSMP, but UVR had considerable effects to that of SMPs. It is believed that by controlling the content of nano-ZnO particles and the linking network structure of polymer molecular chains inside SMP, its UVR absorbability, surface hardness, dynamic mechanical properties and shape memory effects could be enhanced in an acceptable performance to against the UV degradation.

Acknowledgements

This project is supported by the Hong Kong Polytechnic University Grant (G-YK84) and the National Natural Science Foundation of China, Grant Numbers 11225211 and 11272106, for which we are very grateful.

References

[1] Barrett R, Francis W, Abrahamson E, Lake MS, Scherbarth M. Qualification of elastic memory composite hinges for spaceflight applications. In: 47th AIAA/ASME/ASCE/AHS/ASC structures, structural dynamics and materials conference, Newport, Rhode Island; 2006.
[2] Browne AL, Johnson NL. Hood assembly utilizing active materials based mechanisms. U.S. Patent, 0197674; 2008.
[3] Buckley PR, McKinley GH, Wilson TS, Small W, Benett WJ, Bearinger JP, et al. Inductively heated shape memory polymer for the magnetic actuation of medical devices. IEEE Trans Biomed Eng 2006;53(10):2075.
[4] Diffey BL. Sources and measurement of ultraviolet radiation. Methods 2002;28(1):4–13.
[5] Dutta S, Chattopadhyay S, Sarkar A, Chakrabarti M, Sanyal D, Jana D. Role of defects in tailoring structural, electrical and optical properties of ZnO. Prog Mater Sci 2009;54:89–136.
[6] Emeline AV, Ryabchuk VK, Serpone N. Photoreactions occurring on metal-oxide surfaces are not all photocatalytic. Description of criteria and conditions for processes to be photocatalytic. Catal Today 2007;122:91–100.

[7] Gallagher RP, Lee T. Adverse effects of ultraviolet radiation: a brief review. Prog Biophys Mol Biol 2006;92(1):119–31.

[8] Kumar AP, Depan D, Tomer NS, Singh RP. Nanoscale particles for polymer degradation and stabilization—Trends and future perspectives. Prog Polym Sci 2009;34:479–515.

[9] Lendlein A, Langer R. Biodegradable, elastic shape-memory polymers for potential biomedical applications. Science 2002;296:1673.

[10] Leng JS, Wu XL, Liu YJ. Effect of a linear monomer on the thermomechanical properties of epoxy shape-memory polymer. Smart Mater Struct 2009;18:095031.

[11] Liu YJ, Du HY, Liu LW, Leng JS. Shape memory polymers and their composites in aerospace applications: review. Smart Mater Struct 2014;23:023001.

[12] Liu YJ, Lv HB, Lan X, Leng JS, Du SY. Review of electro-active shape-memory polymer composite. Compos Sci Technol 2009;69:2064–8.

[13] Lowry M, Hubble D, Wressell A, Vratsanos M, Pepe F, Hegedus C. Assessment of UV-permeability in nano-ZnO filled coatings via high throughput experimentation. J Coat Technol Res 2008;5(2):233–9.

[14] Lu HB, Liu YJ, Leng JS, Du SY. Qualitative separation of the effect of the solubility parameter on the recovery behavior of shape-memory polymer. Smart Mater Struct 2009;18:085003.

[15] Moezzi A, McDonagh AM, Cortie MB. Zinc oxide particles: synthesis, properties and applications. Chem Eng J 2012;185–186:1–22.

[16] Pastorelli G, Cucci C, Garcia O, Piantanida G, Elnaggar A, Cassar M, et al. Environmentally induced colour change during natural degradation of selected polymers. Polym Degrad Stab 2014;107:198–209.

[17] Rabek JF. Mechanisms of photophysical processes and photochemical reactions in polymers: theory and applications. UK: John Wiley & Sons Ltd; 1987. ISBN: 0 471 91180 1.

[18] Rochetter JM, Ashby VS. Photoresponsive polyesters for tailorable shape memory biomaterials. Macromolecules 2013;46:2134–40.

[19] Salla J, Pandey KK, Srinivas K. Improvement of UV resistance of wood surfaces by using ZnO nanoparticles. Polym Degrad Stab 2012;97(4):592–6.

[20] Serpone N, Dondi D, Albini A. Inorganic and organic UV filters: their role and efficacy in sunscreens and suncare products. Inorg Chim Acta 2007;360(3):794–802.

[21] Strong AB. Plastic: materials and processing. 2nd ed. USA: Clarinda Publication Services; 2000, ISBN 0 13 021626 7.

[22] Takahashi T, Kondo T, Tanaka K, Hattori S, Irie S, Kudoh S, et al. Using collagen artificial skin to estimate the protection effects of UV-cut materials against sunlight under the Antarctic ozone hole. Polym Degrad Stab 2012;97:1002–9.

[23] Tigges B, Moller M, Weichold O. ZnO nanoparticle-containing emulsions for transparent, hydrophobic UV-absorbent films. J Colloid Interface Sci 2010;345:41–5.

[24] UNEP (United Nations Environment Programme). Environmental effects of ozone depletion and its interactions with climate change: 2010 assessment. United Nations Environment Programme, Nairobi, Kenya; 2010.

[25] Wu XL, Zhang WY, Liu YJ, Leng JS. A preliminary study on shape recovery speed of a styrene-based shape memory polymer composite actuated by different heating methods. In: International conference on smart materials and nanotechnology in engineering. Proceedings of SPIE vol. 6423; 2007.

[26] Xu JW, Shi WF, Pang WM. Synthesis and shape memory effects of Si–O–Si cross-linked hybrid polyurethanes. Polymer 2006;47:457–65.

[27] Xu T, Li GQ, Pang SS. Effects of ultraviolet radiation on morphology and thermo-mechanical properties of shape memory polymer based syntactic form. Compos A Appl Sci Manuf 2011;42(10):1525–33.

[28] Zhang DW, Liu YJ, Yu K, Leng JS. Influence of cross-linking agent on thermomechanical properties and shape memory effect of styrene shape memory polymer. J Intell Mater Syst Struct 2011;22:2147.

[29] Zhang ZC, Chu HT, Wang KW, Liu YJ, Leng JS. Multifunctional carbon nano-paper composite. In: Fourth international conference on smart materials and nanotechnology in engineering. Proceedings of SPIE, vol. 8793; 2013.

[30] Zhu Y, Hu J, Yeung LY, Liu Y, Ji F, Yeung KW. Development of shape memory polyurethane fiber with complete shape recoverability. Smart Mater Struct 2006;15:1385.

Composites Part B 90 (2016) 378–385

Contents lists available at ScienceDirect

Composites Part B

journal homepage: www.elsevier.com/locate/compositesb

Effects of silane surfactant on Nano-ZnO and rheology properties of nano-ZnO/epoxy on the UV absorbability of nano-ZnO/epoxy/micron-HGF composite

Tsz-ting Wong [a], Kin-tak Lau [a, *], Wai-yin Tam [a], Julie A. Etches [b], Jang-Kyo Kim [c], Ying Wu [c]

[a] Department of Mechanical Engineering, The Hong Kong Polytechnic University, Hung Hom, Kowloon, Hong Kong
[b] Faculty of Engineering, University of Bristol, United Kingdom
[c] Department of Mechanical and Aerospace Engineering, Hong Kong University of Science and Technology, Hong Kong

A R T I C L E I N F O

Article history:
Received 25 September 2015
Received in revised form
5 January 2016
Accepted 6 January 2016
Available online 15 January 2016

Keywords:
A. Polymer-matrix composites (PMCs)
A. Glass fibre
A. Particle-reinforcement
E. Resin flow

A B S T R A C T

Nano-zinc oxide (nano-ZnO)/epoxy filled micron-hollow glass fibres (micron-HGFs) epoxy composite is opening up a new configuration for fibre reinforced polymer composite (FRPC) with enhanced ultraviolet (UV) resistibility. ZnO nanoparticles having intrinsic UV absorbability were introduced into epoxy and nano-ZnO/epoxy was filled into 100 μm HGF by using vacuum infiltration technique. 4 wt.% 100 nm ZnO/epoxy/100 μm HGF epoxy composite was found to have the highest UV absorbability among other samples. The silane surfactant on ZnO nanoparticle (NP) was evaluated and the rheology of nanofluid (NF) was investigated for the UV absorbability of nanocomposite (NC), which the two parameters determine the dispersion of ZnO nanoparticles and the polymerization shrinkage of nanocomposite. An optimum concentration and good dispersion of ZnO nanoparticles are aimed to be achieved in order to maximize the UV absorbability of nano-ZnO/epoxy/micron-HGF epoxy composite. The silane surfactant on ZnO nanoparticle was found to be ineffective for UV absorption.

1. Introduction

Ultraviolet (UV) is proven to be the major cause of skin cancer on human and deterioration of mechanical properties on polymer-based materials [1,6,8,24]. It causes decolouration, cracks and delamination in carbon and glass fibre polymer composites [1]. As the usage of these composites has been massively increased in aerospace, automobile and civil construction industries, the protection of human bodies and polymer-based composites from UV attack is certainly being a concern worldwide.

ZnO particle is an intrinsically inorganic UV absorber which is proven to have less negative effects to polymer-based materials after UV degradation. This is because it processes UV absorption by physical reaction and it can obtain a full UV absorption in its nano size [9]. ZnO nanoparticles (NPs) have been introduced into polymer-based materials for protecting the materials from UV degradation [9,12] and enhancing their thermal stability [3,10,14,35]. Researchers have developed UV-protective coatings and introduced UV absorption inorganic NPs into polymers for UV protection of polymer-based materials. It is commonly known that UV-protective coating has a wearing problem and embedded particles have a problem of dissolution out from the polymers under UV degradation, since cracks will be induced inside polymers and allow particles to pass through, it is especially critical if the particles are in nano size. Therefore, by introducing HGF as the host to protect ZnO NPs would be a unique solution for the nanocomposite (NC) to process a continuous UV absorption and protection for the entire material throughout the UV degradation and reinforce the base polymer simultaneously [29]. Vacuum infiltration is a well-known technique for the fabrication of self-healing composites, which require to infiltrate resin into hollow fibres, for aerospace applications [5,21,22,29].

The silane surfactant of ZnO NPs and the rheology properties of NF have the relationship with the dispersion of NPs, the polymerization shrinkage and the UV absorbability of NC.

A homogenous dispersion of ZnO NPs can be achieved by electrostatic (physical) or steric stabilization (chemical) methods, for

---

* Corresponding author. Tel.: +852 2766
E-mail address: mmktlau@.

http://dx.doi.org/10.1016/j.compositesb.2016.01.005
1359-8368/

example, by ultrasonication for increasing the magnitude of repulsion to overcome the Van de Waal's attraction of ZnO NP–NP or by surface treatment of doping silane coupling agent on ZnO NP to increase the negative charges on the surface of ZnO NP for increasing the magnitude of repulsion to overcome the hydrogen bond (H-bond) of ZnO NP–NP [14,15,19,33]. The silane surfactant of commonly used γ-aminopropyltriethoxysilane (KH550) on ZnO was proven to be able to improve the dispersion of particles and enhance the compatibility of the particles inside polymers which means it improves the mechanical properties of the NC. The effectiveness of UV absorption of silane-ZnO NC was also investigated. Wu investigated the effects of different surface modification of ZnO particles to UV absorbability and found that KH550-ZnO had lower UV absorbability than other doped-ZnO [33]. In the paper of Mallakpour in 2012, the UV absorbability of KH550-ZnO/PAI was lower than neat PAI [15] and in his paper in 2014, after the chemical modification of PAI, the UV absorbability of KH550-ZnO/PAI was higher than neat PAI, and the higher the concentration of KH550-ZnO, the higher the UV absorbability of the NC [14]. Nicolay also discovered the UV absorbability of KH550-ZnO/sol–gel having the similar results of the research of Mallakpour in 2014 [19]. However, it has not yet achieved a full UV absorbability by implementing silane-ZnO particles into polymers. Contrarily, styrene-based and epoxy-based shape memory polymers (SMPs) were proven to have full UV absorbability at 2 wt.% of 100 nm ZnO particles implemented [31].

The vacuum infiltration pressure has an effect on ZnO NP dispersion and the effect is more significant inside micron-HGF, furthermore, a good rheology properties of NF is achieved by an even dispersion of ZnO NP. The flow behaviour of ZnO/epoxy fluid studied by the rheology test enables to explain the dispersion ability of ZnO inside epoxy and it is important for the fabrication of filled micron-HGF epoxy composite. Sadeghipour [25] pointed out most of the theories of the moduli of composites have their origin in the theory of the viscosity of suspensions. This implies that the rheology properties of NF correlate with the dispersion of NPs and the mechanical properties of the NC. There were several researchers studied the surfactant of NP and the rheology properties of NF in the relationship with the dispersion of NP, the polymerization shrinkage and the UV absorbability of NC. Nasu studied NF rheology, NP dispersion and UV protection property of suspension of titanium dioxides (TiO_2) and ZnO with different surfactant [17,18]. Yang also investigated the surface properties of TiO_2 microparticle in the relationship with fluid rheology properties and particle dispersion [34]. Siddiqui tested the rheology effect of carbon nanotube (CNT)/polymer on the behaviour of polymerization curing [26]. Suganthi examined the influence of the interaction of ZnO NP–polymer–water molecule on the NF transport properties (viscosity and thermal conductivity) [27].

The polymerization shrinkage is an effect from the curing process of polymer materials. Different polymers process different degrees of polymerization shrinkage. Generally, thermosetting plastics are considered having lower degree of polymerization shrinkage than thermoplastics because of the crystalline molecular structure. Epoxy, which is a kind of thermosetting plastics and possesses a relatively high dimensional precision, combining with different reinforcements has been widely used in aerospace applications. Although it has a relatively low polymerization shrinkage, the polymerization shrinkage become accountable if it is inside a micron-HGF. NPs are able to lower the degree of polymerization shrinkage of polymers, especially when ZnO NPs has high thermal conductivity and thermal stability [2,4,11,16,23,28]. Physically, NPs situate between epoxy polymer chains which interrupt and lower the linkage-growth polymerization under curing process. Added that ZnO NP has high heat capacity to accelerate heat energy exchange without changing much its temperature and expansion which helps to stabilize the dimension change of NC under curing. Lowering the rate of linkage-growth and the temperature change during polymerization process could lower the degree of polymerization shrinkage of polymer and the residual stress induced inside NC, so the NC results in better dimensional stability and mechanical properties. There are many studies regarding the implementation of NPs into polymers for increasing their functionality while enhancing the NC dimensional stabilization in medical, optical, manufacturing and coating engineering applications [7,13,20,30,35]. Onbattuvelli and Mahrholz stated that the inclusion of NPs enables to higher the densification of polymer and slower the speed of polymerization which lengthen the fabrication time and lower the degree of polymerization shrinkage [13,20]. Zabihi discovered the optimum thermal properties of NC which occurs at a relatively low concentration of 5 wt.%, of 50 nm ZnO particles [35]. A research proved that after adding 35 vol.% of NPs, the polymerization shrinkage of a polymer composite could be reduced to 0.3% [7].

In a previous experimental study, 4 wt.% 100 nm ZnO/epoxy/100 μm HGF epoxy composite in 0.2 mm intervals of HGFs obtained the best UV absorbability among the samples [32]. In order to understand the phenomenon, NF rheology properties, ZnO NP dispersion characteristic and NC shrinkage behaviour inside micron-HGF were investigated. An optimum concentration and good dispersion of ZnO NP are aimed to be achieved in order to maximize the UV absorbability of nano-ZnO/epoxy/micron-HGF epoxy composite. The silane surfactant on ZnO NP was found to be ineffective for UV absorption.

2. Materials and methods

2.1. Raw materials

Two types of ZnO NPs, 100 nm ZnO (undoped) and 20 nm doped-ZnO, used in this study are produced by American process and French process respectively. Their crystal structures and apparent (bulk) densities (0.560 g/cm^3 of 100 nm ZnO and 0.532 g/cm3of 20 nm doped-ZnO), which representing their deformability, are similar. They are both in spherical shape and in white colour. The surface area of 100 nm ZnO is 31.42 ƒm2 which is 25 times larger than 20 nm doped-ZnO, which means 100 nm ZnO has larger contact surface area with epoxy molecules inside the resin. 20 nm ZnO is coated with a silane coupling agent (KH550) in the weight ratio of 99:1. Silane surfactant on 20 nm ZnO particle is proven to be able to prevent particle agglomeration because of the increased negative charges on the surface of ZnO NP for increasing the magnitude of repulsion to overcome the H-bond of ZnO NP–NP and improve the bonding strength of ZnO NP–EP simultaneously. No solvents were used in all the dispersion processes.

HGF with outer diameter (OD) of 125 μm and inner diameter (ID) of 100 μm is produced by the Department of Aerospace Engineering of University of Bristol. It has a static frictional coefficient of approximately 0.94 and density of 2.63 g/cm^3.

Araldite GY251 and hardener HY956 mixed in the weight ratio of 5:1 was the epoxy resin which is also used as the base polymer.

2.2. ZnO NP dispersion and NC polymerization shrinkage inside micron-HGFs

Neat epoxy and different concentration (2, 4 and 7 wt.%) of ZnO NPs mixed with epoxy underwent 5 mins of mechanical stirring followed by 20 mins of ultrasonication, hardener was added afterwards and the mixture underwent another 5 mins of ultrasonication individually. Resin fluid was infiltrated into a 100 μm

HGF by using vacuum infiltration technique. Vacuum pump with the total ultimate vacuum pressure of 2 Pa was applied constantly for 10 mins to ensure a full infiltration in the HGF of 100 mm long. All filled fibres were cured under room temperature and pressure for 24 h prior to characterization. The dispersion of ZnO NPs and the polymerization shrinkage of nano-ZnO/epoxy inside micron-HGF were characterized by using optical microscope.

2.3. Rheology properties

The fluid samples were prepared with the same procedure mentioned before. They were produced at the same period of time, room temperature and pressure and were kept at 0–3 °C after mixing to ensure the tests were conducted within the pot life of fluid samples. The rheology studies on nano-ZnO/epoxy fluid samples were conducted on rotational Rheometer (ARES#, TA Instruments) using a parallel plane plate geometry with 25 mm diameter and 1 mm gap under isothermal condition. The concentration of ZnO NPs and the intermolecular forces of NP—NP, NPEP and EP—EP have significant effects on the fluid flow of nano-ZnO/epoxy inside micron-HGF and were evaluated by shear stress and viscosity along the shear rate from 0 to 250 s^{-1}. The shear rate is in log scale for easy evaluation.

2.4. UV absorbability

Nano-ZnO/epoxy/micron-HGF epoxy composite with different concentration (2, 4and 7 wt.%) of ZnO NPs and the same thickness of 2 mm were fabricated. Samples are compared regarding their UV absorbability between undoped and doped-ZnO NPs and their different concentration implemented. Neat epoxy/micron-HGF epoxy composite was fabricated for comparison purpose. The nano-ZnO/epoxy infiltrants were prepared with the same procedure mentioned before and the filled composites were cured under room temperature and pressure for 24 h prior to UV absorbability test in the range of UVA to UVC (190 nm–400 nm) by using UV–vis Spectrophotometer (Dynamica DB-20, 190–1100 nm).

3. Results and discussion

3.1. Dispersion characteristic of ZnO NP inside micron-HGFs

Dispersion characteristic of ZnO NPs is governed by the intermolecular strength of NP—NP, NP—EP and EP—EP which can be varied by two major methods: electrostatics (physical) and steric stabilization (chemical) that is the use of ultrasonication treatment during the preparation of resin and the use of surfactant on ZnO NP respectively. The intensity and time of ultrasonication and the concentration of surfactant on ZnO NP are crucially adjusted for achieving an even dispersion of ZnO NPs inside epoxy. The silane surfactant on ZnO NP is commonly used and is proven to be able to prevent particle agglomeration and obtain good bonding strength of NP—EP which correlate with the mechanical properties of the composite. Organic solvent is also commonly used to obtain an even dispersion of ZnO NPs. However, for fabricating nano-ZnO/epoxy/micron-HGF epoxy composite, solvent is not considered because it may not be fully vapourized out from micron-HGF before the resin is fully cured, for which it would eventually affect the mechanical properties of the final composite.

The dispersion characteristics of different concentration of 100 nm ZnO and 20 nm doped-ZnO NPs in epoxy inside individual HGF with inner diameter (ID) of 100 μm were observed under optical microscope as shown in Fig. 1. Neat epoxy without ZnO NPs and air bubbles inside the 100 μm HGF is clear. 2 wt.%, 4 wt.% and 7 wt.% 100 nm ZnO/epoxy and 20 nm doped-ZnO/epoxy exhibit different degrees of particle agglomeration. At 7 wt.% 100 nm ZnO/epoxy and 7 wt.% 20 nm doped-ZnO/epoxy, the particle agglomeration is severe as numbers of white clusters with irregular sizes, shapes and dispersion are distinctively observed inside the 100 μm HGF. Particles agglomerated at 7 wt.% 100 nm ZnO/epoxy impeded the flow of resin which air bubbles and ZnO NPs were blocked to be infiltrated out and through the 100 μm HGF. At 2 wt.% 100 nm ZnO/epoxy, 2 wt.% and 4 wt.% 20 nm doped-ZnO/epoxy, particle agglomeration is hardly observed, instead, the particles are in relatively lower concentration but in even dispersion inside the 100μmHGF. At 4 wt.% 100 nm ZnO/epoxy, particle agglomeration is hardly observed and the particles are in higher concentration and even dispersion inside the 100 μm HGF.

3.2. Rheology properties of NF

Rheology properties of NF can be adopted to determine the infiltration satisfaction of fluid in micron-HGF. There are two major parameters which are used to understand the rheology of fluid: shear stress and viscosity. In the following, two sets of fluid samples regarding their shear stress and viscosity against shear rate are discussed. Two sets of fluid samples as shown in Figs. 2 and 3 are 2 wt.%, 4 wt.% and 7 wt.% (yellow, red and green respectively) of 100 nm ZnO (solid line) and 20 nm doped-ZnO (dashed line) mixed with epoxy. One neat epoxy (black solid line) is a control sample for reference purpose.

In Fig. 2, yield stress indicates the starting shear stress at zero shear rate. It is the stress required to start deforming the microstructure and simulating the flow of fluid. The amount of ZnO NP increases, the yield stress of fluid increases. Particles are interlocked between polymer molecular chains, which decrease the mobility of the microstructure of resin and increases the difficulty of deformation of resin. However, on the other side, particles are able to stabilize the flow of fluid during infiltration process and the polymerization shrinkage of resin during curing process.

Lower shear stresses was sufficient to deform the microstructure of 4 wt.% and 7 wt.% of 100 nm ZnO/epoxy along the shear rate compared to that of 20 nm doped-ZnO/epoxy. The shear stresses required to deform 2 wt.% 100 nm ZnO/epoxy and 2 wt.% 20 nm doped ZnO/epoxy behave similar. The shear stress required to deform 2 wt.% 100 nm ZnO/epoxy is higher upon the shear rate at 1.6 s^{-1}, the shear stress required of it is lower after the point. The silane surfactant on 20 nm ZnO particles may be destroyed by higher shear force and the resin becomes inhomogeneous with particles in irregular sizes, shapes and dispersion, so that a much higher shear stress was required to deform the microstructure of fluid. It is worth noting that the bonding between silane coating and 20 nm ZnO particle is an H-bond which is a kind of secondary weak bond and relatively susceptive to the applied shear force. It could be concluded that the silane surfactant on 20 nm ZnO particle is regarded as an inhibiter to the flow of fluid.

In Fig. 3, 7 wt.% 20 nm doped-ZnO/epoxy is not included for discussion due to its 4 times higher of viscosity along the plateau compared with other fluid samples. The results of viscosity and shear stress against shear rate for all fluid samples are match. Shear stress is the applied force acting on the microstructure of fluid interplaying with the viscosity of fluid which is defined as the internal resistance induced by the intermolecular forces between NP—NP, NP—EP and EP—EP to inhibit the flow of fluid.

Along the plateau, neat epoxy has gradually increasing viscosity with the increasing shear rate, this phenomenon also happens in 20 nm doped-ZnO/epoxy. This could be claimed that the silane surfactant enabled 20 nm ZnO/epoxy to behave similarly as the neat epoxy in terms of their viscosity property. The higher the concentration of 20 nm ZnO particles, the steeper the increasing

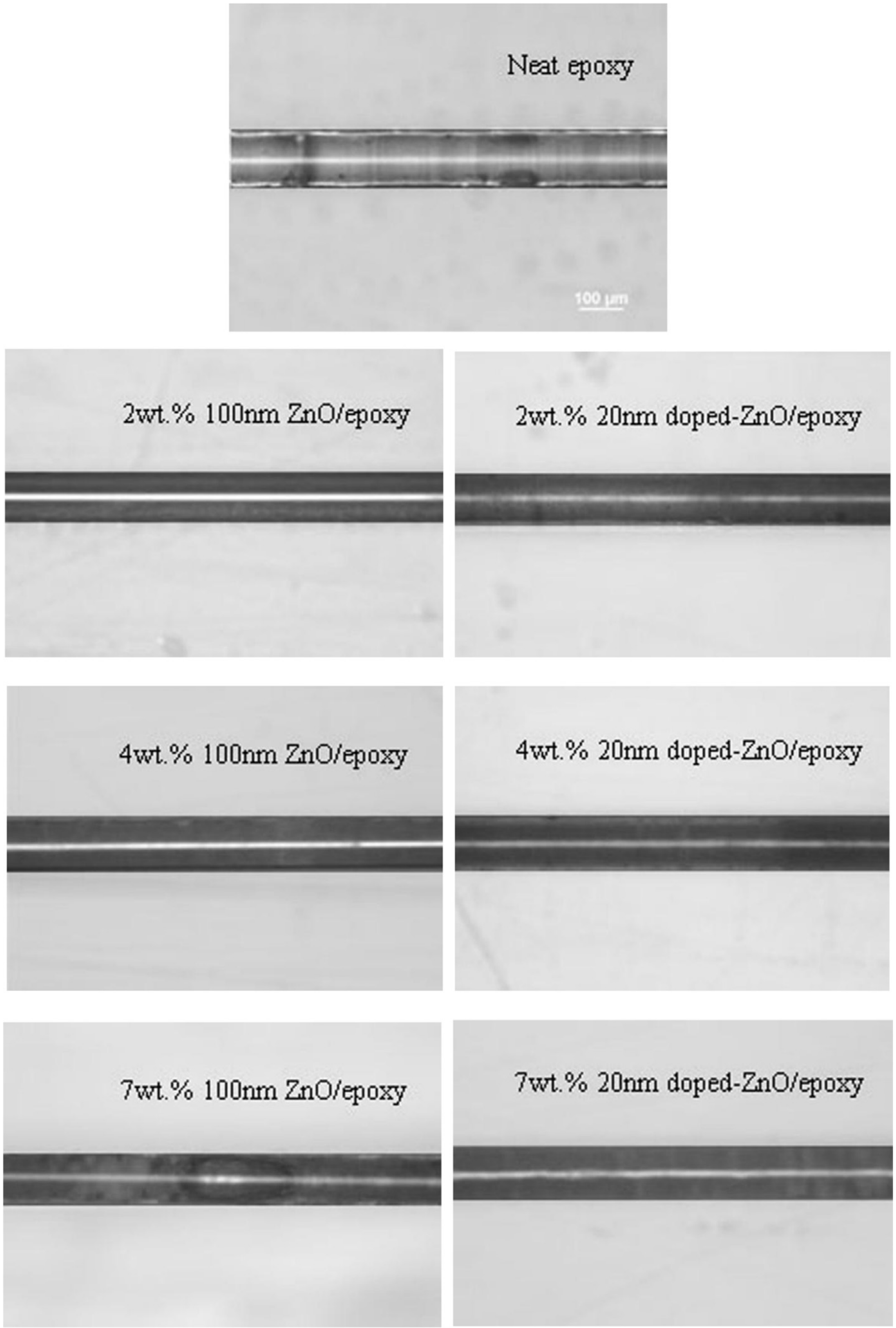

Fig. 1. Particle dispersion of neat epoxy (the topmost), 2 wt.%, 4 wt.% and 7 wt.% of 100 nm ZnO/epoxy (left) and 20 nm doped-ZnO/epoxy (right) inside micron-HGF.

slope of viscosity of the fluid along the plateau. Undoped 100 nm ZnO particles should not be considered as unstable to epoxy but they were adverse the behaviour of epoxy with gradually decreasing slope of viscosity along the plateau. The higher the concentration of 100 nm ZnO particles, the steeper the decreasing slope of viscosity of the fluid along the plateau. ZnO particles regarded as undeformable, so that the Van de Waals' interaction of 100 nm ZnO—EP, the H-bond of silane coating—20 nm ZnO, the H-bond of 20 nm doped-ZnO—EP and the covalent bond of EP—EP are subjected to the applied shear stress and then they are sheared apart resulting in a lower viscosity of the fluid.

Every fluid sample has its initial viscosity and has gradually increasing or decreasing viscosity along its plateau until it reaches a critical viscosity as shown in Fig. 3 The higher the concentration of ZnO NPs, the higher the viscosity of the fluid sample. After the critical viscosity, all fluid samples have a sudden drop of viscosity. 100 nm ZnO/epoxy without silane surfactant drops violently than 20 nm doped-ZnO/epoxy. It could be explained that slipping may occur between the surface of 100 nm ZnO—EP. The silane surfactant on 20 nm ZnO particles should not be regarded as stabilizing the viscosity of fluid if they are destroyed by higher shear force and the resin results as inhomogeneous with particles in irregular sizes, shapes and dispersion which increases the viscosity of fluid and inhibited the flow.

Although the contact surface area of 20 nm doped-ZnO—EP is 25 times lesser than that of 100 nm ZnO—EP, the chemical bonding

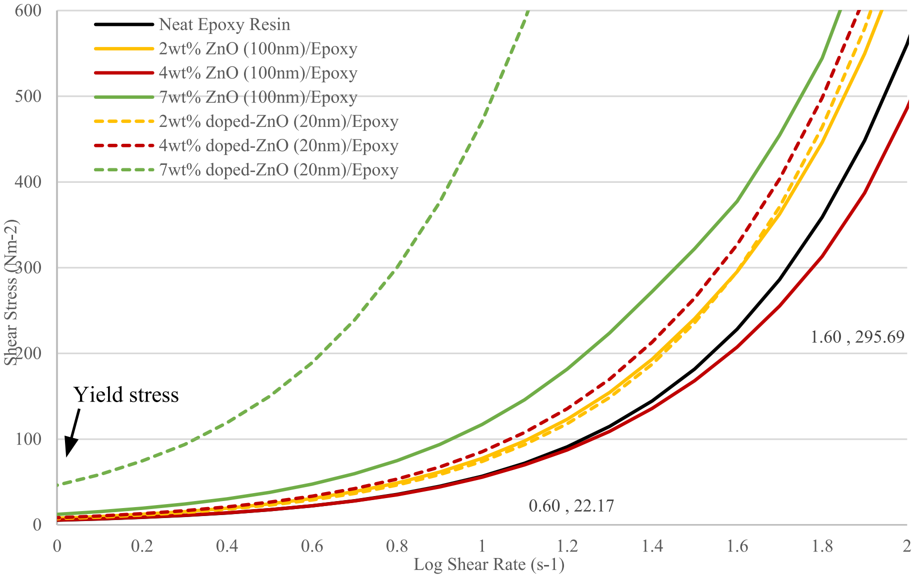

Fig. 2. Shear stress against shear rate of different fluid samples.

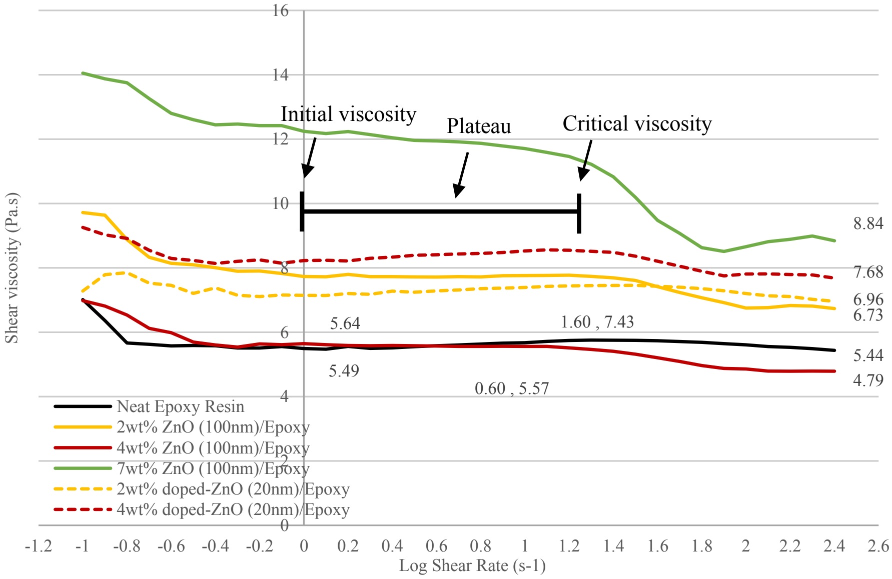

Fig. 3. Shear viscosity against shear rate of different fluid samples.

strength of 20 nm doped-ZnO–EP is much stronger than that of 100 nm ZnO–EP. It could be proven by the rheology results that a larger shear stress was required to deform the microstructure of 20 nm doped-ZnO/epoxy with higher viscosity. Conclusively, 4 wt.% 100 nm ZnO/epoxy has the lowest required shear stress to deform its microstructure and viscosity at 5.5 Pa.s throughout the applied shear rate from 0 to 250 s^{-1} among all the nano-ZnO/epoxy fluid samples.

3.3. Polymerization shrinkage of NC inside micron-HGFs

Different degrees of polymerization shrinkage are observed at the end of nano-ZnO/epoxy as shown in Fig. 4. A higher degree of polymerization shrinkage happens in neat epoxy while a lower degree of polymerization shrinkage appears in resin with higher content of ZnO NPs. The shrinkage angles were measured at the end of resin. The shrinkage angle of neat epoxy, 2, 4 and 7 wt.% ZnO/epoxy are 45°, 53°, 55° and 57° respectively. A resin with high shrinkage angle indicates that it has a low degree of polymerization shrinkage. 100 nm ZnO/epoxy and 20 nm doped-ZnO/epoxy had no influence in the degree of polymerization shrinkage, but the particle agglomerations and the inner surface properties of HGF would affect the shrinkage angle. When the particles agglomerate away from the end of resin, the shrinkage angle is higher and vice versa.

It could be concluded that ZnO NPs helped stabilizing the resin to obtain a lower degree of polymerization shrinkage. The symmetric diagram in Fig. 5 shows the behaviour of resin from infiltration to curing process. During vacuum infiltration, the applied shear stress leads the fluid to fully flow through the 100 μm HGF while frictional force along the inner surface of the 100 μm HGF exerts on the fluid which inhibits the flow. Epoxy resin along the centre moves further beyond than those along the inner surface of

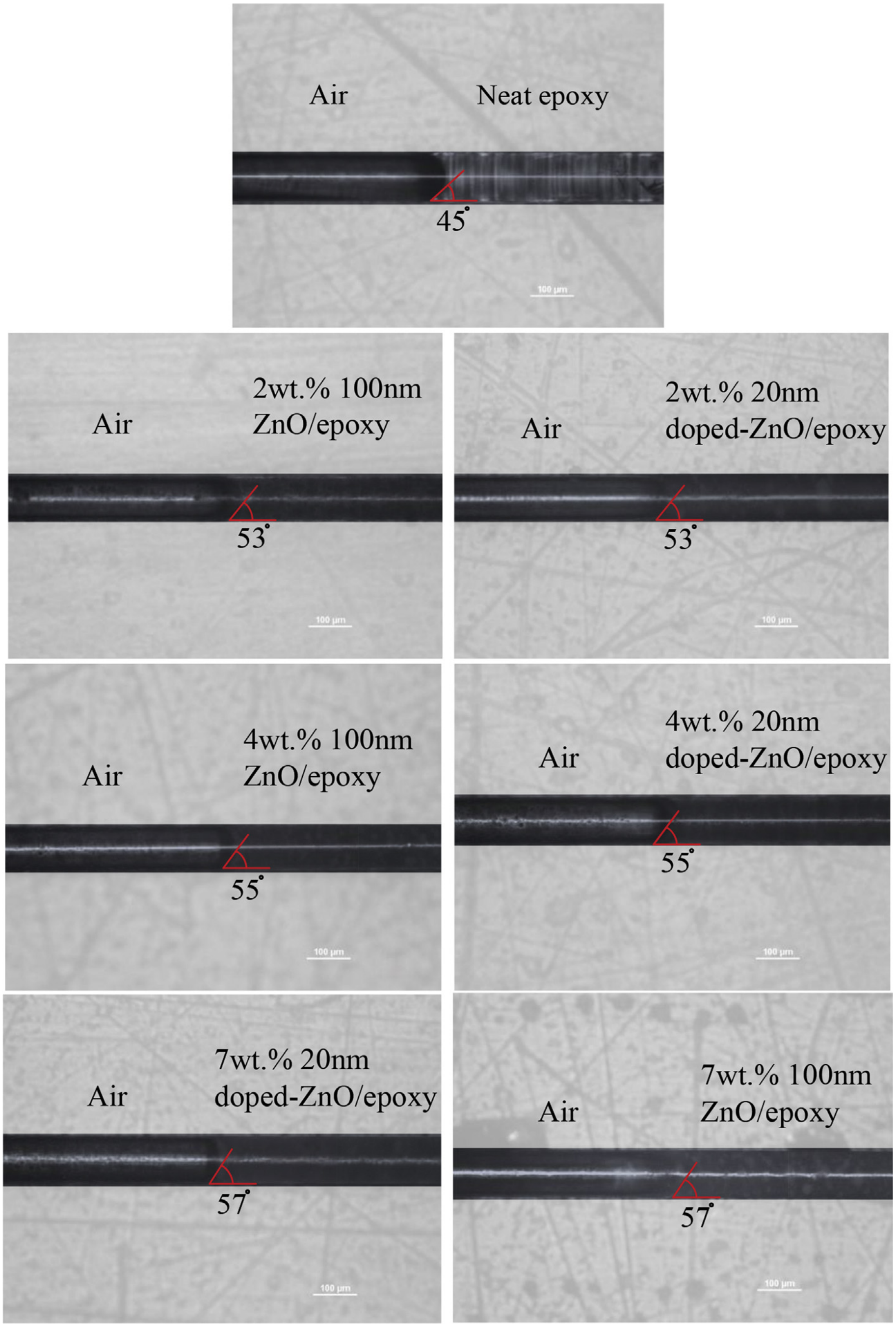

Fig. 4. Polymerization shrinkage of neat epoxy (the topmost), 2 wt.%, 4 wt.% and 7 wt.% of 100 nm ZnO/epoxy (left) and 20 nm doped-ZnO/epoxy (right) inside micron-HGF.

the 100 μm HGF, thus, at the end of fluid is in convex shape. During curing, the fluid shrinks until it is fully cured. Different degrees of curvature can be obtained at the end of nano-ZnO/epoxy attributed to different concentration of ZnO NPs implemented. It is assured that 4 wt.% 100 nm ZnO/epoxy enables to obtain a lower degree of polymerization shrinkage with a high concentration and an even dispersion of ZnO NPs inside the 100 μm HGF.

3.4. *UV absorbability of nano-ZnO/epoxy/micron-HGF epoxy composite*

The UV absorbability results of nano-ZnO/epoxy/micron-HGF epoxy composites agree with the dispersion characteristics of ZnO NPs and the rheology properties of nano-ZnO/epoxy infiltrants. 4 wt.% 100 nm ZnO/epoxy obtains the lowest required shear stress to deform its microstructure and viscosity, a high concentration and an even dispersion of ZnO NPs inside the epoxy, so 4 wt.% 100 nm ZnO/epoxy/100 μm HGF epoxy composite has the highest UVA absorbability (315–400 nm), a full UVB (280–315 nm) and UVC (100–280 nm) absorbability as shown in Fig. 6.

In Fig. 7, it shows the UV absorbability of all composite samples. 2 wt.% 100 nm ZnO/epoxy/100 μm HGF has an even dispersion of ZnO NPs but a lower concentration, however, the UV absorbability of 2 wt.% 100 nm ZnO/epoxy/100 μm HGF/epoxy composite is still higher than neat epoxy/100 μm HGF epoxy composite. 7 wt.% 100 nm ZnO/epoxy/100 μm HGF epoxy composite has UV

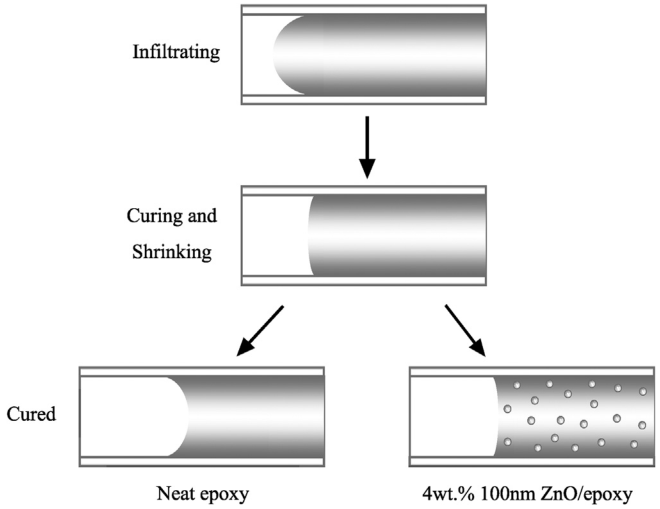

Fig. 5. Schematic diagram showing the polymerization shrinkage of neat epoxy resin and 4 wt.% 100 nm ZnO/epoxy resin during curing process.

absorbability lower than neat/epoxy/100 μm HGF epoxy composite, this happening is the consequence of existing air bubbles inside the 100 μm HGF.

All 20 nm doped-ZnO/epoxy/100 μm HGF epoxy composites have UV absorbability lower than neat/epoxy/100 μm HGF epoxy composite. This obviously shows the silane surfactant on 20 nm ZnO particle inhibits the UV absorption of ZnO NP. It could be interpreted that the silane coating blocks the passage of UV radiation into ZnO NPs for exhibiting the UV absorption, and the silane coating has the refraction property which it refracts the UV radiation into surrounding polymers and pass through the composite. This interpretation is represented by a schematic diagram in Fig. 8.

4. Conclusions

In this study, the relationship of the silane surfactant of ZnO NP and rheology properties of NF with the dispersion of NP and the polymerization shrinkage of NC are discussed to achieve a nano-ZnO/epoxy/micron-HGF epoxy composite with good UV absorbability. The effectiveness of UV absorption of silane surfactant on ZnO NP was evaluated. The following are highlighted from this study.

A. Generally, 100 nm ZnO/epoxy fluid samples have lower shear viscosity and require less shear stress to deform the fluid to flow than that of 20 nm doped-ZnO/epoxy fluid samples. The surfactant on 20 nm ZnO particle is regarded as an inhibiter to the fluid flow.

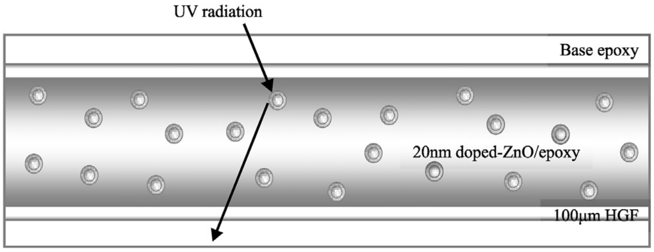

Fig. 8. Schematic diagram showing the refraction of silane surfactant on 20 nm ZnO particles in epoxy inside 100 μm HGF of the epoxy composite.

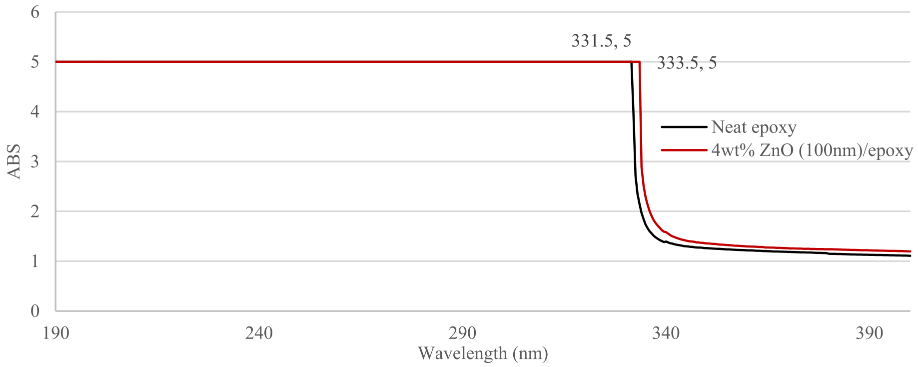

Fig. 6. UV absorbability of neat epoxy and 4 wt.% 100 nm ZnO/epoxy/100 μm HGFs epoxy composite.

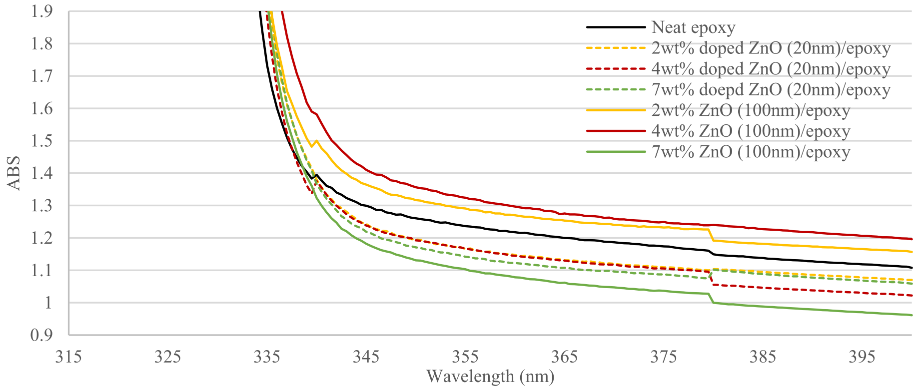

Fig. 7. UV absorbability of all composite samples.

B. Among all the nano-ZnO/epoxy fluid samples, 4 wt.% 100 nm ZnO/epoxy has the lowest viscosity at 5.5 Pa.s and requires the lowest shear stress to deform its microstructure along the shear rate. Under the observation from optical microscope, 4 wt.% 100 nm ZnO NPs obtained an even dispersion in epoxy inside 100 μm HGF. The better the dispersion of ZnO NPs, the lower the viscosity of nano-ZnO/epoxy fluid.
C. Rheological properties are proven to be correlated to the UV absorbability of nano-ZnO/epoxy/micron-HGF epoxy composite. The lower the viscosity and shear stress required to deform the microstructure of nano-ZnO/epoxy fluid, the higher the UV absorbability of nano-ZnO/epoxy/micron-HGF epoxy composite.
D. During vacuum infiltration process, the applied shear stress interferes the intermolecular forces between NP–NP, NP–EP and EP–EP. During curing process, the degree of polymerization shrinkage of resin decides the closeness of NP–NP inside EP. These show they are the factors to influence the dispersion of ZnO NPs and the UV absorbability of nano-ZnO/epoxy/micron-HGF epoxy composite.
E. The use of silane surfactant on ZnO NP and the use of sonication during resin preparation, are accounted for the dispersion of ZnO NPs inside epoxy which is decisive for obtaining a nano-ZnO/epoxy/micron-HGF epoxy composite with good UV absorbability. However, it was found that silane surfactant on ZnO NP was ineffective for UV absorption.
F. To achieve a nano-ZnO/epoxy/micron-HGF epoxy composite with good UV absorbability, optimum concentration and good dispersion of ZnO NPs inside epoxy resin with low polymerization shrinkage are required. And silane surfactant on ZnO NP was not considered to be implemented as it was found to be ineffective for UV absorption.
G. From the experimental results, 4 wt.% 100 nm ZnO/epoxy is able to obtain a low viscosity and shear stress required to deform its microstructure, a good concentration and an even dispersion of ZnO NPs, a low polymerization shrinkage of resin inside the 100 μm HGF and a good UV absorbability of 4 wt.% 100 nm ZnO/epoxy/HGF epoxy composite is then able to be achieved.
H. The mechanical properties of nano-ZnO/epoxy/micron-HGF epoxy composite considering the bonding strength of ZnO NP–EP inside micron-HGF in the relationship with their UV absorbability will be further studied.

Acknowledgement

This project is supported by the Hong Kong Polytechnic University Grant (G-YK84).

References

[1] Awaja F, Nguyen MT, Zhang S, Arhatari B. The investigation of inner structural damage of UV and heat degraded polymer composites using X-ray micro CT. Compos Part A Appl Sci Manuf 2011;42(2):408–18.
[2] Ayrilmis N. Combined effects of boron and compatibilizer on dimensional stability and mechanical properties of wood/HDPE composites. Compos Part B Eng 2013;44:745–9.
[3] Diez-Pascual AM, Xu CP, Luque R. Development and characterization of novel poly(ether ether ketone)/ZnO bionanocomposites. J Mater Chem B 2014;2:3065–78.
[4] Esthappan SK, Nair AB, Joseph R. Effect of crystallite size of zinc oxide on the mechanical, thermal and flow properties of polypropylene/zinc oxide nanocomposites. Compos Part B Eng 2015;69:145–53.
[5] Etches J, Bond I, Mellor P. Manufacture and applications of magnetically active fibre reinforced composites. Smart Mater Struct 2006;15:288–94.
[6] Gallagher RP, Lee T. Adverse effects of ultraviolet radiation: a brief review. Prog Biophys Mol Biol 2006;92(1):119–31.
[7] Hata E, Tomita Y. Order-of-magnitude polymerization-shrinkage suppression of volume gratings recorded in nanoparticle-polymer composites. Opt Lett 2010;35(3):396–8.
[8] Kumar AP, Depan D, Tomer NS, Singh RP. Nanoscale particles for polymer degradation and stabilization – trends and future perspectives. Prog Polym Sci 2009;34:479–515.
[9] Li YQ, Fu SY, Mai YM. Preparation and characterization of transparent ZnO/epoxy nanocomposites with high-UV shielding efficiency. Polymer 2006;47:2127–32.
[10] Li YQ, Kang Y, Xiao HM, Mei SG, Zhang GL, Fu SY. Preparation and characterization of transparent Al doped ZnO/epoxy composite as thermal-insulating coating. Compos Part B Eng 2011;42:2176–80.
[11] Liufu SC, Xiao HN, Li YP. Thermal analysis and degradation mechanism of polyacrylate/ZnO nanocomposites. Polym Degrad Stab 2005;87:103–10.
[12] Lowry M, Hubble D, Wressell A, Vratsanos M, Pepe F, Hegedus C. Assessment of UV-permeability in nano-ZnO filled coatings via high throughput experimentation. J Coat Technol Res 2008;5(2):233–9.
[13] Mahrholz T, Stangle J, Sinapius M. Quantitation of the reinforcement effect of silica nanoparticles in epoxy resins used in liquid composite moulding processes. Compos Part A Appl Sci Manuf 2009;40:235–43.
[14] Mallakpour S, Madani M. The effect of the coupling agents KH550 and KH570 on the nanostructure and interfacial interaction of zinc oxide/chiral poly(amide-imide) nanocomposites containing L-leucine amino acide moieties. J Mater Sci 2014;49:5112–8.
[15] Mallakpour S, Madani M. Use of silane coupling agent for surface modification of zinc oxide as inorganic filler and preparation of poly(amide-imide)/zinc oxide nanocomposite containing phenylalanine moieties. Bull Mater Sci 2012;35(3):333–9.
[16] Moezzi A, McDonagh AM, Cortie MB. Review: zinc oxide particles: synthesis, properties and applications. Chem Eng J 2012;185–186:1–22.
[17] Nasu A, Otsubo Y. Rheology and UV-protecting properties of complex suspensions of titanium dioxides and zinc oxides. J Colloid Interface Sci 2007;310:617–23.
[18] Nasu A, Otsubo Y. Rheology and UV protection properties of suspensions of fine titanium dioxides in a silicone oil. J Colloid Interface Sci 2006;296:558–64.
[19] Nicolay A, Lanzutti A, Poelman M, Ruelle B, Fedrizzi L, Dubois Ph, et al. Elaboration and characterization of a multifunctional silane/ZnO hybrid nanocomposite coating. Appl Surf Sci 2015;327:379–88.
[20] Onbattuvelli VP, Enneti RK, Park SJ, Atre SV. The effects of nanoparticle addition on SiC and AlN powder-polymer mixtures: packing and flow behavior. Int J Refract Metals Hard Mater 2013;36:183–90.
[21] Pang JWC, Bond IP. A hollow fibre reinforced polymer composite encompassing self-healing and enhanced damage visibility. Compos Sci Technol 2005;65:1791–9.
[22] Pang JWC, Bond IP. 'Bleeding composites' – damage detection and self-repair using a biomimetic approach. Compos Part A Appl Sci Manuf 2005;36:183–8.
[23] Pavlicevic J, Spirkova M, Bera O, Jovicic M, Pilic B, Balos S, et al. The influence of ZnO nanoparticles on thermal and mechanical behavior of polycarbonate-based polyurethane composites. Compos Part B Eng 2014;60:673–9.
[24] Rabek JF. Photostabilization of polymers. Principles and applications. Elsevier Applied Science; 1990. p. 1–30. Chapter 1.
[25] Sadeghipour H, Ebadi-Dehaghani H, Ashouri D, Mousavian S, Hashemi-Fesharaki M, Gahrouei MS. Effects of modified and non-modified clay on the rheological behavior of high density polyethylene. Compos Part B Eng 2013;52:164–71.
[26] Siddiqui NA, Khan SU, Ma PC, Li CY, Kim JK. Manufacturing and characterization of carbon fibre/epoxy composite prepregs containing carbon nanotubes. Compos Part A Appl Sci Manuf 2011;42:1412–20.
[27] Suganthi KS, Rajan KS. A formulation strategy for preparation of ZnO-Propylene glycol-water nanofluids with improved transport properties. Int J Heat Mass Transf 2014;71:653–63.
[28] Wacharawichanant S, Thongyai S, Phutthaphan A, Eiamsam-ang C. Effect of particle sizes of zinc oxide on mechanical, thermal and morphological properties of polyoxymethylene/zinc oxide nanocomposites. Polym Test 2008;27:971–6.
[29] Williams G, Trask R, Bond I. A self-healing carbon fibre reinforced polymer for aerospace applications. Compos Part A Appl Sci Manuf 2007;38(6):1525–32.
[30] Wilson KS, Zhang K, Antonucci JM. Systematic variation of interfacial phase reactivity in dental nanocomposites. Biomaterials 2005;26:5095–103.
[31] Wong TT, Lau KT, Tam WY, Leng JS, Wang WX, Li WB, et al. Degradation of nano-ZnO particles filled styrene-based and epoxy-based SMPs under UVA exposure. Compos Struct 2015;132:1056–64.
[32] Wong TT, Tam WY, Etches JA, Wang WX, Leng JS, Lau KT. Feasibility of using ZnO/epoxy filled hollowed glass fibres (HGFs) for UV resistant polymer composites. Mater Lett 2014;128:220–3.
[33] Wu YL, Tok ALY, Boey FYC, Zeng XT, Zhang XH. Surface modification of ZnO nanocrystals. Appl Surf Sci 2007;253:5473–9.
[34] Yang HG, Li CZ, Gu HC, Fang TN. Rheological behavior of titanium dioxide suspensions. J Colloid Interface Sci 2001;236:96–103.
[35] Zabihi O, Mostafavi SM, Ravari F, Khodabandeh A, Hooshafza A, Zare K, et al. The effect of zinc oxide nanoparticles on thermo-physical properties of diglycidyl ether of bisphenol A/2,2′-Diamino-1,1′- binaphthalene nanocomposites. Thermochim Acta 2011;521:49–58.

References

Abdolmaleki A and Bazyar Z. Preparation and characterization of Poly(benzimidazole-amide)/ZnO nanocomposites using silane coupling agent. Polymer-Plastics Technology and Engineering. 2013;52:1542-1549.

Abdolmaleki A, Mallakpour S and Borandeh S. Preparation, characterization and surface morphology of novel optically active poly(ester-amide)/functionalized ZnO bionanocomposites via ultrasonication assisted process. Applied Surface Science. 2011;257:6725-6733.

Abdolmaleki A, Mallakpour S and Borandeh S. The use of novel biodegradable, optically active and nanostructured poly(amide-ester-imide) as a polymer matrix for preparation of modified ZnO based bionanocomposites. Materials Research Bulletin. 2012;47:1123-1129.

Agubra VA and Mahesh HV. Environmental degradation of E-glass/nanocomposite under the combined effect of UV radiation, moisture, and rain. Journal of Polymer Science Part B: Polymer Physics. 2014;52:1024-1029.

Alonso E, Sherman AM, Wallington TJ, Everson MP, Field FR, Roth R and Kirchain RE. Evaluating rare Earth element availability: A case with revolutionary demand from clean technologies. Environmental Science & Technology. 2012;46:3406-3414.

Andrady AL, Hamid SH, Hu X. and Torikai A. Effects of increased solar ultraviolet radiation on materials. Journal of Photochemistry and Photobiology B: Biology. 1998;46(1):96-103.

Awaja F, Moon JB, Zhang S, Gilbert M, Kim CG and Pigram PJ. Surface molecular degradation of 3D glass polymer composite under low earth orbit simulated space environment. Polymer Degradation and Stability. 2010;95:987-996.

Awaja F and Pigram PJ. Surface Molecular Characterisation of different epoxy resin composites subjected to UV accelerated degradation using XPS and ToF-SIMS. Polymer Degradation and Stability. 2009;94:651-658.

Australian Institute of Health and Welfare (AIHW). Cancer in Australia an overview 2014. Cancer series No 90. Cat. No. CAN 88. Canberra. 2014.

Awaja F, Nguyen MT, Zhang S and Arhatari B. The investigation of inner structural damage of UV and heat degraded polymer composites using X-ray micro CT. Composites Part A: Applied Science and Manufacturing. 2011;42(2):408-418.

Bannister DJ, Andrews MC, Cervenka AJ and Young RJ. Analysis of the single-fibre pull-out test by means of Raman spectroscopy: Part II. Micromechanics of deformation for an aramid/epoxy system. Composites Science and Technology. 1995;53:411-421.

Belec L, Nguyen TH, Nguyen DL and Chailan JF. Comparative effects of humid tropical weathering and artificial ageing on a model composite properties from nano- to macro-scale. Composites: Part A. 2015;68:235-241.

Betteridge D, Joyner DJ, Greening F and Shoko NR. The analysis of polymer degradation products by UV-photoelectron spectroscopy. Physica Scripta. 1977;16:339-345.

Bressy C, Ngo VG, Ziarelli F and Margaillan A. New insights into the adsorption of 3-(Trimethoxysilyl)-propylmethacrylate on hydroxylated ZnO nanopowders. Langmuir. 2012;28:3290-3297.

Brodowsky HM, Jenschke W and Mader E. Characterization of interphase properties: Microfatigue of single fibre model composites. Composites: Part A. 2010;41:1579-1586.

Caldwell MM, Bjorn LO, Bornman JF, Flint SD, Kulandaivelu F, Teramura AH and Tevini M. Effects of increased solar ultraviolet radiation on terrestrial ecosystems. Journal of Photochemistry and Photobiology B: Biology. 1998;46:40-52.

Canestraro CD, Rodrigues PC, Marchiori CFN, Schneider CB, Akcelrud L, Koehler M and Roman LS. The role of the double peaked absorption spectrum in the efficiency of solar cells based on donor-acceptor-donor copolymers. Solar Energy Materials & Solar Cells. 2011;95:2287-2294.

Chakrabarti S, Chaudhuri B, Bhattacharjee S, Das P and Dutta BK. Degradation mechanism and kinetic model for photocatalytic oxidation of PVC-ZnO composite film in presence of a sensitizing dye and UV radiation. Journal of Hazardous Materials. 2008;154:230-236.

Chang LN and Chow WS. Accelerated weathering on glass fibre/epoxy/organo-montmorillonite nanocomposites. Journal of Composites Materials. 2010;44(12):1421-1434.

Chawla KK. Composite materials: Science and engineering. Springer, New York. 2012. Third edition. ISBN 978-0-387-74364-6.

Chen X, Yu N, Zhang L, Liu Z, Wang Z and Chen Z. Synthesis of polypyrrole nanoparticles for constructing full-polymer UV/NIR-shielding film. RSC Advances. 2015;5:96888-96895.

Chen YL, Liu B, He XQ, Huang Y and Hwang KC. Failure analysis and the optimal toughness design of carbon nanotube-reinforced composites. Composites Science and Technology. 2010;70:1360-1367.

Chou KF, Han CC and Lee S. Water transport in crosslinked 2-hydroxyethyl methacrylate. Polymer Engineering and Science. 2000;40(4):1004-1014.

Chung DDL. Composite materials: Science and applications. Springer, New York. 2010. Second edition. ISBN 978-1-84882-830-8.

Cockell CS and Knowland J. Ultraviolet radiation screening compounds. Biological Reviews. 1999;74:311-345.

Costenaro D, Carniato F, Gatti G, Marchese L and Bisio C. Preparation of luminescent ZnO nanoparticles modified with aminopropyltriethoxy silane for optoelectronic applications. New Journal of Chemistry. 2013;37:2103-2109.

Cristea MV, Riedl B and Blanchet P. Enhancing the performance of exterior waterborne coatings for wood by inorganic nanosized UV absorbers. Progress in Organic Coatings. 2010;69:432-441.

Deka BK, Mandal M and Maji TK. Effect of nanoparticles on flammability, UV resistance, biodegradability, and chemical resistance of wood polymer nanocomposite. Industrial & Engineering Chemistry Research. 2012;51:11881-11891.

Devi RR, Gogoi K, Konwar BK and Maji TK. Synergistic effect of nanoTiO_2 and nanoclay on mechanical, flame retardancy, UV stability, and antibacterial properties of wood polymer composites. Polymer Bulletin. 2013;70:1397-1413.

Dholakiya B. Polyester: Unsaturated polyester resin for specialty applications. InTech, Chapters. 2012. ISBN 978-953-51-0770-5.

Diallo AK, Dkhil GSB, Didane Y, Margeat O, Ackermann J and Videlot-Ackermann C. Impact of surfactants covering ZnO nanoparticles on solution-processed field-effect transistors: From dispersion state to solid state. Colloids and Surfaces A: Physicochemical and Engineering Aspects. 2016;500:214-221.

Diffey BL. Solar ultraviolet radiation effects on biological systems. Physics in Medicine and Biology. 1991;36(3):299-328.

Diffey BL. Sources and measurement of ultraviolet radiation. Methods. 2002;28(1):4-13.

Dutta S, Chattopadhyay S, Sarkar A, Chakrabarti M, Sanyal D and Jana D. Role of defects in tailoring structural, electrical and optical properties of ZnO. Progress in Materials Science. 2009;54:89-136.

El-Mossalamy EH and Al-Thabaiti SA. Synthesis and thermal studies of poly(N-acryloyl,N'-cyanoacetohydrazide) complexes with Co(II), Fe(III), and UO_2(II) ions. Journal of Applied Polymer Science. 2003;90:3354-3358.

El-Toni AM, Yin S, Sato T, Ghannam T, Al-Hoshan M and Al-Salhi M. Investigation of photocatalytic activity and UV-shielding properties for silica coated titania nanoparticles by solvothermal coating. Journal of Alloys and Compounds. 2010;508:L1-L4.

Emeline AV, Ryabchuk VK and Serpone N. Photoreactions occurring on metal-oxide surfaces are not all photocatalytic: Description of criteria and conditions for processes to be photocatalytic. Catalysis Today. 2007;122:91-100.

Farhad A and Yuan LB. Mechanics of bond and interface shear transfer in optical fibre sensors. Journal of Engineering Mechanics. 1998;124:385-394.

Fleisch TH. Reduction of copper oxides by UV radiation and atomic hydrogen studied by XPS. Applications of Surface Science. 1982;10:51-62.

Francia CD, Ward TC and Claus RO. The single-fibre pull-out test. 1: Review and interpretation. Composites: Part A. 1996;27A:597-612.

Francia CD, Ward TC and Claus RO. The single-fibre pull-out test. 2: Quantitative evaluation of an uncatalysed TGDDM/DDS epoxy cure study. Composites: Part A. 1996;27A:613-624.

French RH, Mullejans H and Jones DJ. Optical properties of aluminum oxide: Determined from vacuum ultraviolet and electron energy-loss spectroscopies. Journal of the American Ceramic Society. 1998;81(10):2549-2557.

Fu SY, Yue CY, Hu X and Mai YM. Analyses of the micromechanics of stress transfer in single- and multi-fiber pull-out tests. Composites Science and Technology. 2000;60:569-579.

Gallagher RP and Lee TK. Adverse effects of ultraviolet radiation: A brief review Review Article. Progress in Biophysics and Molecular Biology. 2006;92(1):119-131.

Gao Y, Xie MY, Liu LQ, Li JZ, Kuang J, Ma WJ, Zhou WY, Xie SS and Zhang Z. Effect of supra-molecular microstructures on the adhesion of SWCNT fibre/iPP interface. Polymer. 2013; 54:456-463.

Garcia-Espinel JD, Castro-Fresno D, Gayo PP and Ballester-Munoz F. Effects of sea water environment on glass fiber reinforced plastic materials used for marine civil engineering constructions. Materials and Design. 2015;66:46-50.

Ghasemi-Kahrizsangi A, Neshati J, Shariatpanahi H and Akbarinezhad E. Improving the UV degradation resistance of epoxy coatings using modified carbon black nanoparticles. Progress in Organic Coatings. 2015;85:199-207.

Gibson AG. The cost effective use of fibre reinforced composites offshore. HSE priced publications. 2003. Pages: 3-23.

Grasset F, Saito N, Li D, Park D, Sakaguchi I, Ohashi N, Haneda H, Roisnel T, Mornet S and Duguet E. Surface modification of zinc oxide nanoparticles by aminopropyltriethoxysilane. Journal of Alloys and Compounds. 2003;360:298-311.

Guillot L, Monney L, Dubois C and Chambaudet A. Testing of organic matrix durability in photochemical ageing using ablation measurements. Polymer Degradation and Stability. 2001;72:209-215.

Hang TTX, Dung NT, Truc TA, Duong NT, Truoc BV, Vu PG, Hoang T, Thanh DTM and Olivier MG. Effect of silane modified nano ZnO on UV degradation of polyurethane coatings. Progress in Organic Coatings. 2015;79:68-74.

Hashmi SSA. Enhanced zinc ion transport in gel polymer electrolyte: effect of nano-sized ZnO dispersion. Journal of Solid State Electrochemistry. 2012;16:3105-3114.

Hata E and Tomita Y. Order-of-magnitude polymerization-shrinkage suppression of volume gratings recorded in nanoparticle-polymer composites. Optics Letters. 2010;35(3):396-398.

Heiting G. Ultraviolet radiation and your eyes. 2016. Available from: http://www.allaboutvision.com/sunglasses/spf.htm.

Heppenstall-Butler M, Bannister DJ and Young RJ. A study of transcrystalline polypropylene/ single-aramid-fibre pull-out behaviour using Raman spectroscopy. Composites: Part A. 1996;27A:833-838.

Hodgkin JH, Simon GP and Varley RJ. Thermoplastic toughening of epoxy resins: a critical review. Polymers for Advanced Technologies. 1998;9:3-10.

Hollaway LC. A review of the present and future utilization of FRP composites in the civil infrastructure with reference to their important in-service properties. Construction and Building Materials. 2010;24:2419-2445.

Hollaway LC. Advanced fibre-reinforced polymer (FRP) composites for structural applications. Editor: Jiping Bai. Woodhead Publishing Limited. 2013. Pages: 582-661.

Holzmann D, Schofberger W, Holzinger D, Schmidt T and Knor G. Functional nanoscale additives for ultra-durable powder-coating polymers. Monatshefte fur chemie. 2011;142:855-860.

Hsiang HI, Chang YL, Chen CY and Yen FS. Silane functional effects on the rheology abrasion resistance of transparent SiO_2/UV-curable resin nano-composites. Materials Chemistry and Physics. 2010;120:476-479.

Hsueh CH. Interfacial debonding and fiber pull-out stresses of fiber-reinforced composites. Materials Science and Engineering: A. 1990;123:1–11.

Hsueh CH. Interfacial debonding and fiber pull-out stresses of fiber-reinforced composites II: non-constant interfacial bond strength. Materials Science and Engineering: A. 1990;125:67–73.

Hu L, Wan Y, He F, Luo HL, Liang H, Li X and Wang J. Effect of coupling treatment on mechanical properties of bacterial cellulose nanofibre-reinforced UPR ecocomposites. Materials Letters. 2009;63:1952-1954.

Huang JJ, Ye YB, Lei ZQ, Ye XJ, Rong MZ and Zhang MQ. Highly luminescent and transparent ZnO quantum dots-epoxy composite used for white light emitting diodes. Physical Chemistry Chemical Physics. 2014;16:5480-5484.

Hulatt J, Hollaway L and Thorne A. Preliminary investigations on the environmental effects on new heavyweight fabrics for use in civil engineering. Composites Part B: Engineering. 2002;33:407-414.

Jacobs JF, Koper GJM and Ursem WNJ. UV protective coatings: A botanical approach. Progress in Organic Coatings. 2007;58:166-171.

Jeeju PP, Sajimol AM, Sreevalsa VG, Varma SJ and Jayalekshmi S. Size-dependent optical properties of transparent, spin-coated polystyrene/ZnO nanocomposite films. Polymer International. 2011;60:1263-1268.

Jiang X and Kong X. Micro-mechanical characteristics of fibre/matrix interfaces in composite materials. Composite Science and Technology. 1999;59(5):635-642.

Jones N. A scarcity of rare metals is hindering green technologies. 2013. Available from:
http://e360.yale.edu/feature/a_scarcity_of_rare_metals_is_hindering_green_technologies/2711/.

Joshy MK, Mathew L and Joseph R. Influence of fiber surface modification on the mechanical performance of Isora-Polyester composites. International Journal of Polymeric Materials and Polymeric Biomaterials. 2009;58:2-20.

Jouni M, Boudenne A, Boiteux G, Massardiar V, Garnier B and Serghei A. Electrical and thermal properties of polyethylene/silver nanoparticle composites. Polymer Composites. 2013;34(5):778-786.

Kaczmarek H, Metzler M and Scigalski F. Photochemical stability of poly(acrylic acid)/silver nanocomposite. Materials Letters. 2014;135:110-114.

Kaczmarek H, Sionkowska A, Kaminska A, Kowalonek J, Swiatek M and Szalla A. The influence of transition metal salts on photo-oxidative degradation of poly(ethylene oxide). Polymer Degradation and Stability. 2001;73:437-441.

Kanimozhi K, Prahunathan P, Selvaraj V and Alagar M. Vinyl silane-functionalized rice husk ash-reinforced unsaturated polyester nanocomposites. RSC Advances. 2014;4:18157-18163.

Karentz D. Ozone Layer. Reference Module in Earth Systems and Environmental Sciences, from Encyclopedia of Ecology. 2008:2615-2621.

Kendall D. Building the future with FRP composites Reinforced Plastics. 2007;51(5):26-33.

Kim HS, Hong SI and Kim SJ. On the rule of mixtures for predicting the mechanical properties of composites with homogeneously distributed soft and hard particles. Journal of Materials Processing Technology. 2001;112(1):109-113.

Kim HY and Lee SY. A steel-reinforced hybrid GFRP deck panel for temporary bridges. Construction and Building Materials. 2012;34:192-200.

Kim D, Jeon K, Lee Y, Seo J, Seo K, Han H and Khan S. Preparation and characterization of UV-cured polyurethane acrylate/ZnO nanocomposite films based on surface modified ZnO. 2012;74:435-442.

Kim JK, Baillie C and Mai YW. Interfacial debonding and fibre pull-out stresses Part I Critical comparison of existing theories with experiments. Journal of Materials Science. 1991;27:3143-3154.

Koyanagi J, Nakatani H and Ogihara S. Comparison of glass-epoxy interface strengths examined by cruciform specimen and single-fiber pull-out tests under combined stress state. Composites: Part A. 2012;43:1819-1827.

Kulyk B, Kapustianyk V, Tsybulskyy V, Krupka O and Sahraoui B. Optical properties of ZnO/PMMA nanocomposite films. Journal of Alloys and Compounds. 2010;502:24-27.

Kumar AP, Depan D, Tomer NS and Singh RP. Nanoscale particles for polymer degradation and stabilization—Trends and future perspectives. Progress in Polymer Science. 2009;34:479–515.

Kyrikou I, Briassoulis D, Hiskakis M and Babou E. Analysis of photo-chemical degradation behaviour of polyethylene mulching film with pro-oxidants. Polymer Degradation and Stability. 2011;96:2237-2252.

Lai WL, Kou SC, Poon CS, Tsang WF, Ng SP and Hung YY. Characterization of flaws embedded in externally bonded CFRP on concrete beams by infrared thermography and shearography. Journal of Nondestructive Evaluation. 2009;28:27-35.

Laidler KJ. The development of the Arrhenius equation. Journal of Chemical Education. 1984;61(6):494-498.

Lampman S. Characterization and failure analysis of plastics. ASM International. 2003. ISBN 0871707869.

Lau KT, Yuan LB, Zhou LM, Wu JS and Woo CH. Strain monitoring in FRP laminates and concrete beams using FBG sensors. Composite Structures. 2001;51:9-20.

Lee BS, Motoyama T, Ichikawa K, Tabata Y and Lee DC. The analysis of surface degradation on UV-treated epoxy/glass fiber by Corona-charging properties. Polymer Degradation and Stability. 1999;66:271-278.

Levchik SV and Weil ED. Thermal decomposition, combustion and flame-retardancy of epoxy resins-a review of the recent literature. Polymer International. 2004;53:1901-1929.

Li H, Chen Y, Ruan C, Gao W and Xie Y. Preparation of organic-inorganic multifunctional nanocomposite coating via sol-gel routes. Journal of Nanoparticle Research. 2001;3:157-160.

Li P, Jiu T, Tang G, Wang G, Li J, Li X and Fang J. Solvents induced ZnO nanoparticles aggregation associated with their interfacial effect on organic solar cells. Applied Materials & Interfaces. 2014;6:18172-18179.

Li R, Pei J and Sun C. Effect of nano-ZnO with modified surface on properties of bitumen. Construction and Building Materials. 2015;98:656-661.

Li YN, Xu WM and Zhang GQ. Effect of coupling agent on nano-ZnO modification and antibacterial activity of ZnO/HDPE nanocomposite films. IOP Conference Series: Materials Science and Engineering. 2015;87:012054-012061.

Li YQ, Fu SY and Mai YW. Preparation and characterization of transparent ZnO/epoxy nanocomposites with high-UV shielding efficiency. Polymer. 2006;47:2127-2132.

Liu GL, Zhu DW, Liao SJ, Ren LY, Cui JZ and Zhou WB. Solid-phase photocatalytic degradation of polyethylene-goethite composite film under UV-light irradiation. Journal of Hazardous Materials. 2009;172:1424-1429.

Liu WG, Zhang XC, Li HY and Liu Z. Effect of surface modification with 3-aminopropyltriethyloxy silane on mechanical and crystallization performances of ZnO/poly(butylenesuccinate) composites. Composites Part B: Engineering. 2012;43:2209-2216.

Liu YF and Kagawa Y. The energy release rate for an interfacial debond crack in a fiber pull-out model. Composites Science and Technology. 2000;60:167-171.

Lowry MS, Hubble DR, Wressell AL, Vratsanos MS, Pepe FR and Hegedus CR. Assessment of UV-permeability in nano-ZnO filled coatings via high throughput experiment. Journal of Coatings Technology and Research. 2008;5(2):233-239.

Luethi B, Reber R, Mayer J, Wintermantel E, Janczak-Rusch J and Rohr L. An energy-based analytical push-out model applied to characterize the interfacial properties of knitted glass fibre reinforced PET. Composites: Part A. 1998;29A:1553-1562.

Ma CCM, Chen YJ and Kuan HC. Polystyrene nanocomposite materials: Preparation, morphology, and mechanical, electrical, and thermal properties. Journal of Applied Polymer Science. 2005;98:2266-2273.

Mallakpour S and Ahmadizadegan H. Manufacture of zinc oxide/chiral poly(amide-imide)-functionalized amino acid and thiazole bionanocomposites: Using ionic liquid and ultrasonic irradiation.. Journal of Thermoplastic Composite Materials. 2015;28(5):672-685.

Mallakpour S and Khani M. Effect of Surface Functionalized Nano-ZnO Structure on Morphology and Properties of Poly(amide-imide) Nanocomposites Containing N-trimellitylimido-L-leucine and 5-(2-benzimidazole)-1,3-phenylenediamine. Synthesis and Reactivity in Inorganic, Metal-Organic, and Nano-Metal Chemistry. 2013;43:1289-1295.

Mallakpour S and Madani M. A facile route for the preparation of novel optically active poly(amide-imide)/functionalized zinc oxide nanocomposites containing pyromellitoyl-bis-L-phenylalanine moieties. Polymer Bulletin. 2012;68:1201-1214.

Mallakpour S and Madani M. A review of current coupling agents for modification of metal oxide nanoparticles. Progress in Organic Coatings. 2015;86:194-207.

Mallakpour S and Madani M. The effect of the coupling agents KH550 and KH570 on the nanostructure and interfacial interaction of zinc oxide/chiral poly(amide-imide) nanocomposites containing L-leucine amino acid moieties. Journal of Materials Science. 2014;49:5112-5118.

Mallakpour S and Madani M. Use of silane coupling agent for surface modification of zinc oxide as inorganic filler and preparation of poly(amide-imide)/zinc oxide nanocomposite containing phenylalanine moieties. Bulletin of Materials Science. 2012;35(3):333-339.

Martyniuk K, Sorensen BF, Modregger P and Lauridsen EM. 3D in situ observations of glass fibre/matrix interfacial debonding. Composites: Part A. 2013;55:63-73.

Musat V, Tabacaru A, Vasile BS and Surdu VA. Size-dependent photoluminescence of zinc oxide quantum dots through organosilane functionalization. RSC Advances. 2014;4:63128-63136.

Meier MAR, Metzger JO and Schubert US. Plant oil renewable resources as green alternatives in polymer science. Chemical Society Reviews. 2007;36:1788-1802.

Meier MAR. Renewable resources for polymer chemistry: A sustainable alternative? Macromolecular Rapid Communications. 2011;32:1297-1298.

Mirmiran A. A new concrete-filled hollow FRP composite column. Composites Part B: Engineering. 1996;263-268.

Moghaddam E, Youzbashi AA, Kazemzadeh A and Eshraghi MJ. Photoluminescence investigation of ZnO quantum dots surface modified with silane coupling agent as a capping agent. Journal of Luminescence. 2015;168:158-162.

Nairn JA. On the use of shear-lag methods for analysis of stress transfer in unidirectional composites. Mechanics of Materials. 1997;26:63-80.

Nguyen T, Dinh C and Do T. Tailoring the assembly, interfaces, and porosity of nanostructures toward enhanced catalytic activity. Chemical Communications. 2015;51:624.

Nguyen T, Pellegrin B, Bernard C, Gu X, Gorham JM, Stutzman P, Stanley D, Shapiro A, Byrd E, Hettenhouser R and Chin J. Fate of nanoparticles during life cycle of polymer nanocomposites. Nanosafe 2010: International Conference on Safe Production and Use of Nanomaterials. Journal of Physics: Conference Series. 2011;304:012060.

Nicolais L, Meo M and Milella Eva. Composite materials: A vision for the future. Springer, New York. 2011. ISBN 978-0-85729-165-3.

Nouneh K, Oyama M, Diaz R, Abd-Lefdil M, Kityk IV and Bousmina M. An approach to surface functionalization of indium tin oxide for regular growth of silver nano-particles and their optical features. Journal of Alloys and Compounds. 2011;509:2631-2638.

Olmos D, Prolongo SG and Gonzalez-Benito J. Thermo-mechanical properties of polysulfone based nanocomposites with well dispersed silica nanoparticles. Composites Part B: Engineering. 2014;61:307-314.

Oral AY, Mensur E, Aslan MH and Basaran E. The preparation of copper(II) oxide thin films and the study of their microstructures and optical properties. Materials Chemistry and Physics. 2004;83:140-144.

Parveen S, Rana S and Fangueiro R. A review on nanomaterial dispersion, microstructure and mechanical properties of carbon nanotube and nanofiber reinforced cementitious composites. Journal of Nanomaterials. 2013;2013:1-19.

Patterson A, Ferreira AP, Banks E, Skeene K, Clarke G, Nicholson S and Rawlinson-Malone C. Modelling drug degradation in a spray dried polymer dispersion using a modified Arrhenius equation. International Journal of Pharmaceutics. 2015;478:348-360.

Paul ND. and Gwynn-Jones D. Ecological roles of solar UV radiation: towards an integrated approach. TRENDS in Ecology and Evolution. 2003;18(1):48-55.

Pepper T. ASM Handbook/ extraction: Polyester resins. FB MVU, Werkstofftechnologien/ Kunststofftechnik. 2003.

Phua DI, Herman K, Balaceanu A, Zakrevski J and Pich A. Reversible size modulation of aqueous microgels via orthogonal or combined application of thermo- and phototriggers. Langmuir. 2016;32:3867-3879.

Pietrzak M and Szalinska H. Reducing the shrinkage and setting dose in polyester resins by addition of metal oxides. Radiation Physics and Chemistry. 1984; 23(4):409-411.

Piggott MR. Why interface testing by single-fibre methods can be misleading. Composites Science and Technology. 1997;57:965-974.

Piggott MR, Sanadi A, Chua PS and Andison D. In Proceeding. 1st International Conference on the Composite Interface (ICCI1). Editors: Ishida H and Koenig JL. Elsevier, London. 1986. Pages:109-121.

Polyakov LM. Effect of UV radiation and vacuum on the strength and failure of polymer films. Mekhanika Polimerov. 1966;2(3):359-364.

Rhodes R, Horie M, Chen H, Wang Zm Turner ML and Saunders BR. Aggregation of zinc oxide nanoparticles: From non-aqueous dispersions to composites used as photoactive layers in hybrid solar cells. Journal of Colloid and Interface Science. 2010;344:261-271.

Rivera T, Olvera L, Martinez A, Molina D, Azorin J, Barrera M, Soto AM, Sosa R and Furetta C. Thermoluminescence properties of copper doped zirconium oxide for UVR dosimetry. Radiation Measurements. 2007;42:665-667.

Rodrigues PC, Berlim LS, Azevedo D, Saavedra NC, Prasad PN, Schreiner WH, Atvars TDZ and Akcelrud L. Electronic structure and optical properties of an alternated fluorene–Benzothiadiazole copolymer: interplay between experimental and theoretical data. The Journal of Physical Chemistry. 2012;116:3681-3690.

Sambandan DR and Ratner D. Sunscreens: An overview and update. Journal of the American Academy of Dermatology. 2011;64(4),748-758.

Sato K, Kondo S, Tsukada M, Ishigaki T and Kamiya H. Influence of solid fraction on the optimum molecular weight of polymer dispersants in aqueous TiO_2 nanoparticle suspensions. Journal of the American Ceramic Society. 2007;90(11):3401-3406.

Scelsi L, Bonner M, Hodzic A, Soutis C, Wilson C, Scaife R and Ridgway K. Potential emissions savings of lightweight composite aircraft components evaluated through life cycle assessment. Polymer Letters. 2011;5(3):209-217.

Schuller Y, Beckert W, Lauke B, Ageorges C and Friedrich K. Single fibre transverse debonding: stress analysis of the Broutman test. Composites: Part A. 2000;31:661-670.

Sebastian KL and Puthur R. Breaking of a polymer – multidimensional classical transition state theory and beyond. Chemical Physics Letters. 1999;304:399-404.

Serpone N, Dondi D and Albini A. Inorganic and organic UV filters: Their role and efficacy in sunscreens and suncare products. Inorganica Chimica Acta. 2007;360:794-802.

Selvi M, Devaraju S, Vengatesan MR, Go JS, Kumar M and Alagar M. The effect of UV radiation on polybenzoxazine/epoxy/OG-POSS nanocomposites. Royal Society of Chemistry. 2014;4:8238-8244.

Shanmugam N, Hussein IA, Badghaish A, Shuaib AN, Furquan SA and Al-Mehthel MH. Evaluation of oil fly ash as a light stabilizer for epoxy composites: accelerated weathering study. Polymer Degradation and Stability. 2015;112:94-103.

Sharma RK and Balani K. Mechanics of ZnO micro-rod and ZnO nanoparticle reinforcement in ultra-high molecular weight polyethylene biocomposite. Journal of Physics D: Applied Physics. 2014;47:345301-315311.

Shenoi RA, Moy SSJ and Hollaway LC. Advanced polymer composites for structural applications in construction: proceedings of the first international conference, held at Southampton University, UK, on 15-17 April 2002. Thomas Telford. 2002. Pages: 3-20.

Shimizu M, Takeda Y, Higashi M and Hiyama T. Synthesis and photophysical properties of dimethoxybis(3,3,3-trifluoropropen-1-yl)benzenes: Compact chromophores exhibiting violet fluorescence in the solid state. Chemistry-An Asian Journal. 2011;6:2536-2544.

Sil D and Chakrabarti S. Photocatalytic degradation of PVC-ZnO composite film under tropical sunlight and artificial UV radiation: A comparative study. Solar Energy. 2010;84:476-485.

Stewart R. Rebounding automotive industry welcome news for FRP. Reinforced Plastics. 2011;55(1):38-44.

Stevanovic MM, Skapin SD, Bracko I, Milenkovic M, Petkovic J, Filipic M and Uskokovic DP. Poly(lactide-co-glycolide)/silver nanoparticles: Synthesis, characterization antimicrobial activity, cytotoxicity assessment and ROS-inducing potential. Polymer. 2012;53:2818-2828.

Stiefel C and Schwack W. Review Article. Photoprotection in changing times – UV filter efficacy and safety, sensitization processes and regulatory aspects. International Jounral of Cosmetic Science. 2015;37:2-30.

Stoecklein W. The examination of UV-absorbers in 2-coat metallic and non-metallic automotive paints. Science & Justice. 1999;39(3):188-195.

Strong AB. Plastic: materials and processing. Prentice-Hall, Inc, New Jersey. 2000. Second edition. ISBN 0 13 021626 7.

Sun Q, Lu Y, Zhang H, Zhao H, Yu H, Xu J, Fu Y, Yang D and Liu Y. Hydrothermal fabrication of rutile TiO_2 submicrospheres on wood surface: An efficient method to prepare UV-protective wood. Materials Chemistry and Physics. 2012;133:253-258.

Taig IC. Principles of design of a carbon fibre composite aircraft wing. Philosophical Transactions of the Royal Society of London. Series A: Mathematical, Physical and Engineering Sciences. 1980;294:565-575.

Tang E, Cheng G, Ma X, Pang X and Zhao Q. Surface modification of zinc oxide nanoparticle by PMAA and its dispersion in aqueous system. Applied Surface Science. 2006;252:5227-5232.

Tang E, Liu H, Sun L, Zheng E and Cheng G. Fabrication of zinc oxide/poly(styrene) grafted nanocomposite latex and its dispersion. European Polymer Journal. 2007;43:4210-4218.

Tcherbi-Narteh A, Hosur M, Triggs E and Jeelani S. Thermal stability and degradation of Diglycidyl Ether of Bisphenol A epoxy modified with different nanoclays exposed to UV radiation. Polymer Degradation and Stability. 2013;98:759-770.

Tcherbi-Narteh A, Hosur M, Triggs E, Owuor P and Jelaani S. Viscoelastic and thermal properties of full and partially cured DGEBA epoxy resin composites modified with Montmorillonite nanoclay exposed to UV radiation. Polymer Degradation and Stability. 2014;101:81-91.

Tejland P, Langhammer C and Andren HO. On the black oxide colour of zirconium alloys. Journal of Nuclear Materials. 2010;400:79-83.

Thomason JL and Yang L. Temperature dependence of the interfacial shear strength in glass-fibre epoxy composites. Composites Science and Technology. 2014;96:7-12.

Tigges B, Moller M and Weichold O. ZnO nanoparticle-containing emulsions for transparent, hydrophobic UV-absorbent films. Journal of Colloid and Interface Science. 2010;345:41-45.

Ukaji E, Furusawa T, Sato M and Suzuki N. The effect of surface modification with silane coupling agent on suppressing the photo-catalytic activity of fine TiO_2 particles as inorganic UV filter. Applied Surface Science. 2007;254:563-569.

United Nations Environment Programme (UNEP). Environmental Effects of Ozone Depletion and Its Interactions with Climate Change: 2010 Assessment. United Nations Environment Programme. Nairobi, Kenya. 2010.

US National Aeronautics and Space Administration (NASA). Ultraviolet radiation. 2001. Available from: www.nasa.gov.

Vidyasagar CC, Naik YA, Venkatesh TG and Viswanatha R. Solid-state synthesis and effect of temperature on optical properties of Cu-ZnO, Cu-CdO and CuO nanoparticles. Powder Technology. 2011;214:337-343.

Volodin AM. Photoinduced phenomena on the surface of wide-band-gap oxide catalysts. Catalysis Today. 2000;58:103-114.

Wagner HD, Ajayan PM and Schulte K. Nanocomposite toughness from a pull-out mechanism. Composites Science and Technology. 2013;83:27-31.

Wan C, Lu Y, Sun Q and Li J. Hydrothermal synthesis of zirconium dioxide coating on the surface of wood with improved UV resistance. Applied Surface Science. 2014;321:38-42.

Wang W, Liu J, Yu X and Yang G. Transparent poly(methyl methacrylate)/ZnO nanocomposites based on KH570 surface modified ZnO quantum dots. Journal of nanoscience and nanotechnology. 2010:10:5196-5201.

Wang X, Zhou S and Wu L. Facile encapsulation of SiO_2 on ZnO quantum dots and its application in waterborne UV-shielding polymer coatings. Journal of Materials Chemistry C. 2013;1:7547-7553.

Woo RSC, Chen Y, Zhu H, Li J, Kim JK and Leung CKY. Environmental degradation of epoxy-organoclay nanocomposites due to UV exposure. Part I: photo-degradation. Composites Science and Technology. 2007;67:3448-3456.

Woo RSC, Zhu H, Leung CKY and Kim JK. Environmental degradation of epoxy-organoclay nanocomposites due to UV exposure. Part II: residual mechanical properties. Composites Science and Technology. 2008;68:2149-2155.

World Health Organization (WHO). Global Solar UV Index: A Practical Guide. Geneva, Switzerland. 2002.

World Meteorological Organization (WMO). Scientific Assessment of Ozone Depletion: 2014. World Meteorological Organization, Global Ozone Research and Monitoring Project – Report No 55. Geneva, Switzerland. 2014.

Xian G, Li H and Su X. Water absorption and hygrothermal ageing of ultraviolet cured glass-fiber reinforced acrylate composites. Polymer Composites. 2012;33(7):1120-1128.

Xiao X, Liu X, Cao G, Zhang C, Xia L, Xu W and Xiao S. Atomic layer deposition TiO_2/Al_2O_3 nanolayer of dyed polyamide/aramid blend fabric for high intensity UV light protection. Polymer Engineering and Science. 2015;55(6):1296-1302.

Xu CJ, Wan JT and Li BG. Monochromatic light-emitting copolymer of methyl methacrylate and Eu-complexed 5-acrylamido-1,10-phenanthroline. Dyes and Pigments. 2013;98:493-498.

Yan J, McNaughter PD, Wang Z, Hodson N, Chen M, Cui Z, O'Brien P and Saunders BR. Controlled aggregation of quantum dot dispersions by added amine bilinkers and effects on hybrid polymer film properties. RSC Advances. 2015;5:95512-95522.

Yan L, Chouw N and Jayaraman K. Effect of UV and water spraying on the mechanical properties of flax fabric reinforced polymer composites used for civil engineering applications. Materials and Design. 2015;71:17-25.

Yang H, Zhu S and Pan N. Studying the mechanisms of titanium dioxide as ultraviolet-blocking additive for films and fabrics by an improved scheme. Journal of Applied Polymer Science. 2004;92:3201-3210.

Yang L and Thomason JL. Interface strength in glass fibre-polypropylene measured using the fibre pull-out and microbond methods. Composites: Part A. 2010;41:1077-1083.

Voytekunas VY, Ng FL and Abadie MJM. Kinetics study of the UV-initiated cationic polymerization of cycloalophatic diepoxide resins. European Polymer Journal. 2008;44:3640-3649.

Yan L, Chouw N and Jayaraman K. Effect of UV and water spraying on the mechanical properties of flax fabric reinforced polymer composites used for civil engineering applications. Materials and Design. 2015;71:17-25.

Yang XF, Li J, Croll SG, Tallman DE and Bierwagen GP. Degradation of low gloss polyurethane aircraft coatings under UV and prohesion alternating exposures. Polymer Degradation and Stability. 2003;80:51-58.

Yang XF, Tallman DE, Bierwagen GP, Croll SG and Rohlik S. Blistering and degradation of polyurethane coatings under different accelerated weathering tests. Polymer Degradation and Stability. 2002;77:103-109.

Yi C, Sun Y, Pi H and Guo S. Low-temperature UV irradiation induced the colour change kinetics and the corresponding structure development of PVC film. Journal of Applied Polymer Science. 2011;122:2588-2593.

Zhang G, Lin H, Morikawa H and Miura M. In-situ growth of ZnO particles on bamboo pulp fabric and its anti-UV property. Fibers and Polymers. 2013;14(11):1803-1807.

Zhang H, Zhu C, Yu J, Shi C and Zhang D. Influence of surface modification on physical and ultraviolet aging resistance of bitumen containing inorganic nanoparticles. Construction and Building Materials. 2015;98:735-740.

Zhang H, Zhu C, Yu J, Tan B and Shi C. Effect of nano-zinc oxide on ultraviolet aging properties of bitumen with 60/80 penetration grade. Materials and Structures. 2015;48:3249-3257.

Zhang SY. A new model for the energy release rate of fibre/matrix interfacial fracture. Composites Science and Technology. 1998;58:163-166.

Zhang X, Liu HY, Mai YW and Diao XX. On steady-state fibre pull-out I The stress field. Composites Science and Technology. 1999;59:2179-2189.

Zhao FM, Okabe T and Takeda N. The estimation of statistical fibre strength by fragmentation tests of single-fibre composites. Composites Science and Technology. 2000;60:1965-1974.

Zhao H and Li RKY. A study on the photo-degradation of zinc oxide (ZnO) filled polypropylene nanocomposites. Polymer. 2006;47:3207-3217.

Zohdy MH, Hossamy MBE, El-Naggar AWM, Fathalla AI and Ali NM. Novel UV-protective formulations for cotton, PET fabrics and their blend utilizing irradiation technique. European Polymer Journal. 2009;45:2926-2934.